Linköping studies in science and technology. Thesis.
No. 1422

Automotive Sensor Fusion for Situation Awareness

Christian Lundquist

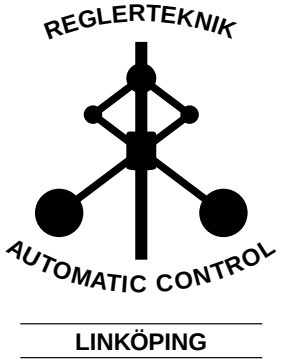

Division of Automatic Control
Department of Electrical Engineering
Linköping University, SE-581 83 Linköping, Sweden
http://www.control.isy.liu.se
lundquist@isy.liu.se

Linköping 2009

This is a Swedish Licentiate's Thesis.

Swedish postgraduate education leads to a Doctor's degree and/or a Licentiate's degree.
A Doctor's Degree comprises 240 ECTS credits (4 years of full-time studies).
A Licentiate's degree comprises 120 ECTS credits,
of which at least 60 ECTS credits constitute a Licentiate's thesis.

Linköping studies in science and technology. Thesis.
No. 1422

Automotive Sensor Fusion for Situation Awareness

Christian Lundquist

lundquist@isy.liu.se
www.control.isy.liu.se
Department of Electrical Engineering
Linköping University
SE-581 83 Linköping
Sweden

ISBN 978-91-7393-492-3 ISSN 0280-7971 LiU-TEK-LIC-2009:30

Printed by LiU-Tryck, Linköping, Sweden 2009

To my family

Abstract

The use of radar and camera for situation awareness is gaining popularity in automotive safety applications. In this thesis situation awareness consists of accurate estimates of the ego vehicle's motion, the position of the other vehicles and the road geometry. By fusing information from different types of sensors, such as radar, camera and inertial sensor, the accuracy and robustness of those estimates can be increased.

Sensor fusion is the process of using information from several different sensors to compute an estimate of the state of a dynamic system, that in some sense is better than it would be if the sensors were used individually. Furthermore, the resulting estimate is in some cases only obtainable through the use of data from different types of sensors. A systematic approach to handle sensor fusion problems is provided by model based state estimation theory. The systems discussed in this thesis are primarily dynamic and they are modeled using state space models. A measurement model is used to describe the relation between the state variables and the measurements from the different sensors. Within the state estimation framework a process model is used to describe how the state variables propagate in time. These two models are of major importance for the resulting state estimate and are therefore given much attention in this thesis. One example of a process model is the single track vehicle model, which is used to model the ego vehicle's motion. In this thesis it is shown how the estimate of the road geometry obtained directly from the camera information can be improved by fusing it with the estimates of the other vehicles' positions on the road and the estimate of the radius of the ego vehicle's currently driven path.

The positions of stationary objects, such as guardrails, lampposts and delineators are measured by the radar. These measurements can be used to estimate the border of the road. Three conceptually different methods to represent and derive the road borders are presented in this thesis. Occupancy grid mapping discretizes the map surrounding the ego vehicle and the probability of occupancy is estimated for each grid cell. The second method applies a constrained quadratic program in order to estimate the road borders, which are represented by two polynomials. The third method associates the radar measurements to extended stationary objects and tracks them as extended targets.

The approaches presented in this thesis have all been evaluated on real data from both freeways and rural roads in Sweden.

Populärvetenskaplig sammanfattning

Användandet av radar och kamera för att skapa en bra situationsmedvetenhet ökar i popularitet i säkerhetsapplikationer för bilar. I den här avhandlingen omfattar situationsmedvetenheten noggranna skattningar av den egna bilens rörelse, de andra bilarnas positioner samt vägens geometri. Genom att fusionera information från flera typer av sensorer, såsom radar, kamera och tröghetssensor, kan noggrannheten och robustheten av dessa skattningar öka.

Sensorfusion är en process där informationen från flera olika sensorer används för att beräkna en skattning av ett systems tillstånd, som på något sätt kan anses vara bättre än om sensorerna användes individuellt. Dessutom kan den resulterande tillståndsskattningen i vissa fall endast erhållas genom att använda data från olika sensorer. Ett systematiskt sätt att behandla sensorfusionsproblemet tillhandahålls genom att använda modellbaserade tillståndsskattningsmetoder. Systemen som diskuteras i den här avhandlingen är huvudsakligen dynamiska och modelleras med tillståndsmodeller. En mätmodell används för att beskriva relationen mellan tillståndsvariablerna och mätningarna från de olika sensorerna. Inom tillståndsskattningens ramverk används en processmodell för att beskriva hur en tillståndsvariabel propagerar i tiden. Dessa två modeller är av stor betydelse för den resulterande tillståndsskattningen och ges därför stort utrymme i den här avhandlingen. Ett exempel på en processmodell är den så kallade enspårs fordonsmodellen, som används för att skatta den egna bilens rörelse. I den här avhandlingen visas hur skattningen av vägens geometri, som erhålls av kameran, kan förbättras genom att fusionera informationen med skattningen av de andra bilarnas positioner på vägen och skattningen av den egna bilens körda radie.

Stationära objekt, såsom vägräcken och lampstolpar uppmäts med radarn. Dessa mätningar kan användas för att skatta vägens kanter. Tre konceptuellt olika metoder att representera och beräkna vägkanterna presenteras i den här avhandlingen. “Occupancy grid mapping” diskretiserar kartan som omger den egna bilen, och sannolikheten att en kartcell är ockuperad skattas. Den andra metoden applicerar ett kvadratiskt program med bivillkor för att skatta vägkanterna, vilka är representerade i form av två polynom. Den tredje metoden associerar radarmätningarna med utsträckta stationära objekt och följer dem som utsträckta mål.

Tillvägagångssätten som presenteras i den här avhandlingen är alla utvärderade på mätdata från svenska motorvägar och landsvägar.

Acknowledgments

First of all I would like to thank my supervisor Professor Fredrik Gustafsson for guidance and inspiring discussions during my research projects and the writing of this thesis. Especially, I want to acknowledge all the good and thrilling ideas popping up during our discussions. I would also like to thank my co-supervisor Dr. Thomas Schön for introducing me to the world of academic research and teaching me all those important details, for example how to write a good, exciting and understandable paper.

I am very grateful to Professor Lennart Ljung for giving me the opportunity to join the Automatic Control group and for creating an inspiring, friendly and professional atmosphere. This atmosphere is maintained by all great colleagues, and I would like to thank you all for being good friends.

This work was supported by the SEnsor Fusion for Safety (SEFS) project within the Intelligent Vehicle Safety Systems (IVSS) program. I would like to thank Lars Danielsson at Volvo Car Corporation and Fredrik Sandblom at Volvo 3P for the recent useful and interesting discussions at Chalmers. I hope that we will have the possibility to cooperate even after the end of the project. Dr. Andreas Eidehall at Volvo Car Corporation helped me a lot with the measurements and fusion framework at the beginning of my research, which I thankfully acknowledge. I would also like to thank Andreas Andersson at Nira Dynamics for fruitful discussions on the German Autobahn and for providing measurement data.

A special thanks to Dr. Umut Orguner who helped me with the target tracking theory and took the time to explain all things I didn't understand. This thesis has been proofread by Karl Granström and Umut Orguner. Your help has improved the quality of this thesis substantially. I acknowledge Ulla Salaneck's help when it comes to practical and administrative stuff. Gustaf Hendeby and Henrik Tidefelt helped me with my LaTeX issues. Thank you all!

From 2004 to 2007 I worked at the company ZF Lenksysteme GmbH with the development of Active Front Steering. I appreciate the encouragement I got from my colleague Dr. Wolfgang Reinelt during this time. With him I wrote my first papers and he also helped me to establish the contact with Professor Lennart Ljung. My former boss Gerd Reimann introduced me to the beautiful world of vehicle dynamics and taught me the importance of performing good experiments and collecting real data.

Finally, I would like to thank my parents and my sister for their never ending support for all that I have undertaken in life this far.

Linköping, October 2009
Christian Lundquist

Contents

1

Introduction

This thesis is concerned with the problem of estimating the motion of a vehicle and the characteristics of its surroundings, i.e. to improve the situation awareness. More specifically, the description of the ego vehicle's surroundings consists in other vehicles and stationary objects as well as the geometry of the road. The signals from several different sensors, including camera, radar and inertial sensor, must be combined and analyzed to compute estimates of various quantities and to detect and classify many objects simultaneously. Sensor fusion allows the system to obtain information that is better than if it was obtained by individual sensors.

Situation awareness is the perception of environmental features, the comprehension of their meaning and the prediction of their status in the near future. It involves being aware of what is happening in and around the vehicle to understand how the subsystems impact on each other.

Sensor fusion is introduced in Section 1.1 and its application within the automotive community is briefly discussed in Section 1.2. The study presented in this thesis was accomplished in a Swedish research project, briefly described in Section 1.3. The sensor fusion framework and its components, such as infrastructure, estimation algorithms and various mathematical models, are all introduced in Section 1.4. Finally, the chapter is concluded with a statement of the contributions in Section 1.5, and the outline of this thesis in Section 1.6.

1.1 Sensor Fusion

Sensor fusion is the process of using information from several different sensors to compute an estimate of the state of a dynamic system. The resulting estimate is in some sense better than it would be if the sensors were used individually. The term better can in this case mean more accurate, more reliable, more available and of higher safety integrity. Furthermore, the resulting estimate may in some cases only be possible to obtain by using

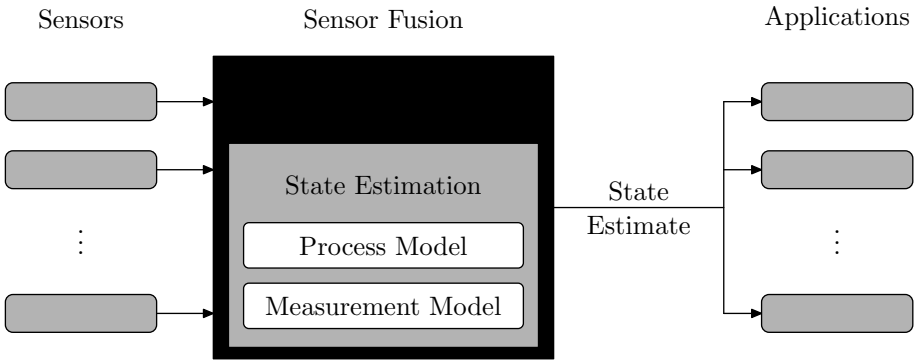

Figure 1.1: *The main components of the sensor fusion framework are shown in the middle box. The framework receives measurements from several sensors, fuses them and produces one state estimate, which can be used by several applications.*

data from different types of sensors. Figure 1.1 illustrates the basic concept of the sensor fusion framework. Many systems have traditionally been stand alone systems with one or several sensors transmitting information to only one single application. Using a sensor fusion approach it might be possible to remove one sensor and still perform the same tasks, or add new applications without the need to add new sensors.

Sensor fusion is required to reduce cost, system complexity and number of components involved and to increase accuracy and confidence of sensing.

1.2 Automotive Sensor Fusion

Within the automotive industry there is currently a huge interest in active safety systems. External sensors are increasingly important and typical examples used in this work are radar sensors and camera systems. Today, a sensor is usually connected to a single function. However, all active safety functions need information about the state of the ego vehicle and its surroundings, such as the lane geometry and the position of other vehicles. The use of signal processing and sensor fusion to replace redundant and costly sensors with software attracted recent attention in IEEE Signal Processing Magazine (Gustafsson, 2009).

The sensors in a modern passenger car can be divided into a number of subgroups; there are internal sensors measuring the motion of the vehicle, external sensor measuring the objects surrounding the vehicle and there are sensors communicating with other vehicles and with the infrastructure. The communication between sensors, fusion framework, actuators and controllers is made possible by the controller area network (CAN). It is a serial bus communication protocol developed by Bosch in the early 1980s and presented by Kiencke et al. (1986) at the SAE international congress in Detroit. An overview of the CAN bus, which has become the de facto standard for automotive communication, is given in Johansson et al. (2005).

Internal sensors are often referred to as proprioceptive sensors in the literature. Typical examples are gyrometers, primarily measuring the yaw rate about the vehicle's vertical

(a) *(b)*

Figure 1.2: *Figure (a) shows the camera in the vehicle, and Figure (b) the front looking radar. Note that this is not serial production mounting. Courtesy of Volvo Car Corporation.*

axis, and accelerometers, measuring the longitudinal and lateral acceleration of the vehicle. The velocity of the vehicle is measured using inductive wheel speed sensors and the steering wheel position is measured using an angle sensor. External sensors are referred to as exteroceptive sensors in the literature, typical examples are radar (RAdio Detection And Ranging), lidar (LIght Detection And Ranging) and cameras.

An example of how a radar and a camera may be mounted in a passenger car is illustrated in Figure 1.2. These two sensors complement each other very well, since the advantage of the radar is the disadvantage of the camera and vice versa. A summary of the two sensors' properties is presented in Table 1.1 and in e.g., Jansson (2005).

As already mentioned, the topic of this thesis is how to estimate the state variables describing the ego vehicle's motion and the characteristics of its surroundings. The ego vehicle is one subsystem, labeled $\mathcal{E}$ in this work. The use of data from the vehicle's actuators, e.g. the transmission and steering wheel, to estimate a change in position over

Table 1.1: *Properties of radar and camera for object detection*

	Camera	**Radar**
Detects	other vehicles, lane markings, pedestrians	other vehicles, stationary objects
Classifies objects	yes	no
Azimuth angle	high accuracy	medium accuracy
Range	low accuracy	very high accuracy
Range rate	not	very high accuracy
Field of View	wide	narrow
Weather Conditions	sensitive to bad visibility	less sensitive

time is referred to as odometry. The ego vehicle's surroundings consists of other vehicles, referred to as targets $\mathcal{T}$, and stationary objects as well as the shape and the geometry of the road $\mathcal{R}$. Mapping is the problem of integrating the information obtained by the sensors into a given representation, see Adams et al. (2007) for a recent overview and Thrun (2002) for a survey. The main focus of this thesis is the ego vehicle $\mathcal{E}$ (odometry) and the road geometry $\mathcal{R}$, which includes stationary objects along the road (mapping). Simultaneous localization and mapping (SLAM) is an approach used by autonomous vehicles to build a map while at the same time keeping track of their current locations, see e.g. Durrant-Whyte and Bailey (2006), Bailey and Durrant-Whyte (2006). This approach is not treated in this thesis.

1.3 Sensor Fusion for Safety

The work in this thesis has been performed within the research project Sensor Fusion for Safety (SEFS), which is funded by the Swedish Intelligent Vehicle Safety Systems (IVSS) program. The project is a collaboration between Volvo Technology, Volvo Cars, Volvo Trucks, Mecel, Chalmers University of Technology and Linköping University.

The overall objective of this project is to obtain sensor fusion competence for automotive safety applications in Sweden by doing research within relevant areas. This goal is achieved by developing a sensor fusion platform, algorithms, modeling tools and a simulation platform. More specifically, the aim is to develop general methods and algorithms for a sensor fusion systems utilizing information from all available sensors in a modern passenger car. The sensor fusion will provide a refined description of the vehicle's environment that can be used by a number of different safety functions. The integration of the data flow requires new specifications with respect to sensor signals, hardware, processing, architectures and reliability.

The SEFS work scope is divided into a number of work packages. These include at a top level, fusion structure, key scenarios and the development of requirement methods. The next level consists in work packages such as pre-processing and modeling, the implementation of a fusion platform and research done on fusion algorithms, into which this thesis can be classified. The use-case work package consists of implementation of software and design of prototypes and demonstrators. Finally, there is an evaluation and validation work package.

During the runtime of the SEFS project, i.e. from 2005 until today, two PhD theses (Schön, 2006, Gunnarsson, 2007) and two licentiate theses (Bengtsson, 2008, Danielsson, 2008) have been produced. An overview of the main results in the project is given in Ahrholdt et al. (2009) and the sensor fusion framework is well described in Bengtsson and Danielsson (2008). Furthermore it is worth mentioning some of the publications produced by the project partners. Motion models for tracked vehicles are covered in Svensson and Gunnarsson (2006), Gunnarsson et al. (2006). A better sensor model of the tracked vehicle is presented in Gunnarsson et al. (2007). Detection of lane departures and lane changes of leading vehicles are studied in Schön et al. (2006), with the goal to increase the accuracy of the road geometry estimate. Computational complexity for systems obtaining data from sensors with different sampling rates and different noise distributions is studied in Schön et al. (2007).

1.4 Components of the Sensor Fusion Framework

A systematic approach to handle sensor fusion problems is provided by nonlinear state estimation theory. Estimation problems are handled using discrete-time model based methods. The systems discussed in this thesis are primarily dynamic and they are modeled using stochastic difference equations. More specifically, the systems are modeled using the discrete-time nonlinear state space model

$$\boldsymbol{x}_{t+1} = f_t(\boldsymbol{x}_t, \boldsymbol{u}_t, \boldsymbol{w}_t, \boldsymbol{\theta}), \tag{1.1a}$$

$$\boldsymbol{y}_t = h_t(\boldsymbol{x}_t, \boldsymbol{u}_t, \boldsymbol{e}_t, \boldsymbol{\theta}), \tag{1.1b}$$

where (1.1a) describes the evolution of the state variable $\boldsymbol{x}$ over time and (1.1b) explains how the state variable $\boldsymbol{x}$ relates to the measurement $\boldsymbol{y}$. The state vector at time t is denoted by $\boldsymbol{x}_t \in \mathbb{R}^{n_x}$, with elements $x_1, \ldots, x_{n_x}$ being real numbers. Sensor observations collected at time t are denoted by $\boldsymbol{y}_t \in \mathbb{R}^{n_y}$, with elements $y_1, \ldots, y_{n_x}$ being real numbers. The model f_t in (1.1a) is referred to as the process model, the system model, the dynamic model or the motion model, and it describes how the state propagates in time. The model h_t in (1.1b) is referred to as the measurement model or sensor model and it describes how the state is propagated into the measurement space. The random vector $\boldsymbol{w}_t$ describes the process noise, which models the fact that the actual state dynamics is usually unknown. The random vector $\boldsymbol{e}_t$ describes the sensor noise. Furthermore, $\boldsymbol{u}_t$ denotes the deterministic input signals and $\boldsymbol{\theta}$ denotes the possibly unknown parameter vector of the model.

The ego vehicle constitutes an important dynamic system in this thesis. The yaw and lateral dynamics are modeled using the so called single track model. This model will be used as an example throughout the thesis. Some of the variables and parameters in the model are introduced in Example 1.1.

Example 1.1: Single Track Ego Vehicle Model

A so called bicycle model is obtained if the wheels at the front and the rear axle of a passenger car are modeled as single wheels. This type of model is also referred to as single track model and a schematic drawing is given in Figure 1.3. Some examples of typical variables and parameters are:

State variables $\boldsymbol{x}$: the yaw rate $\dot{\psi}_E$ and the body side slip angle β, i.e.

$$\boldsymbol{x} = \begin{bmatrix} \dot{\psi}_E & \beta \end{bmatrix}^{\mathrm{T}}. \tag{1.2}$$

Measurements $\boldsymbol{y}$: the yaw rate $\dot{\psi}_E$ and the lateral acceleration a_y, i.e.

$$\boldsymbol{y} = \begin{bmatrix} \dot{\psi}_E & a_y \end{bmatrix}^{\mathrm{T}}, \tag{1.3}$$

which both are measured by an inertial measurement unit (IMU).

Input signals $\boldsymbol{u}$: the steering wheel angle δ_s, which is measured with an angular sensor at the steering column, the longitudinal acceleration $\dot{v}_x$, which is measured by the IMU and the vehicle velocity v_x, which is measured at the wheels, i.e.

$$\boldsymbol{u} = \begin{bmatrix} \delta_s & \dot{v}_x & v_x \end{bmatrix}^{\mathrm{T}}. \tag{1.4}$$

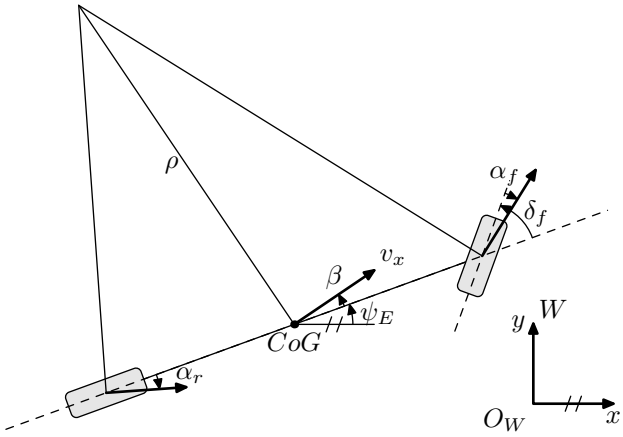

Figure 1.3: *Illustration of the geometry for the single track model, describing the motion of the ego vehicle. The ego vehicle velocity vector v_x is defined from the center of gravity (CoG) and its angle to the longitudinal axis of the vehicle is denoted by β, referred to as the body side slip angle. Furthermore, the slip angles are referred to as α_f and α_r. The front wheel angle is denoted by δ_f and the current driven radius is denoted by ρ.*

Parameters $\boldsymbol{\theta}$: the vehicle mass m, which is weighed before the tests, the steering ratio i_s between the steering wheel angle and the front wheels, which has to be estimated in advance, and the tire parameter C_α, which is estimated on-line, since the parameter value changes due to different road and weather conditions.

The nonlinear models f and h are derived in Section 2.3.

The model (1.1) must describe the essential properties of the system, but it must also be simple enough to be efficiently used within a state estimation algorithm. The model parameters $\boldsymbol{\theta}$ are estimated using techniques from system identification community. The main topic of Chapter 2 is the derivation of the model equations through physical relations and general assumptions. Chapter 3 describes algorithms that are used to compute estimates of the state $\boldsymbol{x}_t$ and the parameter $\boldsymbol{\theta}$ in (1.1).

Before describing the individual steps of the sensor fusion framework another important example is presented in Example 1.2.

Example 1.2: Object Tracking

Other objects, such as vehicles or stationary objects on and along the road, are tracked using measurements from a radar mounted in the ego vehicle. A simple model for one such tracked object is given by using the following variables:

State variables $\boldsymbol{x}$: Cartesian position of tracked targets $i = 1, \ldots, N_x$ in a world fixed coordinate frame W, i.e. $\boldsymbol{x}_i = \begin{bmatrix} x^W & y^W \end{bmatrix}^{\mathrm{T}}$.

Measurements $\boldsymbol{y}$: Range and azimuth angle to objects $m = 1, \ldots, N_y$ measured by the radar in the ego vehicle fixed coordinate frame E, i.e. $\boldsymbol{y}_m = \begin{bmatrix} d^E & \delta \end{bmatrix}^{\mathrm{T}}$.

At every time step t, N_y observations are obtained by the radar. Hence, the radar delivers N_y range and azimuth measurements in a multi-sensor set $\mathbf{Y} = \{\boldsymbol{y}_1, \ldots, \boldsymbol{y}_{N_y}\}$ to the sensor fusion framework. The sensor fusion framework currently also tracks N_x targets. The multi-target state is given by the set $\mathbf{X} = \{\boldsymbol{x}_1, \ldots, \boldsymbol{x}_{N_x}\}$ where $\boldsymbol{x}_1, \ldots, \boldsymbol{x}_{N_x}$ are the individual states.

Obviously, the total number of state variables in the present example is $2N_x$ and the total number of measurements is $2N_y$. This issue may be compared to Example 1.1, where the size of the $\boldsymbol{y}$-vector corresponds to the total number of measurements at time t. Typically, the radar also observes false detections, referred to as clutter, or receives several measurements from the same target, i.e. N_y is seldom equal to N_x for radar sensors.

The different steps of a typical sensor fusion algorithm, as the central part of the larger framework, are shown in Figure 1.4. The algorithm is initiated using a prior guess of the state $\boldsymbol{x}_0$ or, if it is not the first iteration, the state estimate $\hat{\boldsymbol{x}}_{t-1|t-1}$ from the previous time step $t-1$ is used. New measurements $\mathbf{Y}_t$ are collected from the sensors and *preprocessed* at time t. Model (1.1) is used to *predict* the state estimate $\hat{\boldsymbol{x}}_{t|t-1}$ and the measurement $\hat{\boldsymbol{y}}_{t|t-1}$. For Example 1.2 it is necessary to *associate* the radar observations $\mathbf{Y}_t$ with the predicted measurements $\hat{\mathbf{Y}}_{t|t-1}$ of the existing state estimates and to *manage the tracks*, i.e. initiate new states and remove old, invalid states. The data association and track management are further discussed in Section 4.2. Returning to Example 1.1, where the data association and track management are obviously not needed, since there the data association is assumed fixed. Finally, the new measurement $\boldsymbol{y}_t$ is used to improve the state estimate $\hat{\boldsymbol{x}}_{t|t}$ at time t in the so called *measurement update* step. The prediction and measurement update are described in Section 3.2. This algorithm is iterated, $\hat{\boldsymbol{x}}_{t|t}$ is used to predict $\hat{\boldsymbol{x}}_{t+1|t}$, new measurements $\mathbf{Y}_{t+1}$ are collected at time $t+1$ and so on. The state estimation theory, as part of the sensor fusion framework, is discussed further in Chapter 3.

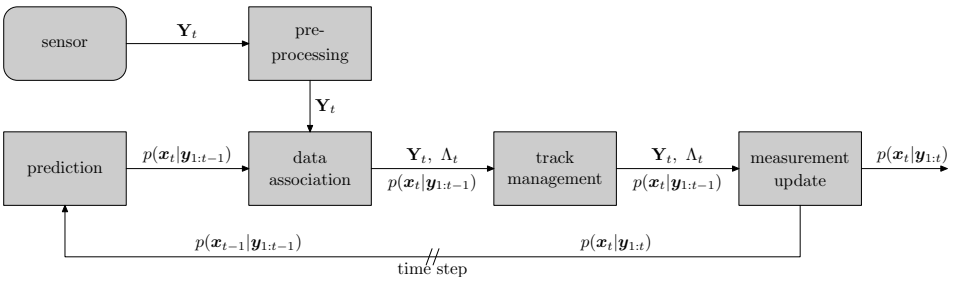

Figure 1.4: *The new measurements $\mathbf{Y}_t$ contain new information and are* associated *to the* predicted *states $\widehat{\mathbf{X}}_{t|t-1}$ and thereafter used to* update *them to obtain the improved state estimates $\widehat{\mathbf{X}}_{t|t}$.*

1.5 Contributions

The main contributions of this thesis are briefly summarized and presented below:

- A method to improve the road curvature estimate, using information from the image processing, the motion of the ego vehicle and the position of the other vehicles on the road is presented in Paper A. Furthermore, a new process model for the road is presented.
- An approach to estimate the tire road interaction is presented in Paper B. The load transfer between the front and rear axles is considered when recursively estimating the stiffness parameters of the tires.
- Two different methods to estimate the road edges and stationary objects along the road are presented in the Papers C and D. The methods are compared to the standard occupancy grid mapping technique, which is presented in Section 4.3.1.

1.6 Outline

There are two parts in this thesis. The objective of the first part is to give a unified overview of the research reported in this thesis. This is accomplished by explaining how the different publications in Part II relate to each other and to the existing theory.

1.6.1 Outline of Part I

The main components of a sensor fusion framework are depicted in Figure 1.1. Part I aims at giving a general description of the individual components of this framework. Chapter 2 is concerned with the inner part of the model based estimation process i.e., the *process model* and the *measurement model* illustrated by the two white rectangles in Figure 1.1. The *estimation process*, illustrated by the gray rectangle, is outlined in Chapter 3. In Chapter 4 some examples including the sensors to the left in Figure 1.1 and the *tracking* or *fusion management*, illustrated by the black rectangle, are described. Chapters 2 and 3 emphasize on the theory and the background of the mathematical relations used in Part II. Finally, the work is summarized and the next steps for future work are given in Chapter 5.

1.6.2 Outline of Part II

Part II consists of a collection of edited papers, introduced below. Besides a short summary of the paper, a paragraph briefly explaining the background and the contribution is provided. The background is concerned with how the research came about, whereas the contribution part states the contribution of the present author.

Paper A: Joint Ego-Motion and Road Geometry Estimation

Lundquist, C. and Schön, T. B. (2008a). Joint ego-motion and road geometry estimation. *Submitted to Information Fusion.*

Summary: We provide a sensor fusion framework for solving the problem of joint ego-motion and road geometry estimation. More specifically we employ a sensor fusion framework to make systematic use of the measurements from a forward looking radar and camera, steering wheel angle sensor, wheel speed sensors and inertial sensors to compute good estimates of the road geometry and the motion of the ego vehicle on this road. In order to solve this problem we derive dynamical models for the ego vehicle, the road and the leading vehicles. The main difference to existing approaches is that we make use of a new dynamic model for the road. An extended Kalman filter is used to fuse data and to filter measurements from the camera in order to improve the road geometry estimate. The proposed solution has been tested and compared to existing algorithms for this problem, using measurements from authentic traffic environments on public roads in Sweden. The results clearly indicate that the proposed method provides better estimates.

Background and contribution: The topic had already been studied in the automatic control group in Linköping by Dr. Thomas B. Schön and Dr. Andreas Eidehall, see e.g., Eidehall et al. (2007), Schön et al. (2006), where a simplified vehicle model was used. The aim of this work was to study if the results could be improved by using a more complex vehicle model, i.e. the single track model, which in addition includes the side slip of the vehicle. The author of this thesis contributed with the idea that the single track model could be used to describe the current driven curvature instead of using a road model based on road construction standards.

Paper B: Recursive Identification of Cornering Stiffness Parameters for an Enhanced Single Track Model

> Lundquist, C. and Schön, T. B. (2009b). Recursive identification of cornering stiffness parameters for an enhanced single track model. In *Proceedings of the 15th IFAC Symposium on System Identification*, pages 1726–1731, Saint-Malo, France.

Summary: The current development of safety systems within the automotive industry heavily relies on the ability to perceive the environment. This is accomplished by using measurements from several different sensors within a sensor fusion framework. One important part of any system of this kind is an accurate model describing the motion of the vehicle. The most commonly used model for the lateral dynamics is the single track model, which includes the so called cornering stiffness parameters. These parameters describe the tire-road contact and are unknown and even time-varying. Hence, in order to fully make use of the single track model, these parameters have to be identified. The aim of this work is to provide a method for recursive identification of the cornering stiffness parameters to be used on-line while driving.

Background and contribution: The tire parameters are included in the single track model, which is used to describe the ego vehicle's motion in all papers in this thesis. This work started as a project in a graduate course in system identification held by Professor Lennart Ljung. The idea to use RLS to estimate the parameters was formulated during discussion between the two authors of this paper. Andreas Andersson at Nira Dynamics and the author of this thesis collected the measurement data during a trip to Germany.

Paper C: Estimation of the Free Space in Front of a Moving Vehicle

Lundquist, C. and Schön, T. B. (2009a). Estimation of the free space in front of a moving vehicle. In *Proceedings of the SAE World Congress*, SAE paper 2009-01-1288, Detroit, MI, USA.

Summary: There are more and more systems emerging making use of measurements from a forward looking radar and a forward looking camera. It is by now well known how to exploit this data in order to compute estimates of the road geometry, tracking leading vehicles, etc. However, there is valuable information present in the radar concerning stationary objects, that is typically not used. The present work shows how radar measurements of stationary objects can be used to obtain a reliable estimate of the free space in front of a moving vehicle. The approach has been evaluated on real data from highways and rural roads in Sweden.

Background and contribution: This work started as a project in a graduate course on convex optimization held by Professor Anders Hansson, who also proposed the idea of using the arctan-function in the predictor. Dr. Thomas Schön established the contact with Dr. Adrian Wills at the University of Newcastle, Australia, whose toolbox was used to efficiently solve the least squares problem.

Paper D: Tracking Stationary Extended Objects for Road Mapping using Radar Measurements

Lundquist, C., Orguner, U., and Schön, T. B. (2009). Tracking stationary extended objects for road mapping using radar measurements. In *Proceedings of the IEEE Intelligent Vehicles Symposium*, pages 405–410, Xi'an, China.

Summary: It is getting more common that premium cars are equipped with a forward looking radar and a forward looking camera. The data is often used to estimate the road geometry, tracking leading vehicles, etc. However, there is valuable information present in the radar concerning stationary objects, that is typically not used. The present work shows how stationary objects, such as guardrails, can be modeled and tracked as extended objects using radar measurements. The problem is cast within a standard sensor fusion framework utilizing the Kalman filter. The approach has been evaluated on real data from highways and rural roads in Sweden.

Background and contribution: The author of this thesis came up with the ideas presented in this paper as he was writing Paper C. Dr. Umut Orguner contributed with his knowledge in the area of target tracking to the realization of the ideas.

1.6.3 Related Publications

Publications of related interest, but not included in this thesis:

Ahrholdt, M., Bengtsson, F., Danielsson, L., and Lundquist, C. (2009). SEFS – results on sensor data fusion system development. In *16th World Congress of ITS*, Stockholm, Sweden

Reinelt, W. and Lundquist, C. (2006a). Controllability of active steering system hazards: From standards to driving tests. In Pimintel, J. R., editor, *Safety Critical Automotive Systems*, ISBN 13: 978-0-7680-1243-9, pages 173–178. SAE International, 400 Commonwealth Drive, Warrendale, PA, USA,

Malinen, S., Lundquist, C., and Reinelt, W. (2006). Fault detection of a steering wheel sensor signal in an active front steering system. In *Preprints of the IFAC Symposium on SAFEPROCESS*, pages 547–552, Beijing, China,

Reinelt, W. and Lundquist, C. (2006b). Mechatronische Lenksysteme: Modellbildung und Funktionalität des Active Front Steering. In Isermann, R., editor, *Fahrdynamik Regelung - Modellbildung, Fahrassistenzsysteme, Mechatronik*, ISBN 3-8348-0109-7, pages 213–236. Vieweg Verlag,

Lundquist, C. and Reinelt, W. (2006a). Back driving assistant for passenger cars with trailer. In *Proceedings of the SAE World Congress*, SAE paper 2006-01-0940, Detroit, MI, USA,

Lundquist, C. and Reinelt, W. (2006b). Rückwärtsfahrassistent für PKW mit Aktive Front Steering. In *Proceedings of the AUTOREG (Steuerung und Regelung von Fahrzeugen und Motoren*, VDI Bericht 1931, pages 45–54, Wiesloch, Germany,

Reinelt, W. and Lundquist, C. (2005). Observer based sensor monitoring in an active front steering system using explicit sensor failure modeling. In *Proceedings of the 16th IFAC World Congress*, Prague, Czech Republic,

Reinelt, W., Lundquist, C., and Johansson, H. (2005). On-line sensor monitoring in an active front steering system using extended Kalman filtering. In *Proceedings of the SAE World Congress*, SAE paper 2005-01-1271, Detroit, MI, USA,

Reinelt, W., Klier, W., Reimann, G., Lundquist, C., Schuster, W., and Großheim, R. (2004). Active front steering for passenger cars: System modelling and functions. In *Proceedings of the first IFAC Symposium on Advances in Automotive Control*, Salerno, Italy.

Patents of related interest, but not included in this thesis:

Lundquist, C. and Großheim, R. (2009). Method and device for determining steering angle information. International Patent WO 2009047020, 2009.04.16 and German Patent DE 102007000958, 2009.05.14,

Lundquist, C. (2008). Method for stabilizing a vehicle combination. U.S. Patent US 2008196964, 2008.08.21 and German Patent DE 102007008342, 2008.08.21,

Reimann, G. and Lundquist, C. (2008). Verfahren zum Betrieb eines elektronisch geregelten Servolenksystems. German Patent DE 102006053029, 2008.05.15,

Reinelt, W., Schuster, W., Großheim, R., and Lundquist, C. (2008c). Verfahren zum Betrieb eines Servolenksystems. German Patent DE 102006052092, 2008.05.08,

Reinelt, W., Schuster, W., Großheim, R., and Lundquist, C. (2008b). Verfahren zum Betrieb eines elektronischen Servolenksystems. German Patent DE 102006043069, 2008.03.27,

Reinelt, W., Schuster, W., Großheim, R., and Lundquist, C. (2008d). Verfahren zum Betrieb eines Servolenksystems. German Patent DE 102006041237, 2008.03.06,

Reinelt, W., Schuster, W., Großheim, R., and Lundquist, C. (2008e). Verfahren zum Betrieb eines Servolenksystems. German Patent DE 102006041236, 2008.03.06,

Reinelt, W., Schuster, W., Großheim, R., and Lundquist, C. (2008a). Verfahren zum Betrieb eines elektronisch geregelten Servolenksystems. German Patent DE 102006040443, 2008.03.06,

Reinelt, W. and Lundquist, C. (2007). Method for assisting the driver of a motor vehicle with a trailer when reversing. German Patent DE 102006002294, 2007.07.19, European Patent EP 1810913, 2007.07.25 and Japanese Patent JP 2007191143, 2007.08.02,

Reinelt, W., Lundquist, C., and Malinen, S. (2007). Automatic generation of a computer program for monitoring a main program to provide operational safety. German Patent DE 102005049657, 2007.04.19,

Lundquist, C. and Reinelt, W. (2006c). Verfahren zur Überwachung der Rotorlage eines Elektromotors. German Patent DE 102005016514, 2006.10.12,

Part I

Background Theory and Applications

2

Models of Dynamic Systems

Given measurements from several sensors the objective is to estimate one or several state variables, either by means of improving a measured signal or by means of estimating a signal which is not, or can not, be directly measured. In either case the relationship between the measured signals and the state variable must be described, and the equations describing this relationship is referred to as the measurement model. When dealing with dynamic or moving systems, as is commonly the case in automotive applications, the objective might be to predict the value of the state variable at the next time step. The prediction equation is referred to as the process model. This section deals with these two types of models.

As mentioned in the introduction in Section 1.4, a general model of dynamic systems is provided by the nonlinear state space model

$$\boldsymbol{x}_{t+1} = f_t(\boldsymbol{x}_t, \boldsymbol{u}_t, \boldsymbol{w}_t, \boldsymbol{\theta}), \tag{2.1a}$$

$$\boldsymbol{y}_t = h_t(\boldsymbol{x}_t, \boldsymbol{u}_t, \boldsymbol{e}_t, \boldsymbol{\theta}). \tag{2.1b}$$

The single track model, introduced in Example 1.1, is used as an example throughout the first sections of this chapter. For this purpose the process and measurement models are given in Example 2.1, while the derivations are provided later in Section 2.3. Most mechanical and physical laws are provided in continuous-time, but computer implementations are made in discrete-time, i.e. the process and measurement models are derived in continuous-time according to

$$\dot{\boldsymbol{x}}(t) = a(\boldsymbol{x}(t), \boldsymbol{u}(t), \boldsymbol{w}(t), \boldsymbol{\theta}, t), \tag{2.2a}$$

$$\boldsymbol{y}(t) = c(\boldsymbol{x}(t), \boldsymbol{u}(t), \boldsymbol{e}(t), \boldsymbol{\theta}, t), \tag{2.2b}$$

and are then discretized. Discretization is the topic of Section 2.1. Special cases of the general state space model (2.1), such as the state space model with additive noise and the linear state space model, are discussed in Section 2.2.

Several models for various applications are given in the papers in Part II, however, the derivations are not always thoroughly described, and the last sections of this chapter are aimed at closing this gap. More specifically, the single track state space model of the ego vehicle given in Example 2.1 is derived in Section 2.3 and compared to other commonly used models. There exist different road models, of which some are treated in Section 2.4. Finally, target tracking models are discussed briefly in Section 2.5.

Example 2.1: Single Track Model

The state variables $\boldsymbol{x}_{\mathcal{E}}$, the input signals $\boldsymbol{u}_{\mathcal{E}}$ and the measurement signals $\boldsymbol{y}_{\text{IMU}}$ of the ego vehicle model were defined in Example 1.1, and are repeated here for convenience

$$\boldsymbol{x}_{\mathcal{E}} = \begin{bmatrix} \dot{\psi}_E & \beta \end{bmatrix}^{\mathrm{T}}, \tag{2.3a}$$

$$\boldsymbol{u}_{\mathcal{E}} = \begin{bmatrix} \delta_f & \dot{v}_x & v_x \end{bmatrix}^{\mathrm{T}}, \tag{2.3b}$$

$$\boldsymbol{y}_{\text{IMU}} = \begin{bmatrix} \dot{\psi}_E^m & a_y^m \end{bmatrix}^{\mathrm{T}}. \tag{2.3c}$$

Note that the front wheel angle δ_f is used directly as an input signal to simplify the example. The continuous-time single track process and measurement models are given by

$$\dot{\boldsymbol{x}}_{\mathcal{E}} = \begin{bmatrix} a_{\mathcal{E}_1} \\ a_{\mathcal{E}_2} \end{bmatrix} = \begin{bmatrix} -\frac{C_{\alpha f} l_f^2 \cos\delta_f + C_{\alpha r} l_r^2}{I_{zz} v_x} \dot{\psi}_E + \frac{-C_{\alpha f} l_f \cos\delta_f + C_{\alpha r} l_r}{I_{zz}} \beta + \frac{C_{\alpha f} l_f \tan\delta_f}{I_{zz}} \\ -\left(1 + \frac{C_{\alpha f} l_f \cos\delta_f - C_{\alpha r} l_r}{v_x^2 m}\right) \dot{\psi}_E - \frac{C_{\alpha f} \cos\delta_f + C_{\alpha r} + \dot{v}_x m}{m v_x} \beta + \frac{C_{\alpha f} \sin\delta_f}{m v_x} \end{bmatrix}, \tag{2.4a}$$

$$\boldsymbol{y}_{\text{IMU}} = \begin{bmatrix} c_{\mathcal{E}_1} \\ c_{\mathcal{E}_2} \end{bmatrix} = \begin{bmatrix} \dot{\psi}_E \\ \frac{-C_{\alpha f} l_f \cos\delta_f + C_{\alpha r} l_r}{m v_x} \dot{\psi}_E - \frac{C_{\alpha f} \cos\delta_f + C_{\alpha r} + m\dot{v}_x}{m} \beta + \frac{C_{\alpha f} \sin\delta_f}{m} \end{bmatrix}, \tag{2.4b}$$

with parameter vector

$$\boldsymbol{\theta} = \begin{bmatrix} l_f & l_r & I_{zz} & m & C_{\alpha f} & C_{\alpha r} \end{bmatrix}, \tag{2.5}$$

where l_f and l_r denotes the distances between the center of gravity of the vehicle and the front and rear axles, respectively. Furthermore, m denotes the mass of the vehicle and I_{zz} denotes the moment of inertia of the vehicle about its vertical axis in the center of gravity. The parameters $C_{\alpha f}$ and $C_{\alpha f}$ are called cornering stiffness and describe the road tire interaction. Typical values for the parameters are given in Table 2.1. The model is derived in Section 2.3.

2.1 Discretizing Continuous-Time Models

The measurements dealt with in this work are sampled and handled as discrete-time variables in computers and electronic control units (ECU). All sensor signals are transferred in sampled form from different sensors to the log-computer on a so called CAN-Bus (Controller Area Network). Hence, the systems discussed in this thesis must also be described

Table 2.1: *Typical ranges for the vehicle parameters used in the single track model.*

m kg	I_{zz} kgm^2	C_α N/rad	$l_f + l_r$ m
$1000 - 2500$	$850 - 5000$	$45000 - 75000$	$2.5 - 3.0$

using discrete-time models according to the state space model in (2.1). Nevertheless, since physical relations commonly are given in continuous-time, the various systems presented in this thesis, such as the single track model in Example 2.1, are derived and represented using continuous-time state space models in the form (2.2). Thus, all continuous-time models in this thesis have to be discretized in order to describe the measurements. Only a few of the motion models can be discretized exactly by solving the sampling formula

$$\boldsymbol{x}_{t+1} = \boldsymbol{x}_t + \int_t^{t+T} a(\boldsymbol{x}(\tau), \boldsymbol{u}(t), \boldsymbol{w}(t), \boldsymbol{\theta}) d\tau, \tag{2.6}$$

analytically, where T denotes the sampling time. A simpler way is to make use of the standard forward Euler method, which approximates (2.2a) according to

$$\boldsymbol{x}_{t+1} \approx \boldsymbol{x}_t + Ta(\boldsymbol{x}_t, \boldsymbol{u}_t, \boldsymbol{w}_t, \boldsymbol{\theta}) \triangleq f_t(\boldsymbol{x}_t, \boldsymbol{u}_t, \boldsymbol{w}_t, \boldsymbol{\theta}). \tag{2.7}$$

This is a very rough approximation with many disadvantages, but it is frequently used because of its simplicity. This method is used in Example 2.2 to discretize the continuous-time vehicle model given in (2.4).

Example 2.2: Discrete-Time Single Track Model

The single track model given in Example 2.1 may be discretized using (2.7) according to

$$\boldsymbol{x}_{\mathcal{E},t+1} = \begin{bmatrix} f_{\mathcal{E}_1} \\ f_{\mathcal{E}_2} \end{bmatrix} = \begin{bmatrix} \dot{\psi}_{E,t} + Ta_{\mathcal{E}_1} \\ \beta_t + Ta_{\mathcal{E}_2} \end{bmatrix}, \tag{2.8a}$$

$$\boldsymbol{y}_{\text{IMU},t} = \begin{bmatrix} h_{\mathcal{E}_1} \\ h_{\mathcal{E}_2} \end{bmatrix} = \begin{bmatrix} c_{\mathcal{E}_1} \\ c_{\mathcal{E}_2} \end{bmatrix}, \tag{2.8b}$$

where T is the sampling time.

Sampling of linear systems is thoroughly described by Rugh (1996). Moreover, different options to sample and linearize non-linear continuous-time systems are described by Gustafsson (2000). The linearization problem is treated in Chapter 3, in a discussion of approximative model based filters such as the extended Kalman filter.

2.2 Special cases of the State Space Model

Special cases of the general state space model (2.1) are treated in this section. These includes the linear state space model in Section 2.2.1 and the state space model with additive noise in Section 2.2.2.

2.2.1 Linear State Space Model

An important special case of the general state space model (2.1) is the linear Gaussian state space model, where f and h are linear functions and the noise is Gaussian,

$$\boldsymbol{x}_{t+1} = F_t(\boldsymbol{\theta})\boldsymbol{x}_t + G_t^u(\boldsymbol{\theta})\boldsymbol{u}_t + G_t^w\boldsymbol{w}_t, \tag{2.9a}$$

$$\boldsymbol{y}_t = H_t(\boldsymbol{\theta})\boldsymbol{x}_t + H_t^u(\boldsymbol{\theta})\boldsymbol{u}_t + \boldsymbol{e}_t, \tag{2.9b}$$

where $\boldsymbol{w}_t \sim \mathcal{N}(0, Q_t)$ and $\boldsymbol{e}_t \sim \mathcal{N}(0, R_t)$. Note that the single track model (2.4) is linear in the state variables, as shown in Example 2.3.

Example 2.3: Linearized Single Track Model

The front wheel angle is usually quite small at higher velocities and the assumptions $\cos\delta_f \approx 1$, $\tan\delta_f \approx \sin\delta_f \approx \delta_f$ therefore applies. The discrete-time single track model (2.8) may be written on the linear form (2.9) according to

$$\dot{\boldsymbol{x}}_{\mathcal{E},t+1} = \begin{bmatrix} 1 - T\frac{C_{\alpha f}l_f^2 + C_{\alpha r}l_r^2}{I_{zz}v_x} & T\frac{-C_{\alpha f}l_f + C_{\alpha r}l_r}{I_{zz}} \\ -T - T\frac{C_{\alpha f}l_f - C_{\alpha r}l_r}{v_x^2 m} & 1 - T\frac{C_{\alpha f} + C_{\alpha r} + \dot{v}_x m}{m v_x} \end{bmatrix} \boldsymbol{x}_{\mathcal{E},t} + \begin{bmatrix} \frac{C_{\alpha f}l_f}{I_{zz}} \\ \frac{C_{\alpha f}}{m v_x} \end{bmatrix} \delta_f + \boldsymbol{w}_t, \tag{2.10a}$$

$$\boldsymbol{y}_{\text{IMU},t} = \begin{bmatrix} 1 & 0 \\ \frac{-C_{\alpha f}l_f + C_{\alpha r}l_r}{m v_x} & -\frac{C_{\alpha f} + C_{\alpha r} + m\dot{v}_x}{m} \end{bmatrix} \boldsymbol{x}_{\mathcal{E},t} + \begin{bmatrix} 0 \\ \frac{C_{\alpha f}}{m} \end{bmatrix} \delta_f + \boldsymbol{e}_t. \tag{2.10b}$$

The model is linear in the input δ_f. However, the inputs $\dot{v}_x$ and v_x are implicitly modeled in the matrices $F_t(\dot{v}_x, v_x, \boldsymbol{\theta})$, $G_t^u(v_x, \boldsymbol{\theta})$ and $H_t(\dot{v}_x, v_x, \boldsymbol{\theta})$.

Several of the radar measurements in Example 1.2 can be associated to the same tracked state. This situation leads to a problem where a batch of measurements $\boldsymbol{y}_i, \ldots, \boldsymbol{y}_j$ is associated to the same state $\boldsymbol{x}_k$. The update of the state with the batch of new measurements may be executed iteratively, as if the measurements were collected at different time steps. Another method, which is used in Paper C, is accomplished by stacking all available measurements in the set $\boldsymbol{y}_{i:j}$ and sensor models $H_{i:j}$ on top of each other in order to form

$$\boldsymbol{Y}_{i:j} = \begin{bmatrix} \boldsymbol{y}_i \\ \vdots \\ \boldsymbol{y}_j \end{bmatrix} \quad \text{and} \quad \boldsymbol{H}_{i:j}(\boldsymbol{\theta}) = \begin{bmatrix} H_i(\boldsymbol{\theta}) \\ \vdots \\ H_j(\boldsymbol{\theta}) \end{bmatrix}, \tag{2.11}$$

respectively. The measurement equation (2.9b) may now be rewritten according to

$$\boldsymbol{Y}_{i:j,t} = \boldsymbol{H}_{i:j,t}(\boldsymbol{\theta})\boldsymbol{x}_{k,t} + \boldsymbol{e}_t. \tag{2.12}$$

Linear state space models and linear system theory in general are thoroughly described by Rugh (1996) and Kailath (1980).

2.2.2 State Space Model with Additive Noise

A special case of the general state space model (2.1) is given by assuming that the noise enters additively and the input signals are subsumed in the time-varying dynamics, which leads to the form

$$\boldsymbol{x}_{t+1} = f_t(\boldsymbol{x}_t, \boldsymbol{\theta}) + \boldsymbol{w}_t, \tag{2.13a}$$
$$\boldsymbol{y}_t = h_t(\boldsymbol{x}_t, \boldsymbol{\theta}) + \boldsymbol{e}_t. \tag{2.13b}$$

In Example 1.1 an ego vehicle model was introduced, where the steering wheel angle, the longitudinal acceleration and the vehicle velocity were modeled as deterministic input signals. This consideration can be motivated by claiming that the driver controls the vehicle's lateral movement with the steering wheel and the longitudinal movement with the throttle and brake pedals. Furthermore, the steering wheel angle and the velocity are measured with less noise than the other measurement signals, and they are often pre-processed to improve the accuracy and remove bias. With these arguments the resulting model, given in Example 2.1, may be employed. The model is in some sense simpler than if these two signals would be assumed to be stochastic measurements, as shown in Example 2.4.

Example 2.4: Single Track Model without Deterministic Input Signals

In classical signal processing it is uncommon to allow deterministic input signals, at least not if these are measured by sensors. The input signals in Example 1.1 should instead be modeled as stochastic measurements. Hence, the measurement vector and the state vector are augmented and the system is remodeled. One example is given by the state space model

$$\boldsymbol{x}_{\mathcal{E},t+1} = \begin{bmatrix} \dot{\psi}_{t+1} \\ \beta_{t+1} \\ \delta_{f,t+1} \\ v_{x,t+1} \\ \dot{v}_{x,t+1} \end{bmatrix} = \begin{bmatrix} f_{\mathcal{E}_1}(\dot{\psi}_t, \beta_t, \delta_{f,t}, v_{x,t}, w_{\dot{\psi},t}, \boldsymbol{\theta}) \\ f_{\mathcal{E}_2}(\dot{\psi}_t, \beta_t, \delta_{f,t}, \dot{v}_{x,t}, v_{x,t}, w_{\beta,t}, \boldsymbol{\theta}) \\ f_{\mathcal{E}_3}(\delta_{f,t}, w_{\delta_f,t}, \boldsymbol{\theta}) \\ v_{x,t} + T\dot{v}_{x,t} \\ \dot{v}_{x,t} + w_{\dot{v}_x,t} \end{bmatrix}, \tag{2.14a}$$

$$\boldsymbol{y}_t = \begin{bmatrix} \dot{\psi}_t^m \\ a_{y,t}^m \\ \delta_{s,t}^m \\ v_{x,t}^m \\ \dot{v}_{x,t}^m \end{bmatrix} = \begin{bmatrix} h_{\mathcal{E}_1}(\dot{\psi}_t, \beta_t, \delta_{f,t}, v_{x,t}, \boldsymbol{\theta}) + e_{\dot{\psi},t} \\ h_{\mathcal{E}_2}(\dot{\psi}_t, \beta_t, \delta_{f,t}, \dot{v}_{x,t}, v_{x,t}, \boldsymbol{\theta}) + e_{\beta,t} \\ h_{\mathcal{E}_3}(\dot{\psi}_t, \beta_t, \delta_{f,t}, \boldsymbol{\theta}) + e_{\delta_s,t} \\ v_{x,t} + e_{v_x,t} \\ \dot{v}_{x,t} + e_{\dot{v}_x,t} \end{bmatrix}, \tag{2.14b}$$

where T is the sample time and the measured signals are labeled with superscript m to distinguish them from the states. The first two rows of the process and measurement models i.e., $f_{\mathcal{E}_1}$, $f_{\mathcal{E}_2}$, $h_{\mathcal{E}_1}$ and $h_{\mathcal{E}_1}$, where given in (2.8). The third measurement signal is the steering wheel angle δ_s, but the third state is the front wheel angle δ_f. A possible measurement model $h_{\mathcal{E}_3}$ will be discussed in Example 3.1. Random walk is assumed for the longitudinal acceleration $\dot{v}_x$ in the process model.

Another way to represent the state space model is given by considering the probability density function (pdf) of different signals or state variables of a system. The transition density $p(\boldsymbol{x}_{t+1}|\boldsymbol{x}_t)$ models the dynamics of the system and if the process noise is assumed additive, the transition model is given by

$$p(\boldsymbol{x}_{t+1}|\boldsymbol{x}_t) = p_w(\boldsymbol{x}_{t+1} - f(\boldsymbol{x}_t, \boldsymbol{u}_t, \boldsymbol{\theta})), \tag{2.15}$$

where p_w denotes the density of the process noise $\boldsymbol{w}$. A fundamental property of the process model is the Markov property,

$$p(\boldsymbol{x}_{t+1}|\boldsymbol{x}_1, \ldots, \boldsymbol{x}_t) = p(\boldsymbol{x}_{t+1}|\boldsymbol{x}_t). \tag{2.16}$$

This means that the state of the system at time t contains all necessary information about the past, which is needed to predict the future behavior of the system.

Furthermore, if the measurement noise is assumed additive then the likelihood function, which describes the measurement model, is given by

$$p(\boldsymbol{y}_t|\boldsymbol{x}_t) = p_e(\boldsymbol{y}_k - h(\boldsymbol{x}_t, \boldsymbol{u}_t, \boldsymbol{\theta})), \tag{2.17}$$

where p_e denotes the density of the sensor noise $\boldsymbol{e}$. The two density functions in (2.15) and (2.17) are often referred to as a hidden Markov model (HMM) according to

$$\boldsymbol{x}_{t+1} \sim p(\boldsymbol{x}_{t+1}|\boldsymbol{x}_t), \tag{2.18a}$$
$$\boldsymbol{y}_t \sim p(\boldsymbol{y}_t|\boldsymbol{x}_t), \tag{2.18b}$$

since $\boldsymbol{x}_t$ is not directly visible in $\boldsymbol{y}_t$. It is a statistical model where one Markov process, that represents the system, is observed through another stochastic process, the measurement model.

2.3 Ego Vehicle Model

The ego vehicle model was introduced in Example 1.1 and the single track model was given in Example 2.1. Before the model equations are derived in Section 2.3.3, the tire road interaction, which is an important part of the model, is discussed in Section 2.3.2. Two other vehicle models, which are commonly used for lane keeping systems are given in Section 2.3.4. However, to derive these models accurately some notation is required, which is the topic of Section 2.3.1.

2.3.1 Notation

The coordinate frames describing the ego vehicle and one leading vehicle are defined in Figure 2.1. The extension to several leading vehicles is straightforward. The inertial world reference frame is denoted by W and its origin is O_W. The ego vehicle's coordinate frame E is located in the center of gravity (CoG) and E_s is at the vision and radar sensor of the ego vehicle. Furthermore, the coordinate frame T_i is associated with the tracked

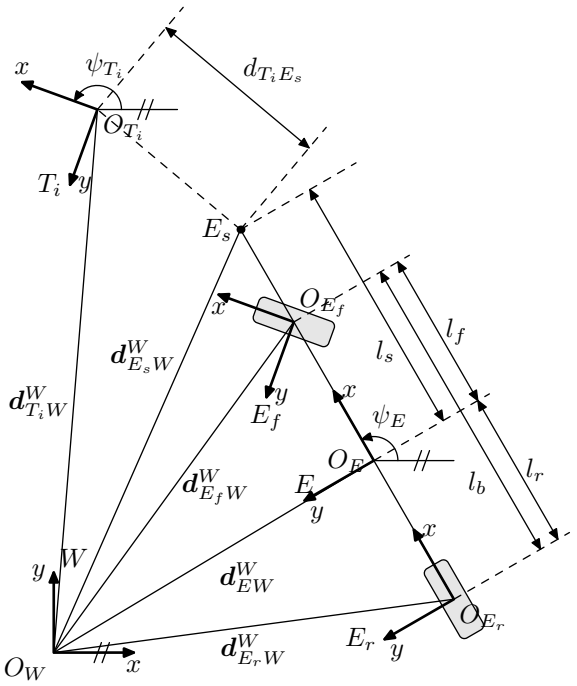

Figure 2.1: *Coordinate frames describing the ego vehicle, with center of gravity in O_E and the radar and camera sensors mounted in E_s. One leading vehicle is positioned in O_{T_i}.*

leading vehicle i, and its origin O_{T_i} is located at the leading vehicle. In this work the planar coordinate rotation matrix

$$R^{WE} = \begin{bmatrix} \cos\psi_E & -\sin\psi_E \\ \sin\psi_E & \cos\psi_E \end{bmatrix} \tag{2.19}$$

is used to transform a vector $\boldsymbol{d}^E$, represented in E, into a vector $\boldsymbol{d}^W$, represented in W, according to

$$\boldsymbol{d}^W = R^{WE}\boldsymbol{d}^E + \boldsymbol{d}^W_{EW}, \tag{2.20}$$

where the yaw angle of the ego vehicle ψ_E is the angle of rotation from W to E. The geometric displacement vector $\boldsymbol{d}^W_{EW}$ is the direct straight line from O_W to O_E represented with respect to the frame W. Velocities are defined as the movement of a frame E relative to the inertial reference frame W, but typically resolved in the frame E, for example v^E_x is the velocity of the E frame in its x-direction. The same convention holds for the acceleration a^E_x. In order to simplify the notation, E is left out when referring to the ego vehicle's velocity and acceleration.

This notation will be used when referring to the various coordinate frames. However, certain frequently used quantities will be renamed, in the interest of readability. The measurements are denoted using superscript m. Furthermore, the notation used for the rigid body dynamics is in accordance with Hahn (2002).

2.3.2 Tire Model

The slip angle α_i is defined as the angle between the central axis of the wheel and the path along which the wheel moves. The phenomenon of side slip is mainly due to the lateral elasticity of the tire. For reasonably small slip angles, at maximum 3° or up to a centripetal force of approximately $0.4\ \mathrm{g}$, it is a good approximation to assume that the lateral friction force of the tire F_i is proportional to the slip angle,

$$F_i = C_{\alpha i}\alpha_i. \tag{2.21}$$

The parameter $C_{\alpha i}$ is referred to as the cornering stiffness of tire i and describes the cornering behavior of the tire. The load transfer to the front axle when braking or to the outer wheels when driving through a curve can be considered by modeling the cornering stiffness as

$$C_{\alpha i} = C_{\alpha i0} + \zeta_{\alpha i}\Delta F_{zi}, \tag{2.22}$$

where $C_{\alpha i0}$ is the equilibrium of the stiffness for tire i and $\zeta_{\alpha i}$ relates the load transfer ΔF_{zi} to the total stiffness. This tire model is treated in Paper B. General information about slip angles and cornering stiffness can be found in the books by e.g. Pacejka (2006), Mitschke and Wallentowitz (2004), Wong (2001).

Most of the ego vehicle's parameters $\boldsymbol{\theta}$, such as the dimensions, the mass and the moment of inertia are assumed time invariant and are given by the vehicle manufacturer. Since the cornering stiffness is a parameter that describes the properties between road and tire it has to be estimated on-line, as described in Paper B, or has to be estimated for the given set, i.e. a batch, of measurements.

To determine how the front and rear cornering stiffness parameters relate to each other and in which range they typically are, a $3\ \mathrm{min}$ measurement sequence, acquired on rural roads, was used. The data used to identify the cornering stiffness parameters was split into two parts, one estimation part and one validation part. This facilitates cross-validation, where the parameters are estimated using the estimation data and the quality of the estimates can then be assessed using the validation data (Ljung, 1999). From Pacejka (2006), Mitschke and Wallentowitz (2004), Wong (2001) it is known that the cornering stiffness values should be somewhere in the range between $20,000$ and $100,000\ \mathrm{N/rad}$. The single track model (2.4) was used and the parameter space was gridded and an exhaustive search was performed. To gauge how good a specific parameter pair is, the simulated yaw rate and lateral acceleration were compared with the measured values according to

$$\mathrm{fit}_1 = 100\left(1 - \frac{|y - \hat{y}|}{|y - \bar{y}|}\right), \tag{2.23}$$

where y is the measured value, $\hat{y}$ is the estimate and $\bar{y}$ is the mean of the measurement, see Ljung (2009). Since there are two signals, two fit-values are obtained, which are combined into a joint fit-value using a weighted sum. In Figure 2.2 a diagonal ridge of the best fit value is clearly visible. For different estimation data sets, different local maxima were found on the ridge. Further, it was assumed that the two parameters should have approximately the same value. This constraint (which forms a cross diagonal or

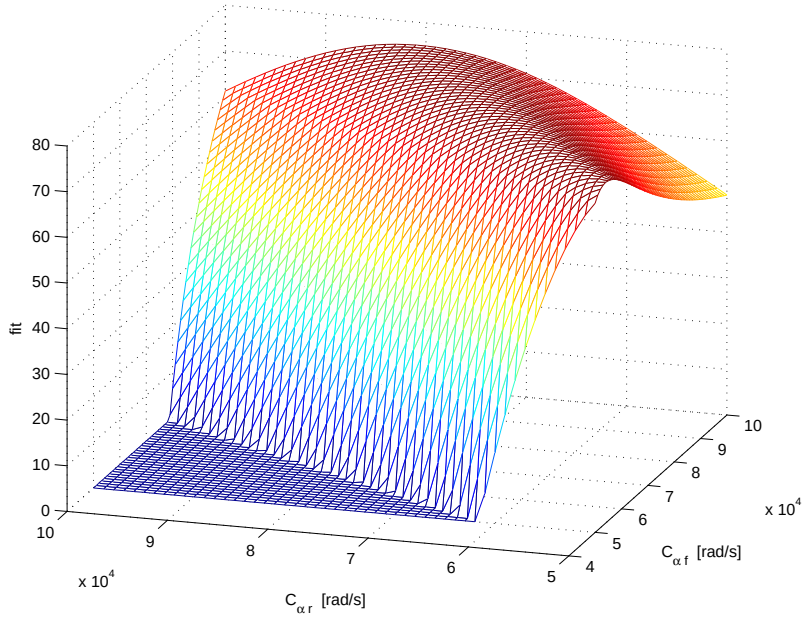

Figure 2.2: *A grid map showing the total fit value of the two outputs and the constraint defined in* (2.24).

orthogonal ridge) is expressed as

$$\text{fit}_2 = 100\left(1 - \frac{|C_{\alpha f} - C_{\alpha r}|}{\left|\frac{(C_{\alpha f}+C_{\alpha r})}{2}\right|}\right), \tag{2.24}$$

and added as a third fit-value to the weighted sum, obtaining the total fit for the estimation data set as

$$\text{total fit} = w_{\psi_E}\text{fit}_{\psi_E} + w_{a_y}\text{fit}_{a_y} + w_2\text{fit}_2, \tag{2.25}$$

where the weights should sum to one, i.e. $w_{\psi_E} + w_{a_y} + w_2 = 1,\ w \geq 0$. The exhaustive search resulted in the values $C_{\alpha f} = 41000\ \text{N/rad}$ and $C_{\alpha r} = 43000\ \text{N/rad}$. The resulting state-space model was validated using the validation data and the result is given in Figure 5 in Paper A.

2.3.3 Single Track Model

In this work the ego vehicle motion is only considered during normal driving situations and not at the adhesion limit. This implies that the single track model, described in e.g., Mitschke and Wallentowitz (2004) is sufficient for the present purposes. This model is also referred to as the bicycle model. The geometry of the single track model with slip angles is shown in Figure 1.3. It is worth mentioning that the velocity vector of the ego

vehicle is typically not in the same direction as the longitudinal axis of the ego vehicle. Instead the vehicle will move along a path at an angle β with the longitudinal direction of the vehicle. Hence, the angle β is defined as,

$$\tan\beta = \frac{v_y}{v_x}, \tag{2.26}$$

where v_x and v_y are the ego vehicle's longitudinal and lateral velocity components, respectively. This angle β is referred to as the float angle in Robert Bosch GmbH (2004) and the vehicle body side slip angle in Kiencke and Nielsen (2005). Lateral slip is an effect of cornering. To turn, a vehicle needs to be affected by lateral forces. These are provided by the friction when the wheels slip.

The Slip Angles

From Figure 2.1 the following geometric constraints, describing the relations between the front axle, rear axle and the origin of the world coordinate frame, are obtained

$$x^W_{E_fW} = l_b\cos\psi_E + x^W_{E_rW}, \tag{2.27a}$$
$$y^W_{E_fW} = l_b\sin\psi_E + y^W_{E_rW}, \tag{2.27b}$$

where E_f and E_r are coordinate frames fixed to the front and rear wheel, respectively. The ego vehicle's velocity at the rear axle is given by

$$R^{E^rW}\dot{\boldsymbol{d}}^W_{E_rW} = \begin{bmatrix} v_x^{E_r} \\ v_y^{E_r} \end{bmatrix}, \tag{2.28}$$

which is rewritten to obtain

$$\dot{x}^W_{E_rW}\cos\psi_E + \dot{y}^W_{E_rW}\sin\psi_E = v_x^{E_r}, \tag{2.29a}$$
$$-\dot{x}^W_{E_rW}\sin\psi_E + \dot{y}^W_{E_rW}\cos\psi_E = v_y^{E_r}. \tag{2.29b}$$

Furthermore, the direction of the tire velocity vectors are given by the constraint equations

$$-\sin(\psi_E-\alpha_r)\,\dot{x}^W_{E^rW} + \cos(\psi_E-\alpha_r)\,\dot{y}^W_{E^rW} = 0, \tag{2.30a}$$
$$-\sin(\psi_E+\delta_f-\alpha_f)\,\dot{x}^W_{E^fW} + \cos(\psi_E+\delta_f-\alpha_f)\,\dot{y}^W_{E^fW} = 0. \tag{2.30b}$$

The equations (2.27), (2.29) and (2.30) are used to obtain

$$\dot{\psi}_1 = \frac{v_x^{E_r}}{l_1}\tan(\delta_f-\alpha_f) - \frac{v_y^{E_r}}{l_1}, \tag{2.31a}$$
$$v_y^{E_r} = -v_x^{E_r}\tan\alpha_r. \tag{2.31b}$$

The velocities $v_x^{E_r}$ and $v_y^{E_r}$ have their origin in the ego vehicle's rear axle, and the velocities in the vehicle's center of gravity are given by $v_x \triangleq v_x^E \approx v_x^{E_r}$ and $v_y \triangleq v_y^E = v_y^{E_r} + \dot{\psi}_E l_r$. The ego vehicles body side slip angle β is defined in (2.26), and by inserting

this relation into (2.31) the following equations are obtained

$$\tan\alpha_r = \frac{\dot{\psi}_E \cdot l_r}{v_x} - \tan\beta, \tag{2.32a}$$

$$\tan(\delta_f - \alpha_f) = \frac{\dot{\psi}_E \cdot l_f}{v_x} + \tan\beta. \tag{2.32b}$$

Small α and β angles ($\tan\alpha \approx \alpha$ and $\tan\beta \approx \beta$) can be assumed during normal driving conditions i.e.,

$$\alpha_r = \frac{\dot{\psi}_E l_r}{v_x} - \beta, \tag{2.33a}$$

$$\alpha_f = -\frac{\dot{\psi}_E l_f}{v_x} - \beta + \tan\delta_f. \tag{2.33b}$$

Process Model

Newton's second law of motion, $F = ma$, is applied to the center of gravity. Only the lateral axis y has to be considered, since the longitudinal movement is a measured input

$$\sum F_i = m\, a_y, \tag{2.34}$$

where

$$a_y = \dot{v}_y + \dot{\psi}_E\, v_x, \tag{2.35}$$

and

$$\dot{v}_y \approx \frac{d}{dt}(\beta v_x) = v_x\dot{\beta} + \dot{v}_x\beta, \tag{2.36}$$

for small angles. By inserting the tire forces F_i, which were defined by the tire model (2.21), into (2.34) the following force equation is obtained

$$C_{\alpha f}\,\alpha_f\cos\delta_f + C_{\alpha r}\,\alpha_r = m(v_x\dot{\psi}_E + v_x\dot{\beta} + \dot{v}_x\beta), \tag{2.37}$$

where m denotes the mass of the ego vehicle. The moment equation

$$\sum M_i = I_{zz}\,\ddot{\psi}_E \tag{2.38}$$

is used in the same manner to obtain the relations for the angular accelerations

$$l_f\, C_{\alpha f}\,\alpha_f\cos\delta_f - l_r\, C_{\alpha r}\,\alpha_r = I_{zz}\,\ddot{\psi}_E, \tag{2.39}$$

where I_{zz} denotes the moment of inertia of the vehicle about its vertical axis in the center of gravity. Inserting the relations for the wheel side slip angles (2.33) into (2.37) and (2.39) results in

$$m(v_x\dot{\psi}_E + v_x\dot{\beta} + \dot{v}_x\beta) = C_{\alpha f}\left(\frac{\dot{\psi}_E l_f}{v_x} + \beta - \tan\delta_f\right)\cos\delta_f + C_{\alpha r}\left(\beta - \frac{\dot{\psi}_E l_r}{v_x}\right), \tag{2.40a}$$

$$I_{zz}\ddot{\psi}_E = l_f\, C_{\alpha f}\left(\frac{\dot{\psi}_E l_f}{v_x} + \beta - \tan\delta_f\right)\cos\delta_f - l_r\, C_{\alpha r}\left(\beta - \frac{\dot{\psi}_E l_r}{v_x}\right). \tag{2.40b}$$

These relations are rewritten according to

$$\ddot{\psi}_E = \beta \frac{-l_f C_{\alpha f} \cos\delta_f + l_r C_{\alpha r}}{I_{zz}} - \dot{\psi}_E \frac{C_{\alpha f} l_f^2 \cos\delta_f + C_{\alpha r} l_r^2}{I_{zz} v_x} + \frac{l_f C_{\alpha f} \tan\delta_f}{I_{zz}}, \tag{2.41a}$$

$$\dot{\beta} = -\beta \frac{C_{\alpha f} \cos\delta_f + C_{\alpha r} + \dot{v}_x m}{m v_x} - \dot{\psi}_E \left(1 + \frac{C_{\alpha f} l_f \cos\delta_f - C_{\alpha r} l_r}{v_x^2 m}\right) + \frac{C_{\alpha f} \sin\delta_f}{m v_x}, \tag{2.41b}$$

to obtain the process model (2.4a).

Measurement Model

The ego vehicle's lateral acceleration in the CoG is given by

$$a_y = v_x(\dot{\psi}_E + \dot{\beta}) + \dot{v}_x \beta. \tag{2.42}$$

By replacing $\dot{\beta}$ with the expression given in (2.41b) and at the same time assuming that $\dot{v}_x\beta$ is small and can be neglected, the following relation is obtained

$$\begin{aligned} a_y &= v_x(\dot{\psi}_E + \dot{\beta}) \\ &= -\beta \frac{C_{\alpha f} \cos\delta_f + C_{\alpha r} + m\dot{v}_x}{m} + \dot{\psi}_E \frac{-C_{\alpha f} l_f \cos\delta_f + C_{\alpha r} l_r}{m v_x} + \frac{C_{\alpha f}}{m} \sin\delta_f, \end{aligned} \tag{2.43}$$

which is the measurement equation in (2.4b).

2.3.4 Single Track Model with Road Interaction

There are several different way to model the ego vehicle. The single track model (2.4) is used in all papers in Part II, but in Paper A a comparison is made with two other approaches. These are based on different vehicle models, which are discussed in this section.

The first model is commonly used for autonomous driving and lane keeping. This model is well described by e.g. Dickmanns (2007) and Behringer (1997). Note that the ego vehicle's motion is modeled with respect to a road fixed coordinate frame, unlike the single track model in Section 2.3.3, which is modeled in a Cartesian world coordinate frame.

The relative angle between the vehicle's longitudinal axis and the tangent of the road is denoted ψ_{RE}. Ackermann's steering geometry is used to obtain the relation

$$\dot{\psi}_{RE} = \frac{v_x}{l_b}\delta_f - v_x \cdot c_0, \tag{2.44}$$

where the current curvature of the road c_0 is the inverse of the road's radius. The lateral displacement of the vehicle in the lane is given by

$$\dot{l}_E = v_x(\psi_{RE} + \beta). \tag{2.45}$$

A process model for the body side slip angle was given in (2.41b), but since the yaw rate $\dot{\psi}_E$ is not part of the model in this section, equation (2.41b) has to be rewritten according to

$$\dot{\beta} = -\frac{C_{\alpha f}\cos\delta_f + C_{\alpha r} + \dot{v}_x m}{m v_x}\beta - \left(1 + \frac{C_{\alpha f} l_f \cos\delta_f - C_{\alpha r} l_r}{v_x^2 m}\right)\frac{v_x}{l_b}\tan\delta_f + \frac{C_{\alpha f}}{m v_x}\sin\delta_f, \quad (2.46)$$

which is further simplified by assuming small angles, to obtain a linear model according to

$$\dot{\beta} = -\frac{C_{\alpha f} + C_{\alpha r}}{m v_x}\beta + \left(\frac{C_{\alpha f}}{m v_x} - \frac{v_x}{l_b}\right)\delta_f. \quad (2.47)$$

Recall Example 2.4, where no deterministic input signals were used. Especially the steering wheel angle might have a bias, for example if the sensor is not calibrated, which leads to an accumulation of the side slip angle β in (2.47). Other reasons for a steering wheel angle bias is track torsion or strong side wind, which the driver compensates for with the steering wheel. The problem is solved by introducing an offset to the front wheel angel as a state variable according to

$$\delta_f^m = \delta_f + \delta_f^{\text{offs}}. \quad (2.48)$$

To summarize, the state variable vector is defined as

$$\boldsymbol{x}_{\mathcal{E}_3} = \begin{bmatrix} \psi_{RE} \\ l_E \\ \beta \\ \delta_f \\ \delta_f^{\text{offs}} \end{bmatrix} = \begin{bmatrix} \text{relative angle between vehicle and road} \\ \text{lateral displacement of vehicle in lane} \\ \text{vehicle body side slip angle} \\ \text{front wheel angle} \\ \text{front wheel angle bias offset} \end{bmatrix} \quad (2.49)$$

and the process model is given by

$$\begin{bmatrix} \dot{\psi}_{RE} \\ \dot{l}_E \\ \dot{\beta} \\ \dot{\delta}_f \\ \dot{\delta}_f^{\text{offs}} \end{bmatrix} = \begin{bmatrix} \frac{v_x}{l_b}\delta_f - v_x \cdot c_0 \\ v_x(\psi_{RE} + \beta) \\ -\frac{C_{\alpha f}+C_{\alpha r}}{m v_x}\beta + \left(\frac{C_{\alpha f}}{m v_x} - \frac{v_x}{l_b}\right)\delta_f \\ w_{\delta_f} \\ 0 \end{bmatrix}. \quad (2.50)$$

Note that the curvature c_0 is included in (2.44) and in the process model above. The road geometry is the topic of the next section. The curvature c_0 can either be modeled as a deterministic input signal or as a state variable as shown in Example 2.5. This model is used in the approach called "fusion 3" in Paper A, and the state vector is denoted $\boldsymbol{x}_{\mathcal{E}_3}$.

Another and simpler vehicle model is obtained if the side slip angle is omitted and the yaw rate $\dot{\psi}_E$ is used instead of the steering wheel angle. The model is described together with results in Eidehall (2007), Eidehall et al. (2007), Eidehall and Gustafsson (2006), Gern et al. (2000, 2001), Zomotor and Franke (1997). The state variable vector is then defined as

$$\boldsymbol{x}_{\mathcal{E}_2} = \begin{bmatrix} \psi_{RE} & l_E \end{bmatrix}^{\mathrm{T}}, \quad (2.51)$$

and the process model is simply given by

$$\begin{bmatrix} \dot{\psi}_{RE} \\ \dot{l}_E \end{bmatrix} = \begin{bmatrix} v_x c_0 + \dot{\psi}_E \\ v_x \psi_{RE} \end{bmatrix}, \tag{2.52}$$

where the yaw rate $\dot{\psi}_E$ is modeled as an input signal and the curvature c_0 is modeled either as an input signal or as a state variable in combination with a road model. This model, in combination with the road model (2.56) described in the next section, is used in the approach called "fusion 2" in Paper A, and the state vector is $\boldsymbol{x}_{\mathcal{E}_2}$.

More advanced vehicle models with more degrees of freedom, including the two track model, are described by Schofield (2008).

2.4 Road Model

The road, as a construction created by humans, possesses no dynamics; it is a static time invariant object in the world coordinate frame. The building of roads is subject to road construction standards such as VGU (2004a,b), hence, the modeling of roads is geared to these specifications. However, if the road is described in the ego vehicle's coordinate frame and the vehicle is moving along the road it is possible and indeed useful to describe the characteristics of the road using time varying state variables.

A road consists of straight and curved segments with constant radius and of varying length. The sections are connected through transition curves, so that the driver can use smooth and constant steering wheel movements instead of stepwise changes when passing through road segments. More specifically, this means that a transition curve is formed as a clothoid, whose curvature c changes linearly with its curve length x_c according to

$$c(x_c) = c_0 + c_1 \cdot x_c. \tag{2.53}$$

Note that the curvature c is the inverse of the radius. Now, suppose x_c is fixed to the ego vehicle, i.e. $x_c = 0$ at the position of the ego vehicle. When driving along the road and passing through different road segments c_0 and c_1 will not be constant, but rather time varying state variables

$$\boldsymbol{x}_{\mathcal{R}_1} = \begin{bmatrix} c_0 \\ c_1 \end{bmatrix} = \begin{bmatrix} \text{curvature at the ego vehicle} \\ \text{curvature derivative} \end{bmatrix}. \tag{2.54}$$

Using (2.53) a change in curvature at the position of the vehicle is given by

$$\left.\frac{dc(x_c)}{dt}\right|_{x_c=0} = \dot{c}_0 = \frac{dc_0}{dx_c} \cdot \frac{dx_c}{dt} = c_1 \cdot v_x, \tag{2.55}$$

where v_x is the ego vehicle's longitudinal velocity. This relation was introduced by Dickmanns and Zapp (1986), who posted the following process model

$$\begin{bmatrix} \dot{c}_0 \\ \dot{c}_1 \end{bmatrix} = \begin{bmatrix} 0 & v_x \\ 0 & 0 \end{bmatrix} \begin{bmatrix} c_0 \\ c_1 \end{bmatrix} + \begin{bmatrix} 0 \\ w_{c_1} \end{bmatrix}. \tag{2.56}$$

This model is sometimes also referred to as the simple clothoid model. Note that the road is modeled in a road aligned coordinate frame, with the components (x_c, y_c). There

are several advantages using road aligned coordinate frames, especially when it comes to the process models of the other vehicles on the same road, which can be greatly simplified. However, the flexibility of the process model is reduced and basic dynamic relations such as Newton's and Euler's laws cannot be directly applied. The road model (2.53) is transformed into Cartesian coordinates (x^R, y^R) using

$$x^R(x_c) = \int_0^{x_c} \cos\left(\chi(x)\right) dx \approx x_c, \tag{2.57a}$$

$$y^R(x_c) = \int_0^{x_c} \sin\left(\chi(x)\right) dx \approx \frac{c_0}{2} x_c^2 + \frac{c_1}{6} x_c^3, \tag{2.57b}$$

where the heading angle χ is defined as

$$\chi(x) = \int_0^{x} c(\lambda) d\lambda = c_0 x + \frac{c_1}{2} x^2. \tag{2.57c}$$

The origin of the two frames is fixed to the ego vehicle, hence, integration constants (x_0^R, y_0^R) are omitted. Example 2.5 shows how the simple clothoid model can be combined with the ego vehicle model described in Section 2.3.4 into one state space model.

Example 2.5: Single Track Model with Road Interaction

An alternative single track model was proposed in Section 2.3.4. The vehicle is modeled in a road aligned coordinate frame and the process model (2.50) includes the curvature c_0, which was considered as a state variable in this section. Hence, the vehicle model (2.50) can be augmented with a road model e.g., the simple clothoid model (2.56), to describe the vehicle's motion, the shape of the road and their interaction according to the linear state space model

$$\begin{bmatrix} \dot{\psi}_{RE} \\ \dot{l}_E \\ \dot{\beta} \\ \dot{\delta}_f \\ \dot{\delta}_f^{\text{offs}} \\ \dot{c}_0 \\ \dot{c}_1 \end{bmatrix} = \begin{bmatrix} 0 & 0 & 0 & \frac{v_x}{l_b} & 0 & -v_x & 0 \\ v_x & 0 & v_x & 0 & 0 & 0 & 0 \\ 0 & 0 & \frac{C_{\alpha f}+C_{\alpha r}}{m v_x} & \frac{C_{\alpha f}}{m v_x} - \frac{v_x}{l_b} & 0 & 0 & 0 \\ 0 & 0 & 0 & 0 & 0 & 0 & 0 \\ 0 & 0 & 0 & 0 & 0 & 0 & 0 \\ 0 & 0 & 0 & 0 & 0 & 0 & v_x \\ 0 & 0 & 0 & 0 & 0 & 0 & 0 \end{bmatrix} \begin{bmatrix} \psi_{RE} \\ l_E \\ \beta \\ \delta_f \\ \delta_f^{\text{offs}} \\ c_0 \\ c_1 \end{bmatrix} + \begin{bmatrix} 0 \\ 0 \\ 0 \\ w_{\delta_f} \\ 0 \\ 0 \\ w_{c_1} \end{bmatrix}, \tag{2.58a}$$

$$\begin{bmatrix} \psi_{RE}^m \\ l_E^m \\ \delta_f^m \\ c_0^m \end{bmatrix} = \begin{bmatrix} 1 & 0 & 0 & 0 & 0 & 0 & 0 \\ 0 & 1 & 0 & 0 & 0 & 0 & 0 \\ 0 & 0 & 0 & 1 & 1 & 0 & 0 \\ 0 & 0 & 0 & 0 & 0 & 1 & 0 \end{bmatrix} \begin{bmatrix} \psi_{RE} \\ l_E \\ \beta \\ \delta_f \\ \delta_f^{\text{offs}} \\ c_0 \\ c_1 \end{bmatrix} + \begin{bmatrix} e_{\psi_{RE}} \\ e_{l_E} \\ e_{\delta_f} \\ e_{c_0} \end{bmatrix}. \tag{2.58b}$$

The velocity v_x is modeled as a deterministic input signal and the measurements

$$\boldsymbol{y}_{\text{camera}} = \begin{bmatrix} \psi_{RE}^m & l_E^m & c_0^m \end{bmatrix}^{\mathrm{T}} \tag{2.59}$$

are obtained using a camera and a computer vision algorithm. The front wheel angle δ_f^m is derived from the steering wheel angle, which is measured by the steering wheel angle sensor. This model is similar to the model denoted "fusion 3" in Paper A.

A problem appears when two or more clothoid segments, with different parameters c_0 and c_1, are observed in the same camera view. The parameter c_0 will change continuously during driving, whereas c_1 will be constant in each segment and change stepwise at the segment transition. This leads to a dirac impulse in $\dot{c}_1$ at the transition. The problem can be solved by assuming a high process noise w_{c_1}, but this leads to less precise estimation of the state variables when no segment transitions occur in the camera view. To solve this problem Dickmanns (1988) proposed an averaging curvature model, which is best described with an example. Assume that the ego vehicle is driving on a straight road (i.e., $c_0 = c_1 = 0$) and that the look ahead distance of the camera is $\bar{x}_c$. A new segment begins at the position $x_c' < \bar{x}_c$, which means that there is a step in c_1 and c_0 is ramped up, see Figure 2.3. The penetration into the next segment is $l_c = \bar{x}_c - x_c'$. The idea of this model, referred to as averaging or spread-out dynamic curvature model, with the new state variables c_{0m} and c_{1m}, is that it generates the true lateral offset $y^R(\bar{x}_c)$ at the look ahead distance $\bar{x}_c$, i.e.

$$y_{\text{real}}^R(\bar{x}_c) = y_{\text{model}}^R(\bar{x}_c), \tag{2.60}$$

but it is continuously spread out in the range $(0, \bar{x}_c)$. The lateral offset of the real road as a function of the penetration l_c, for $0 \leq l_c \leq \bar{x}_c$, is

$$y_{\text{real}}^R(l_c) = \frac{c_1}{6} l_c^3, \tag{2.61}$$

since the first segment is straight. The lateral offset of the averaging model as a function of the penetration l_c is

$$y_{\text{model}}^R(l_c) = \frac{c_{0m}(l_c)}{2} \bar{x}_c^2 + \frac{c_{1m}(l_c)}{6} \bar{x}_c^3, \tag{2.62}$$

at the look ahead distance $\bar{x}_c$. The equation

$$c_1 \frac{l_c^3}{\bar{x}_c^2} = 3c_{0m}(l_c) + c_{1m}(l_c)\bar{x}_c, \tag{2.63}$$

is obtained by inserting (2.61) and (2.62) into (2.60). By differentiating (2.63) with respect to l_c and using the relations $\frac{dc_1}{dl_c} = 0$, $\frac{dc_{0m}(l_c)}{dl_c} = c_{1m}(l_c)$ and $\frac{d(\cdot)}{dl_c} = \frac{d(\cdot)}{dt} \cdot \frac{dt}{dl_c}$ the following equation is obtained

$$\dot{c}_{1m} = 3\frac{v_x}{\bar{x}_c}(c_1(l_c/\bar{x}_c)^2 - c_{1m}), \tag{2.64}$$

for $l_c < \bar{x}_c$. Since $(l_c/\bar{x}_c)^2$ is unknown it is usually set to 1 (Dickmanns, 2007), which finally yields

$$\dot{c}_{1m} = 3\frac{v_x}{\bar{x}_c}(c_1 - c_{1m}). \tag{2.65}$$

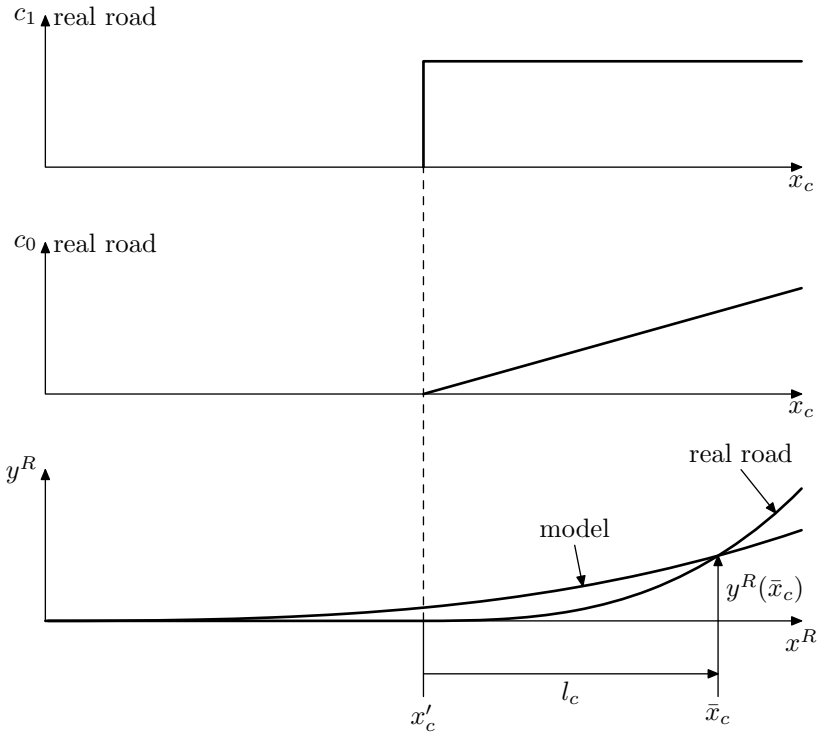

Figure 2.3: *A straight and a curved road segment are modeled with the averaging road model. The two upper plots shows the parameters c_1 and c_0 of the real road, the bottom plot shows the real and the modeled roads in a Cartesian coordinate frame.*

The state variable vector of the averaging model is defined as

$$\boldsymbol{x}_{\mathcal{R}_2} = \begin{bmatrix} c_{0m} \\ c_{1m} \\ c_1 \end{bmatrix} = \begin{bmatrix} \text{curvature at the ego vehicle} \\ \text{averaged curvature derivative} \\ \text{curvature derivative of the foremost segment} \end{bmatrix}, \tag{2.66}$$

and the process model is given by augmenting the simple clothoid model (2.56) with (2.65) according to

$$\begin{bmatrix} \dot{c}_{0m} \\ \dot{c}_{1m} \\ \dot{c}_1 \end{bmatrix} = \begin{bmatrix} 0 & v_x & 0 \\ 0 & -3\frac{v_x}{\bar{x}_c} & 3\frac{v_x}{\bar{x}_c} \\ 0 & 0 & 0 \end{bmatrix} \begin{bmatrix} c_{0m} \\ c_{1m} \\ c_1 \end{bmatrix} + \begin{bmatrix} 0 \\ 0 \\ w_{c_1} \end{bmatrix}. \tag{2.67}$$

The model is driven by the process noise w_{c_1}, which also influences the other states. The averaging model is well described in the recent book by Dickmanns (2007) and some early results using the model are presented by e.g. Dickmanns and Mysliwetz (1992).

A completely different approach is proposed in Paper A, where the process model describes the driven path of the ego vehicle instead of using road construction standards. The shape of the road is given under the assumption that the ego vehicle is driving on the road and the angle between the road and the ego vehicle is measured by the camera and

included as a state variable. The advantage of this approach is that the ego vehicle's path can be modeled more accurately than an unknown road, since there are a lot of sensors available in the vehicle and most vehicle dimensions are known. This model, denoted "fusion 1", is compared with two other approaches in Section 5.3 in Paper A, including a model, denoted "fusion 3", which is similar to the one presented in Example 2.5.

2.5 Target Model

In this work, only measurements from the ego vehicle's sensors are available; that is the target's motion is measured using the ego vehicle's radar and camera. This is the reason for why the target model is simpler than the ego vehicle model. The targets play an important role in the sensor fusion framework presented in this work, but little effort has been spent modeling their motion. Instead standard models from target tracking literature are used. A survey of different process models and measurement models are given by Rong Li and Jilkov (2003) and Rong Li and Jilkov (2001), respectively. The subject is also covered in the books by Blackman and Popoli (1999) and Bar-Shalom et al. (2001). One typical target model is given in Example 2.6.

Example 2.6: Coordinated Turn Model

The coordinated turn model is commonly used to model moving targets. The ego vehicle's radar and camera measures the range $d^m_{T_iE_s}$, the range rate $\dot{d}^m_{T_iE_s}$ and the azimuth angle $\delta^m_{T_iE_s}$ to target number i as described in the introduction in Example 1.2 and shown in Figure 2.1. The states of the coordinated turn model in polar velocity are given by

$$\boldsymbol{x}_{\mathcal{T}} = \begin{bmatrix} x^W_{T_iW} \\ y^W_{T_iW} \\ \psi_{T_i} \\ v_x^{T_i} \\ \dot{\psi}_{T_i} \\ a_x^{T_i} \end{bmatrix} = \begin{bmatrix} x\text{-position in } W\text{-frame} \\ y\text{-position in } W\text{-frame} \\ \text{heading angle} \\ \text{longitudinal velocity} \\ \text{yaw rate} \\ \text{longitudinal acceleration} \end{bmatrix}. \tag{2.68}$$

The process and measurement models are given by

$$\begin{bmatrix} \dot{x}^W_{T_iW} \\ \dot{y}^W_{T_iW} \\ \dot{\psi}_{T_i} \\ \dot{v}_x^{T_i} \\ \ddot{\psi}_{T_i} \\ \dot{a}_x^{T_i} \end{bmatrix} = \begin{bmatrix} v_x^{T_i} \cos\psi_{T_i} \\ v_x^{T_i} \sin\psi_{T_i} \\ \dot{\psi}_{T_i} \\ a_x^{T_i} \\ 0 \\ 0 \end{bmatrix} + \begin{bmatrix} 0 \\ 0 \\ 0 \\ 0 \\ w_{\ddot{\psi}_{T_i}} \\ w_{\dot{a}_x^{T_i}} \end{bmatrix} \tag{2.69a}$$

$$\begin{bmatrix} d^m_{T_iE_s} \\ \dot{d}^m_{T_iE_s} \\ \delta^m_{T_iE_s} \end{bmatrix} = \begin{bmatrix} \sqrt{\left(x^W_{T_iW} - x^W_{EW} - x^E_{E_sE}\right)^2 + \left(y^W_{T_iW} - y^W_{EW} - y^E_{E_sE}\right)^2} \\ v_x^{T_i} \cos\left(-(\psi_{T_i} - \psi_E) + \delta_{T_iE_s}\right) - v_x \cos\delta_{T_iE_s} \\ \arctan\frac{y^W_{T_iW}}{x^W_{T_iW}} - \psi_E - \psi_{E_sE} \end{bmatrix} + \boldsymbol{e}_{\mathcal{T}} \tag{2.69b}$$

where $(x^E_{E_sE}, y^E_{E_sE}, \psi_{E_sE})$ represents the sensor mounting position and orientation in the ego vehicle coordinate frame E. The single track ego vehicle state variable vector and state space model (2.4) has to be augmented with the ego vehicle's position in the world frame (x^W_{EW}, y^W_{EW}), since it is included in the measurement model of the target (2.69b).

3

Estimation Theory

This thesis is concerned with estimation problems, i.e. given measurements $\boldsymbol{y}$ the aim is to estimate the parameter $\boldsymbol{\theta}$ or the state $\boldsymbol{x}$ in (1.1). Both problems rely on the same theoretical basis and the same algorithms can be used. The parameter estimation problem is a part of the system identification process, which also includes the derivation of the model structure, discussed in the previous chapter. The state estimation problem utilizes the model and its parameters to solve for the states. When estimating $\boldsymbol{x}$ it is assumed that $\boldsymbol{\theta}$ is known and vice versa. The parameter is estimated in advance if $\boldsymbol{\theta}$ is time invariant or in parallel with the state estimation problem if $\boldsymbol{\theta}$ is assumed to be time varying. Example 3.1 illustrates how the states and parameters may be estimated.

Example 3.1: Parameter and State Estimation

Consider the single track model introduced in Example 1.1 and its equations derived in Section 2.3. The front wheel angle δ_f is considered to be a state variable in Example 2.4 and the steering wheel angle δ_s is treated as a measurement. The measurement equation is in its simplest form a constant ratio given by

$$\delta_s = h(\delta_f, \theta) = i_s \cdot \delta_f. \tag{3.1}$$

The parameter $\theta = i_s$ is assumed to be time invariant. The state δ_f must be known in order to identify the parameter θ. Usually the parameter is estimated off-line in advance using a test rig where the front wheel angle is measured with highly accurate external sensors. The parameter is then used within the model in order to estimate the states on-line while driving.

The tire parameter C_α is assumed to change with weather and road conditions, hence it is a time varying parameter. It has to be identified on-line at time t using the state estimates from the previous time step $t-1$, which in turn were estimated using the parameter estimate from time step $t-1$.

For various reasons some systems are only modeled by a likelihood function. Often these systems are static and there exists no Markov transition density. However, most systems in this thesis are modeled by both a prediction and a likelihood function. In system identification, the model parameter is estimated without physically describing the parameter's time dependency, hence static estimation theory is used. The state can be estimated in more or less the same way. However, the process model (1.1a) is often given and its time transition information is exploited to further improve the state estimate.

The origins of the estimation research field can be traced back to the work by Gauss in 1795 on least squares (Abdulle and Wanner, 2002) and Bayes (1763) on conditional probabilities. Bayes introduced an important theorem which has come to be referred to as Bayes' theorem,

$$p(\boldsymbol{x}, \boldsymbol{\theta}|\boldsymbol{y}) = \frac{p(\boldsymbol{y}|\boldsymbol{x}, \boldsymbol{\theta})p(\boldsymbol{x}, \boldsymbol{\theta})}{p(\boldsymbol{y})}, \tag{3.2}$$

with which it is possible to calculate the inverse probability $p(\boldsymbol{x}, \boldsymbol{\theta}|\boldsymbol{y})$ given a prior probability $p(\boldsymbol{x}, \boldsymbol{\theta})$ and the likelihood function $p(\boldsymbol{y}|\boldsymbol{x}, \boldsymbol{\theta})$. Note that both the measurement and the state or parameter are treated as random variables. Another view of the estimation problem was introduced by Fisher (1922), who claimed that the probability of an estimate should be seen as a relative frequency of the state or parameter, given data from long-run experiments. Fisher also treats the measurement as a random variable. The main difference to Bayes' approach is that in Fisher's approach there is a true state or parameter which is treated as deterministic, but unknown. To accentuate the different views, the likelihood is often written using $\ell(\boldsymbol{x}, \boldsymbol{\theta})$ to emphasize that the likelihood is regarded as a function of the state $\boldsymbol{x}$ and the parameter $\boldsymbol{\theta}$.

After this brief historical background, the remainder of this chapter is outlined as follows. In Section 3.1, static estimation methods based on both Fishers and Bayes theories, are discussed. These methods can be used for both state and parameter estimation. In Section 3.2, dynamic estimation methods are discussed. These methods are within the scope of this thesis only used for state estimation and are based solely on Bayes' theories.

3.1 Static Estimation Theory

The general estimation problem consists of finding the estimates $\hat{\boldsymbol{x}}$ and $\hat{\boldsymbol{\theta}}$ that minimize a given loss function $V(\boldsymbol{x}, \boldsymbol{\theta}; \boldsymbol{y})$. This problem is separated into a parameter estimation problem and a state estimation problem according to

$$\hat{\boldsymbol{\theta}} = \arg\min_{\boldsymbol{\theta}} V(\boldsymbol{\theta}; \boldsymbol{x}, \boldsymbol{y}), \tag{3.3a}$$

$$\hat{\boldsymbol{x}} = \arg\min_{\boldsymbol{x}} V(\boldsymbol{x}; \boldsymbol{\theta}, \boldsymbol{y}). \tag{3.3b}$$

How to separate a typical estimation problem into these two parts is shown Example 3.2.

General estimation techniques are covered by most textbooks on this topic, e.g. Kay (1993), Kailath et al. (2000), Ljung (1999). There are many estimation methods available, however, in this section the focus is on the methods used in Part II of this thesis.

Example 3.2: Parameter and State Estimation

Consider the linear single track model in Example 2.3. Suppose that the state variables are measured with external and highly accurate sensors. The yaw rate is measured with an extra IMU and the body side slip angle β is measured with a so called Correvit® sensor, which uses optical correlation technology. This sensor incorporates a high intensity light source that illuminates the road surface, which is optically detected by the sensor via a two-phase optical grating system. Now, the parameter $\boldsymbol{\theta}$ can be estimated, according to (3.3a).

Conversely, if $\boldsymbol{\theta}$ is known and $\boldsymbol{y}$ is measured, the state variables $\boldsymbol{x}$ can be estimated using (3.3b).

This section covers estimation problems without any process model $f(\,\cdot\,)$, where a set of measurements is related to a parameter only via the measurement model $h(\,\cdot\,)$. Furthermore, only an important and special case where the measurement model is linear in $\boldsymbol{x}$ is considered. The linear measurement model was given in (2.9b) and is repeated here for convenience

$$\boldsymbol{y}_t = H_t(\boldsymbol{\theta})\boldsymbol{x}_t + \boldsymbol{e}_t. \tag{3.4}$$

In the system identification community the nomenclature deviates slightly and (3.4) is there referred to as a regression model

$$\boldsymbol{y}_t = \varphi_t^{\mathrm{T}}\boldsymbol{\theta}_t + \boldsymbol{e}_t, \tag{3.5}$$

with the regressor φ. The nomenclature in (3.5) is used in the Papers B and C. Nevertheless, the nomenclature presented in (3.4) is used in this section in order to conform to the rest of this chapter. That means that in the algorithms in this section h and $\boldsymbol{x}$ can be substituted by φ and $\boldsymbol{\theta}$, respectively.

3.1.1 Least Squares Estimator

The least squares (LS) estimate is defined as the solution to the optimization problem, where the squared errors between the predicted measurements and the actual measurements are minimized according to,

$$\hat{\boldsymbol{x}}_t^{LS} = \arg\min_{\boldsymbol{x}} \sum_{k=1}^{t} ||\boldsymbol{y}_k - h_k(\boldsymbol{x})||_2^2. \tag{3.6}$$

The solution for the linear case is given in Algorithm 3.1.

If the measurement covariance $R = \mathrm{Cov}\,(\boldsymbol{e})$ is known, or in practice at least assumed to be known, then the weighted least squares (WLS) estimate is given by the optimization problem

$$\hat{\boldsymbol{x}}_t^{WLS} = \arg\min_{\boldsymbol{x}} \sum_{k=1}^{t} (\boldsymbol{y}_k - h_k(\boldsymbol{x}))^{\mathrm{T}} R_k^{-1} (\boldsymbol{y}_k - h_k(\boldsymbol{x})). \tag{3.7}$$

The solution for the linear case is given in Algorithm 3.2, and Example 3.3 illustrates how the single track vehicle model can be reformulated to estimate the parameters using the WLS.

Algorithm 3.1: Least Squares

The least squares estimate and its covariance are given by

$$\hat{\boldsymbol{x}}_t^{LS} = \left(\sum_{k=1}^{t} H_k^{\mathrm{T}} H_k\right)^{-1} \sum_{k=1}^{t} H_k^{\mathrm{T}} \boldsymbol{y}_k = \left(\boldsymbol{H}^{\mathrm{T}}\boldsymbol{H}\right)^{-1} \boldsymbol{H}^{\mathrm{T}}\boldsymbol{Y}, \tag{3.8a}$$

$$\mathrm{Cov}\left(\hat{\boldsymbol{x}}^{LS}\right) = (\boldsymbol{H}^{\mathrm{T}}\boldsymbol{H})^{-1}(\boldsymbol{H}^{\mathrm{T}}\boldsymbol{R}\boldsymbol{H})(\boldsymbol{H}^{\mathrm{T}}\boldsymbol{H})^{-1} \triangleq P^{LS}. \tag{3.8b}$$

The last equality is the batch solution, where $\boldsymbol{H}$ and $\boldsymbol{Y}$ were defined in (2.11)*. Furthermore, the measurement noises $R_k = \mathrm{Cov}\left(\boldsymbol{e}_k\right)$ are forming the main diagonal of $\boldsymbol{R}$ according to $\boldsymbol{R} = \mathrm{diag}(R_1, \ldots, R_t)$.*

Algorithm 3.2: Weighted Least Squares

The weighted least squares estimator and its covariance matrix are given by

$$\hat{\boldsymbol{x}}_t^{WLS} = \left(\sum_{k=1}^{t} H_k^{\mathrm{T}} R_k^{-1} H_k\right)^{-1} \sum_{k=1}^{t} H_k^{\mathrm{T}} R_k^{-1} \boldsymbol{y}_k = \left(\boldsymbol{H}^{\mathrm{T}}\boldsymbol{R}^{-1}\boldsymbol{H}\right)^{-1} \boldsymbol{H}^{\mathrm{T}}\boldsymbol{R}^{-1}\boldsymbol{Y}, \tag{3.9a}$$

$$\mathrm{Cov}\left(\hat{\boldsymbol{x}}^{WLS}\right) = (\boldsymbol{H}^{\mathrm{T}}\boldsymbol{R}^{-1}\boldsymbol{H})^{-1} \triangleq P^{WLS}, \tag{3.9b}$$

where the weighting matrix is the noise covariance $\boldsymbol{R}$.

Example 3.3: Parameter and State Estimation

Consider the linear single track model in Example 2.3 and the separation of the parameter and the state estimation problems in Example 3.2. Suppose that the vehicle's mass m and the dimensions l_f and l_r are known. Furthermore, suppose that the state variable $\boldsymbol{x}$ may be measured as described in Example 3.2. Consider the measurement equation (2.10b); the parameter estimation problem can now be formulated in the form (3.4) or (3.5) according to

$$\boldsymbol{y} = H(\boldsymbol{x}, \boldsymbol{u}, l_f, l_r, m) \begin{bmatrix} C_{\alpha f} \\ C_{\alpha r} \end{bmatrix} + \boldsymbol{e}, \tag{3.10}$$

and the parameters $C_{\alpha f}, C_{\alpha r}$ can be solved for using e.g. WLS in (3.7). Furthermore, the inverse of the moment of inertia $1/I_{zz}$ may be estimated off-line by writing the process model (2.10a) in the form (3.5) according to

$$\boldsymbol{x}_{t+1} = H(\boldsymbol{x}_t, \boldsymbol{u}, l_v, l_f, m, C_{\alpha f}, C_{\alpha r}) \cdot \frac{1}{I_{zz}} + \boldsymbol{w}. \tag{3.11}$$

Another example, where the WLS estimator is applied, is given in Paper C. The left and right borders of a road are modeled by polynomials and the coefficients are the parameters which are estimated given a batch of measurements from a radar.

3.1.2 Recursive Least Squares

Consider the LS estimator in Section 3.1.1. If the state $\boldsymbol{x}$ varies with time it is a good idea to weigh recent measurements higher than older ones. Introduce a forgetting factor $0 < \lambda \leq 1$ in the loss function (3.3) according to

$$V(\boldsymbol{x}, \boldsymbol{y}) = \sum_{k=1}^{t} \lambda^{t-k} ||\boldsymbol{y}_k - h_k(\boldsymbol{x})||_2^2. \tag{3.12}$$

In the linear case the solution is given by the recursion in Algorithm 3.3. For a detailed account of the RLS algorithm and recursive identification in general, see e.g. Ljung (1999), Ljung and Söderström (1983).

In many practical applications the parameter estimate lies within a certain region. Some possibilities to constrain the parameter, under the assumption that the constrained region is a closed convex region in the parameter space, denoted $D_{\mathcal{M}}$, are described by Goodwin and Sin (1984) and Ljung (1999). The simplest approach is to project the new estimate $\hat{\boldsymbol{x}}_t$ back into $D_{\mathcal{M}}$ by taking the old value $\hat{\boldsymbol{x}}_{t-1}$ according to

$$\hat{\boldsymbol{x}}_t = \begin{cases} \hat{\boldsymbol{x}}_t & \text{if } \hat{\boldsymbol{x}}_t \in D_{\mathcal{M}} \\ \hat{\boldsymbol{x}}_{t-1} & \text{if } \hat{\boldsymbol{x}}_t \notin D_{\mathcal{M}} \end{cases}, \tag{3.13}$$

or by projecting $\hat{\boldsymbol{x}}_t$ orthogonally onto the surface of $D_{\mathcal{M}}$, before continuing.

Another approach is the constrained least-squares algorithm described by Goodwin and Sin (1984). If $\hat{\boldsymbol{x}}_t \notin D_{\mathcal{M}}$, then the coordinate basis for the parameter space is transformed by defining

$$\boldsymbol{\rho} = P_{t-1}^{-1/2} \boldsymbol{x}, \tag{3.14}$$

where

$$P_{t-1}^{-1} = P_{t-1}^{-\mathrm{T}/2} P_{t-1}^{-1/2}. \tag{3.15}$$

The image of $D_{\mathcal{M}}$ under the linear transformation (3.14) is denoted $\bar{D}_{\mathcal{M}}$. The image $\hat{\boldsymbol{\rho}}_t$ of $\hat{\boldsymbol{x}}_t$, under $P_{t-1}^{-1/2}$, is orthogonally projected onto the boundary of $\bar{D}_{\mathcal{M}}$ to yield $\hat{\boldsymbol{\rho}}_t'$. Finally, the parameter $\hat{\boldsymbol{x}}_t$ is obtained by projecting back $\hat{\boldsymbol{\rho}}_t'$ under $P_{t-1}^{1/2}$ according to

$$\hat{\boldsymbol{x}}_t = \hat{\boldsymbol{x}}_t' \triangleq P_{t-1}^{1/2} \hat{\boldsymbol{\rho}}_t' \tag{3.16}$$

and continue.

An example of how the RLS estimator can be used for on-line estimation of the stiffness parameters of the tires in a passenger car is given Paper B. The parameters in this example tend to drift when the system is not excited enough, for example when driving at a constant velocity on a straight road. The parameters are therefore constrained using the simple idea given in (3.13).

Algorithm 3.3: Recursive Least Squares

The recursive least squares solution is given by the recursion

$$\hat{\boldsymbol{x}}_t = \hat{\boldsymbol{x}}_{t-1} + K_t \left(\boldsymbol{y}_t - H_t^{\mathrm{T}} \hat{\boldsymbol{x}}_{t-1} \right), \tag{3.17a}$$

$$K_t = P_{t-1} H_t \left(\lambda_t \Lambda_t + H_t^{\mathrm{T}} P_{t-1} H_t \right)^{-1}, \tag{3.17b}$$

$$P_t = \frac{1}{\lambda_t} \left(P_{t-1} - P_{t-1} H_t (\lambda_t \Lambda_t + H_t^{\mathrm{T}} P_{t-1} H_t)^{-1} H_t^{\mathrm{T}} P_{t-1} \right), \tag{3.17c}$$

where $P_t = \mathrm{Cov}(\hat{\boldsymbol{x}}_t)$ and Λ denote a weighting matrix, which can be used to acknowledge the relative importance of the different measurements.

3.1.3 Probabilistic Point Estimates

The maximum likelihood estimate, first introduced by Fisher (1912, 1922), is defined by

$$\hat{\boldsymbol{x}}_t^{ML} = \arg\max_{\boldsymbol{x}_t} p(\boldsymbol{y}_{1:t} | \boldsymbol{x}_t). \tag{3.18}$$

Put into words, the estimate is chosen to be the parameter most likely to produce the obtained measurements.

The posterior $p(\boldsymbol{x}_t | \boldsymbol{y}_{1:t})$ contains all known information about the state of the target at time t. The maximum a posterior (MAP) estimator is defined by

$$\hat{\boldsymbol{x}}_t^{MAP} = \arg\max_{\boldsymbol{x}_t} p(\boldsymbol{x}_t | \boldsymbol{y}_{1:t}) = \arg\max_{\boldsymbol{x}_t} p(\boldsymbol{y}_{1:t} | \boldsymbol{x}_t) p(\boldsymbol{x}_t), \tag{3.19}$$

or put in words, find the most likely estimate of the parameter given the measurements $\boldsymbol{y}_{1:t}$. Bayes' theorem (3.2) and the fact that the maximization is performed over $\boldsymbol{x}_t$ is used in the second equality of (3.19). The ML and MAP estimates are not considered in this work, but mentioned here to complete the view.

3.2 Filter Theory

The topic of this section is recursive state estimation based on dynamic models. The iteration process of the state space estimation was briefly described in words in Section 1.4. The state estimation theory is influenced by the Bayesian view, which implies that the solution to the estimation problem is provided by the filtering probability density function (pdf) $p(\boldsymbol{x}_t | \boldsymbol{y}_{1:t})$. The introduction to this section will be rather general using the model defined in (2.18). Bayes' theorem was introduced in (3.2) and is used to derive the recursive Bayes filter equations

$$p(\boldsymbol{x}_{t+1} | \boldsymbol{y}_{1:t}) = \int p(\boldsymbol{x}_{t+1} | \boldsymbol{x}_t) p(\boldsymbol{x}_t | \boldsymbol{y}_{1:t}) d\boldsymbol{x}_t, \tag{3.20a}$$

$$p(\boldsymbol{x}_t | \boldsymbol{y}_{1:t}) = \frac{p(\boldsymbol{y}_t | \boldsymbol{x}_t) p(\boldsymbol{x}_t | \boldsymbol{y}_{1:t-1})}{p(\boldsymbol{y}_t | \boldsymbol{y}_{1:t-1})}, \tag{3.20b}$$

with the denominator

$$p(\boldsymbol{y}_t|\boldsymbol{y}_{1:t-1}) = \int p(\boldsymbol{y}_t|\boldsymbol{x}_t)p(\boldsymbol{x}_t|\boldsymbol{y}_{1:t-1})d\boldsymbol{x}_t. \tag{3.20c}$$

These equations describe the time evolution

$$\cdots \rightarrow \boldsymbol{x}_{t|t} \rightarrow \boldsymbol{x}_{t+1|t} \rightarrow \boldsymbol{x}_{t+1|t+1} \rightarrow \cdots \tag{3.21}$$

of the random state vector $\boldsymbol{x}$. The Bayes posterior density function $p(\boldsymbol{x}_t|\boldsymbol{y}_{1:t})$ conditioned on the time sequence $\boldsymbol{y}_{1:t} = \{\boldsymbol{y}_1, \ldots, \boldsymbol{y}_t\}$ of measurements accumulated at time t is the probability density function of $\boldsymbol{x}_{t|t}$. The probability density function $p(\boldsymbol{x}_{t+1}|\boldsymbol{y}_{1:t})$ is the time prediction of the posterior $p(\boldsymbol{x}_t|\boldsymbol{y}_{1:t})$ to the time step of the next measurement $\boldsymbol{y}_{t+1}$. Note that the Bayes normalization factor given by (3.20c) is independent of $\boldsymbol{x}$. In practice the numerator of (3.20b) is calculated and then simply normalized, since the integral of the posterior density function must be unitary.

If $p(\boldsymbol{y}_t|\boldsymbol{x}_t)$, $p(\boldsymbol{x}_{t+1}|\boldsymbol{x}_t)$ and $p(\boldsymbol{x}_t)$ are linear and Gaussian then (3.20a) and (3.20b) are reduced to the Kalman filter prediction and measurement update, respectively. The Kalman filter is treated in Section 3.2.1. In contrast, if $p(\boldsymbol{y}_t|\boldsymbol{x}_t)$, $p(\boldsymbol{x}_{t+1}|\boldsymbol{x}_t)$ and $p(\boldsymbol{x}_t)$ are nonlinear, but still assumed Gaussian, several approximations of (3.20a) and (3.20b) exist. The two most common filters are the extended Kalman Filter and the unscented Kalman filter, which are outlined in the Sections 3.2.2 and 3.2.3, respectively. Other methods, including methods that approximate other density functions than Gaussian, are neatly covered by Hendeby (2008) and Schön (2006). The most popular approaches are the particle filter and the marginalized particle filter, see e.g. Ristic et al. (2004), Arulampalam et al. (2002), Cappe et al. (2007), Djuric et al. (2003), Karlsson (2005), Schön et al. (2005).

3.2.1 The Linear Kalman Filter

The linear state space representation subject to Gaussian noise, which were given in (2.9), is the simplest special case when it comes to state estimation. The model is repeated here for convenience;

$$\boldsymbol{x}_{t+1} = F_t(\boldsymbol{\theta})\boldsymbol{x}_t + G_t^u(\boldsymbol{\theta})\boldsymbol{u}_t + G_t^w\boldsymbol{w}_t, \qquad \boldsymbol{w} \sim \mathcal{N}(0, Q), \tag{3.22a}$$

$$\boldsymbol{y}_t = H_t(\boldsymbol{\theta})\boldsymbol{x}_t + H_t^u(\boldsymbol{\theta})\boldsymbol{u}_t + \boldsymbol{e}_t, \qquad \boldsymbol{e} \sim \mathcal{N}(0, R). \tag{3.22b}$$

The linear model (3.22) has two important properties. All density functions involved in the model and state estimation are Gaussian and a Gaussian density function is completely parametrized by the mean and the covariance, i.e. the first and second order moment. Hence, the Bayesian recursion (3.20) is simplified to only propagating the mean and covariance of the involved probability density functions. The most well known estimation algorithm is the Kalman Filter (KF), derived by Kalman (1960) and Kalman and Bucy (1961), and shown in Algorithm 3.4. Example 3.4 shows how the single track vehicle model, introduced in Example 1.1, may be rewritten to be used with the Kalman filter, which in turn is used to estimate the states.

Algorithm 3.4: Kalman Filter

Consider the linear state space model (3.22)*. The Kalman filter is given by the two following steps.*

Prediction

$$\hat{\boldsymbol{x}}_{t|t-1} = F_{t-1}\hat{\boldsymbol{x}}_{t-1|t-1} + G^u_{t-1}\boldsymbol{u}_{t-1} \tag{3.23a}$$
$$P_{t|t-1} = F_{t-1}P_{t-1|t-1}F^{\mathrm{T}}_{t-1} + G^w_{t-1}Q_{t-1}G^{w\mathrm{T}}_{t-1} \tag{3.23b}$$

Measurement Update

$$K_t = P_{t|t-1}H^{\mathrm{T}}_t(H_tP_{t|t-1}H^{\mathrm{T}}_t + R_t)^{-1} \tag{3.24a}$$
$$\hat{\boldsymbol{x}}_{t|t} = \hat{\boldsymbol{x}}_{t|t-1} + K_t(\boldsymbol{y}_t - H_t\hat{\boldsymbol{x}}_{t|t-1} - H^u_t\boldsymbol{u}_t) \tag{3.24b}$$
$$P_{t|t} = (I - K_tH_t)P_{t|t-1} \tag{3.24c}$$

Example 3.4: Linearized Single Track Model

The single track vehicle model was introduced in Example 1.1 and the model equations were derived in Section 2.3. The process model (2.4a) and the measurement model (2.4b) are linear in the state variables and can be written in the form

$$\begin{bmatrix}\dot{\psi}_{t+1}\\ \beta_{t+1}\end{bmatrix} = F_t(\dot{v}_x, v_x, \boldsymbol{\theta})\begin{bmatrix}\dot{\psi}_t\\ \beta_t\end{bmatrix} + G^u_t(v_x, \boldsymbol{\theta})\delta_f + \boldsymbol{w}_t, \qquad \boldsymbol{w} \sim \mathcal{N}(0, Q), \tag{3.25a}$$
$$\begin{bmatrix}\dot{\psi}^m_t\\ a_{y,t}\end{bmatrix} = H_t(\dot{v}_x, v_x, \boldsymbol{\theta})\begin{bmatrix}\dot{\psi}_t\\ \beta_t\end{bmatrix} + H^u_t(\boldsymbol{\theta})\delta_f + \boldsymbol{e}_t, \qquad \boldsymbol{e} \sim \mathcal{N}(0, R), \tag{3.25b}$$

as shown in Example 2.3. Since the inputs $\dot{v}_x$ and v_x are present in F_t, G^u_t and H_t, these matrices must be recalculated at each time step before being used in the Kalman filter (Algorithm 3.4) to estimate the states.

3.2.2 The Extended Kalman Filter

In general, most complex automotive systems tend to be nonlinear. When it comes to solving state estimation problems in sensor fusion frameworks, nonlinear models are commonly applied. This holds also for the work presented in this thesis, but the problems are restricted by the assumption that the process and measurement noise is Gaussian. The most common representation of nonlinear systems is the state space model given in (1.1), repeated here for convenience;

$$\boldsymbol{x}_{t+1} = f_t(\boldsymbol{x}_t, \boldsymbol{u}_t, \boldsymbol{w}_t, \boldsymbol{\theta}), \qquad \boldsymbol{w} \sim \mathcal{N}(0, Q), \tag{3.26a}$$
$$\boldsymbol{y}_t = h_t(\boldsymbol{x}_t, \boldsymbol{u}_t, \boldsymbol{e}_t, \boldsymbol{\theta}), \qquad \boldsymbol{e} \sim \mathcal{N}(0, R). \tag{3.26b}$$

The basic idea behind the extended Kalman filter (EKF) is to approximate the nonlinear model (3.26) by a linear model and apply the Kalman filter locally. The local approximation is obtained by computing a first order Taylor expansion around the current estimate. The result is the extended Kalman filter, which is given in Algorithm 3.5. Early practical applications and examples of the EKF are described in the works by Smith et al. (1962), Schmidt (1966). An early reference where the EKF is treated is Jazwinski (1970), other standard references are Anderson and Moore (1979), Kailath et al. (2000) .

The linearization used in the EKF assumes that all second and higher order terms in the Taylor expansion are negligible. This is certainly true for many systems, but for some systems this assumption can significantly degrade the estimation performance. Higher order EKF are discussed by Bar-Shalom and Fortmann (1988) and Gustafsson (2000). This problem will be revisited in the next section.

3.2.3 The Unscented Kalman Filter

The EKF is sufficient for many applications. However, to use an EKF the gradients of $f_t(\,\cdot\,)$ and $h_t(\,\cdot\,)$ must be calculated, which in some cases is either hard to do analytically or computational expensive to do numerically. An alternative approach, called the unscented Kalman filter (UKF) was proposed by Julier et al. (1995), Julier and Uhlmann (1997) and further refined by e.g. Julier and Uhlmann (2002, 2004), Julier (2002). Instead

Algorithm 3.5: Extended Kalman Filter

Consider the state space model (3.26)*. The extended Kalman filter is given by the two following steps.*

Prediction

$$\hat{\boldsymbol{x}}_{t|t-1} = f_{t-1}(\hat{\boldsymbol{x}}_{t-1|t-1}, \boldsymbol{u}_{t-1}, 0, \boldsymbol{\theta}) \tag{3.27a}$$
$$P_{t|t-1} = F_{t-1}P_{t-1|t-1}F_{t-1}^{\mathrm{T}} + G_{t-1}Q_{t-1}G_{t-1}^{\mathrm{T}} \tag{3.27b}$$

where

$$F_t = \left.\frac{\partial f_t(\boldsymbol{x}_t, \boldsymbol{u}_t, 0, \boldsymbol{\theta})}{\partial \boldsymbol{x}_t}\right|_{\boldsymbol{x}_t=\hat{\boldsymbol{x}}_{t|t}} \qquad G_t = \left.\frac{\partial f_t(\hat{\boldsymbol{x}}_{t|t}, \boldsymbol{u}_t, \boldsymbol{w}_t, \boldsymbol{\theta})}{\partial \boldsymbol{w}_t}\right|_{\boldsymbol{w}_t=0} \tag{3.27c}$$

Measurement Update

$$K_t = P_{t|t-1}H_t^{\mathrm{T}}(H_tP_{t|t-1}H_t^{\mathrm{T}} + R_t)^{-1} \tag{3.28a}$$
$$\hat{\boldsymbol{x}}_{t|t} = \hat{\boldsymbol{x}}_{t|t-1} + K_t(\boldsymbol{y}_t - h_t(\hat{\boldsymbol{x}}_{t|t-1}, \boldsymbol{u}_t, 0, \boldsymbol{\theta})) \tag{3.28b}$$
$$P_{t|t} = (I - K_tH_t)P_{t|t-1} \tag{3.28c}$$

where

$$H_t = \left.\frac{\partial h_t(\boldsymbol{x}_t, \boldsymbol{u}_t, 0, \boldsymbol{\theta})}{\partial \boldsymbol{x}_t}\right|_{\boldsymbol{x}_t=\hat{\boldsymbol{x}}_{t|t-1}} \tag{3.28d}$$

of linearizing $f_t(\,\cdot\,)$ and $h_t(\,\cdot\,)$, the unscented transform (UT) is used to approximate the moments of the prediction $p(\boldsymbol{x}_{t+1}|\boldsymbol{x}_t)$ and the likelihood $p(\boldsymbol{y}_t|\boldsymbol{x}_t)$. Thereby the UKF to some extent also considers the second order terms of the models, which is not done by the EKF.

The principle of the unscented transform is to carefully and deterministically select a set of points, called sigma points, of the initial stochastic variable $\boldsymbol{x}$, such that their mean and covariance equal those of $\boldsymbol{x}$. Then the sigma points are passed through the non-linear function and based on the output the resulting mean and covariance are derived. In case the process noise and measurement noise are not additive, sigma points are selected from an augmented state space, which includes the state $\boldsymbol{x}$, the process noise $\boldsymbol{w}$ and the measurement noise $\boldsymbol{e}$ in one augmented state vector

$$\hat{\boldsymbol{x}}^a_{t|t} = \begin{bmatrix} \hat{\boldsymbol{x}}_{t|t} \\ \mathrm{E}\left(\boldsymbol{w}_t\right) \\ \mathrm{E}\left(\boldsymbol{e}_{t+1}\right) \end{bmatrix}, \tag{3.29}$$

with dimension $n_a = n_{\boldsymbol{x}} + n_{\boldsymbol{w}} + n_{\boldsymbol{e}}$ and the corresponding covariance matrix

$$P^a_{t|t} = \begin{bmatrix} P_{t|t} & 0 & 0 \\ 0 & Q_t & 0 \\ 0 & 0 & R_{t+1} \end{bmatrix}. \tag{3.30}$$

If the noise is additive, then the noise covariances can be added directly to the estimated covariances of the non-augmented sigma points.

There exist many possibilities to choose the sigma points, a thorough discussion about different alternatives is presented by Julier and Uhlmann (2004). In the present work only the standard form is reproduced. The basic principle is to choose one sigma point in the mean of $\boldsymbol{x}^a$ and $2n_a$ points symmetrically on a given contour, described by the state covariance P^a. The sigma points χ^i and the associated weights $w^{(i)}$ are chosen as

$$\chi^{(0)} = \hat{\boldsymbol{x}}^a \qquad w^{(0)} = w^{(0)} \tag{3.31a}$$

$$\chi^{(i)} = \chi^{(0)} + \left(\sqrt{\frac{n_a}{1-w^{(0)}} P^a}\right)_i \qquad w^{(i)} = \frac{1-w^{(0)}}{2n_a} \tag{3.31b}$$

$$\chi^{(i+n_a)} = \chi^{(0)} - \left(\sqrt{\frac{n_a}{1-w^{(0)}} P^a}\right)_i \qquad w^{(i+n_a)} = \frac{1-w^{(0)}}{2n_a} \tag{3.31c}$$

for $i = 1, \ldots, n_a$, where $(\sqrt{A})_i$ is the i^{th} column of any matrix B, such that $A = BB^{\mathrm{T}}$. The augmented state vector makes it possible to propagate and estimate nonlinear influences that the process noise and the measurement noise have on the state vector and the measurement vector, respectively. The weight on the mean $w^{(0)}$ is used for tuning and according to Julier and Uhlmann (2004) preferable properties for Gaussian density functions are obtained by choosing $w^{(0)} = 1 - \frac{n_a}{3}$. After the sigma points have been acquired, the augmented state vector can be partitioned according to

$$\chi^a_{t|t} = \begin{bmatrix} \chi^{\boldsymbol{x}}_{t|t} \\ \chi^{\boldsymbol{w}}_t \\ \chi^{\boldsymbol{e}}_{t+1} \end{bmatrix}. \tag{3.31d}$$

Algorithm 3.6: Unscented Kalman Filter

Consider the state space model (3.26)*. The unscented Kalman filter is given by the following steps, which are iterated in the filter.*

Choose sigma points *according to* (3.31)

Prediction

$$\hat{\boldsymbol{x}}_{t|t-1} = \sum_{i=0}^{2n_a} w^{(i)} \chi^{\boldsymbol{x},(i)}_{t|t-1} \tag{3.32a}$$

$$P_{t|t-1} = \sum_{i=0}^{2n_a} w^{(i)} \left(\chi^{\boldsymbol{x},(i)}_{t|t-1} - \hat{\boldsymbol{x}}_{t|t-1} \right) \left(\chi^{\boldsymbol{x},(i)}_{t|t-1} - \hat{\boldsymbol{x}}_{t|t-1} \right)^{\mathrm{T}} \tag{3.32b}$$

where

$$\chi^{\boldsymbol{x},(i)}_{t|t-1} = f_{t-1} \left(\chi^{\boldsymbol{x},(i)}_{t-1|t-1}, \boldsymbol{u}_{t-1}, \chi^{\boldsymbol{w},(i)}_{t-1|t-1}, \boldsymbol{\theta} \right) \tag{3.32c}$$

Measurement Update

$$\hat{\boldsymbol{x}}_{t|t} = \hat{\boldsymbol{x}}_{t|t-1} + P_{\boldsymbol{xy}} P^{-1}_{\boldsymbol{yy}} (\boldsymbol{y}_t - \hat{\boldsymbol{y}}_{t|t-1}) \tag{3.33a}$$

$$P_{t|t} = P_{t|t-1} - P_{\boldsymbol{xy}} P^{-1}_{\boldsymbol{yy}} P^{\mathrm{T}}_{\boldsymbol{xy}} \tag{3.33b}$$

where

$$\boldsymbol{y}^{(i)}_{t|t-1} = h_t \left(\chi^{\boldsymbol{x},(i)}_{t|t-1}, \boldsymbol{u}_t, \chi^{\boldsymbol{e},(i)}_{t|t-1}, \boldsymbol{\theta} \right) \tag{3.33c}$$

$$\hat{\boldsymbol{y}}_{t|t-1} = \sum_{i=0}^{2n_a} w^{(i)} \boldsymbol{y}^{(i)}_{t|t-1} \tag{3.33d}$$

$$P_{\boldsymbol{yy}} = \sum_{i=0}^{2n_a} w^{(i)} \left(\boldsymbol{y}^{(i)}_{t|t-1} - \hat{\boldsymbol{y}}_{t|t-1} \right) \left(\boldsymbol{y}^{(i)}_{t|t-1} - \hat{\boldsymbol{y}}_{t|t-1} \right)^{\mathrm{T}} \tag{3.33e}$$

$$P_{\boldsymbol{xy}} = \sum_{i=0}^{2n_a} w^{(i)} \left(\chi^{\boldsymbol{x},(i)}_{t|t-1} - \hat{\boldsymbol{x}}_{t|t-1} \right) \left(\boldsymbol{y}^{(i)}_{t|t-1} - \hat{\boldsymbol{y}}_{t|t-1} \right)^{\mathrm{T}} \tag{3.33f}$$

The rest of the UKF is summarized in Algorithm 3.6.

An advantage of the UKF, compared to the EKF, is that the second order bias correction term is implicitly incorporated in the mean estimate. Example 3.5 shows an important problem where the second order term should not be neglected.

Example 3.5: Tracked Radar Object

The radar target tracking problem was introduced in Example 1.2 and the model was defined in Section 2.5. The sensor model converts the Cartesian state variables to polar measurements. This is one of the most important and commonly used transformations for sensors measuring range and azimuth angle. Usually the azimuth angle error of these type of sensors is significantly larger than the range error. This also holds for the sensors used in this thesis.

Let the sensor be located at the origin and the target at $(x, y) = (0, 1)$ in this simple, though commonly used example (Julier and Uhlmann, 2004). Measurements may be simulated by adding Gaussian noise to the actual polar value $(r, \psi) = (1, \pi/2)$ of the target localization. A plot of several hundred state estimates, produced in a Monte Carlo simulation, forms a banana shaped arc around the true value $(x, y) = (0, 1)$, as shown in Figure 3.1. The azimuth error causes this band of Cartesian points to be stretched around the circumference of a circle, with the result that the mean of these points lies somewhat closer to the origin than the point $(0, 1)$. In the figure it is clearly shown that that the UT estimate ($\times$) lies close to the mean of the measurements ($\circ$). Furthermore, it is shown that the linearized state estimate ($+$) produced by the EKF is biased and the variance in the y component is underestimated.

As a result of the linearization in the EKF, the second order terms are neglected, which produces a bias error in the mean as shown in Example 3.5. In Julier and Uhlmann (2004) it is shown how the UT calculates the projected mean and covariance correctly to the second order terms.

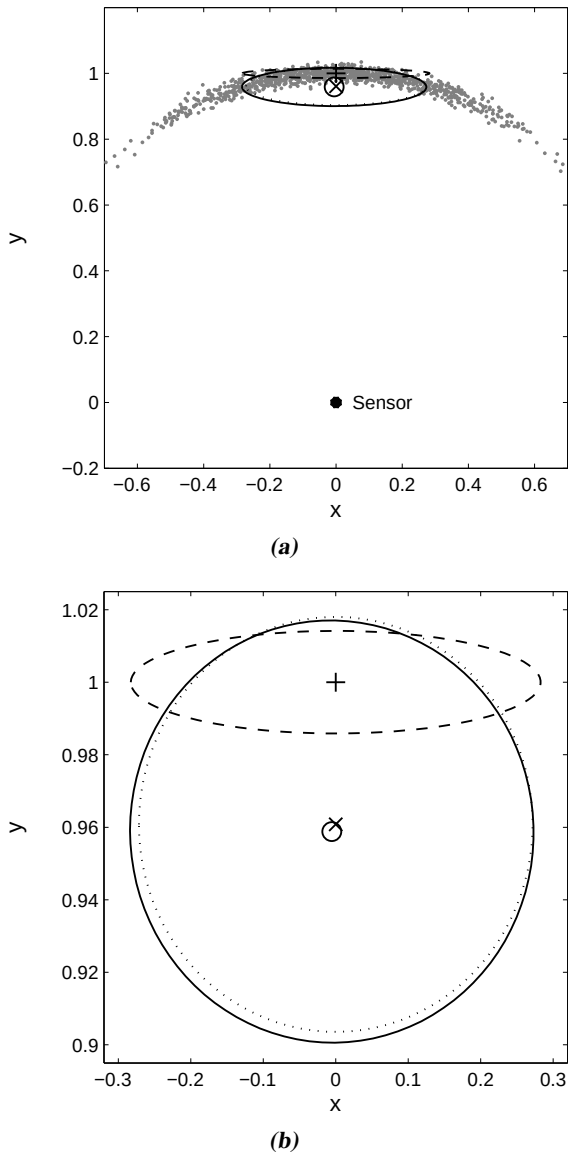

(a)

(b)

Figure 3.1: *A Monte Carlo simulation of the problem in Example 3.5 is shown in Figure (a). The sensor, for example a radar, is in the position* $(0, 0)$ *and the true position of the target is in the position* $(0, 1)$*. The mean of the measurements is at* $\circ$ *and the uncertainty ellipse is solid. The linearized mean is at* $+$ *and its ellipse is dashed. The UT mean is at* $\times$ *and its uncertainty ellipse is dotted. Figure (b) is a zoom. Note that the scaling in the* x *and the* y *axis are different.*

4

The Sensor Fusion Framework

The components of the sensor fusion framework were illustrated in Figure 1.1 in the introduction. The inner boxes, i.e. the process and measurement models, have been discussed in Chapter 2, where several examples were given. Furthermore, these models were used in the estimation algorithms, covered in Chapter 3, to estimate parameters and state variables. The present chapter deals with the outer box, that is the "surrounding infrastructure".

Instead of considering the individual components, the sensor fusion framework can also be represented as an iterative process according to Figure 1.4. In view of this interpretation, the present chapter deals with the sensor data processing, the data association and the track management.

Practical design principles and implementation strategies, e.g. to manage asynchronous sensor data and out-of-sequence-measurements are not considered in this work. However, these topics, with application to automotive systems, are treated in the recent paper by Bengtsson and Danielsson (2008).

The chapter begins with a brief presentation of the experimental setup in Section 4.1. Multi-target multi-sensor tracking, including data association and track management, is treated in Section 4.2. The chapter is concluded with Section 4.3 treating road border and free space estimation. There are many alternatives when it comes to estimating and representing the free road area in front of the ego vehicle. Two methods are presented in the papers C and D in Part II, and a third method is described in Section 4.3.1. The three approaches are compared and their advantages and disadvantages are discussed in Section 4.3.2.

4.1 Experimental Setup

During the time of this work measurements from three different vehicles were used. The vehicles and some of their sensors are shown in Figure 4.1.

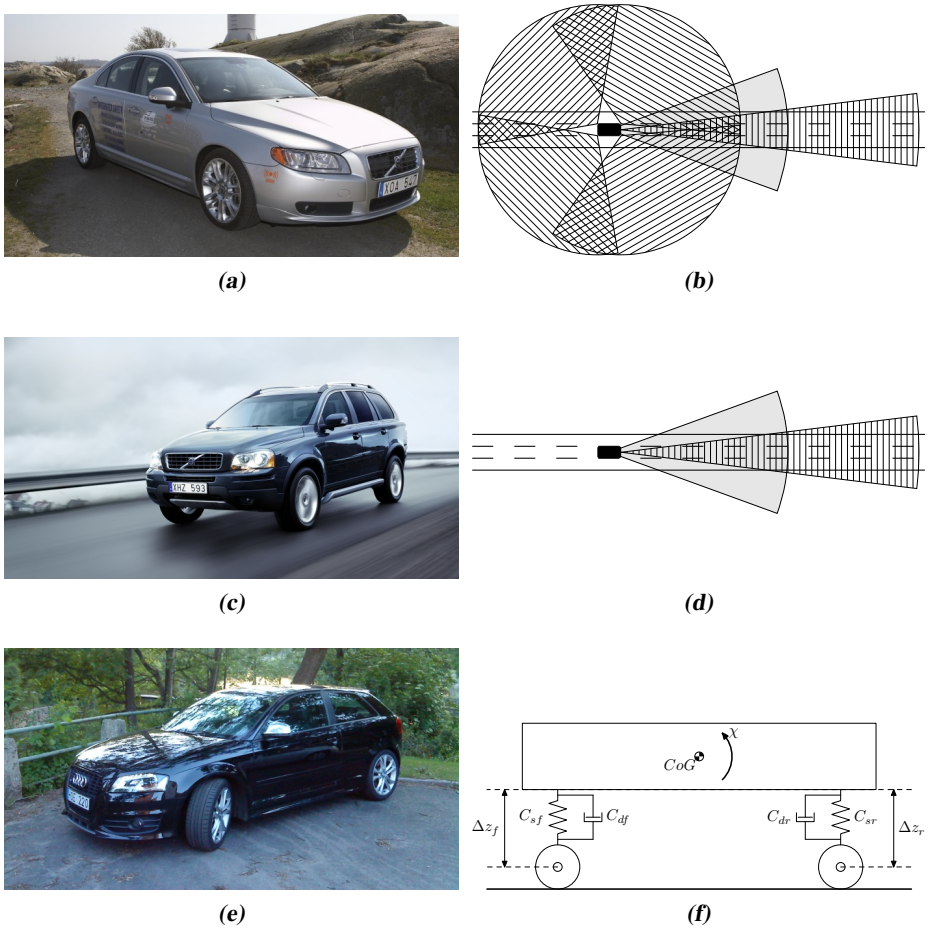

Figure 4.1: *The Volvo S80 in Figure (a) is equipped with 5 radars and one camera, as illustrated in Figure (b). The field of view is illustrated as striped zones for the radar and a gray zone for the camera. Figure (c) shows the Volvo XC90, which is equipped only with one long range radar and one camera, compare with Figure (d). Finally, the Audi S3 in Figure (e) is not equipped with any exteroceptive sensors, but with axle height sensors as illustrated in Figure (f). Note that the drawings are not true to scale. Courtesy of Volvo Car Corporation.*

All three vehicles were equipped with standard, serial production IMU, steering wheel angle sensor and wheel speed sensors. The Volvo XC90 was equipped with a forward looking 77 GHz mechanically scanning frequency modulated continuous-wave (FMCW) radar and a forward looking vision sensor (camera), measuring range and bearing angle to the targets. Computer vision is included in the image sensor and comprehends object and lane detection and provides for example the lane curvature. In addition, the Volvo S80 was equipped with four wide field of view 24 GHz radars at the corners of the vehicle. The range of the forward looking radar is approximately 200 m, whereas it is approximately 50 m for the four other radars.

The Audi S3 was equipped with neither radar nor camera. In this vehicle the vertical position of the front and the rear suspension is measured with axle height sensor, and can be used to derive the pitch angle. A summary of the sensor equipment of the prototypes is given in Table 4.1.

The results in this thesis are based on tests performed on public roads. Hence, no specific test procedures are realized and no reference values are provided.

4.2 Target Tracking

Radar measurements originate from objects, referred to as targets, or from false detections, referred to as clutter. The target tracking collects the measurement data including one or more observations of targets and partitions the data into sets of observations, referred to as tracks. Measurements associated to one track are supposed to be produced by the same source.

The track management handles the tracks and ensures that only tracks with sufficient quality are kept within the sensor fusion framework. If measurements are likely to originate from a new target, then the track management starts a new track and chooses a suitable prior $p(\boldsymbol{x}_0|\boldsymbol{y}_0)$ to initiate the tracking filter. If a track is not observed for a number of time steps it is removed.

When the tracks are observed a number of time steps, quantities such as position and velocity can be estimated. Furthermore, new measurements are first considered for the update of existing tracks and a data association algorithm is used to determine which measurement corresponds to which track. This is the topic of Section 4.2.1. If multiple measurements are received from the same target, i.e. when the size of the target is large

Table 4.1: *Overview of the sensors equipment in the prototypes.*

		S80	**XC90**	**S3**
proprioceptive sensors	IMU	X	X	X
	steering wheel angle sensor	X	X	X
	wheel speed sensor	X	X	X
	axle height sensors			X
exteroceptive sensors	forward looking radar	X	X	
	forward looking camera	X	X	
	rear radar	X		
	side radar	X		

compared to the sensor resolution, it can be modeled and tracked as a so called extended target. Different approaches to take care of the measurements and to appropriately model the target are discussed in Section 4.2.2.

4.2.1 Data Association

This section would not be needed if only the state variables of the ego vehicle, introduced in Example 1.1 are estimated, because in that case it is obvious how the measurements are associated with the state variables. In the object tracking problem, introduced in Example 1.2, it is no longer obvious which measurement should update which track. There are many methods available for finding likely measurement-to-track associations, i.e. for solving the data association problem, see e.g., Bar-Shalom and Fortmann (1988), Blackman and Popoli (1999). However, the task is seldom easy, due to noisy measurements, multiple reflections on each target and erroneous detections caused by spurious reflections.

The first step in the data association process is called gating. Gates are constructed around the predicted measurement $\hat{\boldsymbol{y}}_{i,t|t-1}$ of each track i to eliminate unlikely pairings and thereby to limit the number of measurement-to-track associations. This reduces the number of measurements that are examined by the data association algorithm. The residual between a measurement $\boldsymbol{y}_{j,t}$ and a predicted measurement $\hat{\boldsymbol{y}}_{i,t|t-1}$ is

$$\tilde{\boldsymbol{y}}_{i,j,t|t-1} = \boldsymbol{y}_{j,t} - \hat{\boldsymbol{y}}_{i,t|t-1}, \tag{4.1}$$

and it is assumed Gaussian distributed according to

$$\tilde{\boldsymbol{y}}_{i,j,t|t-1} \sim \mathcal{N}(0, S_{i,t}), \tag{4.2}$$

where $S_{i,t}$ is the innovation covariance. The gate $\mathcal{G}_i$ is defined as the region

$$\mathcal{G}_i \triangleq \left\{ \boldsymbol{y} \middle| (\boldsymbol{y} - \hat{\boldsymbol{y}}_{i,t|t-1})^{\mathrm{T}} S_{i,t}^{-1} (\boldsymbol{y} - \hat{\boldsymbol{y}}_{i,t|t-1}) \leq U_{\mathcal{G}} \right\}, \tag{4.3}$$

where $U_{\mathcal{G}}$ is the gating threshold. The measurements $\boldsymbol{y}_{j,t} \in \mathcal{G}_i$ are considered as candidates for updating the track $\boldsymbol{x}_{i,t}$ in the data association algorithm.

Now, different conflicts occur. There are several measurements falling within the same gate and there are also measurements falling within more than one gate. There exist many techniques to solve these conflicts, which are considered to be the main part of the data association process. The simplest association algorithm is called nearest neighbor (NN). This approach searches for a unique pairing, i.e. one track $\boldsymbol{x}_{i,t}$ is only updated by one observation $\boldsymbol{y}_{j,t}$. There are some possibilities to decide which measurement actually is the nearest. Common approaches are to choose the measurement with the smallest error $\tilde{\boldsymbol{y}}_{i,j,t|t-1}$ or the smallest statistical distance

$$d^2(\tilde{\boldsymbol{y}}_{i,j,t|t-1}) = \tilde{\boldsymbol{y}}_{i,j,t|t-1}^{\mathrm{T}} S_{i,t}^{-1} \tilde{\boldsymbol{y}}_{i,j,t|t-1} \tag{4.4}$$

which is also known as the Mahalanobis distance, see e.g., Bar-Shalom et al. (2001). Another method is to choose the measurement with the largest likelihood according to

$$\ell(\boldsymbol{y}_{j,t}, \hat{\boldsymbol{y}}_{i,t|t-1}) = \mathcal{N}\left(\boldsymbol{y}_{j,t}; \hat{\boldsymbol{y}}_{i,t|t-1}, S_{i,t}\right). \tag{4.5}$$

Besides the two books mentioned above a nice overview concerning data association and track handling is given in the recent work by Svensson (2008).

4.2.2 Extended Object Tracking

In classical target tracking problems the objects are modeled as point sources and it is assumed that only one measurement is received from each target at each time step. In automotive applications, the targets are at a close distance and of such a large size that individual features can be resolved by the sensor. A target is denoted extended whenever the target extent is larger than the sensor resolution, and it is large enough to occupy multiple resolution cells of the sensor. Put in other words, if a target should be classified as extended does not only depend on its physical size, but rather on the physical size relative to the sensor resolution.

The methods used to track extended objects are very similar to the ones used for tracking a group of targets moving in formation. Extended object tracking and group tracking is thoroughly described in e.g., Ristic et al. (2004). The bibliography Waxman and Drummond (2004) provides a comprehensive overview of existing literature in the area of group and cluster tracking. There exist some different approaches to represent, i.e. to model, the extended target, of which four methods are described in this section.

Point Features

The first and most traditional method is to model the target as a set of point features in a target reference frame, each of which may contribute at most one sensor measurement. The exact location of a feature in the target reference frame is often assumed uncertain. However, if the appearance of the target is known and especially if typical radar reflection points are known, then the location of the features in the target reference frame can be assumed known. The motion of an extended target is modeled through the process model in terms of the translation and rotation of the target reference frame relative to a world coordinate frame, see e.g., Dezert (1998).

For an application in two dimensions the point features are defined as

$$\mathbf{P}^T = \left\{ \boldsymbol{p}_i^T \right\}_{i=1}^{N_p} \quad \text{with} \quad \boldsymbol{p}_i^T = \begin{bmatrix} x_{p_i T}^T & y_{p_i T}^T \end{bmatrix}^{\mathrm{T}} \tag{4.6}$$

in the target's coordinate frame T. The position $\boldsymbol{d}_{TW}^W = \begin{bmatrix} x_{TW}^W & y_{TW}^W \end{bmatrix}^{\mathrm{T}}$ of the target's origin and the orientation ψ_T of the target's frame is tracked relative to the world coordinate frame. The state vector is defined as

$$\boldsymbol{x} = \begin{bmatrix} \boldsymbol{d}_{TW}^W & \psi_T & \dot{\boldsymbol{d}}_{TW}^W & \dot{\psi}_T & \mathbf{P}^W \end{bmatrix}^{\mathrm{T}}, \tag{4.7}$$

where the point features $\mathbf{P}^W = \left\{ \boldsymbol{p}_i^W \right\}_{i=1}^{N_p}$ are expressed with respect to the world coordinate frame W. The point features in the target's coordinate frame can be mapped into a point in the world frame, as they are defined in the state vector, through the transform

$$\boldsymbol{p}_i^W = R^{WT} \boldsymbol{p}_i^T + \boldsymbol{d}_{TW}^W, \tag{4.8}$$

where the rotation matrix R^{WT} was defined previously in (2.19).

The process model for the frame can for example be a constant velocity model, where the velocities are modeled as a first order Gaussian random walk. The uncertainty about

the exact position of the point feature is modeled according to

$$p(\mathbf{P}_t^W|\boldsymbol{d}_{TW}^W,\psi_T)=\prod_{i=1}^{N_p}\mathcal{N}(p_{i,t}^W|R^{WT}(\psi_T)p_i^T+\boldsymbol{d}_{TW}^W,w_pI_2), \tag{4.9}$$

which means that the uncertainty is assumed isotropic around the mean location of the point and with known variance w_p.

At each time step a set of N_y measurements $\mathbf{Y}=\{\boldsymbol{y}_i\}_{i=1}^{N_y}$ is received and has to be associated to the states. Not all measurements arise from a point feature, some are due to false detections (clutter). The association hypotheses are derived through some data association algorithm. In Vermaak et al. (2005) a method is proposed where the association hypotheses are included in the state vector and the output of the tracking filter is a joint posterior density function of the state vector and the association hypotheses. Furthermore, a multi-hypothesis likelihood is obtained by marginalizing over all the association hypotheses. An alternative solution is also proposed using a particle filter, where the unknown hypotheses are sampled from a well designed proposal density function.

An automotive radar sensor model developed for simulation purposes is proposed in Bühren and Yang (2006), where it is assumed that radar sensors often receive measurements from specific reflection centers on a vehicle. These reflection centers can be tracked in a filter and valuable information regarding the vehicle's orientation can be extracted as shown in Gunnarsson et al. (2007). A difficulty in solving the data association problem is the large number of association hypotheses available. To reduce the complexity Gunnarsson et al. (2007) propose an approach where detections are associated with reflector groups. The spatial Poisson distribution, discussed in the subsequent section, is considered to be inappropriate, since the number of vehicle detections is assumed essentially known and not adequately modeled by a Poisson process.

Spatial Distribution

Instead of modeling the target as a number of point features, which are assumed to be explicit measurement sources, the target is represented by a spatial probability distribution. It is more likely that a measurement comes from a region of high spatial density than from a sparse region. In Gilholm and Salmond (2005), Gilholm et al. (2005) it is assumed that the number of received target and clutter measurements are Poisson distributed, hence several measurements may originate from the same target. Each target related measurement is an independent sample from the spatial distribution. The spatial model could be a bounded distribution, such as a uniform pdf or an unbounded distribution, such as a Gaussian. The Poisson assumption allows the problem, or more specifically the evaluation of the likelihood, to be solved without association hypotheses. The spatial distribution is preferable where the point source models are poor representations of reality, that is in cases where the measurement generation is diffuse.

In Gilholm and Salmond (2005) two simple examples are given. One where the principle axis of the extended target is aligned with the velocity vector, i.e. a target is represented by a one dimensional uniform stick model. In the other example, a Gaussian mixture model is assumed for the target. A Kalman filter implementation with explicit constructions of assignment hypotheses is derived from the likelihood in Gilholm and Salmond

(2005), whereas in Gilholm et al. (2005), a particle filter is applied directly given the likelihood which is represented by the Poisson spatial model of the stick. Hence, the need to construct explicit measurement-target assignment hypotheses is avoided in Gilholm et al. (2005).

Boers et al. (2006) present a similar approach, but since raw data is considered, no data association hypotheses are needed. The method to use raw data, i.e. consider the measurements without applying a threshold, is referred to as track before detect. A one dimensional stick target is assumed also by Boers et al. (2006), but unlike Gilholm and Salmond (2005), the target extent is assumed unknown. The state vector is given by the stick's center position and velocity as well as the stick's extension according to

$$\boldsymbol{x} = \begin{bmatrix} x & y & \dot{x} & \dot{y} & L \end{bmatrix}^{\mathrm{T}}. \tag{4.10}$$

The process model is a simple constant velocity model and the length L is modeled as a random walk. The likelihood function is given by the probability distribution

$$p(\boldsymbol{y}|\boldsymbol{x}) = \int p(\boldsymbol{y}|\tilde{\boldsymbol{x}})p(\tilde{\boldsymbol{x}}|\boldsymbol{x})d\tilde{\boldsymbol{x}}, \tag{4.11}$$

where the spatial extension is modeled by the pdf $p(\tilde{\boldsymbol{x}}|\boldsymbol{x})$ and $\tilde{\boldsymbol{x}}$ is assumed to be a point source from an extended target with center given by the state vector $\boldsymbol{x}$. Hence, a measurement is received from a source $\tilde{\boldsymbol{x}}$ with likelihood $p(\boldsymbol{y}|\tilde{\boldsymbol{x}})$.

Elliptical Shaped Target

In many papers dealing with the shape of a target it is assumed that the sensor, e.g. radar, is also able to measure one or more dimensions of the target's extent. A high-resolution radar sensor may provide measurements of a targets down-range extent, i.e. the extension of the objects along the line-of-sight. The information of the target's extent is incorporated in the tracking filter and aids the tracking process to maintain track on the target when it is close to other objects.

An elliptical target model, to represent an extended target or a group of targets, is proposed in Drummond et al. (1990). The idea was improved by Salmond and Parr (2003), where the sensor not only provides measurements of point observations, but rather range, bearing and down-range extent. The prime motivation of the study is to aid track retention for closely spaced moving targets. Furthermore, the state vector includes the position, velocity and the size of the ellipse. An EKF is used in Salmond and Parr (2003), but it is concluded that the filter may diverge under certain conditions, since the relation between the down-range extent measurement of the target and the position and velocity coordinates in the state vector is highly nonlinear. The same problem is studied in Ristic and Salmond (2004), where a UKF is implemented and tested. Even though the UKF shows better performance it is concluded that neither the EKF nor the UKF are suitable for this problem. The problem is further studied by Angelova and Mihaylova (2008), where other filter techniques, based on Monte Carlo algorithms, are proposed. In this paper the size of the ellipse takes values from a set of standard values, i.e. the algorithm estimates the type of object from a list, under the assumption that typical target sizes are known.

A group of objects moving collectively may also be modeled as an extended target. The ellipse model is used to model a formation of aircraft in Koch (2008).

Line Shaped Target

In paper D the road borders are modeled as extended objects in the form of lines. A line is expressed as a third order polynomial in its coordinate frame. Since the road borders are assumed to be stationary, the frames are not included in the state vector. Furthermore, stationary points such as delineators and lamp posts are also modeled in paper D. The nearest neighbor algorithm is used to associate measurements from stationary observations $\mathcal{S}_m$ to the targets. Here it is assumed that an extended line target $\mathcal{L}_j$ can give rise to several measurements, but a point target $\mathcal{P}_i$ can only contribute to one measurement. Since the likelihood of a line $\ell_{\mathcal{S}_m\mathcal{L}_j}$ is a one dimensional spatial density function, but the likelihood of a point $\ell_{\mathcal{S}_m\mathcal{P}_i}$ is given by a two dimensional density function, a likelihood ratio test is applied to determine the measurement-to-track association problem. The likelihood ratio for a measurement $\boldsymbol{y}_{\mathcal{S}_m}$ is given by

$$\Lambda(\boldsymbol{y}_{\mathcal{S}_m}) \triangleq \frac{\ell_{\mathcal{S}_m\mathcal{P}_i}}{\ell_{\mathcal{S}_m\mathcal{L}_j}}. \tag{4.12}$$

The corresponding likelihood ratio test is

$$\Lambda(\boldsymbol{y}_{\mathcal{S}_m}) \underset{H_1}{\overset{H_0}{\gtrless}} \eta, \tag{4.13}$$

where H_0 and H_1 correspond to hypotheses that the measurement $\boldsymbol{y}_{\mathcal{S}_m}$ is associated to the point $\mathcal{P}_i$ and to the line $\mathcal{L}_j$, respectively. The threshold is selected as $\eta < 1$, since the density function of a point is two dimensional and the density function of a line is one dimensional. More theory about likelihood ratio test is given by e.g., van Trees (1968).

4.3 Estimating the Free Space using Radar

In this section three conceptually different methods to estimate stationary objects along the road, or more specifically to estimate the road borders, are introduced and compared. The first method considered in Section 4.3.1 is occupancy grid mapping, which discretizes the map surrounding the ego vehicle and the probability of occupancy is estimated for each grid cell. The second method applies a constrained quadratic program in order to estimate the road borders and is described in detail in Paper C. The problem is stated as a constrained curve fitting problem. The third method, described in Paper D and briefly introduced in Section 4.2.2, associates the radar measurements to extended stationary objects and tracks them as extended targets. This section is concluded in Section 4.3.2 by comparing the three approaches.

4.3.1 Occupancy Grid Map

The objective is to compute a map of the environment surrounding the ego vehicle using as few variables as possible. A map is defined over a continuous space and it can be discretized with, e.g. a grid approximation. The size of the map can be reduced to a certain area surrounding the ego vehicle. In order to keep a constant map size while the vehicle is moving, some parts of the map are thrown away and new parts are initiated.

Occupancy grid mapping (OGM) is one method for tackling the problem of generating consistent maps from noisy and uncertain data under the assumption that the ego vehicle pose, i.e. position and heading, is known. These maps are very popular in the robotics community, especially for all sorts of autonomous vehicles equipped with laser scanners. Indeed several of the DARPA urban challenge vehicles (Buehler et al., 2008a,b,c) used OGM's. This is because they are easy to acquire, and they capture important information for navigation. The OGM was introduced by Elfes (1987) and an early introduction is given by Moravec (1988). To the best of the author's knowledge, Borenstein and Koren (1991) were the first to utilize OGM for collision avoidance. Examples of OGM in automotive applications are given in Vu et al. (2007), Weiss et al. (2007). A solid treatment can be found in the recent textbook by Thrun et al. (2005).

This section begins with a brief introduction to occupancy grid maps, according to Thrun et al. (2005). Using this theory and a sensor with high resolution usually gives a nice looking bird eye's view map. However, since a standard automotive radar is used, producing only a few range and bearing measurements at every time sample, some modifications are introduced as described in the following sections.

Background

The planar map $\boldsymbol{m}$ is defined in the world coordinate frame W and is represented by a matrix. The goal of any occupancy grid mapping algorithm is to calculate the filtering probability density function of the map

$$p(\boldsymbol{m}|\boldsymbol{y}_{1:t}, \boldsymbol{x}_{\mathcal{E},1:t}), \tag{4.14}$$

where $\boldsymbol{m}$ denotes the map, $\boldsymbol{y}_{1:t} \triangleq \{\boldsymbol{y}_1, \ldots, \boldsymbol{y}_t\}$ denotes the set of all measurements up to time t, and $\boldsymbol{x}_{\mathcal{E},1:t}$ denotes the path of the ego vehicle defined through the discrete-time sequence of all previous positions. An occupancy grid map is partitioned into finitely many grid cells

$$\boldsymbol{m} = \{m_i\}_{i=1}^{N_m}. \tag{4.15}$$

The probability of a cell being occupied $p(m_i)$ is specified by a number ranging from 1 for occupied to 0 for free. The notation $p(m_i)$ will be used to refer to the probability that a grid cell is occupied. A disadvantage with this design is that it not enables to represent dependencies between neighboring cells.

The occupancy grid map was originally developed to primarily be used with measurements from a laser scanner. A laser is often mounted on a rotating shaft and generates a range measurement for every angular step of the mechanical shaft, i.e. a bearing angle. This means that the continuously rotating shaft produces many range and bearing measurements during every cycle. The OGM algorithms transform the polar coordinates of the measurements into Cartesian coordinates in a fixed world or map frame. After completing one mechanical measurement cycle the sensor provides the measurements for use.

The algorithm loops through all cells and increases the occupancy probability $p(m_i)$ if the cell was occupied according to the measurement $\boldsymbol{y}_t$. Otherwise the occupancy value either remains unchanged or is decreased, depending on if the range to the cell is greater or less than the measured range. The latter implies that the laser beam did pass this cell

without observing any obstacles. If the measured range is great or the cell size is small, it might be necessary to consider the angular spread of the laser beam and increase or decrease the occupancy probability of several cells with respect to the beam width.

The map is assumed not to be changed during sensing. Problems of this kind, where a state does not change over time are solved with binary Bayes filter, of which OGM is one example. In this case the state can either be free $m_i = 0$ or occupied $m_i = 1$. A standard technique to avoid numerical instabilities for probabilities close to 0 and to avoid truncation problems close to 0 and 1 is to use the log odds representation of occupancy

$$\ell_{i,t} = \log \frac{p(m_i|\boldsymbol{y}_{1:t}, \boldsymbol{x}_{\mathcal{E},1:t})}{1 - p(m_i|\boldsymbol{y}_{1:t}, \boldsymbol{x}_{\mathcal{E},1:t})}, \tag{4.16}$$

or put in words, the odds of a state is defined as the ratio of the probability of this event $p(m_i|\boldsymbol{y}_{1:t}, \boldsymbol{x}_{\mathcal{E},1:t})$ divided by the probability of its complement $1 - p(m_i|\boldsymbol{y}_{1:t}, \boldsymbol{x}_{\mathcal{E},1:t})$. The probabilities are easily recovered using

$$p(m_i|\boldsymbol{y}_{1:t}, \boldsymbol{x}_{\mathcal{E},1:t}) = 1 - \frac{1}{1 + \exp \ell_{i,t}}. \tag{4.17}$$

Note that the filter uses the inverse measurement model $p(\boldsymbol{m}|\boldsymbol{y}, \boldsymbol{x})$. Using Bayes' rule it can be shown that the binary Bayes filter in log odds form is

$$\ell_{i,t} = \ell_{i,t-1} + \log \frac{p(m_i|\boldsymbol{y}_t, \boldsymbol{x}_{\mathcal{E},t})}{1 - p(m_i|\boldsymbol{y}_t, \boldsymbol{x}_{\mathcal{E},t})} - \log \frac{p(m_i)}{1 - p(m_i)}, \tag{4.18}$$

where $p(m_i)$ represents the prior probability. The log odds ratio of the prior before processing any measurements is defined as

$$\ell_{i,0} = \log \frac{p(m_i)}{1 - p(m_i)}. \tag{4.19}$$

Typically $p(m_i) = 0.5$ is assumed, since before having measurements nothing is known about the surrounding environment. This value yields $\ell_0 = 0$.

OGM with Radar Measurements

The radar system provides range and bearing measurements for observed targets at every measurement cycle. The main difference to a laser is that there is not one range measurement for every angular position of the moving sensor. The number of observations depends on the environment. In general there are much fever observations compared to a laser sensor. There is also a limit on the number of objects transmitted by the radar equipment on the CAN-bus. Moving objects, which are distinguished by measurements of the Doppler shift, are prioritized and more likely to be transmitted than stationary objects. Furthermore, it is assumed that the opening angle of the radar beam is small compared to the grid cell size. With these the OGM algorithm was changed to loop through the measurements instead of the cells, in order to decrease the computational load. A radar's angular uncertainty is usually larger than its range uncertainty. When transforming the polar coordinates of the radar measurements into the Cartesian coordinates of the map, the uncertainties can either be transformed in the same manner or it can simply be assumed that the uncertainty increases with the range.

Experiments and Results

Figure 4.2a shows an OGM example of a highway situation. The ego vehicle's camera view is shown in Figure 4.2c. The size of the OGM is 401×401 m, with the ego vehicle in the middle cell. Each cell represents a 1×1 m square. The gray-level in the occupancy map indicates the probability of occupancy $p(\boldsymbol{m}|\boldsymbol{y}_{1:t}, \boldsymbol{x}_{\mathcal{E},1:t})$, the darker the grid cell, the more likely it is to be occupied. The map shows all major structural elements as they are visible at the height of the radar. This is a problem if the road is undulated and especially if the radar observes obstacles over and behind the guardrail. In this case the occupancy probability of a cell might be decreased even though it was previously believed to be occupied, since the cell is between the ego vehicle and the new observation. The impact of this problem can be reduced by tuning the filter well.

It is clearly visible in Figure 4.2a that the left border is sharper than the right. The only obstacle on the left side is the guardrail, which gives rise to the sharp edge, whereas on the right side there are several obstacles behind the guardrail, which also cause reflections, e.g. noise barrier and vegetation. A closer look in Figure 4.2b reveals that there is no black line of occupied cells representing the guardrail as expected. Instead there is a region with mixed probability of occupancy and after about 5 m the gray region with initial valued cells tell us that nothing is known about these cells.

In summary the OGM generates a good-looking overview of the traffic situation, but not much information for a collision avoidance system. Given the sparse radar measurements it is inefficient to represent the occupancy information as a rather huge square matrix with most of its elements equal to 0.5, which indicates that nothing is known about these cells.

4.3.2 Comparison of Free Space Estimation Approaches

The presented methods, i.e. the OGM in the previous section, the constrained curve fitting problem in Paper C and the extended stationary objects tracks in Paper D, do not depend on the fact that only one radar sensor is used. In fact it is straightforward to add more sensor information from additional sensors. In other words, the approach introduced here fits well within a future sensor fusion framework where additional sensors, such as cameras and additional radars, are incorporated.

The properties of the three approaches are compared and summarized below.

The results of the presented methods are better than expected, given the fact that only measurements delivered by standard automotive sensors are used. The main drawback of the presented methods is that the result can be unstable or erroneous if there are too few measurement points or if the measurements stem from other objects than the guardrail. However, the problem of having too few measurements or having measurements from the wrong objects is very hard to solve with any algorithm.

The representation form of the OGM is a square matrix with the log odds of each grid cell. Since most of the environment is unknown many of the matrix elements are equal to the initial log odds. In this example, a 401×401 matrix is used, implying that the environment is described by 160801 parameters. The number of parameters

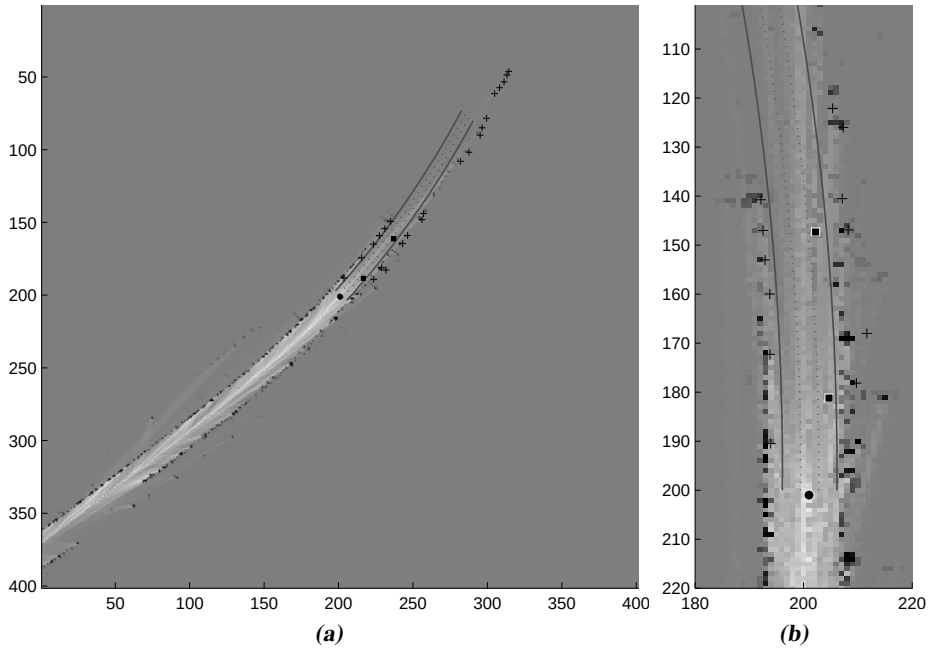

(c)

Figure 4.2: *The filled circle at position* $(201, 201)$ *in the occupancy grid map in Figure (a) is the ego vehicle, the* $+$ *are the radar observations obtained at this time sample, the black squares are the two leading vehicles that are currently tracked. Figure (b) shows a zoom of the OGM in front of the ego vehicle. The gray-level in the figure indicates the probability of occupancy, the darker the grid cell, the more likely it is to be occupied. The shape of the road is given as solid and dashed lines, calculated as described in Lundquist and Schön (2008b). The camera view from the ego vehicle is shown in Figure (c), the concrete walls, the guardrail and the pillar of the bridge are interesting landmarks. Furthermore, the two tracked leading vehicles are clearly visible in the right lane.*

used for the constrained curve fitting is 8 and 12 for the linear and nonlinear model, respectively. The start and endpoint of valid segments can be limited by the user, even though no vector with more than 100 elements was observed during the tests. A line modeling the extended objects is represented by 5 parameters and one coordinate frame which is defined by its position and heading, i.e. 3 parameters. The author observed at maximum 20 lines, adding up to 160 parameters. However, it is suggested that the user limits the number of lines to 10, adding up to 80 parameters.

The computational time does of course depend on the hardware on which the algorithm is implemented, but it is still worth comparing the proposed algorithms. The average computational times over a sequence of 1796 samples for the presented methods are given in Table 4.2. Note that the times given in this table include the complete algorithms, including initialization and coordinate frame transformations. The times given in Table 1 in Paper C only compare the optimization algorithms. All of the algorithms can be made more efficient by fine tuning the code. However, the potential of the extended object tracking is assumed to be highest. This is because time implicitly depends on the number of tracked objects, which can be reduced by merging tracks and associating measurements to fewer tracks.

Table 4.2: *Average computational time for one sample.*

Method	**Time [ms]**
Occupancy Grid Mapping, Section 4.3.1	14.9
Linear Predictor, Paper C	109.5
Nonlinear Predictor, Paper C	137.2
Extended Object Tracking, Paper D	28.6

The flexibility of the OGM and the extended object tracking must be said to be higher. The OGM is not tied to any form of the road border or the stationary objects. The extended objects can be modeled in various types of shapes. The constrained curve fitting problem is the least flexible in that it only models the left and right border lines.

5

Concluding Remarks

In the first part an overview of the basics behind the research reported in this thesis has been presented. This part also aims at explaining how the papers in Part II relate to each other and to the existing theory. A conclusion of the results is given in Section 5.1 and ideas for future work are discussed in Section 5.2.

5.1 Conclusion

The work presented in this thesis has dealt with the problem of estimating the motion of a vehicle and representing and estimating its surroundings, i.e. improving the situation awareness. The surroundings consist of other vehicles and stationary objects, as well as the shape and the geometry of the road. Here, a major part of the work is not only the estimation problem itself, but also the way in which to represent the environment, i.e. the mapping problem. Paper A is concerned with estimating the lane geometry, i.e. the lane markings are described by a polynomial and the coefficients are the states to estimate. This problem can be solved with a camera and computer vision, but by fusing the data obtained from the image processing with information about the ego vehicle's motion and the other vehicles' movement on the road, the road geometry estimate can be improved. The other vehicles are tracked primarily by using measurements from a radar. The motion of the ego vehicle is estimated by combining measurements from the vehicle's IMU, steering wheel angle sensor and wheel velocity sensors in a model based filter. The model is in this case the so called single track model or bicycle model, in which the tire road interaction plays a major role. This interaction can be considered as a constant parameter, which is estimated off-line in advance, or the parameter can be considered time varying and be estimated on-line while driving. This is the topic of Paper B.

The surroundings of a vehicle is more complicated than the shape of the lane markings. In this thesis three conceptually different methods to estimate the road borders and the stationary objects along the road are studied and compared. The first method consid-

ered in Section 4.3.1 is occupancy grid mapping, which discretizes the surroundings into a number of grid cells. The probability of occupancy is estimated for each grid cell using radar data regarding the position of the stationary objects. The second method, described in detail in Paper C, consists in a constrained quadratic program in order to estimate the road borders. The problem is formulated as a constrained curve fitting problem, and the road borders are represented as two polynomials. The third method, described in Paper D, associates the radar measurements to extended stationary objects in the form of curved lines and tracks these lines as extended targets.

The approaches have been evaluated on real data from both freeways and rural roads in Sweden. The results are encouraging and surprisingly good at times, not perfect but much more informative than the raw measurements. Problems typically occur when there are too few measurements or if the measurements stem from other objects than the road side objects.

5.2 Future Research

The radar and camera data used in this thesis is generally preprocessed. Nevertheless, the preprocessing is not covered in this thesis. Specifically, more effort can be spent on the image processing to increase the information content. For example within the area of odometry the estimate could be more accurate if the camera information is used in addition to the measurements in Example 1.1. This is called visual odometry and it would probably improve the estimate of the body side slip angles, especially during extreme maneuvers where the tire road interaction is strongly nonlinear. Since only one camera is used, the inverse depth parametrization introduced by Civera et al. (2008) is an interesting approach, see e.g., Schön and Roll (2009) for an automotive example on visual odometry. To verify the state estimates more accurate reference values are needed as well.

The stationary objects along the road are treated as extended targets in this thesis. This approach requires comprehensive data association. The probability hypothesis density (PHD) filter, based on a finite random set description of the targets is a newly developed approach to propagate the intensity of these sets of states in time, see e.g., Mahler (2003), Vo and Ma (2006), Erdinc et al. (2006). It is an elegant method that avoids the combinatorial problem that arises from data association in a multi-sensor multi-target framework. A first example of an intensity map describing the density of stationary targets along the road is shown in Figure 5.1. In this thesis only radar data has been used to estimate the position of stationary objects. However, the camera captures information about the objects along the road and this source of information should be better used.

Currently there is a lot of activity within the computer vision community to enable non-planar road models, making use of parametric models similar to the ones used in this paper. A very interesting avenue for future work is to combine the ideas presented in this thesis with information from a camera about the height differences on the road side within a sensor fusion framework. This would probably improve the estimates, especially in situations when there are too few radar measurements available.

Parameter and model uncertainty in general are not treated in this thesis. One important aspect is how to model the process noise, i.e. how it shall best be included into the process model. In all applications discussed in this thesis the process noise is assumed

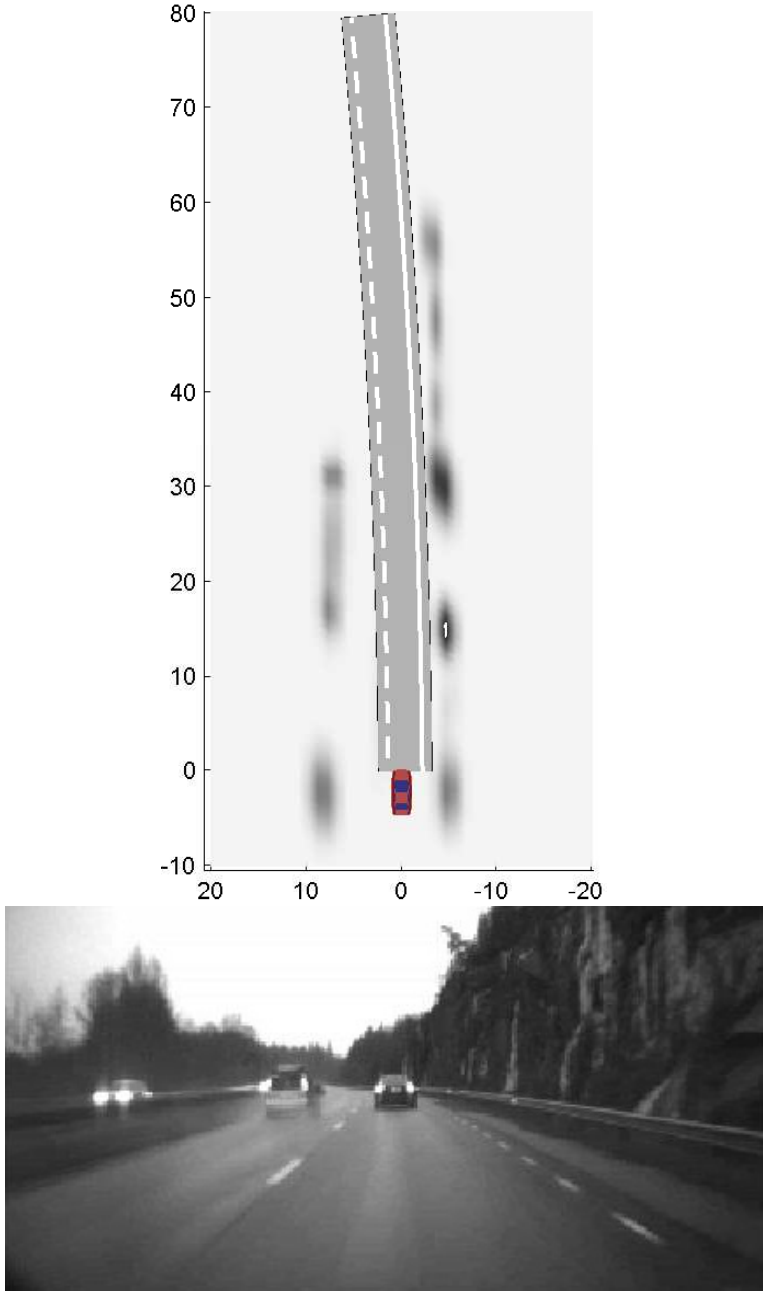

Figure 5.1: *Illustration of stationary target estimation. The intensity map of the PHD filter is illustrated using a gray scale, the darker the area, the higher the density of stationary targets. Here, only measurements from the radar are used. The photo shows the driver's view.*

additive. Can the state estimate computed in a filter be improved by modeling the process noise differently? Another aspect is how to treat bias and variance of the parameter $\boldsymbol{\theta}$. Bias and variance of $\boldsymbol{\theta}$ is propagated to a bias and a variance increase of the states $\boldsymbol{x}$. How can this impact on $\boldsymbol{x}$ be reduced? These two aspects are interesting and would improve many results if they are thoroughly considered.

Bibliography

Abdulle, A. and Wanner, G. (2002). 200 years of least squares method. *Elemente der Mathematik*, 57:45–60.

Adams, M., Wijesoma, W., and Shacklock, A. (2007). Autonomous navigation: Achievements in complex environments. *IEEE Instrumentation & Measurement Magazine*, 10(3):15–21.

Ahrholdt, M., Bengtsson, F., Danielsson, L., and Lundquist, C. (2009). SEFS – results on sensor data fusion system development. In *16th World Congress of ITS*, Stockholm, Sweden.

Anderson, B. D. O. and Moore, J. B. (1979). *Optimal Filtering*. Information and system science series. Prentice Hall, Englewood Cliffs, NJ, USA.

Angelova, D. and Mihaylova, L. (2008). Extended object tracking using Monte Carlo methods. *IEEE Transactions on Signal Processing*, 56(2):825–832.

Arulampalam, M. S., Maskell, S., Gordon, N., and Clapp, T. (2002). A tutorial on particle filters for online nonlinear/non-Gaussian Bayesian tracking. *IEEE Transactions on Signal Processing*, 50(2):174–188.

Bailey, T. and Durrant-Whyte, H. (2006). Simultaneous localization and mapping (SLAM): Part II. *IEEE Robotics & Automation Magazine*, 13(3):108–117.

Bar-Shalom, Y. and Fortmann, T. E. (1988). *Tracking and Data Association*. Mathematics in science and engineering. Academic Press, Orlando, FL, USA.

Bar-Shalom, Y., Rong Li, X., and Kirubarajan, T. (2001). *Estimation with Applications to Tracking and Navigation*. John Wiley & Sons, New York.

Bayes, T. (1763). An essay towards solving a problem in the doctrine of chances. *The Philosophical Transactions*, 53:370–418.

Behringer, R. (1997). *Visuelle Erkennung und Interpretation des Fahrspurverlaufes durch Rechnersehen für ein autonomes Straßenfahrzeug*, volume 310 of *Fortschrittsberichte VDI, Reihe 12*. VDI Verlag, Düsseldorf, Germany. Also as: PhD Thesis, Universität der Bundeswehr, 1996.

Bengtsson, F. (2008). *Models for Tracking in automotive safety systems*. Licentiate Thesis No R012/2008, Department of Signals and Systems, Chalmers University of Technology.

Bengtsson, F. and Danielsson, L. (2008). Designing a real time sensor data fusion system with application to automotive safety. In *15th World Congress of ITS*, New York, USA.

Bühren, M. and Yang, B. (2006). Simulation of automotive radar target lists using a novel approach of object representation. In *Proceedings of the IEEE Intelligent Vehicles Symposium*, pages 314–319.

Blackman, S. S. and Popoli, R. (1999). *Design and Analysis of Modern Tracking Systems*. Artech House, Inc., Norwood, MA, USA.

Boers, Y., Driessen, H., Torstensson, J., Trieb, M., Karlsson, R., and Gustafsson, F. (2006). Track-before-detect algorithm for tracking extended targets. In *IEE Proceedings on Radar and Sonar Navigation*, volume 153, pages 345–351.

Borenstein, J. and Koren, Y. (1991). The vector field histogram-fast obstacle avoidance for mobile robots. *IEEE Transactions on Robotics and Automation,*, 7(3):278–288.

Buehler, M., Iagnemma, K., and Singh, S., editors (2008a). Special Issue on the 2007 DARPA Urban Challenge, Part I, volume 25 (8). *Journal of Field Robotics*.

Buehler, M., Iagnemma, K., and Singh, S., editors (2008b). Special Issue on the 2007 DARPA Urban Challenge, Part II, volume 25 (9). *Journal of Field Robotics*.

Buehler, M., Iagnemma, K., and Singh, S., editors (2008c). Special Issue on the 2007 DARPA Urban Challenge, Part III, volume 25 (10). *Journal of Field Robotics*.

Cappe, O., Godsill, S., and Moulines, E. (2007). An overview of existing methods and recent advances in sequential Monte Carlo. *Proceedings of the IEEE*, 95(5):899–924.

Civera, J., Davison, A., and Montiel, J. (2008). Inverse depth parametrization for monocular SLAM. *IEEE Transactions on Robotics*, 24(5):932–945.

Danielsson, L. (2008). *Tracking Theory for Preventive Safety Systems*. Licentiate Thesis No R004/2008, Department of Signals and Systems, Chalmers University of Technology.

Dezert, J. C. (1998). Tracking maneuvering and bending extended target in cluttered environment. In *Proceedings of Signal and Data Processing of Small Targets*, volume 3373, pages 283–294. SPIE.

Dickmanns, E. (1988). Dynamic computer vision for mobile robot control. In *Proceedings of the 19th International Symposium on Industrial Robots*, Sydney, Australia.

Dickmanns, E. D. (2007). *Dynamic Vision for Perception and Control of Motion*. Springer, London, UK.

Dickmanns, E. D. and Mysliwetz, B. D. (1992). Recursive 3-D road and relative ego-state recognition. *IEEE Transactions on pattern analysis and machine intelligence*, 14(2):199–213.

Dickmanns, E. D. and Zapp, A. (1986). A curvature-based scheme for improving road vehicle guidance by computer vision. In *Proceedings of the SPIE Conference on Mobile Robots*, volume 727, pages 161–198, Cambridge, MA, USA.

Djuric, P. M., Kotecha, J. H., Zhang, J., Huang, Y., Ghirmai, T., Bugallo, M. F., and Miguez, J. (2003). Particle filtering. *Signal Processing Magazine, IEEE*, 20(5):19–38.

Drummond, O. E., Blackman, S. S., and Pretrisor, G. C. (1990). Tracking clusters and extended objects with multiple sensors. In Drummond, O. E., editor, *Proceedings of Signal and Data Processing of Small Targets*, volume 1305, pages 362–375. SPIE.

Durrant-Whyte, H. and Bailey, T. (2006). Simultaneous localization and mapping (SLAM): Part I. *IEEE Robotics & Automation Magazine*, 13(2):99–110.

Eidehall, A. (2007). *Tracking and threat assessment for automotive collision avoidance*. PhD thesis No 1066, Linköping Studies in Science and Technology, Linköping, Sweden.

Eidehall, A. and Gustafsson, F. (2006). Obtaining reference road geometry parameters from recorded sensor data. In *Proceedings of the IEEE Intelligent Vehicles Symposium*, pages 256–260, Tokyo, Japan.

Eidehall, A., Pohl, J., and Gustafsson, F. (2007). Joint road geometry estimation and vehicle tracking. *Control Engineering Practice*, 15(12):1484–1494.

Elfes, A. (1987). Sonar-based real-world mapping and navigation. *IEEE Journal of Robotics and Automation*, 3(3):249–265.

Erdinc, O., Willett, P., and Bar-Shalom, Y. (2006). A physical-space approach for the probability hypothesis density and cardinalized probability hypothesis density filters. In Drummond, O. E., editor, *Proceedings of Signal and Data Processing of Small Targets*, volume 6236, page 623619. SPIE.

Fisher, R. A. (1912). On an absolute criterion for fitting frequency curves. *Messenger of Mathematics*, 41:155–160.

Fisher, R. A. (1922). On the mathematical foundations of theoretical statistics. *Philosophical Transactions of the Royal Society Series A*, 222:309–368.

Gern, A., Franke, U., and Levi, P. (2000). Advanced lane recognition - fusing vision and radar. In *Proceedings of the IEEE Intelligent Vehicles Symposium*, pages 45–51, Dearborn, MI, USA.

Gern, A., Franke, U., and Levi, P. (2001). Robust vehicle tracking fusing radar and vision. In *Proceedings of the international conference of multisensor fusion and integration for intelligent systems*, pages 323–328, Baden-Baden, Germany.

Gilholm, K., Godsill, S., Maskell, S., and Salmond, D. (2005). Poisson models for extended target and group tracking. In Drummond, O. E., editor, *Proceedings of Signal and Data Processing of Small Targets*, volume 5913, page 59130R. SPIE.

Gilholm, K. and Salmond, D. (2005). Spatial distribution model for tracking extended objects. In *IEE Proceedings of Radar, Sonar and Navigation*, volume 152, pages 364–371.

Goodwin, G. C. and Sin, K. S. (1984). *Adaptive filtering prediction and control*. Prentice-Hall, Englewood Cliffs.

Gunnarsson, J. (2007). *Models and Algorithms - with applications to vehicle tracking and frequency estimation*. PhD thesis No 2628, Department of Signals and Systems, Chalmers University of Technology.

Gunnarsson, J., Svensson, L., Bengtsson, E., and Danielsson, L. (2006). Joint driver intention classification and tracking of vehicles. In *Nonlinear Statistical Signal Processing Workshop, 2006 IEEE*, pages 95–98.

Gunnarsson, J., Svensson, L., Danielsson, L., and Bengtsson, F. (2007). Tracking vehicles using radar detections. In *Proceedings of the IEEE Intelligent Vehicles Symposium*, pages 296–302, Istanbul, Turkey.

Gustafsson, F. (2000). *Adaptive Filtering and Change Detection*. John Wiley & Sons, New York, USA.

Gustafsson, F. (2009). Automotive safety systems. *Signal Processing Magazine, IEEE*, 26(4):32–47.

Hahn, H. (2002). *Rigid body dynamics of mechanisms. 1, Theoretical basis*, volume 1. Springer, Berlin, Germany.

Hendeby, G. (2008). *Performance and Implementation Aspects of Nonlinear Filtering*. PhD thesis No 1161, Linköping Studies in Science and Technology, Linköping, Sweden.

Jansson, J. (2005). *Collision Avoidance Theory with Applications to Automotive Collision Mitigation*. PhD thesis No 950, Linköping Studies in Science and Technology, Linköping, Sweden.

Jazwinski, A. H. (1970). *Stochastic processes and filtering theory*. Mathematics in science and engineering. Academic Press, New York, USA.

Johansson, K. H., Törngren, M., and Nielsen, L. (2005). Vehicle applications of controller area network. In Hristu-Varsakelis, D. and Levine, W. S., editors, *Handbook of Networked and Embedded Control Systems*, pages 741–765. Birkhäuser.

Julier, S. (2002). The scaled unscented transformation. In *Proceedings of the American Control Conference*, volume 6, pages 4555–4559.

Julier, S. and Uhlmann, J. (2002). Reduced sigma point filters for the propagation of means and covariances through nonlinear transformations. In *Proceedings of the American Control Conference*, volume 2, pages 887–892.

Julier, S., Uhlmann, J., and Durrant-Whyte, H. (1995). A new approach for filtering nonlinear systems. In *American Control Conference, 1995. Proceedings of the*, volume 3, pages 1628–1632.

Julier, S. J. and Uhlmann, J. K. (1997). New extension of the Kalman filter to nonlinear systems. In *Signal Processing, Sensor Fusion, and Target Recognition VI*, volume 3068, pages 182–193. SPIE.

Julier, S. J. and Uhlmann, J. K. (2004). Unscented filtering and nonlinear estimation. *Proceedings of the IEEE*, 92(3):401–422.

Kailath, T. (1980). *Linear systems*. Prentice Hall, Englewood Cliffs, NJ, USA.

Kailath, T., Sayed, A. H., and Hassibi, B. (2000). *Linear Estimation*. Information and System Sciences Series. Prentice Hall, Upper Saddle River, NJ, USA.

Kalman, R. E. (1960). A new approach to linear filtering and prediction problems. *Transactions of the ASME, Journal of Basic Engineering*, 82:35–45.

Kalman, R. E. and Bucy, R. S. (1961). New results in linear filtering and prediction theory. *Transactions of the ASME – Journal of Basic Engineering, Series 83D*, pages 95–108.

Karlsson, R. (2005). *Particle Filtering for Positioning and Tracking Applications*. PhD thesis No 924, Linköping Studies in Science and Technology, Linköping, Sweden.

Kay, S. M. (1993). *Fundamentals of Statistical Signal Processing, Volume I: Estimation Theory*. Prentice Hall Signal Processing. Prentice Hall, Upper Saddle River, NJ, USA.

Kiencke, U., Dais, S., and Litschel, M. (1986). Automotive serial controller area network. Technical Report 860391, SAE International Congress.

Kiencke, U. and Nielsen, L. (2005). *Automotive Control Systems*. Springer, Berlin, Heidelberg, Germany, second edition.

Koch, J. W. (2008). Bayesian approach to extended object and cluster tracking using random matrices. *IEEE Transactions on Aerospace and Electronic Systems*, 44(3):1042–1059.

Ljung, L. (1999). *System identification, Theory for the user*. System sciences series. Prentice Hall, Upper Saddle River, NJ, USA, second edition.

Ljung, L. (2009). *System identification toolbox 7 – user's guide*. MathWorks, Natick, Mass.

Ljung, L. and Söderström, T. (1983). *Theory and Practice of Recursive Identification*. The MIT Press series in Signal Processing, Optimization, and Control. The MIT Press, Cambridge, Massachusetts.

Lundquist, C. (2008). Method for stabilizing a vehicle combination. U.S. Patent US 2008196964, 2008.08.21 and German Patent DE 102007008342, 2008.08.21.

Lundquist, C. and Großheim, R. (2009). Method and device for determining steering angle information. International Patent WO 2009047020, 2009.04.16 and German Patent DE 102007000958, 2009.05.14.

Lundquist, C., Orguner, U., and Schön, T. B. (2009). Tracking stationary extended objects for road mapping using radar measurements. In *Proceedings of the IEEE Intelligent Vehicles Symposium*, pages 405–410, Xi'an, China.

Lundquist, C. and Reinelt, W. (2006a). Back driving assistant for passenger cars with trailer. In *Proceedings of the SAE World Congress*, SAE paper 2006-01-0940, Detroit, MI, USA.

Lundquist, C. and Reinelt, W. (2006b). Rückwärtsfahrassistent für PKW mit Aktive Front Steering. In *Proceedings of the AUTOREG (Steuerung und Regelung von Fahrzeugen und Motoren*, VDI Bericht 1931, pages 45–54, Wiesloch, Germany.

Lundquist, C. and Reinelt, W. (2006c). Verfahren zur Überwachung der Rotorlage eines Elektromotors. German Patent DE 102005016514, 2006.10.12.

Lundquist, C. and Schön, T. B. (2008a). Joint ego-motion and road geometry estimation. *Submitted to Information Fusion*.

Lundquist, C. and Schön, T. B. (2008b). Road geometry estimation and vehicle tracking using a single track model. In *Proceedings of the IEEE Intelligent Vehicles Symposium*, pages 144–149, Eindhoven, The Netherlands.

Lundquist, C. and Schön, T. B. (2009a). Estimation of the free space in front of a moving vehicle. In *Proceedings of the SAE World Congress*, SAE paper 2009-01-1288, Detroit, MI, USA.

Lundquist, C. and Schön, T. B. (2009b). Recursive identification of cornering stiffness parameters for an enhanced single track model. In *Proceedings of the 15th IFAC Symposium on System Identification*, pages 1726–1731, Saint-Malo, France.

Mahler, R. (2003). Multitarget Bayes filtering via first-order multitarget moments. *IEEE Transactions on Aerospace and Electronic Systems*, 39(4):1152–1178.

Malinen, S., Lundquist, C., and Reinelt, W. (2006). Fault detection of a steering wheel sensor signal in an active front steering system. In *Preprints of the IFAC Symposium on SAFEPROCESS*, pages 547–552, Beijing, China.

Mitschke, M. and Wallentowitz, H. (2004). *Dynamik der Kraftfahrzeuge*. Springer, Berlin, Heidelberg, 4th edition.

Moravec, H. (1988). Sensor fusion in certainty grids for mobile robots. *AI Magazine*, 9(2):61–74.

Pacejka, H. B. (2006). *Tyre and Vehicle Dynamics*. Elsevier, Amsterdam, second edition.

Reimann, G. and Lundquist, C. (2008). Verfahren zum Betrieb eines elektronisch geregelten Servolenksystems. German Patent DE 102006053029, 2008.05.15.

Reinelt, W., Klier, W., Reimann, G., Lundquist, C., Schuster, W., and Großheim, R. (2004). Active front steering for passenger cars: System modelling and functions. In *Proceedings of the first IFAC Symposium on Advances in Automotive Control*, Salerno, Italy.

Reinelt, W. and Lundquist, C. (2005). Observer based sensor monitoring in an active front steering system using explicit sensor failure modeling. In *Proceedings of the 16th IFAC World Congress*, Prague, Czech Republic.

Reinelt, W. and Lundquist, C. (2006a). Controllability of active steering system hazards: From standards to driving tests. In Pimintel, J. R., editor, *Safety Critical Automotive Systems*, ISBN 13: 978-0-7680-1243-9, pages 173–178. SAE International, 400 Commonwealth Drive, Warrendale, PA, USA.

Reinelt, W. and Lundquist, C. (2006b). Mechatronische Lenksysteme: Modellbildung und Funktionalität des Active Front Steering. In Isermann, R., editor, *Fahrdynamik Regelung - Modellbildung, Fahrassistenzsysteme, Mechatronik*, ISBN 3-8348-0109-7, pages 213–236. Vieweg Verlag.

Reinelt, W. and Lundquist, C. (2007). Method for assisting the driver of a motor vehicle with a trailer when reversing. German Patent DE 102006002294, 2007.07.19, European Patent EP 1810913, 2007.07.25 and Japanese Patent JP 2007191143, 2007.08.02.

Reinelt, W., Lundquist, C., and Johansson, H. (2005). On-line sensor monitoring in an active front steering system using extended Kalman filtering. In *Proceedings of the SAE World Congress*, SAE paper 2005-01-1271, Detroit, MI, USA.

Reinelt, W., Lundquist, C., and Malinen, S. (2007). Automatic generation of a computer program for monitoring a main program to provide operational safety. German Patent DE 102005049657, 2007.04.19.

Reinelt, W., Schuster, W., Großheim, R., and Lundquist, C. (2008a). Verfahren zum Betrieb eines elektronisch geregelten Servolenksystems. German Patent DE 102006040443, 2008.03.06.

Reinelt, W., Schuster, W., Großheim, R., and Lundquist, C. (2008b). Verfahren zum Betrieb eines elektronischen Servolenksystems. German Patent DE 102006043069, 2008.03.27.

Reinelt, W., Schuster, W., Großheim, R., and Lundquist, C. (2008c). Verfahren zum Betrieb eines Servolenksystems. German Patent DE 102006052092, 2008.05.08.

Reinelt, W., Schuster, W., Großheim, R., and Lundquist, C. (2008d). Verfahren zum Betrieb eines Servolenksystems. German Patent DE 102006041237, 2008.03.06.

Reinelt, W., Schuster, W., Großheim, R., and Lundquist, C. (2008e). Verfahren zum Betrieb eines Servolenksystems. German Patent DE 102006041236, 2008.03.06.

Ristic, B., Arulampalam, S., and Gordon, N. (2004). *Beyond the Kalman Filter: Particle filters for tracking applications*. Artech House, London, UK.

Ristic, B. and Salmond, D. J. (2004). A study of a nonlinear filtering problem for tracking an extended target. In *Proceedings of the 7th International Conference on Information Fusion*, Stockholm, Sweden.

Robert Bosch GmbH, editor (2004). *Automotive Handbook*. SAE Society of Automotive Engineers, 6th edition.

Rong Li, X. and Jilkov, V. (2001). Survey of maneuvering target tracking: Part III. Measurement models. In *Proceedings of Signal and Data Processing of Small Targets*, volume 4473, pages 423–446. SPIE.

Rong Li, X. and Jilkov, V. (2003). Survey of maneuvering target tracking: Part I. Dynamic models. *IEEE Transactions on Aerospace and Electronic Systems*, 39(4):1333–1364.

Rugh, W. J. (1996). *Linear System Theory*. Information and system sciences series. Prentice Hall, Upper Saddle River, NJ, USA, second edition.

Salmond, D. and Parr, M. (2003). Track maintenance using measurements of target extent. In *IEE Proceedings on Radar and Sonar Navigation*, volume 150, pages 389–395.

Schmidt, S. F. (1966). Application of state-space methods to navigation problems. *Advances in Control Systems*, 3:293–340.

Schön, T. B. and Roll, J. (2009). Ego-motion and indirect road geometry estimation using night vision. In *Proceedings of the IEEE Intelligent Vehicles Symposium*, pages 30–35.

Schofield, B. (2008). *Model-Based Vehicle Dynamics Control for Active Safety*. PhD thesis, Department of Automatic Control, Lund University, Sweden.

Schön, T. B. (2006). *Estimation of Nonlinear Dynamic Systems – Theory and Applications*. PhD thesis No 998, Linköping Studies in Science and Technology, Department of Electrical Engineering, Linköping University, Sweden.

Schön, T. B., Eidehall, A., and Gustafsson, F. (2006). Lane departure detection for improved road geometry estimation. In *Proceedings of the IEEE Intelligent Vehicle Symposium*, pages 546–551, Tokyo, Japan.

Schön, T. B., Gustafsson, F., and Nordlund, P.-J. (2005). Marginalized particle filters for mixed linear/nonlinear state-space models. *IEEE Transactions on Signal Processing*, 53(7):2279–2289.

Schön, T. B., Törnqvist, D., and Gustafsson, F. (2007). Fast particle filters for multi-rate sensors. In *Proceedings of the 15th European Signal Processing Conference*, Poznań, Poland.

Smith, G. L., Schmidt, S. F., and McGee, L. A. (1962). Application of statistical filter theory to the optimal estimation of position and velocity on board a circumlunar vehicle. Technical Report TR R-135, NASA.

Svensson, D. (2008). *Multiple Model Filtering and Data Association with Application to Ground Target Tracking*. Licentiate Thesis No R017/2008, Department of Signals and Systems, Chalmers University of Technology.

Svensson, L. and Gunnarsson, J. (2006). A new motion model for tracking of vehicles. In *Proceedings of the 14th IFAC Symposium on System Identification*, Newcastle, Australia.

Thrun, S. (2002). Robotic mapping: A survey. In *Exploring Artificial Intelligence in the New Millenium*. Morgan Kaufmann.

Thrun, S., Burgard, W., and Fox, D. (2005). *Probabilistic Robotics*. Intelligent Robotics and Autonomous Agents. The MIT Press, Cambridge, MA, USA.

van Trees, H. L. (1968). *Detection, Estimation, and Modulation Theory*. John Wiley & Sons, New York, USA.

Vermaak, J., Ikoma, N., and Godsill, S. J. (2005). Sequential Monte Carlo framework for extended object tracking. *IEE Proceedings of Radar, Sonar and Navigation*, 152(5):353–363.

VGU (2004a). *Vägar och gators utformning – Grundvärden*. Vägverket, Swedish Road Administration, Borlänge, Sweden. 2004:80.

VGU (2004b). *Vägar och gators utformning – Landsbygd - Vägrum*. Vägverket, Swedish Road Administration, Borlänge, Sweden. 2004:80.

Vo, B.-N. and Ma, W.-K. (2006). The Gaussian mixture probability hypothesis density filter. *IEEE Transactions on Signal Processing*, 54(11):4091–4104.

Vu, T. D., Aycard, O., and Appenrodt, N. (2007). Online localization and mapping with moving object tracking in dynamic outdoor environments. In *Proceedings of the IEEE Intelligent Vehicles Symposium*, pages 190–195.

Waxman, M. J. and Drummond, O. E. (2004). A bibliography of cluster (group) tracking. In *Proceedings of Signal and Data Processing of Small Targets*, volume 5428, pages 551–560. SPIE.

Weiss, T., Schiele, B., and Dietmayer, K. (2007). Robust driving path detection in urban and highway scenarios using a laser scanner and online occupancy grids. In *Proceedings of the IEEE Intelligent Vehicles Symposium*, pages 184–189.

Wong, J. (2001). *Theory Of Ground Vehicles*. John Wiley & Sons, New York, USA, third edition.

Zomotor, Z. and Franke, U. (1997). Sensor fusion for improved vision based lane recognition and object tracking with range-finders. In *Proceedings of IEEE Conference on Intelligent Transportation System*, pages 595–600, Boston, MA, USA.

Part II

Publications

Paper A

Joint Ego-Motion and Road Geometry Estimation

Authors: Christian Lundquist and Thomas B. Schön.

Edited version of paper originally submitted to *Information Fusion, Special Issue on Information Fusion for Cognitive Automobiles.*

Edited version of paper originally published in *Proceedings of the IEEE Intelligent Vehicle Symposium*, pages 144-149, Eindhoven, The Netherlands, 2008.

Preliminary version published as Technical Report LiTH-ISY-R-2844, Department of Electrical Engineering, Linköping University, Linköping, Sweden.

Joint Ego-Motion and Road Geometry Estimation

Christian Lundquist and Thomas B. Schön

Department of Electrical Engineering,
Linköping University,
SE–581 83 Linköping, Sweden.
E-mail: (lundquist, schon)@isy.liu.se.

Abstract

We provide a sensor fusion framework for solving the problem of joint ego-motion and road geometry estimation. More specifically we employ a sensor fusion framework to make systematic use of the measurements from a forward looking radar and camera, steering wheel angle sensor, wheel speed sensors and inertial sensors to compute good estimates of the road geometry and the motion of the ego vehicle on this road. In order to solve this problem we derive dynamical models for the ego vehicle, the road and the leading vehicles. The main difference to existing approaches is that we make use of a new dynamic model for the road. An extended Kalman filter is used to fuse data and to filter measurements from the camera in order to improve the road geometry estimate. The proposed solution has been tested and compared to existing algorithms for this problem, using measurements from authentic traffic environments on public roads in Sweden. The results clearly indicate that the proposed method provides better estimates.

Keywords: sensor fusion, single track model, bicycle model, road geometry estimation, extended Kalman filter.

1 Introduction

We are in this paper concerned with the problem of integrated ego-motion and road geometry estimation using information from several sensors. The sensors used to this end are a forward looking camera and radar, together with inertial sensors, a steering wheel sensor and wheel speed sensors. The solution is obtained by casting the problem within an existing sensor fusion framework. An important part of this solution is the nonlinear state-space model. The state-space model contains the dynamics of the ego vehicle, the

road geometry, the leading vehicles and the measurement relations. It can then be written in the form

$$\boldsymbol{x}_{t+1} = f(\boldsymbol{x}_t, \boldsymbol{u}_t) + \boldsymbol{w}_t, \tag{1a}$$

$$\boldsymbol{y}_t = h(\boldsymbol{x}_t, \boldsymbol{u}_t) + \boldsymbol{e}_t, \tag{1b}$$

where $\boldsymbol{x}_t \in \mathbb{R}^{n_x}$ denotes the state vector, $\boldsymbol{u}_t \in \mathbb{R}^{n_u}$ denotes the input signals, $\boldsymbol{y}_t \in \mathbb{R}^{n_y}$ denotes the measurements, $\boldsymbol{w}_t \in \mathbb{R}^{n_w}$ and $\boldsymbol{e}_t \in \mathbb{R}^{n_e}$ denote the process and measurement noise, respectively. The process model equations, describing the evolution of the state over time are denoted by $f : \mathbb{R}^{n_x} \times \mathbb{R}^{n_u} \to \mathbb{R}^{n_x}$. Furthermore, the measurement model describing how the measurements from the vision system, the radar and the inertial sensors relate to the state is given by $h : \mathbb{R}^{n_x} \times \mathbb{R}^{n_u} \to \mathbb{R}^{n_y}$. When we have a model in the form (1) we have transformed the problem into a standard nonlinear state estimation problem, where the task is to compute estimates of the state based on the information in the measurements. There are many different ways of solving this problem and we will in this work make use of the popular Extended Kalman Filter (EKF), described by e.g. Smith et al. (1962), Schmidt (1966), Anderson and Moore (1979).

The problem studied in this paper is by no means new, it is the proposed solution that is new. For some early, still very interesting and relevant work on this problem we refer to Dickmanns and Zapp (1986), Dickmanns and Mysliwetz (1992). From the camera we can produce estimates of the road geometry based on measurements of the lane markings. This problem is by now rather mature, see e.g. the survey by McCall and Trivedi (2006) and the recent book by Dickmanns (2007) for solid accounts. The next step in the development was to make use of the radar information as well. Using radar measurements we can track the leading vehicles, that is, we can estimate the position and velocity of the leading vehicles. Under the assumption that the leading vehicles drive on the same road as the ego vehicle, their positions contain valuable information about the road geometry. This idea was introduced by Zomotor and Franke (1997), Gern et al. (2000, 2001) and has been further refined by Eidehall et al. (2007), Eidehall (2007). The combination of radar and vision as well as the advantages and disadvantages of these sensors are discussed by Hofmann et al. (2000, 2003). Furthermore, the ego vehicle model used by Hofmann et al. (2000, 2003) is comparable with the one used in the present work. The four wheel speeds are used to estimate the path of the ego vehicle, which unlike the present work is separated from the leading vehicles dynamics and the lane estimate.

The leading vehicles are used to improve the road geometry in the present work; however the opposite is also possible as the recent work by Schubert et al. (2009), Weigel et al. (2009) shows, where the vehicle detection algorithm benefits from the lane information. Vision and radar are used by Schubert et al. (2009), whereas vision and lidar are used by Weigel et al. (2009). Muller et al. (2009) used lidar to detect the leading vehicle, and the movement of the leading vehicle is then used to estimate the lane and the driven path, which in turn is used to autonomously follow this vehicle. This works well even for curved and narrow roads. Unmarked and winding rural roads may be hard to detect, recent research in this area is presented by Loose et al. (2009), where stereo vision and image radar are used within a marginalized particle filter to obtain 3D information and improve the task of lane recognition. Information obtained from road-side structures may be used to improve the estimate of the lane shape and the position of the vehicle within the lane, as showed by Watanabe et al. (2009), where only a monocular camera is used.

Furthermore, at construction sites it is hard to identify the temporary lanes, a method for this using color images and beacon extraction is presented by Gumpp et al. (2009). Wedel et al. (2008) present an algorithm for free space estimation, capable of handling non-planar roads, using a stereo camera system.

Lane tracking has also been tackled using radar sensors, see e.g. Kaliyaperumal et al. (2001), Lakshmanan et al. (1997), Nikolova and Hero (2000), Ma et al. (2000) and laser sensors, see e.g. Wijesoma et al. (2004). There have been several approaches making use of reflections from the road boundary, such as crash barriers and reflection posts, to compute information about the free space, see e.g. Kirchner and Heinrich (1998), Kirchner and Ameling (2000), Sparbert et al. (2001) for some examples using laser scanners and Lundquist et al. (2009), where radar is used.

To summarize, our approach is able to improve the performance by making use of a dynamic model of the ego vehicle and a new dynamic model of the road at the same time as we make use of the motion of the leading vehicles. The new road process model describes the curvature of the ego vehicle's currently driven path. This should be compared with existing road models, used in most of the publications mentioned above, where the road's curvature is modeled according to road construction standards. The advantage of our new road model is that we are able to directly include information of the ego vehicles motion into the estimate of the road geometry.

In the subsequent section we provide a brief introduction to the sensor fusion framework we work with and explain how the present problem fits into this framework. An essential part of this framework is the dynamical model (1a), which is derived in Section 3. Furthermore, the corresponding measurement model (1b) is introduced in Section 4. In Section 5 the proposed solution is evaluated using measurements from real and relevant traffic environments from public roads in Sweden. Finally, the conclusions are given in Section 6. For convenience we provide a list of the relevant notation in the appendix.

2 Sensor Fusion

In order to successfully solve the problem under study in this work it is imperative to have a good understanding of sensor fusion. Sensor fusion is defined as the process of using information from *several different sensors* to compute an *estimate* of the state of a *dynamical system*.

We need a dynamic model and a measurement model in the form (1) in order to be able to produce an estimate of the state. These models are derived in detail in Section 3 and Section 4. However, for the sake of the present discussion we will briefly discuss the model here. The state vector $\boldsymbol{x}_t$ consists of three parts according to

$$\boldsymbol{x}_t = \begin{bmatrix} \boldsymbol{x}_{\mathcal{E},t} \\ \boldsymbol{x}_{\mathcal{R},t} \\ \boldsymbol{x}_{\mathcal{T},t} \end{bmatrix}, \tag{2}$$

where $\boldsymbol{x}_{\mathcal{E},t}$ denotes the state of the ego vehicle, $\boldsymbol{x}_{\mathcal{R},t}$ denotes the state of the road and $\boldsymbol{x}_{\mathcal{T},t}$ denotes the state of one leading vehicle (also referred to as a target). In deriving the evolution of these states over time we will end up with continuous-time differential

equations in the form

$$\dot{\boldsymbol{x}}(t) = f(\boldsymbol{x}(t), \boldsymbol{u}(t)). \tag{3}$$

However, according to (1) we required the model to be in discrete time. The simplest way of obtaining a difference equation from (3) is to make use of the standard forward Euler method, which approximates (3) according to

$$\boldsymbol{x}_{t+T} = \boldsymbol{x}_t + Tf(\boldsymbol{x}_t, \boldsymbol{u}_t) \triangleq g(\boldsymbol{x}_t, \boldsymbol{u}_t), \tag{4}$$

where T denotes the sample time. The measurement model is of course already in discrete time.

The *estimate* of the state is computed by a state estimator of some kind. This state estimator makes use of the measurements from the different sensors to produce an estimate of the so called filtering probability density function (pdf) $p(\boldsymbol{x}_t|\boldsymbol{y}_{1:t})$, where $\boldsymbol{y}_{1:t} \triangleq \{\boldsymbol{y}_i\}_{i=1}^t$ denotes all the measurements from time 1 to time t. This density function contains all there is to know about the state $\boldsymbol{x}_t$, given the information in the measurements $\boldsymbol{y}_{1:t}$. Once an approximation of $p(\boldsymbol{x}_t|\boldsymbol{y}_{1:t})$ is available it can be used to form many different estimates and the most commonly used estimate is the conditional mean estimate

$$\hat{\boldsymbol{x}}_{t|t} = \mathrm{E}(\boldsymbol{x}_t|\boldsymbol{y}_{1:t}). \tag{5}$$

This estimate will be used in the present work as well.

Since we are looking for an algorithm capable of working in real-time it is important to understand how the filtering pdf evolves over time. Now, it is well-known (see e.g. Jazwinski (1970)) that a sequential solution can be obtained according to

$$p(\boldsymbol{x}_t|\boldsymbol{y}_{1:t}) = \frac{p(\boldsymbol{y}_t|\boldsymbol{x}_t)p(\boldsymbol{x}_t|\boldsymbol{y}_{1:t-1})}{\int p(\boldsymbol{y}_t|\boldsymbol{x}_t)p(\boldsymbol{x}_t|\boldsymbol{y}_{1:t-1})d\boldsymbol{x}_t}, \tag{6a}$$

$$p(\boldsymbol{x}_{t+1}|\boldsymbol{y}_{1:t}) = \int p(\boldsymbol{x}_{t+1}|\boldsymbol{x}_t)p(\boldsymbol{x}_t|\boldsymbol{y}_{1:t})d\boldsymbol{x}_t. \tag{6b}$$

Here, it is also worth mentioning that since we have assumed additive noise in the model (1), we have explicit expressions for $p(\boldsymbol{x}_{t+1}|\boldsymbol{x}_t)$ and $p(\boldsymbol{y}_t|\boldsymbol{x}_t)$ according to

$$p(\boldsymbol{x}_{t+1}|\boldsymbol{x}_t) = p_{\boldsymbol{w}_t}(\boldsymbol{x}_{t+1} - f(\boldsymbol{x}_t, \boldsymbol{u}_t)), \tag{7a}$$

$$p(\boldsymbol{y}_t|\boldsymbol{x}_t) = p_{\boldsymbol{e}_t}(\boldsymbol{y}_t - h(\boldsymbol{x}_t, \boldsymbol{u}_t)), \tag{7b}$$

where $p_{\boldsymbol{w}_t}(\,\cdot\,)$ and $p_{\boldsymbol{e}_t}(\,\cdot\,)$ denote the pdf's for the process and the measurement noise, respectively.

In the special case, where the equations in the model (1) are linear and the noise is Gaussian, the multidimensional integrals in (6) allows for an analytical solution, the Kalman filter (Kalman, 1960). For a derivation of this kind, see e.g. Schön (2006). However, the problem is that for the general nonlinear, non-Gaussian case that we are facing, there does not exist any closed form solution to (6). Hence, we are forced to make approximations of some kind. The most commonly used approximation is provided by the extended Kalman filter (EKF). The idea underlying the EKF is very simple, approximate the nonlinear model with a linear model subject to Gaussian noise and apply the Kalman

filter to this approximation. For a solid account of the EKF we refer to Anderson and Moore (1979), Kailath et al. (2000). Lately the so called particle filter, introduced by Gordon et al. (1993), has become increasingly popular. This filter often provides a better solution, but it typically requires much more computational effort. For the present application the EKF provides an approximation that is good enough. For a more thorough account of the framework for nonlinear estimation briefly introduced above we refer to Schön (2006).

Before we end our brief overview on the sensor fusion problem it is important to stress that a successful sensor fusion framework will, besides the modeling and filtering parts mentioned above, rely on a certain surrounding infrastructure. This surrounding infrastructure deals with issues such as time synchronization between the various sensors, calibration, sensor-near signal processing, track handling, etc. This part of the framework should not be overlooked and a solid treatment of the provided infrastructure is accounted for by Bengtsson and Danielsson (2008) for the problem at hand. Despite this it is worth mentioning that the leading vehicles are incorporated into the estimation problem using rather standard techniques from target tracking, such as nearest neighbor data association and track counters in order to decide when to stop tracking a certain vehicle, etc. These are all important parts of the system we have implemented, but it falls outside the scope of this paper and since the techniques are rather standard we simply refer to the general treatments given in e.g. Blackman and Popoli (1999), Bar-Shalom et al. (2001).

3 Dynamic Models

As mentioned in the introduction our sensor fusion framework needs a state-space model describing the dynamics of the ego vehicle, the road and the leading vehicles. In this section we will derive the differential equations describing the motion of the ego vehicle (Section 3.2), the road (Section 3.3) and the leading vehicles (Section 3.4), also referred to as targets. Finally, in Section 3.5 we summarize these equations and form the process model of the state-space model. However, before we embark on deriving these equations we introduce the overall geometry and some necessary notation in Section 3.1.

3.1 Geometry and Notation

The coordinate frames describing the ego vehicle and one leading vehicle are defined in Figure 1. The inertial world reference frame is denoted by W and its origin is O_W. The ego vehicle's coordinate frame E is located in the center of gravity (CoG) and E_s is at the vision and radar sensor of the ego vehicle. Furthermore, T_i is associated with the observed and tracked leading vehicle i and its origin O_{T_i} is located at the leading vehicle. In this work we will use the planar coordinate transformation matrix

$$R^{WE} = \begin{bmatrix} \cos\psi_E & -\sin\psi_E \\ \sin\psi_E & \cos\psi_E \end{bmatrix} \tag{8}$$

to transform a vector, represented in E, into a vector, represented in W, where the yaw angle of the ego vehicle ψ_E is the angle of rotation from W to E. The geometric displacement vector $\boldsymbol{d}^W_{EW}$ is the direct straight line from O_W to O_E represented with respect

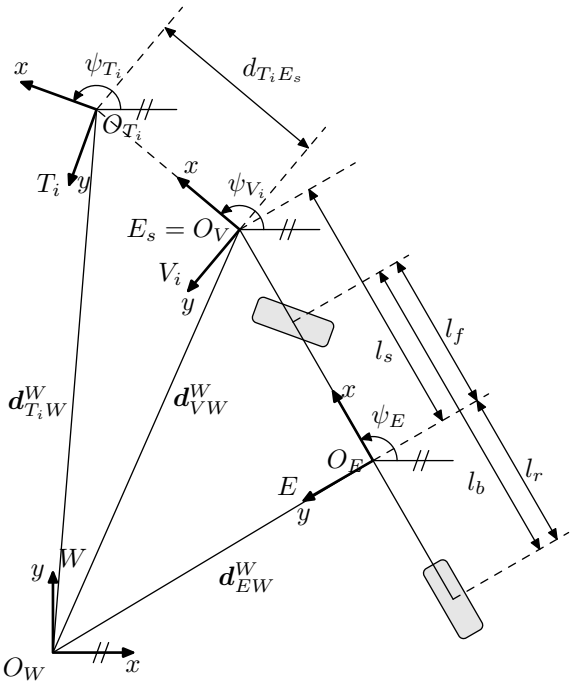

Figure 1: *Coordinate frames describing the ego vehicle, with center of gravity in O_E and the radar and camera sensors mounted in E_s. One leading vehicle is positioned in O_{T_i}.*

to the frame W. Velocities are defined as the movement of a frame E relative to the inertial reference frame W, but typically resolved in the frame E, for example v_x^E is the velocity of the E frame in its x-direction. The same convention holds for the acceleration a_x^E. In order to simplify the notation we leave out E when referring to the ego vehicle's velocity and acceleration. This notation will be used when referring to the various coordinate frames. However, certain frequently used quantities will be renamed, in the interest of readability. The measurements are denoted using superscript m. Furthermore, the notation used for the rigid body dynamics is in accordance with Hahn (2002).

3.2 Ego Vehicle

We will only be concerned with the ego vehicle motion during normal driving situations and not at the adhesion limit. This implies that the single track model is sufficient for the present purposes. This model is also referred to as the bicycle model, see e.g. Mitschke and Wallentowitz (2004), Wong (2001) for a solid treatment. The geometry of the single track model with slip angles is shown in Figure 2. It is here worth to point out that the velocity vector of the ego vehicle is typically not in the same direction as the longitudinal axis of the ego vehicle. Instead the vehicle will move along a path at an angle β with the

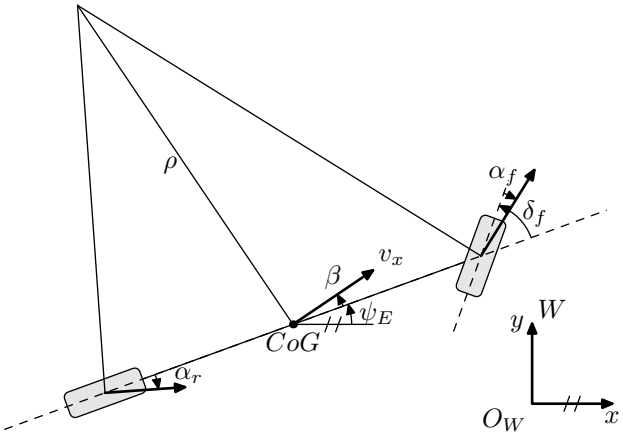

Figure 2: *In the single track model the wheels on each axle are modeled as single units. The velocity vector v_x, with the float angle β to the longitudinal axis of the vehicle, is attached at the center of gravity. Furthermore, the wheel slip angles are referred to as α_f and α_r. The front wheel angle is denoted by δ_f and the current radius is denoted by ρ.*

longitudinal direction of the vehicle. Hence, the angle β is defined as,

$$\tan\beta = \frac{v_y}{v_x}, \tag{9}$$

where v_x and v_y are the ego vehicle's longitudinal and lateral velocity components, respectively. This angle β is referred to as the float angle (Robert Bosch GmbH, 2004) or the vehicle body side slip angle (Kiencke and Nielsen, 2005).

The slip angle α_i is defined as the angle between the central axis of the wheel and the path along which the wheel moves. The phenomenon of side slip is mainly due to the lateral elasticity of the tire. For reasonably small slip angles, at maximum 3 deg, it is a good approximation to assume that the lateral friction force of the tire F_i is proportional to the slip angle,

$$F_i = C_{\alpha i}\alpha_i. \tag{10}$$

The parameter $C_{\alpha i}$ is called cornering stiffness and describes the cornering behavior of the tire. The load transfer to the front axle when braking or to the outer wheels when driving trough a curve influences the parameter value. A model considering these influences is given by Lundquist and Schön (2009).

Following this brief introduction to the ego vehicle geometry, we are now ready to give an expression describing the evolution of yaw angle ψ_E and the float angle β over

time

$$\ddot{\psi}_E = \beta \frac{-C_{\alpha f} l_f \cos\delta_f + C_{\alpha r} l_r}{I_{zz}} - \dot{\psi}_E \frac{C_{\alpha f} l_f^2 \cos\delta_f + C_{\alpha r} l_r^2}{I_{zz} v_x} + \frac{C_{\alpha f} l_f \tan\delta_f}{I_{zz}}, \quad (11a)$$

$$\dot{\beta} = -\beta \frac{C_{\alpha f} \cos\delta_f + C_{\alpha r} + \dot{v}_x m}{m v_x} - \dot{\psi}_E \left(1 + \frac{C_{\alpha f} l_f \cos\delta_f - C_{\alpha r} l_r}{v_x^2 m}\right) + \frac{C_{\alpha f} \sin\delta_f}{m v_x}, \quad (11b)$$

where m denotes the mass of the vehicle and I_{zz} denotes the moment of inertia of the vehicle about its vertical axis in the center of gravity. These single track model equations are well-known in the literature, see e.g. Kiencke and Nielsen (2005).

3.3 Road Geometry

We start this section by defining the road variables and expressing a typical way to parameterize a road. The section is continued with a derivation of a new model for the road that makes use of the dynamic motion of the ego vehicle.

Background

The most essential component in describing the road geometry is the curvature c, which we will define as the curvature of the white lane marking to the left of the ego vehicle. An overall description of the road geometry is given in Figure 3. The heading angle ψ_R is defined as the tangent of the road at the level of the ego vehicle in the world reference frame W, see Figure 4. The angle ψ_{RE} is the angle between the tangent of the road curvature and the longitudinal axis of the ego vehicle. Note that this angle can be measured by sensors mounted on the ego vehicle. Furthermore, we define δ_R as

$$\delta_R \triangleq \psi_{RE} - \beta, \quad (12)$$

i.e., the angle between the ego vehicles direction of motion (velocity vector) and the road curvature tangent.

The road curvature c is typically parameterized according to

$$c(x_c) = c_0 + c_1 x_c, \quad (13)$$

where x_c is the position along the road in a road aligned coordinate frame and $x_c = 0$ at the vehicles center of gravity. Furthermore, c_0 describes the local curvature at the ego vehicle position and c_1 is the distance derivative (hence, the rate of change) of c_0. It is common to make use of a road aligned coordinate frame when deriving an estimator for the road geometry, a good overview of this approach is given by Eidehall (2007). There are several advantages using road aligned coordinate frames, particularly the motion models of the other vehicles on the same road can be greatly simplified. However, the

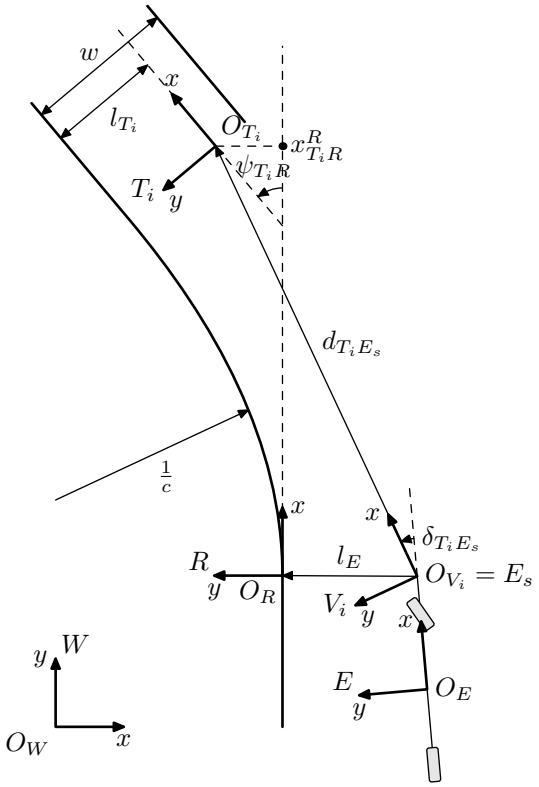

Figure 3: *Relations between one leading vehicle in O_{T_i}, the ego vehicle and the road. The distance between the ego vehicle's longitudinal x-axis and the white lane to its left is $l_E(t)$. The leading vehicle's distance to the lane marking is l_{T_i} and its heading angle in the road frame R is ψ_{T_iR}. The lane width is w.*

flexibility of the motion models is reduced and basic dynamic relations such as Newton's and Euler's laws cannot be directly applied. Since we are using a single track model of the ego vehicle, we will make use of a Cartesian coordinate frame. A good polynomial approximation of the shape of the road curvature is given by

$$y^E = l_E + x^E \tan\psi_{RE} + \frac{c_0}{2}(x^E)^2 + \frac{c_1}{6}(x^E)^3, \tag{14}$$

where $l_E(t)$ is defined as the time dependent distance between the ego vehicle and the lane marking to the left, see e.g. Dickmanns and Mysliwetz (1992), Eidehall (2007).

The following dynamic model is often used for the road

$$\dot{c}_0 = v_x c_1, \tag{15a}$$
$$\dot{c}_1 = 0, \tag{15b}$$

which can be interpreted as a velocity dependent integration. It is interesting to note that (15) reflects the way in which roads are commonly built (Dickmanns and Mysliwetz,

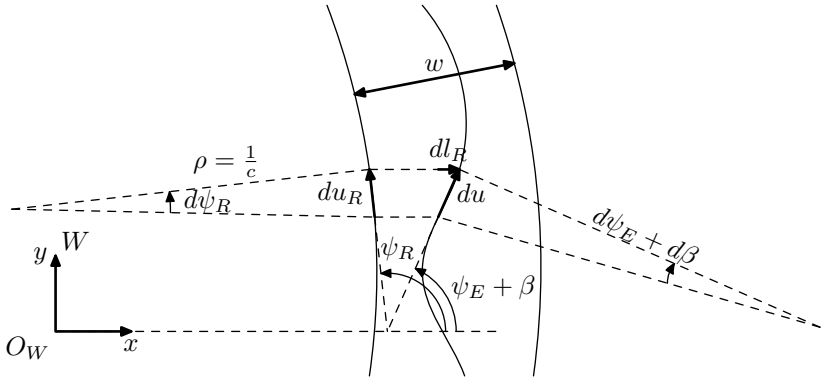

Figure 4: *Infinitesimal segments of the road curvature du_R and the driven path du are shown together with the angles $\delta_R = \psi_R - (\psi_E + \beta)$.*

1992). However, we will now derive a new dynamic model for the road, that makes use of the road geometry introduced above.

A New Dynamic Road Model

Assume that du_R is an infinitesimal part of the road curvature or an arc of the road circle with the angle $d\psi_R$, see Figure 4. A segment of the road circle can be described as

$$du_R = \frac{1}{c_0} d\psi_R, \tag{16}$$

which after division with the infinitesimal change in time dt is given by

$$\frac{du_R}{dt} = \frac{1}{c_0} \frac{d\psi_R}{dt}. \tag{17}$$

Assuming that the left hand side can be reformulated according to

$$\frac{du_R}{dt} = v_x \cos \delta_R \approx v_x, \tag{18}$$

this yields

$$v_x = \frac{1}{c_0} \dot{\psi}_R. \tag{19}$$

The angle ψ_R can be expressed as

$$\psi_R = \psi_E + \beta + \delta_R, \tag{20}$$

by rewriting (12). Re-ordering equation (19) and using the derivative of (20) to substitute $\dot{\psi}_R$ yields

$$\dot{\delta}_R = c_0 v_x - (\dot{\psi}_E + \dot{\beta}), \tag{21}$$

which by substituting $\dot{\beta}$ with (11b) according to

$$\dot{\delta}_R = c_0 v_x - \beta \frac{-C_{\alpha f}\cos\delta_f - C_{\alpha r} - \dot{v}_x m}{m v_x} + \dot{\psi}_E \frac{C_{\alpha f} l_f \cos\delta_f - C_{\alpha r} l_r}{v_x^2 m} - \frac{C_{\alpha f}\sin\delta_f}{m v_x} \quad (22)$$

results in a differential equation of the road angle δ_R. A similar relation has been used by Dickmanns and Mysliwetz (1992), Litkouhi et al. (1993).

We also need a differential equation for the road curvature, which can be found by differentiating (21) w.r.t. time,

$$\ddot{\delta}_R = \dot{c}_0 v_x + c_0 \dot{v}_x - \ddot{\psi}_E - \ddot{\beta}. \quad (23)$$

From the above equation we have

$$\dot{c}_0 = \frac{\ddot{\delta}_R + \ddot{\psi}_E + \ddot{\beta} - c_0 \dot{v}_x}{v_x}. \quad (24)$$

Let us assume that $\ddot{\delta}_R = 0$. Furthermore, differentiating $\dot{\beta}$, from (11b), w.r.t. time and inserting this together with $\ddot{\psi}_E$, given in (11a), into the above expression yields the differential equation

$$\begin{aligned}\dot{c}_0 = \frac{1}{(I_{zz} m^2 v_x)^4}\Big(& C_{\alpha r}^2 (I_{zz} + l_r^2 m)(-\dot{\psi}_E l_r + \beta v_x) \\ & + C_{\alpha f}^2 (I_{zz} + l_f^2 m)(\dot{\psi}_E l_f + (\beta - \delta_f) v_x) \\ & + C_{\alpha r} I_{zz} m(-3\dot{\psi}_E \dot{v}_x l_r + 3\beta \dot{v}_x v_x + \dot{\psi}_E v_x^2) \\ & + \dot{v}_x I_{zz} m^2 v_x (2\beta \dot{v}_x + v_x(\dot{\psi}_E - c_0 v_x)) \\ & + C_{\alpha f}(C_{\alpha r}(I_{zz} + l_r(-l_f)m)(\dot{\psi}_E l_b - 2\dot{\psi}_E l_r + 2\beta v_x - \delta_f v_x) \\ & + I_{zz} m(3\dot{\psi}_E \dot{v}_x l_f + (3\beta - 2\delta_f)\dot{v}_x v_x + (\dot{\delta}_f + \dot{\psi}_E) v_x^2))\Big) \end{aligned} \quad (25)$$

for the road curvature.

In this model c_0 is defined at the ego vehicle and thus describes the currently driven curvature, whereas for the curvature described by the state-space model (15) and by the polynomial (13) it is not entirely obvious where c_0 is defined.

Finally, we need a differential equation describing how the distance $l_E(t)$ between the ego vehicle and the lane markings changes over time. Assume again an infinitesimal arc du of the circumference describing the ego vehicle's curvature. By contemplating Figure 4 we have

$$dl_E = du \sin\delta_R, \quad (26)$$

where δ_R is the angle between the ego vehicle's velocity vector and the road. Dividing this equation with an infinitesimal change in time dt and using (18) yield the differential equation

$$\dot{l}_E = v_x \sin\delta_R, \quad (27)$$

which concludes the derivation of the road geometry model.

3.4 Leading Vehicles

The leading vehicles are also referred to as targets $\mathcal{T}_i$. The coordinate frame T_i moving with target i has its origin located in O_{T_i}, as we previously saw in Figure 3. It is assumed that the leading vehicles are driving on the road, quite possibly in a different lane. More specifically, it is assumed that they are following the road curvature and thus that their heading is in the same direction as the tangent of the road.

From Figure 3 it is obvious that,

$$\boldsymbol{d}^W_{EW} + \boldsymbol{d}^W_{E_sE} + \boldsymbol{d}^W_{T_iE_s} - \boldsymbol{d}^W_{T_iW} = 0, \tag{28}$$

or more explicitly,

$$x^W_{EW} + l_s \cos\psi_E + d_{T_iE_s} \cos(\psi_{E_s} + \delta_{T_iE_s}) - x^W_{T_iW} = 0, \tag{29a}$$

$$y^W_{EW} + l_s \sin\psi_E + d_{T_iE_s} \sin(\psi_{E_s} + \delta_{T_iE_s}) - y^W_{T_iW} = 0, \tag{29b}$$

where $d_{T_iE_s}$ is the distance from the ego vehicle's sensor to the leading vehicle, $\delta_{T_iE_s}$ is the relative angle to the leading vehicle and ψ_{E_s} is the mounting orientation of the sensor. It is worth noticing that the azimuth angle $\delta_{T_iE_s}$ can be measured by a sensor mounted on the vehicle.

Let us introduce the coordinate frame V_i whith origin O_{V_i} at the ego vehicle's sensor and with its x-axis pointing at the target T_i i.e., its heading angle ψ_{V_i} is defined by

$$\psi_{V_i} \triangleq \psi_{E_s} + \delta_{T_iE_s}. \tag{30}$$

The target $\mathcal{T}_i$ is assumed to have zero lateral velocity in the V_i frame, i.e., $\dot{y}^{V_i} = 0$, since it is always fixed to the x^{V_n}-axis. If we transform this relation to the world frame W, using the geometry of Figure 1 we have

$$R^{V_iW} \cdot \dot{\boldsymbol{d}}^W_{T_iW} = \begin{pmatrix} \cdot \\ 0 \end{pmatrix}, \tag{31}$$

where the top equation of the vector equality is non-descriptive and the bottom equation can be rewritten as

$$-\dot{x}^W_{T_iW} \sin\psi_{V_i} + \dot{y}^W_{T_iW} \cos\psi_{V_i} = 0. \tag{32}$$

The velocity vector of the ego vehicles is applied in the center of gravity O_E. The derivative of (29) is used together with the velocity components of the ego vehicle and (32) to get an expression for the derivative of the relative angle to the leading vehicle w.r.t. time according to

$$(\dot{\delta}_{T_iE_s} + \dot{\psi}_E) d_{T_iE_s} + \dot{\psi}_E l_s \cos\delta_{T_iE_s} + v_x \sin(\beta - \delta_{T_iE_s}) = 0, \tag{33}$$

where the assumtion $\psi_E = \psi_{E_s}$ is made. This equation is rewritten, forming the differential equation

$$\dot{\delta}_{T_iE_s} = -\frac{\dot{\psi}_E l_s \cos\delta_{T_iE_s} + v_x \sin(\beta - \delta_{T_iE_s})}{d_{T_iE_s}} - \dot{\psi}_E \tag{34}$$

of the relative angle $\dot{\delta}_{T_iE_s}$ to the leading vehicles.

3.5 Summarizing the Dynamic Model

The state-space models derived in the previous sections are nonlinear and they are given in continuous time. Hence, in order to make use of these equations in the EKF we will first linearize them and then make use of (4) in order to obtain a state-space model in discrete time according to (1). This is a rather standard procedure, see e.g. Gustafsson (2000), Rugh (1996). At each time step, the nonlinear state-space model is linearized by evaluating the Jacobian (i.e., the partial derivatives) of the $g(\boldsymbol{x}, \boldsymbol{u})$-matrix introduced in (4) at the current estimate $\hat{\boldsymbol{x}}_{t|t}$. It is worth noting that this Jacobian is straightforwardly computed off-line using symbolic or numerical software, such as MATHEMATICA. Hence, we will not go through the details here. However, for future reference we will briefly summarize the continuous-time dynamic model here.

In the final state-space model the three parts (ego vehicle, road and leading vehicles) of the dynamic model are augmented, resulting in a state vector of dimension $6+4 \cdot$ (Number of leading vehicles). Hence, the size of the state vector varies with time, depending on the number of leading vehicles that are tracked at a specific instance of time.

The ego vehicle model is described by the following states,

$$\boldsymbol{x}_{\mathcal{E}} = \begin{bmatrix} \dot{\psi}_E & \beta & l_E \end{bmatrix}^{\mathrm{T}}, \tag{35}$$

i.e., the yaw rate, the float angle and the distance to the left lane marking. The front wheel angle δ_f, which is calculated from the measured steering wheel angle, and the ego vehicle longitudinal velocity v_x and acceleration $\dot{v}_x$ are modeled as input signals,

$$\boldsymbol{u}_t = \begin{bmatrix} \delta_f & v_x & \dot{v}_x \end{bmatrix}^{\mathrm{T}}. \tag{36}$$

The nonlinear state-space model $\dot{\boldsymbol{x}}_{\mathcal{E}} = f_{\mathcal{E}}(\boldsymbol{x}, \boldsymbol{u})$ is given by

$$f_{\mathcal{E}}(\boldsymbol{x}, \boldsymbol{u}) = \begin{bmatrix} \beta \frac{-C_{\alpha f} l_f \cos\delta_f + C_{\alpha r} l_r}{I_{zz}} - \dot{\psi}_E \frac{C_{\alpha f} l_f^2 \cos\delta_f + C_{\alpha r} l_r^2}{I_{zz} v_x} + \frac{C_{\alpha f} l_f \tan\delta_f}{I_{zz}} \\ -\beta \frac{C_{\alpha f} \cos\delta_f + C_{\alpha r} + \dot{v}_x m}{m v_x} - \dot{\psi}_E \left(1 + \frac{C_{\alpha f} l_f \cos\delta_f - C_{\alpha r} l_r}{v_x^2 m}\right) + \frac{C_{\alpha f} \sin\delta_f}{m v_x} \\ v_x \sin\delta_R \end{bmatrix}. \tag{37}$$

The corresponding differential equations were previously given in (11a), (11b) and (27), respectively. Note that (37) is linear in $\dot{\psi}_E$ and β and nonlinear in δ_R.

The states describing the road $\boldsymbol{x}_{\mathcal{R}}$ are the road curvature c_0 at the ego vehicle position, the angle δ_R between the ego vehicles direction of motion and the road curvature tangent and the width of the lane w, i.e.,

$$\boldsymbol{x}_{\mathcal{R}} = \begin{bmatrix} c_0 & \delta_R & w \end{bmatrix}^{\mathrm{T}}. \tag{38}$$

The differential equations for c_0 and δ_R were given in (25) and (22), respectively. When it comes to the width of the current lane w, we have

$$\dot{w} = 0, \tag{39}$$

motivated by the fact that w does not change as fast as the other variables, i.e., the non-linear state-space model $\dot{\boldsymbol{x}}_{\mathcal{R}} = f_{\mathcal{R}}(\boldsymbol{x}, \boldsymbol{u})$ is given by

$$f_{\mathcal{R}}(\boldsymbol{x}, \boldsymbol{u}) = \begin{bmatrix} \dot{c}_0 \\ c_0 v_x + \beta \frac{C_{\alpha f}\cos\delta_f + C_{\alpha r} + \dot{v}_x m}{m v_x} + \dot{\psi}\frac{C_{\alpha f} l_f \cos\delta_f - C_{\alpha r} l_r}{v_x^2 m} - \frac{C_{\alpha f}\sin\delta_f}{m v_x} \\ 0 \end{bmatrix}. \quad (40)$$

A target is described by the following states; azimuth angle $\delta_{T_i E_s}$, lateral position l_{T_i} of the target, distance between the target and the ego vehicle $d_{T_i E_s}$ and relative velocity between the target and the ego vehicle $\dot{d}_{T_i E_s}$. Hence, the state vector is given by

$$\boldsymbol{x}_{\mathcal{T}} = \begin{bmatrix} \delta_{T_i E_s} & l_{T_i} & \dot{d}_{T_i E_s} & d_{T_i E_s} \end{bmatrix}^{\mathrm{T}}. \quad (41)$$

The derivative of the azimuth angle was given in (34). It is assumed that the leading vehicle's lateral velocity is small, implying that $\dot{l}_{T_n} = 0$ is a good assumption (compare with Figure 3). Furthermore, it can be assumed that the leading vehicle accelerates similar to the ego vehicle, thus $\ddot{d}_{T_i E_s} = 0$ (compare with e.g. Eidehall (2007)). The state-space model $\dot{\boldsymbol{x}}_{\mathcal{T}} = f_{\mathcal{T}}(\boldsymbol{x}, \boldsymbol{u})$ of a leading vehicle (target) is

$$f_{\mathcal{T}}(\boldsymbol{x}, \boldsymbol{u}) = \begin{bmatrix} -\frac{\dot{\psi}_E l_s \cos\delta_{T_i E_s} + v_x \sin(\beta - \delta_{T_i E_s})}{d_{T_i E_s}} - \dot{\psi}_E \\ 0 \\ 0 \\ \dot{d}_{T_i E_s} \end{bmatrix}. \quad (42)$$

Note that the dynamic models given in this section are nonlinear in $\boldsymbol{u}$.

4 Measurement Model

The measurement model (1b) describes how the measurements $\boldsymbol{y}_t$ relates to the state variables $\boldsymbol{x}_t$. In other words, it describes how the measurements enter the estimator. We will make use of superscript m to denote measurements. Let us start by introducing the measurements relating directly to the ego vehicle motion, by defining

$$\boldsymbol{y}^1 = \begin{bmatrix} \dot{\psi}_E^m & a_y^m \end{bmatrix}^{\mathrm{T}}, \quad (43)$$

where $\dot{\psi}_E^m$ and a_y^m are the measured yaw rate and the measured lateral acceleration, respectively. They are both measured with the ego vehicle's inertial sensor in the center of gravity (CoG). The ego vehicle lateral acceleration in the CoG is

$$a_y = v_x(\dot{\psi}_E + \dot{\beta}) + \dot{v}_x \beta. \quad (44)$$

By replacing $\dot{\beta}$ with the expression given in (11b) and at the same time assuming that $\dot{v}_x\beta \approx 0$ we obtain

$$\begin{aligned} a_y &= v_x(\dot{\psi}_E + \dot{\beta}) \\ &= -\beta\frac{C_{\alpha f}\cos\delta_f + C_{\alpha r} + m\dot{v}_x}{m} + \dot{\psi}_E\frac{-C_{\alpha f} l_f \cos\delta_f + C_{\alpha r} l_r}{m v_x} + \frac{C_{\alpha f}}{m}\sin\delta_f. \end{aligned} \quad (45)$$

From this it is clear that the measurement of the lateral acceleration contains information about the ego vehicle states. Hence, the measurement equation corresponding to (43) is given by

$$h^1 = \begin{bmatrix} \dot{\psi}_E \\ -\beta\frac{C_{\alpha f}\cos\delta_f + C_{\alpha r} + m\dot{v}_x}{m} + \dot{\psi}_E\frac{-C_{\alpha f}l_f\cos\delta_f + C_{\alpha r}l_r}{mv_x} + \frac{C_{\alpha f}}{m}\sin\delta_f \end{bmatrix}. \tag{46}$$

The vision system provides measurements of the road geometry and the ego vehicle position on the road according to

$$\boldsymbol{y}^2 = \begin{bmatrix} c_0^m & \psi_{RE}^m & w^m & l_E^m \end{bmatrix}^{\mathrm{T}} \tag{47}$$

and the corresponding measurement equations are given by

$$h^2 = \begin{bmatrix} c_0 & (\delta_R + \beta) & w & l_E \end{bmatrix}^{\mathrm{T}}. \tag{48}$$

In order to include measurements of a leading vehicle we require that it is detected both by the radar and the vision system. The range $d^m_{T_iE_s}$ and the range rate $\dot{d}^m_{T_iE_s}$ are measured by the radar. The azimuth angle is also measured by the radar, but not used directly in this framework. Instead, the accuracy of the angle estimate is improved by using the camera information. We will not describe these details here, since it falls outside the scope of this work. The corresponding measurement vector is

$$\boldsymbol{y}^3 = \begin{bmatrix} \delta^m_{T_iE_s} & \dot{d}^m_{T_iE_s} & d^m_{T_iE_s} \end{bmatrix}^{\mathrm{T}}. \tag{49}$$

Since these are state variables, the measurement equation is obviously

$$h^3 = \begin{bmatrix} \delta_{T_iE_s} & \dot{d}_{T_iE_s} & d_{T_iE_s} \end{bmatrix}^{\mathrm{T}}. \tag{50}$$

The fact that the motion of the leading vehicles reveals information about the road geometry allows us to make use of their motion in order to improve the road geometry estimate. This will be accomplished by introducing a nontrivial artificial measurement equation according to

$$h^4 = l_E + (\delta_R + \beta)d_{T_iE_s}\cos\delta_{T_iE_s} + \frac{c_0}{2}(d_{T_iE_s}\cos\delta_{T_iE_s})^2 + \frac{l_{T_i}}{\cos\psi_{T_iR}}, \tag{51}$$

which is derived from Figure 3 and describes the predicted lateral distance of a leading vehicle in the ego vehicles coordinate frame E. In order to model the road curvature we introduce the road coordinate frame R, with its origin O_R on the white lane marking to the left of the ego vehicle. This implies that the frame R is moving with the frame E of the ego vehicle. The angle $\psi_{T_iR} \triangleq \psi_{T_i} - \psi_R$ is derived by considering the road's slope at the position of the leading vehicle, i.e.,

$$\psi_{T_iR} = \arctan\frac{dy^R}{dx^R} = \arctan c_0 x^R, \tag{52}$$

where $x^R = x^R_{T_iR}$, see Figure 3. The Cartesian x-coordinate of the leading vehicle $\mathcal{T}_i$ in the R-frame is

$$x^R_{T_iR} \approx x^E_{T_iE_s} \approx d_{T_iE_s}\frac{\cos\delta_{T_iE_s}}{\cos\psi_{RE}}. \tag{53}$$

The sensors only provide range $d^m_{T_iE_sn}$ and azimuth angle $\delta^m_{T_iE_s}$. Hence, the corresponding quasi-measurement is

$$\boldsymbol{y}^4 = d^m_{T_iE_s} \sin(\delta^m_{T_iE_s}), \tag{54}$$

describing the measured lateral distance to a leading vehicle in the ego vehicle's coordinate frame. This might seem a bit ad hoc at first. However, the validity of the approach has recently been justified in the literature, see e.g. Teixeira et al. (2007).

5 Experiments and Results

The experiments presented in this section are based on measurements acquired on public roads in Sweden during normal traffic conditions. The test vehicle is a Volvo XC90 equipped with a forward looking 77 GHz mechanically scanning FMCW radar and a forward looking vision sensor (camera), measuring the distances and angles to the targets. The image sensor includes object and lane detection and provides for example the lane curvature. Information about the ego vehicle motion, such as the steering wheel angle, yaw rate, etc. were acquired directly from the CAN bus.

Before stating the main results in this section we outline how to estimate the parameters of the ego vehicle and how the filter is tuned. Subsequently we state the results of the ego vehicle validation. We compare our road curvature estimates with two other sensor fusion approaches as well as one road model.

5.1 Parameter Estimation and Filter Tuning

Most of the ego vehicle's parameters, such as the dimensions, the mass and the moment of inertia were provided by the vehicle manufacturer. Since the cornering stiffness is a parameter which describes the properties between road and tire it has to be estimated for the given set of measurements. An on-line method to estimate the cornering stiffness parameter using recursive least square is presented by Lundquist and Schön (2009). However, in the present work an exhaustive search was accomplished off-line using a batch of measurements to estimate $C_{\alpha f}$ and $C_{\alpha r}$. A state-space model with the differential equations given in (11a) and (11b) and with the yaw rate $\dot{\psi}_E$ and the float angle β in the state vector was used for this purpose. Furthermore, the front wheel angle δ_f and the ego vehicle longitudinal velocity v_x were modeled as input signals. The measurements were provided by the yaw rate $\dot{\psi}^m_E$ and the lateral acceleration a^m_y. The corresponding measurement equation was given in (46). The data used to identifying the cornering stiffness parameters was split into two parts, one estimation part and one validation part. This facilitates cross-validation, where the parameters are estimated using the estimation data and the quality of the estimates can then be assessed using the validation data (Ljung, 1999).

The approach is further described by Lundquist and Schön (2008a). The resulting state-space model with the estimated parameters was validated using the validation data and the result is given in Figure 5.

The process and measurement noise covariances are the design parameters in the extended Kalman filter (EKF). It is assumed that the covariances are diagonal and that there are no cross correlations between the measurement noise and the process noise. The

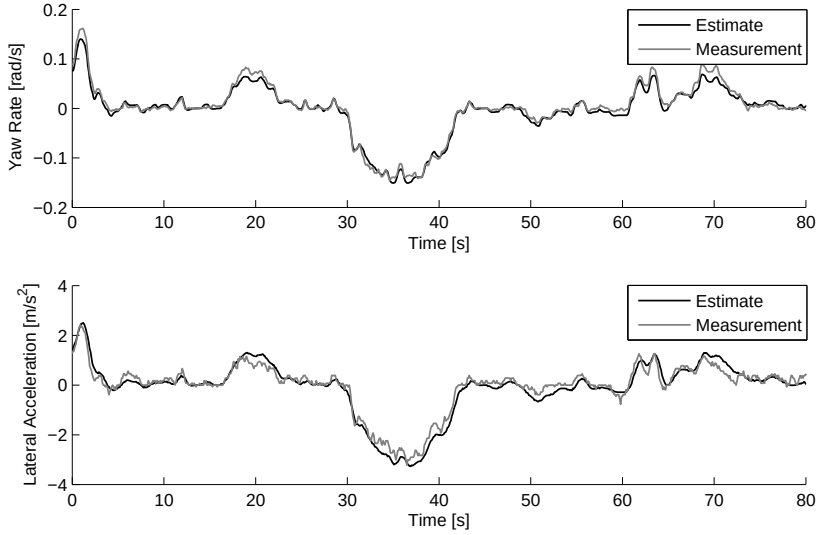

Figure 5: *Comparing the simulated result of the nonlinear state-space model (black) with measured data (gray) of a validation data set. The upper plot shows the yaw rate and the lower shows the lateral acceleration.*

present filter has ten states and ten measurement signals, which implies that 20 parameters have to be tuned. The tuning was started using physical intuition of the error in the process equations and the measurement signals. In a second step, the covariance parameters were tuned simply by trying to minimize the root mean square error (RMSE) of the estimated $\hat{c}_0$ and the reference curvature c_0. The estimated curvature was obtained by running the filter using the estimation data set. The calculation of the reference value is described by Eidehall and Gustafsson (2006). The chosen design parameters were validated on a different data set and the results are discussed in the subsequent sections.

5.2 Validation Using Ego Vehicle Signals

The state variables of the ego vehicle are according to (35), the yaw rate, the float angle and the distance to the left lane marking. The estimated and the measured yaw rate signals are, as expected, very similar. As described in Section 5.1, the parameters of the vehicle model were optimized with respect to the yaw rate, hence it is no surprise that the fusion method decreases the residual further. A measurement sequence acquired on a rural road is shown in Figure 6a. Note that the same measurement sequence is used in Figures 5 to 7, which will make it easier to compare the estimated states.

The float angle β is estimated, but there is no reference or measurement signal to compare it to. An example is shown in Figure 6b. For velocities above $30 - 40$ km/h, the float angle appears more or less like the mirror image of the yaw rate, and by comparing with Figure 6a, we can conclude that the sequence is consistent.

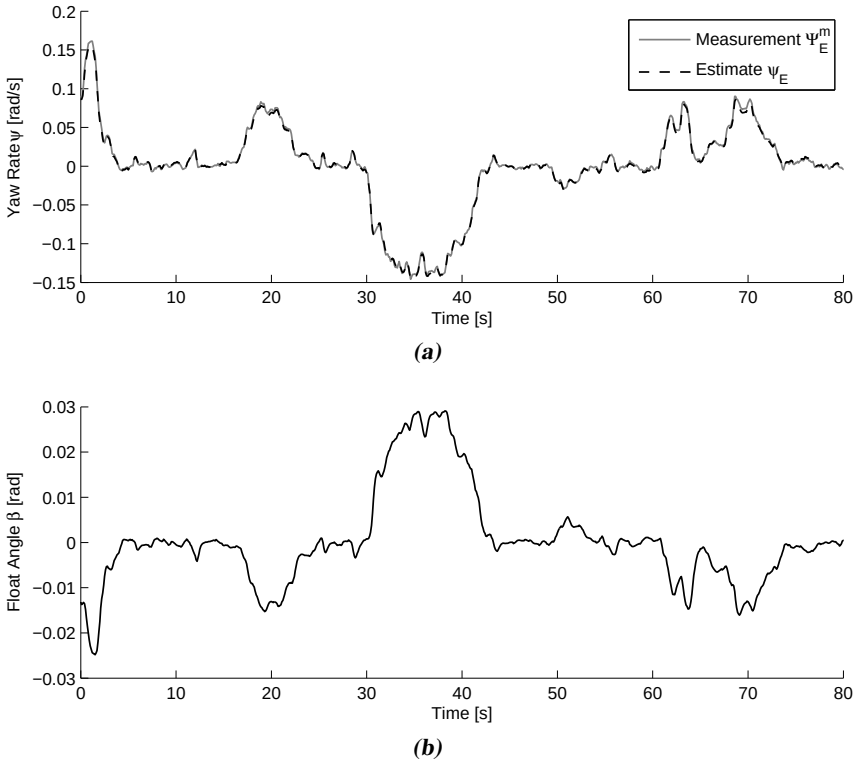

Figure 6: *A comparison between the ego vehicle's measured (gray) and estimated yaw rate (black dashed) using the sensor fusion approach in this paper is shown in (a). The estimated float angle β for the same data sequence is shown in (b).*

The measurement signal of the distance to the left white lane marking l_E^m is produced by the vision system OLR (Optical Lane Recognition). Bad lane markings or certain weather conditions can cause errors in the measurement signal. The estimated state l_E of the fusion approach is very similar to the pure OLR signal.

5.3 Road Curvature Estimation

An essential idea with the sensor fusion approach introduced in this paper is to make use of the single track ego vehicle model in order to produce better estimates of the road curvature. In this section we will compare this approach to approaches based on other models of the ego vehicle and the road geometry.

Fusion 1 is the sensor fusion approach shown in this paper.

Fusion 2 is a similar approach, thoroughly described by Eidehall (2007). An important difference to fusion 1 is that the ego vehicle is modeled with a constant velocity model, which is less complex. The float angle β is not estimated. Furthermore, the road is modeled according to (15) and a road aligned coordinate frame is used. This

method is similar to the approaches used by e.g. Zomotor and Franke (1997), Gern et al. (2000, 2001).

Fusion 3 comprehends the ego vehicle model of fusion 1 and the road model of fusion 2, i.e., substituting (25) by (15) and introducing the seventh state c_1. Furthermore, a Cartesian coordinate frame is used. This method, but without considering the leading vehicles is similar to the ones described by e.g. Dickmanns and Mysliwetz (1992) and Behringer (1997).

Model is the ego vehicle and road state-space model given in this paper, described by the motion models (37) and (40) and the measurement models (46) and (48), without the extended Kalman filter.

The curvature estimate $\hat{c}_0$ from the sensor fusion approaches, the model and the raw measurement from the optical lane recognition are compared to a reference value. The reference value is computed off-line using a geometric method described by Eidehall and Gustafsson (2006), which applies a least square curve fitting to a sliding window. The entire data set i.e., also future values of the ego vehicle movement, is used to derive the reference value. The accuracy of the method was validated on a test track, where the ground truth is well defined, and the results are good as reported by Eidehall and Gustafsson (2006).

A typical result of a comparison is shown in Figure 7. The data stems from a rural road, which explains the curvature values. It can be seen that the estimates from the sensor fusion approaches give better results than using the OLR alone, as was expected. The OLR estimate is rather noisy compared to the fused estimates. This is not surprising, since the raw OLR has less information. A camera view from the curve at time $32\ \mathrm{s}$ is shown in Figure 8a.

The curvature estimate from the state-space model described in this paper is denoted by model and is shown as a dash-dotted black line. The absolute position is not measured, which leads to a clearly visible bias in the estimate of c_0. The bias is transparent in Figure 7, but it also leads to a large RMSE value in Table 1. Fusion 3 also delivers a decent result, but it is interesting to notice that the estimate seems to follow the incorrect OLR at time $35\ \mathrm{s}$. The same behavior holds for fusion 2 in Figure 7.

To get a more aggregate view of the performance, we provide the root mean square error (RMSE) for longer measurement sequences in Table 1. The fusion approaches improve the road curvature estimate by making use of the information about the leading vehicles, that is available from the radar and the vision systems. However, since we are interested in the curvature estimate also when there are no leading vehicles in front of the ego vehicle, this case will be studied as well. It is straightforward to study this case, it is just a matter of not providing the measurements of the leading vehicles to the algorithms. The RMSE values found without information about the leading vehicles are given in the columns marked *no* in Table 1.

These results should ideally be compared to data where information about the leading vehicles is considered, but during the $78\ \mathrm{min}$ drive there were not always another car in front of us. Only for about $50\ \%$ of the time there existed other vehicles, which we could track. Hence, for the sake of comparability we give the RMSE values for those sequences where at least one leading vehicle was tracked, bearing in mind that these are based on

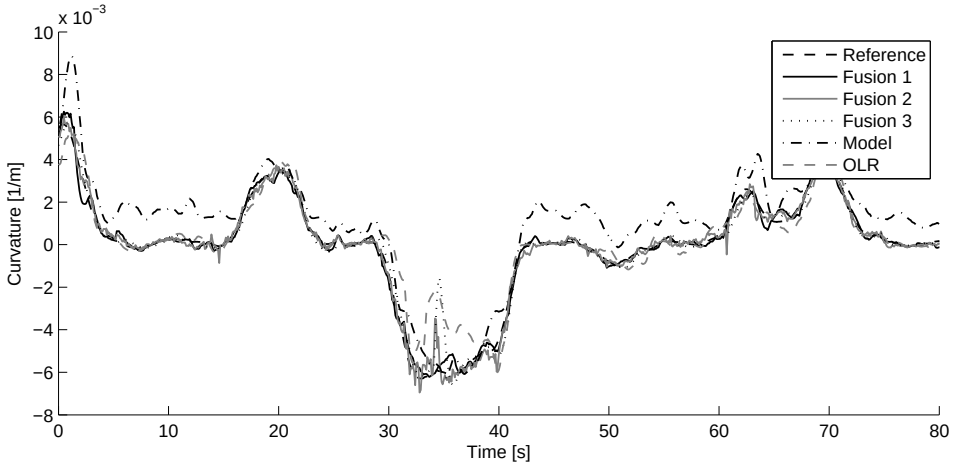

Figure 7: *Results from the three fusion approaches (fusion 1 solid black line, fusion 2 gray line and fusion 3 dotted line) and the OLR (dashed gray line), showing the curvature estimate $\hat{c}_0$. As can be seen, the curvature estimate can be improved by taking the other vehicles (gray line) and the ego vehicle's driven curvature in to account (solid black line). The model (dash-dotted) is estimating the derivative of the curvature and the absolute position is not measured, which leads to the illustrated bias. The dashed line is the reference curvature.*

(a) ***(b)***

Figure 8: *Two different camera views are shown. In (a) the lane markings are excellent and the leading vehicles are close and clearly visible. This is the traffic situation at 32 s in the Figures 5 to 7. Although the circumstances seem perfect, the OLR, Fusion 2 and 3 have problems estimating the curvature, as seen in Figure 7. The traffic situation shown in (b) is more demanding, mainly due to the weather conditions and large distance to the leading vehicle.*

only about $50\ \%$ of the data. The corresponding columns in Table 1 are marked *only*. Finally, we also give the RMSE values for the complete data, where other vehicles were considered whenever *possible*.

It is interesting to see that the advantage of fusion 1, which uses a more accurate ego vehicle and road model, in comparison to fusion 2 is particularly noticeable when

Table 1: *Comparison of the root mean square error (RMSE) of the road curvature c_0 in $[1/m]$ for the three fusion approaches and the pure measurement signal OLR for two longer measurement sequences acquired on public roads in Sweden. Three cases were considered, using only those measurements where a leading vehicle could be tracked, using the knowledge of the leading vehicles position whenever possible or not at all and thereby simulating the lonely driver. Note that all RMSE values should be multiplied by 10^{-3}.*

	Highway			Rural road		
Time	44 min			34 min		
OLR $[10^{-3}/m]$	0.385			3.60		
Model $[10^{-3}/m]$	0.356			2.10		
Leading vehicles used?	only	possible	no	only	possible	no
Fusion 1 $[10^{-3}/m]$	0.176	0.184	0.189	1.48	1.13	1.18
Fusion 2 $[10^{-3}/m]$	0.231	0.228	0.230	1.53	2.84	2.91
Fusion 3 $[10^{-3}/m]$	0.203	0.210	0.205	1.32	2.01	1.94

driving alone on a rural road, the RMSE for fusion 1 is then 1.18, whereas the RMSE for fusion 2 is 2.91. The reason for this is first of all that we are driving on a rather curvy road which implies that any additional information will help improving the curvature estimate. Here, the additional information is the improved ego vehicle and road models used in fusion 1. Furthermore, the fact that there are no leading vehicles that could aid the fusion algorithm when driving alone creates a greater disadvantage for fusion 2, since it is its main additional information. Fusion 3, which uses the single track vehicle model of fusion 1, but the road model of fusion 2, seems to position itself between those two.

Comparing the rural road results based only on those measurements where other vehicles were tracked, we see an interesting pattern. The curvature estimate of fusion 2 and fusion 3 is improved by the additional information, but the estimate of fusion 1 is declined. The error values of the three fusion approaches are also in the same range. The explanation of this behavior can be found by analyzing the measurement sequences. If the leading vehicle is close-by, as for example in Figure 8a, it helps improving the results. However, if the leading vehicle is more distant, the curvature at this position might not be the same as it is at the ego vehicle's position, which leads to a degraded result. In (Lundquist and Schön, 2008b) the authors presented preliminary results based on much shorter measurement sequences, where the leading vehicles were more close-by and the estimate of fusion 1 was improved by the existence of leading vehicles. The problem could be solved by letting the measurement noise $\boldsymbol{e}$ of the measurement equation (51) depend on the distance to the leading vehicle.

The highway is rather straight and as expected not much accuracy could be gained in using an improved dynamic vehicle model. It is worth noticing that the OLR's rural road RMSE value is about 10 times higher than the highway value, but the model's RMSE increases only about six times when comparing the rural road values with the highway. Comparing the RMSE values in the columns marked *possible*; the RMSE for fusion 1 also increases about six times, but that of fusion 2 increases as much as twelve times

when comparing the highway measurements with the rural road.

A common problem with these road estimation methods is that it is hard to distinguish between the case when the leading vehicle is entering a curve and the case when the leading vehicle is performing a lane change. With the approach in this paper the information about the ego vehicle motion, the OLR and the leading vehicles is weighted together in order to form an estimate of the road curvature. The fusion approach in this paper produces an estimate of the lateral position l_{T_n} of the leading vehicle which seems reasonable. The results are thoroughly described by Lundquist and Schön (2008b).

6 Conclusions

In this contribution we have derived a method for joint ego-motion and road geometry estimation. The presented sensor fusion approach combines the information from sensors present in modern premium cars, such as radar, camera and IMU, with a dynamic model. This model, which consists of a new dynamic motion model of the road, is the core of this contribution. The road geometry is estimated by considering the information from the optical lane recognition of the camera, the position of the leading vehicles, obtained by the radar and the camera, and by making use of a dynamic ego vehicle motion model, which takes IMU-data and the steering wheel angle as input. If one of these three parts fails, for example there might not be any leading vehicles or the lane markings are bad, as in Figure 8b, then the sensor fusion framework will still deliver an estimate.

The presented sensor fusion framework has been evaluated together with two other fusion approaches on real and relevant data from both highway and rural roads in Sweden. The data consists of $78\ \mathrm{min}$ driving on various road conditions, also including snow-covered pavement. The approach presented in this paper obtained the best results in all situations, when compared to the other approaches, but it is most prominent when driving alone on a rural road. If there are no leading vehicles that can be used, the improved road and ego vehicle models still supports the road geometry estimation and delivers a more accurate result.

Acknowledgement

The authors would like to thank Dr. Andreas Eidehall at Volvo Car Corporation for fruitful discussions. Furthermore, they would like to thank the SEnsor Fusion for Safety (SEFS) project within the Intelligent Vehicle Safety Systems (IVSS) program and the strategic research center MOVIII, funded by the Swedish Foundation for Strategic Research (SSF) for financial support.

References

Anderson, B. D. O. and Moore, J. B. (1979). *Optimal Filtering*. Information and system science series. Prentice Hall, Englewood Cliffs, NJ, USA.

Bar-Shalom, Y., Rong Li, X., and Kirubarajan, T. (2001). *Estimation with Applications to Tracking and Navigation*. John Wiley & Sons, New York.

Behringer, R. (1997). *Visuelle Erkennung und Interpretation des Fahrspurverlaufes durch Rechnersehen für ein autonomes Straßenfahrzeug*, volume 310 of *Fortschrittsberichte VDI, Reihe 12*. VDI Verlag, Düsseldorf, Germany. Also as: PhD Thesis, Universität der Bundeswehr, 1996.

Bengtsson, F. and Danielsson, L. (2008). Designing a real time sensor data fusion system with application to automotive safety. In *15th World Congress of ITS*, New York, USA.

Blackman, S. S. and Popoli, R. (1999). *Design and Analysis of Modern Tracking Systems*. Artech House, Inc., Norwood, MA, USA.

Dickmanns, E. D. (2007). *Dynamic Vision for Perception and Control of Motion*. Springer, London, UK.

Dickmanns, E. D. and Mysliwetz, B. D. (1992). Recursive 3-D road and relative ego-state recognition. *IEEE Transactions on pattern analysis and machine intelligence*, 14(2):199–213.

Dickmanns, E. D. and Zapp, A. (1986). A curvature-based scheme for improving road vehicle guidance by computer vision. In *Proceedings of the SPIE Conference on Mobile Robots*, volume 727, pages 161–198, Cambridge, MA, USA.

Eidehall, A. (2007). *Tracking and threat assessment for automotive collision avoidance*. PhD thesis No 1066, Linköping Studies in Science and Technology, Linköping, Sweden.

Eidehall, A. and Gustafsson, F. (2006). Obtaining reference road geometry parameters from recorded sensor data. In *Proceedings of the IEEE Intelligent Vehicles Symposium*, pages 256–260, Tokyo, Japan.

Eidehall, A., Pohl, J., and Gustafsson, F. (2007). Joint road geometry estimation and vehicle tracking. *Control Engineering Practice*, 15(12):1484–1494.

Gern, A., Franke, U., and Levi, P. (2000). Advanced lane recognition - fusing vision and radar. In *Proceedings of the IEEE Intelligent Vehicles Symposium*, pages 45–51, Dearborn, MI, USA.

Gern, A., Franke, U., and Levi, P. (2001). Robust vehicle tracking fusing radar and vision. In *Proceedings of the international conference of multisensor fusion and integration for intelligent systems*, pages 323–328, Baden-Baden, Germany.

Gordon, N. J., Salmond, D. J., and Smith, A. F. M. (1993). Novel approach to nonlinear/non-Gaussian Bayesian state estimation. In *IEE Proceedings on Radar and Signal Processing*, volume 140, pages 107–113.

Gumpp, T., Nienhuser, D., Liebig, R., and Zollner, J. (2009). Recognition and tracking of temporary lanes in motorway construction sites. In *Proceedings of the IEEE Intelligent Vehicles Symposium*, pages 305–310, Xi'an, China.

Gustafsson, F. (2000). *Adaptive Filtering and Change Detection*. John Wiley & Sons, New York, USA.

Hahn, H. (2002). *Rigid body dynamics of mechanisms. 1, Theoretical basis*, volume 1. Springer, Berlin, Germany.

Hofmann, U., Rieder, A., and Dickmanns, E. (2000). Ems-vision: application to hybrid adaptive cruise control. In *Proceedings of the IEEE Intelligent Vehicles Symposium*, pages 468–473, Dearborn, MI, USA.

Hofmann, U., Rieder, A., and Dickmanns, E. (2003). Radar and vision data fusion for hybrid adaptive cruise control on highways. *Machine Vision and Applications*, 14(1):42 – 49.

Jazwinski, A. H. (1970). *Stochastic processes and filtering theory*. Mathematics in science and engineering. Academic Press, New York, USA.

Kailath, T., Sayed, A. H., and Hassibi, B. (2000). *Linear Estimation*. Information and System Sciences Series. Prentice Hall, Upper Saddle River, NJ, USA.

Kaliyaperumal, K., Lakshmanan, S., and Kluge, K. (2001). An algorithm for detecting roads and obstacles in radar images. *IEEE Transactions on Vehicular Technology*, 50(1):170–182.

Kalman, R. E. (1960). A new approach to linear filtering and prediction problems. *Transactions of the ASME, Journal of Basic Engineering*, 82:35–45.

Kiencke, U. and Nielsen, L. (2005). *Automotive Control Systems*. Springer, Berlin, Heidelberg, Germany, second edition.

Kirchner, A. and Ameling, C. (2000). Integrated obstacle and road tracking using a laser scanner. In *Proceedings of the IEEE Intelligent Vehicles Symposium*, pages 675–681, Dearborn, MI, USA.

Kirchner, A. and Heinrich, T. (1998). Model based detection of road boundaries with a laser scanner. In *Proceedings of the IEEE Intelligent Vehicles Symposium*, pages 93–98, Stuttgart, Germany.

Lakshmanan, S., Kaliyaperumal, K., and Kluge, K. (1997). Lexluther: an algorithm for detecting roads and obstacles in radar images. In *Proceedings of the IEEE Conference on Intelligent Transportation System*, pages 415–420, Boston, MA, USA.

Litkouhi, B., Lee, A., and Craig, D. (1993). Estimator and controller design for lanetrak, a vision-based automatic vehicle steering system. In *Proceedings of the 32nd IEEE Conference on Decision and Control*, volume 2, pages 1868 – 1873, San Antonio, Texas.

Ljung, L. (1999). *System identification, Theory for the user*. System sciences series. Prentice Hall, Upper Saddle River, NJ, USA, second edition.

Loose, H., Franke, U., and Stiller, C. (2009). Kalman particle filter for lane recognition on rural roads. In *Proceedings of the IEEE Intelligent Vehicles Symposium*, pages 60–65, Xi'an, China.

Lundquist, C., Orguner, U., and Schön, T. B. (2009). Tracking stationary extended objects for road mapping using radar measurements. In *Proceedings of the IEEE Intelligent Vehicles Symposium*, pages 405–410, Xi'an, China.

Lundquist, C. and Schön, T. B. (2008a). Road geometry estimation and vehicle tracking using a single track model. Technical Report LiTH-ISY-R-2844, Department of Electrical Engineering, Linköping University, SE-581 83 Linköping, Sweden.

Lundquist, C. and Schön, T. B. (2008b). Road geometry estimation and vehicle tracking using a single track model. In *Proceedings of the IEEE Intelligent Vehicles Symposium*, pages 144–149, Eindhoven, The Netherlands.

Lundquist, C. and Schön, T. B. (2009). Recursive identification of cornering stiffness parameters for an enhanced single track model. In *Proceedings of the 15th IFAC Symposium on System Identification*, pages 1726–1731, Saint-Malo, France.

Ma, B., Lakshmanan, S., and Hero, A. (2000). Simultaneous detection of lane and pavement boundaries using model-based multisensor fusion. *IEEE Transactions on Intelligent Transportation Systems*, 1(3):135–147.

McCall, J. C. and Trivedi, M. M. (2006). Video-based lane estimation and tracking for driver assistance: Servey, system, and evaluation. *IEEE Transactions on Intelligent Transportation Systems*, 7(1):20–37.

Mitschke, M. and Wallentowitz, H. (2004). *Dynamik der Kraftfahrzeuge*. Springer, Berlin, Heidelberg, 4th edition.

Muller, A., Manz, M., Himmelsbach, M., and Wunsche, H. (2009). A model-based object following system. In *Proceedings of the IEEE Intelligent Vehicles Symposium*, pages 242–249, Xi'an, China.

Nikolova, M. and Hero, A. (2000). Segmentation of a road from a vehicle-mounted radar and accuracy of the estimation. In *Proceedings of the IEEE Intelligent Vehicles Symposium*, pages 284–289, Dearborn, MI, USA.

Robert Bosch GmbH, editor (2004). *Automotive Handbook*. SAE Society of Automotive Engineers, 6th edition.

Rugh, W. J. (1996). *Linear System Theory*. Information and system sciences series. Prentice Hall, Upper Saddle River, NJ, USA, second edition.

Schmidt, S. F. (1966). Application of state-space methods to navigation problems. *Advances in Control Systems*, 3:293–340.

Schön, T. B. (2006). *Estimation of Nonlinear Dynamic Systems – Theory and Applications*. PhD thesis No 998, Linköping Studies in Science and Technology, Department of Electrical Engineering, Linköping University, Sweden.

Schubert, R., Wanielik, G., and Schulze, K. (2009). An analysis of synergy effects in an omnidirectional modular perception system. In *Proceedings of the IEEE Intelligent Vehicles Symposium*, pages 54–59, Xi'an, China.

Smith, G. L., Schmidt, S. F., and McGee, L. A. (1962). Application of statistical filter theory to the optimal estimation of position and velocity on board a circumlunar vehicle. Technical Report TR R-135, NASA.

Sparbert, J., Dietmayer, K., and Streller, D. (2001). Lane detection and street type classification using laser range images. In *Proceedings of the IEEE Intelligent Transportation Systems Conference*, pages 454–459, Oakland, CA, USA.

Teixeira, B. O. S., Chandrasekar, J., Torres, L. A. B., Aguirre, L. A., and Bernstein, D. S. (2007). State estimation for equality-constrained linear systems. In *Proceedings of the 46th Conference on Decision and Control (CDC)*, pages 6220–6225, New Orleans, LA, USA.

Watanabe, A., Naito, T., and Ninomiya, Y. (2009). Lane detection with roadside structure using on-board monocular camera. In *Proceedings of the IEEE Intelligent Vehicles Symposium*, pages 191–196, Xi'an, China.

Wedel, A., Franke, U., Badino, H., and Cremers, D. (2008). B-spline modeling of road surfaces for freespace estimation. In *Proceedings of the IEEE Intelligent Vehicles Symposium*, pages 828–833, Eindhoven, The Netherlands.

Weigel, H., Lindner, P., and Wanielik, G. (2009). Vehicle tracking with lane assignment by camera and Lidar sensor fusion. In *Proceedings of the IEEE Intelligent Vehicles Symposium*, pages 513–520, Xi'an, China.

Wijesoma, W. S., Kodagoda, K. R. S., and Balasuriya, A. P. (2004). Road-boundary detection and tracking using ladar sensing. *IEEE Transactions on Robotics and Automation*, 20(3):456–464.

Wong, J. (2001). *Theory Of Ground Vehicles*. John Wiley & Sons, New York, USA, third edition.

Zomotor, Z. and Franke, U. (1997). Sensor fusion for improved vision based lane recognition and object tracking with range-finders. In *Proceedings of IEEE Conference on Intelligent Transportation System*, pages 595–600, Boston, MA, USA.

Paper B

Recursive Identification of Cornering Stiffness Parameters for an Enhanced Single Track Model

Authors: Christian Lundquist and Thomas B. Schön.

Edited version of paper originally published in *Proceedings of the 15th IFAC Symposium on System Identification*, Saint-Malo, France, 2009.

Preliminary version published as Technical Report LiTH-ISY-R-2893, Department of Electrical Engineering, Linköping University, Linköping, Sweden.

Recursive Identification of Cornering Stiffness Parameters for an Enhanced Single Track Model

Christian Lundquist and Thomas B. Schön

Department of Electrical Engineering,
Linköping University,
SE–581 83 Linköping, Sweden.
E-mail: (lundquist, schon)@isy.liu.se.

Abstract

The current development of safety systems within the automotive industry heavily relies on the ability to perceive the environment. This is accomplished by using measurements from several different sensors within a sensor fusion framework. One important part of any system of this kind is an accurate model describing the motion of the vehicle. The most commonly used model for the lateral dynamics is the single track model, which includes the so called cornering stiffness parameters. These parameters describe the tire-road contact and are unknown and even time-varying. Hence, in order to fully make use of the single track model, these parameters have to be identified. The aim of this work is to provide a method for recursive identification of the cornering stiffness parameters to be used on-line while driving.

Keywords: Recursive estimation, Recursive least square, Vehicle dynamics, Gray box model, Tire-road interaction.

1 Introduction

In Lundquist and Schön (2008a) the authors presented a new approach to estimate the road curvature by fusing the information from a camera, a radar, inertial sensors, a steering wheel sensor and wheel speed sensors, making use of an accurate vehicle model. This model is an enhanced single track model, which is also referred to as the bicycle model in the literature. This model contains several parameters, some of which are known and others that are unknown and hence have to be identified. The cornering behavior of the vehicle is strongly connected to the tire characteristics. The parameters of the tires are often assumed to be constant, and this was also the case in Lundquist and Schön (2008a).

In the present contribution we will show a way to identify these parameters in real time when driving.

To be more specific, the cornering stiffness parameter $C_{\alpha i}$ ($i = f,\, r$ for the front and the rear tires, respectively) describes the cornering behavior of the tire. The cornering stiffness parameters are used to describe the relation between the lateral friction force of the tires F_i and the slip angles α_i,

$$F_i = C_{\alpha i}\alpha_i, \qquad i = f,\, r. \tag{1}$$

The slip angle is defined as the angle between the central axis of the wheel and the path along which the wheel moves. Hence, the cornering stiffness parameters have to be included in the model describing the motion of the vehicle. Rather than modeling the cornering stiffness as just a scalar, as indicated in (1), we will model it to be able to account for its dependence of the load transfer from the rear axle to the front axle when braking and vice versa when accelerating. This implies that besides the lateral and yaw dynamics we have to model the vertical motion of the vehicle as well. In this contribution we will derive a rather simple model for the vertical motion, including only the pitch angle and its derivative. The pitch angle is the angle between ground and the longitudinal axis of the vehicle. In modeling the pitching motion we end up with a linear state-space model, containing several unknown parameters, i.e. it is a linear gray-box model. These parameters can be identified using standard techniques (Ljung, 1999, Graebe, 1990). Finally, we can make use of the dynamic models describing the pitch, the lateral and the yaw motion of the vehicle to form an appropriate recursive least squares problem for identifying the cornering stiffness parameters on-line.

The problem of estimating the cornering stiffness parameters in the single track model is by no means new. However, our approach is, to the best of the authors knowledge, new in the sense that we make use of the vertical motion as well in order to estimate the stiffness parameters. Furthermore, as a spin-off contribution we provide a way for identifying the pitch dynamics of a vehicle. There are several previous approaches for identifying the cornering stiffness parameters based solely on the lateral dynamics, see e.g. Wesemeier and Isermann (2006), Sienel (1997), Sierra et al. (2006), Baffet et al. (2007). Grip et al. (2008) used a nonlinear observer to estimate the side slip angle. It is the fact that we have access to measurements of the pitching motion, via the vertical position of the front and the rear suspension, that allows us to take the load transfer into account when identifying the cornering stiffness parameters.

2 Longitudinal and Pitch Dynamics

When a vehicle brakes or accelerates a vertical motion is induced in the vehicle body, the vehicle is said to pitch. This motion does not only depend on the vertical vibration characteristics and the longitudinal brake or drive force, but also on the type of suspension. Nevertheless, we will only consider a simple model of the vertical motion, describing how the pitch angle changes over time. In Section 2.1 we provide a brief derivation of the pitch dynamics used in this work, for a more detailed account, see e.g. Mitschke and Wallentowitz (2004). There are several unknown parameters in the model of the pitch dynamics that have to be estimated from data. This is the topic of Section 2.2.

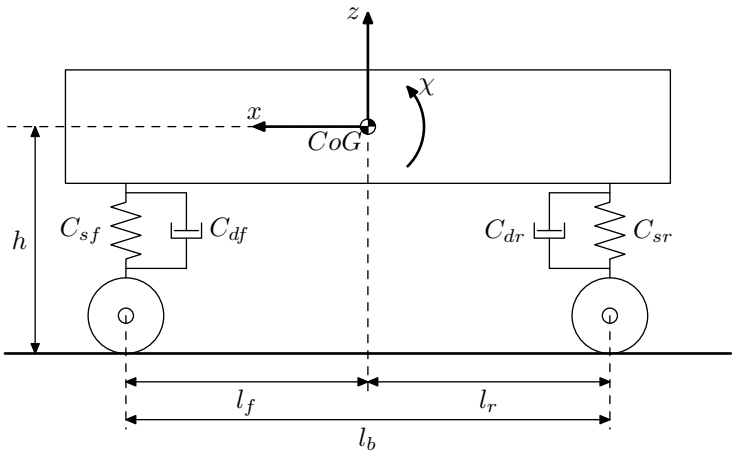

(a) *Definition of the variables used to describe the vertical motion of the vehicle.*

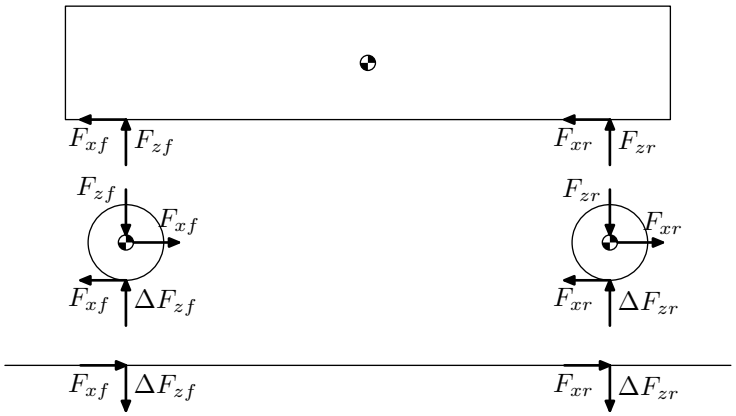

(b) *Vertical and longitudinal forces acting on the vehicle, relevant for our model.*

Figure 1: *Side view of the vehicle, introducing the variables used to model the vertical motion of the vehicle.*

2.1 Modeling

In Figure 1 we provide a side view of the vehicle, where the variables necessary for the present derivation are defined. First of all, let us write down the spring and damper equations,

$$F_{zf} = -C_{sf}(z - l_f\chi) - C_{df}(\dot{z} - l_f\dot{\chi}), \tag{2a}$$
$$F_{zr} = -C_{sr}(z + l_r\chi) - C_{dr}(\dot{z} + l_r\dot{\chi}), \tag{2b}$$

where C_{sf}, C_{sr}, C_{df} and C_{dr} are the front (f) and the rear (r) spring (s) and damper (d) constants, respectively. The vertical position of the complete chassis is denoted by z. We also assume that the pitch angles are small, implying that $l_i \tan\chi \approx l_i\chi$, $i = f, r$.

The vehicle body's kinetic motion equation in the vertical direction is given by

$$m\ddot{z} = F_{zr} + F_{zf}, \tag{3}$$

where F_{zr} and F_{zf} are the vertical spring and damper forces of the front and rear axle, respectively.

The longitudinal kinetic equation of the vehicle's body is given by

$$m\ddot{x} = F_{xf} + F_{xr} - F_{\text{air}}, \tag{4}$$

where F_{xf} and F_{xr} are the longitudinal forces acting on the wheel traction (positive values) or braking force (negative values) and F_{air} is the drag, given by

$$F_{\text{air}} = c_W A \frac{\rho}{2} v_x^2, \tag{5}$$

where the air density ρ is approximately $1.23\ \text{kg/m}^3$ at $1.0133\ \text{bar}$ and $15\ ^\circ\text{C}$ (Mitschke and Wallentowitz, 2004). The cross section is A and the drag coefficient is c_W.

Finally, let us write down the torque equilibrium

$$\ddot{\chi} I_{yy} = -F_{zf} l_f + F_{zr} l_r - (F_{xf} + F_{xr})h - F_{\text{air}}(h_{\text{air}} - h), \tag{6}$$

where h and h_{air} are the heights of the center of gravity and the center of drag, respectively.

These equations are comprehensive and not all states and parameters are known. Some of the parameters are given by the vehicle manufacturer, other parameters must be identified. Let us first investigate what we know about the vehicle, i.e. what we are measuring with the standard sensors. In our vehicle[1] we measure the following variables related to the longitudinal and the pitch motion,

- the vertical position of the front and the rear suspension, Δz_f and Δz_r,
- the longitudinal acceleration a_x,
- the longitudinal velocity v_x and
- the torque and revolution at the internal combustion engine.

The ratio between the front and the rear wheel's longitudinal forces differ depending on whether the vehicle is driving or braking.

The brake force is by construction higher on the front wheels than on the rear wheels. This brake force ratio contributes to a torque around the front wheels. When driving or coasting, the traction forces apply on the driven axle. Our vehicle is all wheel driven and the traction forces on the front and the rear wheels are approximately equal. Hence, the resulting traction force is not applied on the same position as the resulting brake force and in addition whether braking or driving it leads to a non-symmetric pitch behavior.

[1] The measurements were collected in cooperation with Nira Dynamics AB using an Audi S3.

2.2 Identification

In order to estimate the spring and damper constants, we form a linear gray-box model and the parameters are identified using standard prediction error methods (Ljung, 1999). In this gray-box model we make use of the suffix χ to clarify that it models the pitch dynamics. Define the states

$$\boldsymbol{x}_\chi = \begin{bmatrix} z & \dot{z} & \chi & \dot{\chi} \end{bmatrix}^{\mathrm{T}}, \tag{7}$$

and the input signals

$$\boldsymbol{u}_\chi = \begin{bmatrix} a_x & v_x^2 \end{bmatrix}^{\mathrm{T}}. \tag{8}$$

Here it is worth noting that the velocity signal is squared before it is used as an input signal. Finally, the output is defined according to

$$\boldsymbol{y}_\chi = \begin{bmatrix} \Delta z_f & \Delta z_r \end{bmatrix}^{\mathrm{T}}. \tag{9}$$

To simplify things, we assume $C_s \triangleq C_{sf} = C_{sr}$ and $C_d \triangleq C_{df} = C_{dr}$. The parameters to be identified are

$$\boldsymbol{\theta}_\chi = \begin{bmatrix} C_s & C_d & l_f & h_{\text{air}} \end{bmatrix}^{\mathrm{T}}. \tag{10}$$

Let us now substitute the traction forces using (4) and the spring and damper forces (2) into (3) and (6) according to

$$\begin{aligned} m\ddot{z} &= -(2C_s)z - (2C_d)\dot{z} + (C_s l_f - C_s(l_b - l_f))\varphi \\ &\quad + (C_d l_f - C_d(l_b - l_f))\dot{\varphi} \qquad (11a) \\ I_{yy}\ddot{\chi} &= (C_s l_f - C_s(l_b - l_f))z + (C_d l_f - C_d(l_b - l_f))\dot{z} \\ &\quad - (C_s l_f^2 + C_s(l_b - l_f)^2)\chi - (C_d l_f^2 + C_d(l_b - l_f)^2)\dot{\chi} \\ &\quad - m\ddot{x}h - F_{\text{air}}h_{\text{air}}. \qquad (11b) \end{aligned}$$

The relation between the pitch angle χ and the measurements $\boldsymbol{y}_\chi$

$$\chi = \arctan\left(\frac{\Delta z_r - \Delta z_f}{l_b}\right) \approx \frac{\Delta z_r - \Delta z_f}{l_b} \tag{12}$$

is used to derive a measurement equation, which together with (11) finally brings us to the state-space model

$$\begin{aligned} \dot{x}_\chi &= \begin{bmatrix} 0 & 1 & 0 & 0 \\ -\frac{2C_s}{m} & -\frac{2C_d}{m} & \frac{C_s l_f - C_s l_r}{m} & \frac{C_d l_f - C_d l_r}{m} \\ 0 & 0 & 0 & 1 \\ \frac{C_s l_f - C_s l_r}{I_{yy}} & \frac{C_d l_f + C_d l_r}{I_{yy}} & -\frac{C_s l_f^2 + C_s l_r^2}{I_{yy}} & -\frac{C_d l_f^2 + C_d l_r^2}{I_{yy}} \end{bmatrix} x_\chi \\ &\quad + \begin{bmatrix} 0 & 0 \\ 0 & 0 \\ 0 & 0 \\ -\frac{mh}{I_{yy}} & -\frac{F_{\text{air}}h_{\text{air}}}{I_{yy}} \end{bmatrix} u_\chi, \qquad (13a) \\ y_\chi &= \begin{bmatrix} 1 & 0 & -l_f & 0 \\ 1 & 0 & l_r & 0 \end{bmatrix} x_\chi, \qquad (13b) \end{aligned}$$

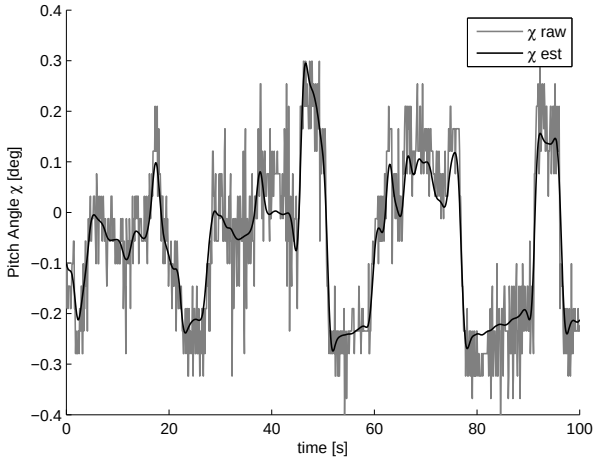

Figure 2: *Illustration of the model validation. The gray line corresponds to the raw measurement of the pitch angle, calculated from the measurements using* (9)*. The black line corresponds to the pitch angle produced by the identified model.*

where $l_r = l_b - l_f$. Measurements with acceleration and brake maneuvers excites the system and are suitable for estimating the parameters. The measurements from the standard sensors are noisy and are therefore filtered before being used for identification purposes. Since the identification can be performed off-line, a zero-phase forward and backward filter is employed. We used two different data sets collected the same day, but on different routs for estimation and validation. More information about the data is presented in Section 5.

A data sequence from the German Autobahn was used to identify the following parameters

$$\widehat{C}_s = 8.24 \cdot 10^4, \qquad \hat{l}_f = 1.45,$$
$$\widehat{C}_d = 4.45 \cdot 10^3, \qquad \hat{h}_{\text{air}} = 0.19,$$

and a validation sequence from a different data set is shown in Figure 2. The raw pitch angle, directly calculated from the measurements using (9) is shown together with the pitch angles computed by our model. Clearly the model match the measurements, indicating that our model is able to capture the pitching dynamics. The corresponding longitudinal acceleration a_x, which is used as input signal to the model is shown in Figure 3. Whenever the vehicle accelerates this will result in a vertical motion, or in other words the pitch angle will change as a result of acceleration. That this is indeed the case for our model should be clear by comparing Figure 2 to Figure 3. For example, at time $t = 45$ s there is a negative acceleration (i.e. the vehicle is braking), intuitively this leads to a positive pitching motion (recall the definition of the pitch angle χ in Figure 1(a)).

The input and output signals are corrupted with noise and the state-space model (13) is used within a Kalman filter framework to estimate the states. The load transfer is derived using the spring and damper forces (2) and the estimated states from the Kalman filter

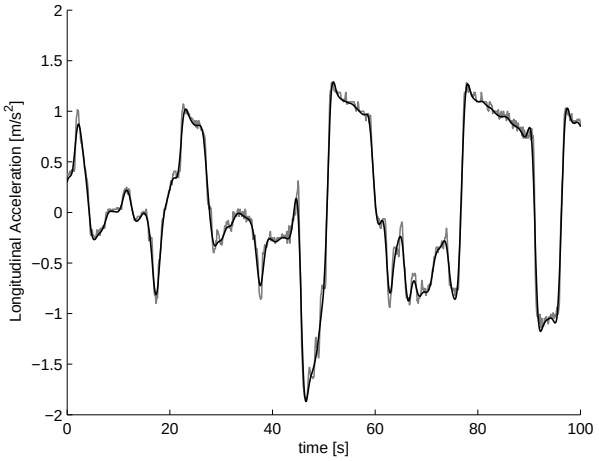

Figure 3: *Here the longitudinal acceleration a_x, which is one of the inputs to the model, is shown. The gray line shows the raw measurement signal and the black line shows the filtered signal.*

according to

$$\Delta F_{zf} = C_{sf} l_f \chi + C_{df} l_f \dot{\chi}, \tag{14a}$$

$$\Delta F_{zr} = -C_{sr} l_r \chi - C_{dr} l_r \dot{\chi}. \tag{14b}$$

3 Lateral and Yaw Dynamics

We will only be concerned with the vehicle motion during normal driving situations and not at the adhesion limit. This implies that the single track model is sufficient for our purposes (Mitschke and Wallentowitz, 2004). The geometry of the single track model with slip angles is provided in Figure 4. It is here worth to point out that the velocity vector of the vehicle is typically not in the same direction as the longitudinal axis of the vehicle. Instead the vehicle will move along a path at an angle β with the longitudinal direction of the vehicle. Hence, the angle β is defined as,

$$\tan \beta = \frac{v_y}{v_x}, \tag{15}$$

where v_x and v_y are the vehicle's longitudinal and lateral velocity components, respectively. This angle β is referred to as the float angle (Robert Bosch GmbH, 2004) or the vehicle body side slip angle (Kiencke and Nielsen, 2005). Lateral slip is an effect of cornering. To turn, a vehicle needs to be affected by lateral forces. These are provided by the friction when the wheels slip.

The slip angle $\alpha_i, i = f, r$ is defined as the angle between the central axis of the wheel and the path along which the wheel moves. The phenomenon of side slip is mainly due to the lateral elasticity of the tire. For reasonably small slip angles, at maximum 3° or up

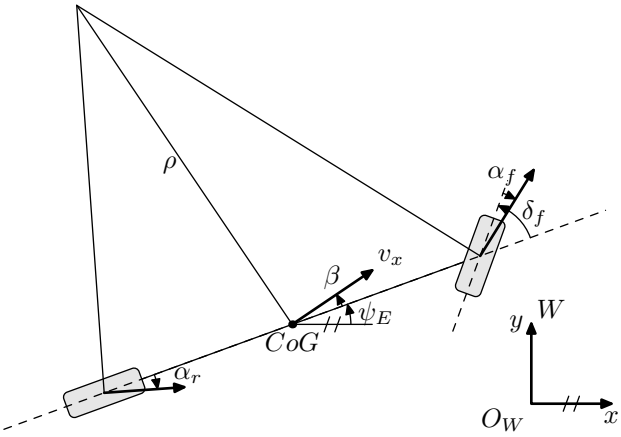

Figure 4: *In the single track model the wheels on each axle are modeled as single units. The velocity vector v_x, with the float angle β to the longitudinal axis of the vehicle, is attached at the center of gravity. Furthermore, the wheel slip angles are referred to as α_f and α_r. The front wheel angle is denoted by δ_f and the current radius is denoted by ρ.*

to a centripetal force of approximately $4\ \mathrm{m/s^2}$, it is a good approximation to assume that the lateral friction force of the tire F_i is proportional to the slip angle,

$$F_i = C_{\alpha i}\alpha_i, \qquad i = f,\, r. \tag{16}$$

The parameter $C_{\alpha i}$ is called cornering stiffness and describes the cornering behavior of the tire. The load transfer to the front axle when braking or to the rear axle when driving can be considered by identifying the cornering stiffness as a parabolic function according to Mitschke and Wallentowitz (2004)

$$C_{\alpha i} = \left(C_{\alpha i0} - C_{\alpha i1}\frac{F_{zi}}{F_{zi,\mathrm{nom}}}\right)F_{zi}, \qquad i = f, r. \tag{17}$$

The nominal normal force $F_{zi,\mathrm{nom}}$ is constant and specified by the tire manufacturer. The current vertical force F_{zi} is given by the normal force at stationary conditions $F_{zi,\mathrm{stat}}$ and the load transfer ΔF_{zi} according to

$$F_{zi} = F_{zi,\mathrm{stat}} + \Delta F_{zi}, \tag{18}$$

where the load transfer ΔF_{zi} is given in (14).

We can now derive a nonlinear state-space model for the vehicle lateral and yaw dynamics, using the following state vector

$$\boldsymbol{x}_\psi = \begin{bmatrix}\dot{\psi}_E & \beta\end{bmatrix}^{\mathrm{T}}, \tag{19}$$

i.e., the yaw rate $\dot{\psi}_E$ and the float angle β. The front wheel angle δ_f and the vehicle longitudinal velocity v_x are both modelled as input signals,

$$\boldsymbol{u}_\psi = \begin{bmatrix}\delta_f & v_x\end{bmatrix}^{\mathrm{T}}, \tag{20}$$

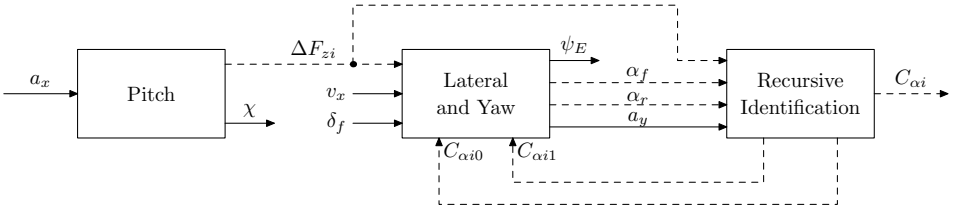

Figure 5: *Illustration of our approach to recursive identification of the cornering stiffness parameters. The solid lines corresponds to input signals (arrows pointing to the box) or measurement signals (arrows pointing away from the box) and the dashed lines corresponds to state or parameter estimates that are not directly measured. The pitch dynamics was treated in Section 2 and this is where the load transfer ΔF_{zi} is computed, which is used in forming the regression vector* (27)*. Furthermore, by making use of the lateral and yaw dynamics we can estimate the slip angles and the lateral accelerations which are also needed in solving the recursive identification problem.*

and the measurements consists of the yaw rate and the lateral acceleration,

$$\boldsymbol{y}_\psi = \begin{bmatrix} \dot{\psi}_E & a_y \end{bmatrix}^{\mathrm{T}}. \tag{21}$$

The complete details of this derivation, within the present framework, are provided by Lundquist and Schön (2008b).

4 Recursive Identification

Our approach to recursive identification of the cornering stiffness parameters is illustrated in Figure 5. The main idea is to make use of both the pitch, the lateral and the yaw dynamics in order to form an appropriate identification problem. The equations modelling the dynamics have already been derived in Section 2 and Section 3. In this section we will pose the resulting recursive identification problem, starting with the regression model in Section 4.1 and the recursive solution is briefly described in Section 4.2.

4.1 Regression Model

The cornering stiffness parameters are identified using a linear regression model according to

$$\boldsymbol{y}_t = \varphi_t^{\mathrm{T}} \boldsymbol{\theta} + \boldsymbol{e}_t, \tag{22}$$

where $\boldsymbol{y}_t$ denote the measurements, φ_t denote the regression vector, $\boldsymbol{\theta}$ denote the parameters to be identified and $\boldsymbol{e}_t$ denote the measurement noise. To be more specific, the parameter vector is given by

$$\boldsymbol{\theta} = \begin{bmatrix} C_{\alpha f0} & C_{\alpha f1} & C_{\alpha r0} & C_{\alpha r1} \end{bmatrix}^{\mathrm{T}}. \tag{23}$$

Furthermore, the measurement vector is chosen as

$$\boldsymbol{y} = \begin{bmatrix} F_{yf} & F_{yr} \end{bmatrix}^{\mathrm{T}}, \tag{24}$$

where the lateral forces are computed using Newton's equation according to

$$F_{yf} = m_y a_{yf} = m\frac{l_r}{l_b}\left(a_{y,m} + l_f\ddot{\psi}_E\right)\cos\delta_f, \tag{25a}$$

$$F_{yr} = m_y a_{yr} = m\frac{l_f}{l_b}\left(a_{y,m} - l_r\ddot{\psi}_E\right). \tag{25b}$$

Furthermore, using (16) and (17) we have

$$F_{yf} = \left(C_{\alpha f0} - C_{\alpha f1}\frac{F_{zf}}{F_{zf,\text{nom}}}\right)F_{zf}\alpha_f, \tag{26a}$$

$$F_{yr} = \left(C_{\alpha r0} - C_{\alpha r1}\frac{F_{zr}}{F_{zr,\text{nom}}}\right)F_{zr}\alpha_r, \tag{26b}$$

implying that the regression matrix is given by

$$\varphi = \begin{bmatrix} F_{zf}\alpha_f & 0 \\ -F_{zf}\alpha_f\frac{F_{zf}}{F_{zf,\text{nom}}} & 0 \\ 0 & F_{zr}\alpha_r \\ 0 & -F_{zr}\alpha_r\frac{F_{zr}}{F_{zr,\text{nom}}} \end{bmatrix}. \tag{27}$$

The only thing that is missing is expressions for the slip angles. In order to derive these, let us start by considering the longitudinal velocities

$$v_x\cos\beta = v_{xr}\cos\alpha_r = v_{xf}\cos\left(\delta_f - \alpha_f\right), \tag{28}$$

which must all be equal, since the vehicle would stretch otherwise. The lateral velocities differer by the yaw rate according to

$$v_{xf}\sin\left(\delta_f - \alpha_f\right) = l_f\dot{\psi}_E + v_x\sin\beta, \tag{29a}$$

$$v_{xr}\sin\alpha_r = l_r\dot{\psi}_E - v_x\sin\beta. \tag{29b}$$

By combining these velocity equations we arrive at

$$\tan(\delta_f - \alpha_f) = \frac{\dot{\psi}_E l_f}{v_x\cos\beta} + \tan\beta, \tag{30a}$$

$$\tan\alpha_r = -\tan\beta + \frac{\dot{\psi}_E l_r}{v_x\cos\beta}. \tag{30b}$$

Under normal driving conditions we can assume small α and β angles, i.e. that $\tan\alpha = \alpha$ and $\tan\beta = \beta$ hold, which results in the following expressions for the slip angles

$$\alpha_f = -\frac{\dot{\psi}_E l_f}{v_x} - \beta + \tan\delta_f, \tag{31a}$$

$$\alpha_r = -\beta + \frac{\dot{\psi}_E l_r}{v_x}. \tag{31b}$$

This means that we can use the measurements v_x and δ_f and the estimated states $\dot{\psi}_E$ and β to calculate the slip angles.

4.2 Constrained Recursive Least Squares

The cornering stiffness parameters $\boldsymbol{\theta}$, given in (23), can now be estimated on-line by making use of the recursive solution to the following least squares problem,

$$\hat{\boldsymbol{\theta}} = \underset{\boldsymbol{\theta} \in D_{\mathcal{M}}}{\arg\min} \frac{1}{2} \sum_{k=1}^{t} \lambda^{t-k} (\boldsymbol{y}_k - \varphi_k^{\mathrm{T}} \boldsymbol{\theta})^{\mathrm{T}} \Lambda^{-1} (\boldsymbol{y}_k - \varphi_k^{\mathrm{T}} \boldsymbol{\theta}), \tag{32}$$

where $0 < \lambda \leq 1$ is the so called forgetting factor. Furthermore, Λ denote a weighting matrix, which can be used to acknowledge the relative importance of the different measurements. It is possible to let λ and/or Λ be time varying. This can for instance be used to model the fact that the parameters are not identifiable during low excitation, i.e., when accelerations or velocities are missing. Finally, $D_{\mathcal{M}}$ is used to denote the set of values over which $\boldsymbol{\theta}$ ranges in the given model structure i.e., enforcing constraints on the parameter $\boldsymbol{\theta}$. The unconstrained recursive solution to (32) is given by

$$\hat{\boldsymbol{\theta}}_t = \hat{\boldsymbol{\theta}}_{t-1} + K_t \left(\boldsymbol{y}_t - \varphi_t^{\mathrm{T}} \hat{\boldsymbol{\theta}}_{t-1} \right), \tag{33a}$$

$$K_t = P_{t-1} \varphi_t \left(\lambda_t \Lambda_t + \varphi_t^{\mathrm{T}} P_{t-1} \varphi_t \right)^{-1}, \tag{33b}$$

$$P_t = \frac{1}{\lambda_t} \left(P_{t-1} - P_{t-1} \varphi_t (\lambda_t \Lambda_t + \varphi_t^{\mathrm{T}} P_{t-1} \varphi_t)^{-1} \varphi_t^{\mathrm{T}} P_{t-1} \right). \tag{33c}$$

This is commonly referred to as the recursive least square (RLS) algorithm. For a detailed account of the RLS algorithm and recursive identification in general we refer to Ljung (1999), Ljung and Söderström (1983).

The constraint $\boldsymbol{\theta} \in D_{\mathcal{M}}$ can be enforced by simply projecting the estimates back into $D_{\mathcal{M}}$ when necessary (Ljung, 1999),

$$\hat{\boldsymbol{\theta}}_t = \begin{cases} \hat{\boldsymbol{\theta}}_t & \text{if } \hat{\boldsymbol{\theta}}_t \in D_{\mathcal{M}} \\ \hat{\boldsymbol{\theta}}_{t-1} & \text{if } \hat{\boldsymbol{\theta}}_t \notin D_{\mathcal{M}} \end{cases} \tag{34}$$

5 Experiments and Results

The measurements used to illustrate and evaluate the approach proposed in this work were collected during normal driving conditions. Note that we are only using measurements that are directly available on the CAN bus in our test vehicle.

The cornering stiffness parameters are identified using the RLS algorithm given in (32) using the model given in (22) – (27), with $\Lambda = I$ and $\lambda = 0.99$. Furthermore, the cornering stiffness parameters $\boldsymbol{\theta}$ have to belong to the following set $D_{\mathcal{M}}$,

$$\begin{aligned} 20000 < C_{\alpha i} < 120000, \quad & i = f, r, \\ \boldsymbol{\theta} > 0, & \\ C_{\alpha i 0} > C_{\alpha i 1}, \quad & i = f, r. \end{aligned} \tag{35}$$

The projection (34) is typically active in the beginning of the data sequence or when the system is not exited, i.e. at low velocities or at low lateral accelerations.

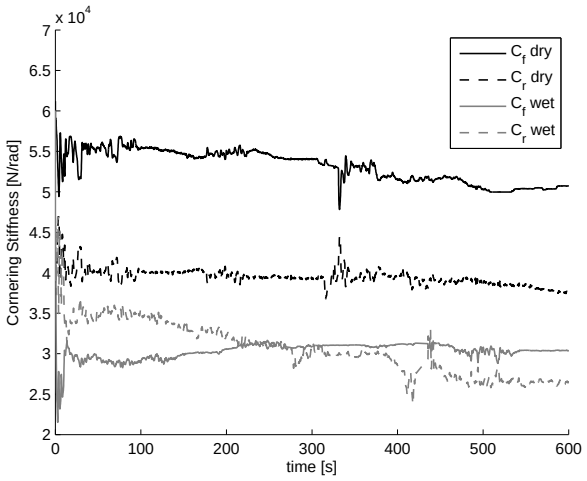

Figure 6: *Identified cornering stiffness parameters as a function of time for two different cases, wet and dry asphalt, respectively.*

Let us start out by providing an illustration of the identified cornering stiffness parameters in Figure 6. The measurements were collected in a test vehicle, which starts from a crossover, accelerates to approximately $100\ \mathrm{km/h}$ and follows a rural road for $10\ \mathrm{min}$. Since we do not have access to the true values for the cornering stiffness parameters it is impossible to directly evaluate the accuracy. However, one interesting comparison is made in the figure. That is that there is a significant difference in the value depending on whether the asphalt is dry or wet. This was expected, since the cornering stiffness parameters describes the tire-road contact, which of course varies with wet/dry asphalt. The stiffness is higher on dry asphalt than on a wet and slippery road.

In Figure 7 we try to illustrate the fact that when the longitudinal acceleration is small, the covariance given in (33c) increase and as soon as there is a significant longitudinal acceleration present, the covariance is reduced. This illustrates the excitation problems inherent in this problem.

The slip angles are computed according to (31) and the result is illustrated in Figure 8. Since there are no measurements, we cannot objectively evaluate these estimates. However, based on knowledge about the test drive it can at least be said that the slip angles agrees with the expectation.

The experiments were performed on various public roads in Germany and the results are encouraging. In order to thoroughly validate the results it is necessary to carry out more dedicated experiments and use reference measurement equipment.

6 Conclusion

The contribution of this paper is a method for recursive identification of the cornering stiffness parameters that are essential for the single track model. Both the vertical, the lateral and the yaw dynamics are used to form the resulting regression problem that is

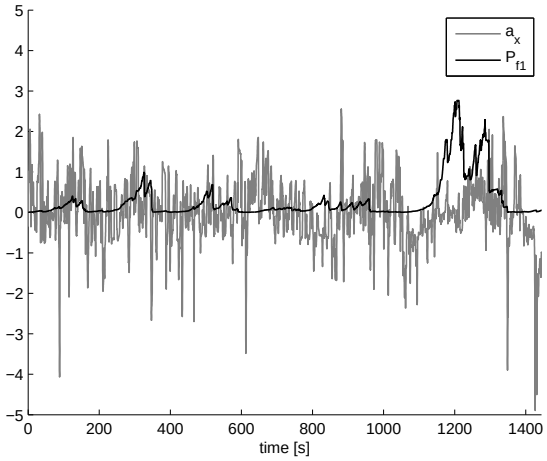

Figure 7: *Illustration of the longitudinal acceleration and the covariance associated to the parameter $C_{\alpha f1}$. The plot shows that whenever there is little excitation in the acceleration, the covariance grows and as soon as there is significant acceleration present, the covariance is reduced.*

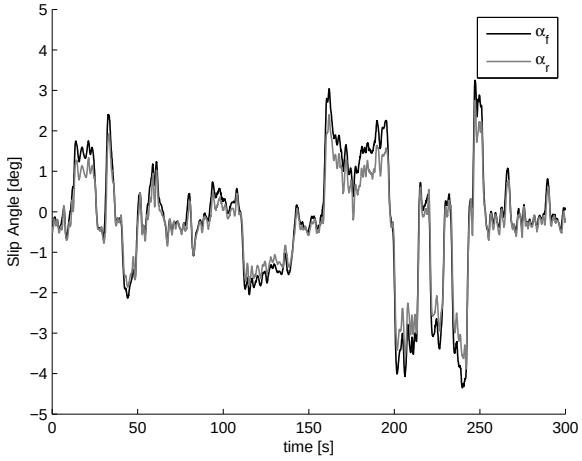

Figure 8: *The calculated slip angles during part of the time window used in Figure 7.*

solved using a constrained RLS algorithm. In order to find the vertical (pitch) dynamics we had to solve a linear gray-box problem. The method has been successfully evaluated on real measurements.

Acknowledgement

The authors would like to thank Andreas Andersson at Nira Dynamics for fruitful discussions on the German Autobahn and for providing the data. Furthermore, they would like to thank the SEnsor Fusion for Safety (SEFS) project within the Intelligent Vehicle Safety Systems (IVSS) program and the strategic research center MOVIII, funded by the Swedish Foundation for Strategic Research (SSF) for financial support.

References

Baffet, G., Charara, A., and Lechner, D. (2007). Experimental evaluation of a sliding mode observer for tire-road forces and an extended Kalman filter for the vehicle side slip angle. In *Proceedings of the 46th IEEE Conference on Decision and Control*, pages 3877–3882, New Orleans, LA, USA.

Graebe, S. (1990). *Theory and Implementation of Gray Box Identification*. PhD thesis, Royal Institute of Technology, Stockholm, Sweden.

Grip, H. F., Imsland, L., Johansen, T. A., Fossen, T. I., Kalkkuhl, J. C., and Suissa, A. (2008). Nonlinear vehicle side-slip estimation with friction adaptation. *Automatica*, 44(3):611 – 622.

Kiencke, U. and Nielsen, L. (2005). *Automotive Control Systems*. Springer, Berlin, Heidelberg, Germany, second edition.

Ljung, L. (1999). *System identification, Theory for the user*. System sciences series. Prentice Hall, Upper Saddle River, NJ, USA, second edition.

Ljung, L. and Söderström, T. (1983). *Theory and Practice of Recursive Identification*. The MIT Press series in Signal Processing, Optimization, and Control. The MIT Press, Cambridge, Massachusetts.

Lundquist, C. and Schön, T. B. (2008a). Road geometry estimation and vehicle tracking using a single track model. In *Proceedings of the IEEE Intelligent Vehicles Symposium*, pages 144–149, Eindhoven, The Netherlands.

Lundquist, C. and Schön, T. B. (2008b). Road geometry estimation and vehicle tracking using a single track model. Technical Report LiTH-ISY-R-2844, Department of Electrical Engineering, Linköping University, SE-581 83 Linköping, Sweden.

Mitschke, M. and Wallentowitz, H. (2004). *Dynamik der Kraftfahrzeuge*. Springer, Berlin, Heidelberg, 4th edition.

Robert Bosch GmbH, editor (2004). *Automotive Handbook*. SAE Society of Automotive Engineers, 6th edition.

Sienel, W. (1997). Estimation of the tire cornering stiffness and its application to active car steering. In *Proceedings of the 36th Conference on Decision and Control*, pages 4744–4749, San Diego, CA, USA.

Sierra, C., Tseng, E., Jain, A., and Peng, H. (2006). Cornering stiffness estimation based on vehicle lateral dynamics. *Vehicle System Dynamics*, 44(1):24–38.

Wesemeier, D. and Isermann, R. (2006). Identification of the vehicle cornering stiffness by parallel identification and simulation. In *Proceedings of the 4th IFAC Symposium on Mechatronic Systems*, Heidelberg, Germany.

Paper C

Estimation of the Free Space in Front of a Moving Vehicle

Authors: Christian Lundquist and Thomas B. Schön.

Edited version of paper originally published in the Special Publication *Intelligent Vehicle Initiative (IVI) Technology Advanced Controls of the SAE World Congress*, SAE paper 2009-01-1288, Detroit, MI, USA, 2009.

Preliminary version published as Technical Report LiTH-ISY-R-2892, Department of Electrical Engineering, Linköping University, Linköping, Sweden.

Estimation of the Free Space in Front of a Moving Vehicle

Christian Lundquist and Thomas B. Schön

Department of Electrical Engineering,
Linköping University,
SE–581 83 Linköping, Sweden.
E-mail: (lundquist, schon)@isy.liu.se.

Abstract

There are more and more systems emerging making use of measurements from a forward looking radar and a forward looking camera. It is by now well known how to exploit this data in order to compute estimates of the road geometry, tracking leading vehicles, etc. However, there is valuable information present in the radar concerning stationary objects, that is typically not used. The present work shows how radar measurements of stationary objects can be used to obtain a reliable estimate of the free space in front of a moving vehicle. The approach has been evaluated on real data from highways and rural roads in Sweden.

Keywords: road geometry, weighted least squares, quadratic program, road borders, free space estimation, automotive radar, road mapping

1 Introduction

For a collision avoidance system it is imperative to have a reliable *map* of the environment surrounding the ego vehicle. This map, consisting of both stationary and moving objects, has to be built in real time using measurements from the sensors present in the ego vehicle. This is currently a very active research topic within the automotive industry and many other areas as well. Great progress has been made, but much remains to be done. Current state-of-the-art when it comes to the problem of building maps for autonomous vehicles can be found in the recent special issues by Buehler et al. (2008a,b,c) on the 2007 DARPA Urban Challenge. In these contributions measurements from expensive and highly accurate sensors are used, while we in the present paper utilize measurements from off-the-shelf automotive radars.

In this contribution we consider the problem of estimating the *free space* in front of the vehicle, making use of radar measurements originating from stationary objects. The free space is defined as the space where a ground vehicle can manoeuvre without colliding with other objects. Another name for the free space is the drivable space.

The present solution makes use of an already existing sensor fusion framework by Lundquist and Schön (2008a), which among other things provided a good road geometry estimate. This framework improves the raw vision estimate of the road geometry by fusing it with radar measurements of the leading vehicles. The idea is that the motion of the leading vehicles reveals information about the road geometry, as described by e.g., Zomotor and Franke (1997), Gern et al. (2000, 2001). Hence, if the leading vehicles can be accurately tracked, their motion can be used to improve the road geometry estimates. Furthermore, we used a solid dynamic model of the ego vehicle allowing us to further refine the estimates by incorporating several additional proprioceptive sensor measurements readily available on the CAN bus. The resulting, rather simple, yet useful *map* of the environment surrounding the ego vehicle consists in

- Road geometry, typically parameterized using road curvature and curvature rate.
- Position and velocity of the leading vehicles.
- Ego vehicle position, orientation and velocity.

This information can and has indeed been used to design simpler collision avoidance systems. However, in order to devise more advanced systems, more information about the environment surrounding the ego vehicle is needed. The purpose of this paper is to exploit information already delivered by the radar sensor in order to compute a more complete map. Hence, there is no need to introduce any new sensors, it is just a matter of *making better use of the sensor information that is already present* in a modern premium car. To be more precise, it is the radar echoes from stationary objects that are used to estimate the road borders, which determines the free space in front of the ego vehicle. The radar measurements used originate from for instance, guardrails and concrete walls. Obviously these stationary radar measurements are not enough to fully explain the road borders. However, as we will see, there is surprisingly much information present in these measurements.

The *key* in our approach is to make use of the road curvature estimate from the sensor fusion framework by Lundquist and Schön (2008a) mentioned above to sort the stationary radar measurements according to which side of the road they originate from. These measurements are then used together with the estimates from the sensor fusion to dynamically form a suitable constrained quadratic program (QP) for estimating the free space in front of the vehicle. This QP models the temporal correlation that exists in roads and the fact that the road shape cannot change arbitrarily fast.

The approach has been evaluated on real data from highways and rural roads in Sweden. The test vehicle is a Volvo S80 equipped with a forward looking 77 GHz mechanically scanned FMCW radar and a forward looking vision sensor (camera).

2 Related Work

We have also investigated a completely different approach to represent the map of the free space in front of the ego vehicle based on so call occupancy grid maps (OGM). This is a commonly used method for tackling the problem of generating consistent maps from uncertain measurements of stationary object under the assumption that the ego vehicle pose is known. Occupancy grid maps are very popular in the robot community, especially for all sorts of autonomous vehicles equipped with laser scanners, indeed several of the DARPA vehicles, described by e.g., Buehler et al. (2008a,b,c), used OGM's. The OGM was introduced by Elfes (1987) and a solid treatment can be found in the recent textbook by Thrun et al. (2005).

The map is discretized into a number of cells with an associated probability of occupancy. The map is represented by a matrix, with each element corresponding to a map-cell. Figure 1a shows an OGM computed for the highway situation given in the ego vehicle's camera view in Figure 1b. The ego vehicle is positioned at $(200, 200)$, indicated by the filled circle. The gray-level in the occupancy map indicates the probability of occupancy, the darker the grid cell, the more likely it is to be occupied. As can be seen in Figure 1a, the OGM generates a good-looking *overview* of the traffic situation. However, since the measurements are obtained from a standard automotive radar the results are not very informative for a collision avoidance system, better accuracy is needed. For a more complete description of the application of the OGM to the present problem we refer to Lundquist et al. (2009).

The work presented here is clearly related to lane tracking, which by now is a very well-studied problem, see e.g., McCall and Trivedi (2006) for a recent survey using cameras. In fact the required sensor fusion framework by Lundquist and Schön (2008a) makes use of the estimates from a visual lane tracker. The recent book by Dickmanns (2007) contains a lot of interesting information about detecting and tracking lanes using cameras. Lane tracking has also been tackled using radar sensors, see e.g., Kaliyaperumal et al. (2001), Lakshmanan et al. (1997), Nikolova and Hero (2000), Ma et al. (2000) and laser sensors, see e.g. Wijesoma et al. (2004). Using laser scanners there have been several approaches making use of reflections from the road boundary, such as crash barriers and reflection posts, to compute information about the free space, see e.g., Kirchner and Heinrich (1998), Kirchner and Ameling (2000), Sparbert et al. (2001). Furthermore, the use of a side looking radar to measure the lateral distance to a sidewall is described in various papers, e.g., Mayhan and Bishel (1982), Tamiya et al. (1996), Fukae et al. (1996). The intended application in these papers by Mayhan and Bishel (1982), Tamiya et al. (1996), Fukae et al. (1996) were automatic lateral control. Here, we have no specific application in mind, we just try to obtain the best possible map based on the available sensor information. This map can then be used by any control system.

Wedel et al. (2008) presents an algorithm for free space estimation, capable of handling non-planar roads, using a stereo camera system. Similar to the present paper the authors make use of a parametric model of the road ahead. An interesting avenue for future work is to combine the idea presented in this paper with the ideas of Wedel et al. (2008) within a sensor fusion framework.

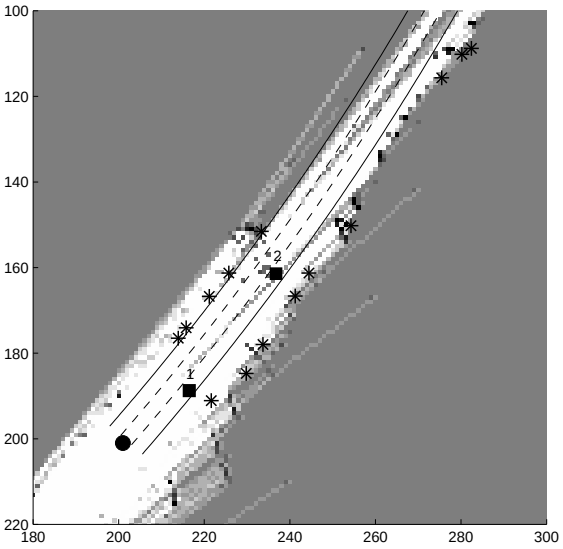

(a)

(b)

Figure 1: *The filled circle at position* $(200, 200)$ *in the occupancy grid map in Figure (a) is the ego vehicle, the stars are the radar observations obtained at this time sample, the black squares with numbers 1 and 2 are the two leading vehicles that are currently tracked. The gray-level in the figure indicates the probability of occupancy, the darker the grid cell, the more likely it is to be occupied. The shape of the road is given as solid and dashed lines, calculated as described by Lundquist and Schön (2008a). The camera view from the ego vehicle is shown in Figure (b), the concrete walls, the guardrail and the pillar of the bridge are interesting landmarks. Furthermore, the two tracked leading vehicles are clearly visible in the right lane.*

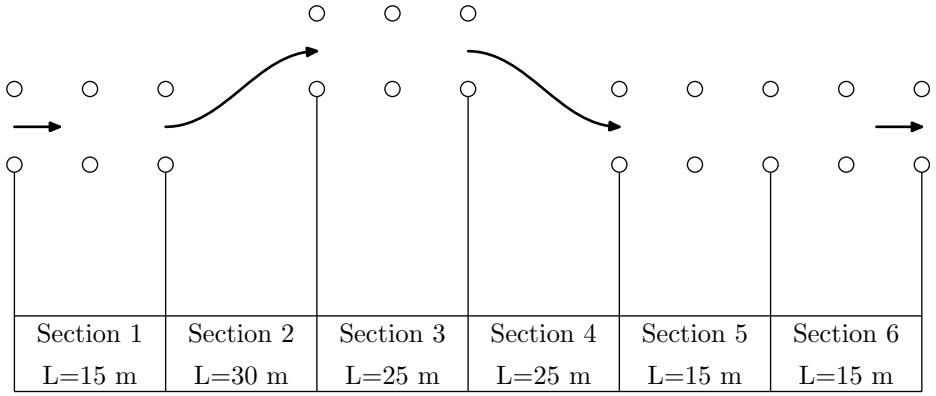

Figure 2: *ISO* 3888 *double lane change maneuver according to ISO (1999).*

3 Problem Formulation

An important question is how the information of the free space should be represented and for which distances ahead of the vehicle that it is needed. We will start by addressing the latter through an example, the standard double lane change maneuver according to ISO (1999). In this maneuver a vehicle has to overtake an obstacle and come back to its original lane as shown in Figure 2. Assume that the ego vehicle is entering section 1 at a velocity of $100\ \mathrm{km/h}$ and that there is an obstacle straight ahead in section 3. The free space, i.e. the distance to the left and right road borders has to be known in order to autonomously overtake the obstacle as shown in the figure. This means that an automatic collision avoidance system needs to have information about the free space at least three sections ahead in order to make a decision on where to steer the vehicle. From this simple, yet informative, calculation we conclude that the road must be well estimated for at least $60\ \mathrm{m}$ ahead when driving at approximately $100\ \mathrm{km/h}$.

In this paper we will use the planar coordinate rotation matrix

$$R^{WE} = \begin{bmatrix} \cos\psi_E & -\sin\psi_E \\ \sin\psi_E & \cos\psi_E \end{bmatrix} \tag{1}$$

to transform a vector, represented in the vehicle's coordinate system E, into a vector, represented in the reference coordinate system W, where ψ_E is the angle of rotation from W to E. We will refer to this angle as the yaw angle of the vehicle. The point O_W is the origin of W and O_E is the origin of E situated in the vehicles center of gravity. The geometric displacement vector $\boldsymbol{d}^W_{EW}$ is the direct straight line from W to E represented with respect to the frame W. The angles and distances are shown in Figure 3.

A stationary object $\mathcal{S}_i$ may be observed by the ego vehicles radar in the point S_i. The radar in the ego vehicle measures the azimuth angle $\delta_{S_iE_s}$ and the range $d_{S_iE_s} = ||r^E_{S_iE_s}||_2$ to the stationary object. These are transformed into Cartesian coordinates according to

$$\boldsymbol{y}_{\mathcal{S}_i} = \begin{bmatrix} x^E_{S_iE_s} \\ y^E_{S_iE_s} \end{bmatrix} = \begin{bmatrix} d_{S_iE_s}\cos\delta_{S_iE_s} \\ d_{S_iE_s}\sin\delta_{S_iE_s} \end{bmatrix} \tag{2}$$

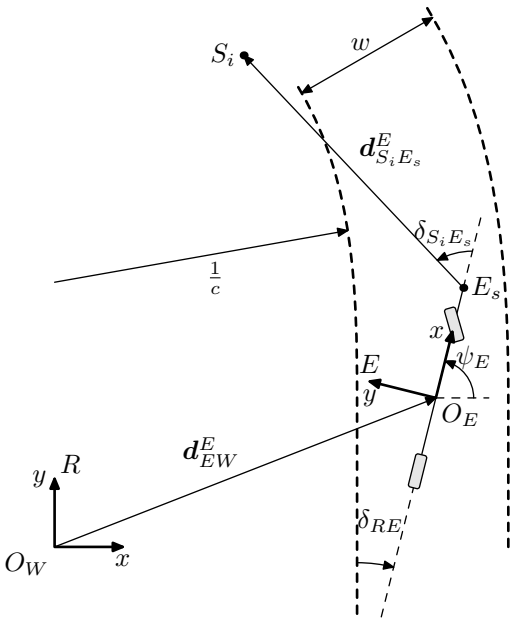

Figure 3: *The ego vehicle's coordinate frame E has its origin O_E situated in the vehicle's center of gravity. A stationary object $\mathcal{S}_i$ is observed at a distance $||\boldsymbol{d}^W_{S_iE_s}||_2$ and an angle $\delta_{S_iE_s}$ with respect to the vehicles radar, which is mounted in the radiator cowling at E_s. The lane width is w, the angle between the ego vehicle and the road is denoted ψ_{RE} and the road curvature is c.*

in the vehicle coordinate frame E.

All the observations of stationary objects $\mathbf{Y}_{\mathcal{S}} = \{\boldsymbol{y}_{\mathcal{S}_i}\}_{i=1}^{N_s}$ from the radar are sorted into two ordered sets, one for the left side $\mathbf{Y}_{\mathcal{S}l}$ and one for the right side $\mathbf{Y}_{\mathcal{S}r}$ of the road. In order to be able to perform this sorting we need some information about the road geometry, otherwise it is of course impossible. Lundquist and Schön (2008a) provide a sensor fusion framework for sequentially estimating the parameters l_E, ψ_{RE}, c_0 in the following model of the road's white lane markings,

$$y^E = l_E + \psi_{RE}x^E + \frac{c_0}{2}(x^E)^2, \tag{3}$$

where x^E and y^E are expressed in the ego vehicle's coordinate frame E. The angle between the longitudinal axis of the vehicle and the road lane is ψ_{RE}, see Figure 3. It is assumed that this angle is small and hence the approximation $\sin\psi_{RE} \approx \psi_{RE}$ is used. The curvature parameter is denoted by c_0 and the offset between the ego vehicle and the white lane is denoted by l_E.

The information about the road shape in (3) can now be used to decide if an observation should be sorted into the left set according to

$$\mathbf{Y}_{\mathcal{S}l} = \left\{\boldsymbol{y}_{\mathcal{S}_i} \in \mathbf{Y}_{\mathcal{S}} \mid y^E_{S_iE_s} \geq l_E + \psi_{RE}x^E_{S_iE_s} + \frac{c_0}{2}(x^E_{S_iE_s})^2\right\} \tag{4}$$

or the right set according to

$$\mathbf{Y}_{\mathcal{S}r} = \left\{ \boldsymbol{y}_{\mathcal{S}_i} \in \mathbf{Y}_{\mathcal{S}} \mid y^E_{S_iE_s} < l_E + \psi_{RE} x^E_{S_iE_s} + \frac{c_0}{2}(x^E_{S_iE_s})^2 \right\}. \tag{5}$$

Observations which lay more than $200\ \mathrm{m}$ behind the vehicle are removed from the set. The two sets $\mathbf{Y}_{\mathcal{S}l}$ and $\mathbf{Y}_{\mathcal{S}r}$ are resorted at every sample, according to the new curvature estimate.

Given the data in $\mathbf{Y}_{\mathcal{S}l}$ we seek a road border model, provided by a predictor

$$\hat{y}^E_{S_iE_s}(x^E_{S_iE_s}, \boldsymbol{\theta}), \tag{6}$$

where $\boldsymbol{\theta}$ denotes a parameter vector describing the road boarders. The exact form of this predictor is introduced in the subsequent section, where two different predictors are derived. The data in $\mathbf{Y}_{\mathcal{S}r}$ in treated analogously. The road boarder parameters $\boldsymbol{\theta}$ are estimated by solving the following least-square problem

$$\min_{\boldsymbol{\theta}} \quad \sum_{i=1}^{N} \lambda_i \left(y^E_{S_iE_s} - \hat{y}^E_{S_iE_s}(x^E_{S_iE_s}, \boldsymbol{\theta}) \right)^2, \tag{7}$$

where N is the number of observations and λ_i is a weighting factor. The problem (7) is formulated as if there is only an error in the y-coordinate. Obviously there are errors present also in the x-coordinate. This can be taken care of by formulating a so called errors-in-variables problem (within the optimization literature this problem is referred to as a total least squares problem), see e.g., Björck (1996). However, for the sake of simplicity we have chosen to stick to an ordinary least squares formulation in this work.

4 Road Border Model

In this section we will derive and analyze two different predictor models, one linear and one nonlinear.

An important problem to be solved is to decide which radar measurements that should be used in estimating the parameters. Later in this section we will introduce suitable constraints that must be satisfied. This will allow us to remove non-relevant data, i.e., outliers.

4.1 Predictor

The two ordered sets $\mathbf{Y}_{\mathcal{S}l}$ and $\mathbf{Y}_{\mathcal{S}r}$ are handled analogously. Hence, only the processing related to the left set is described here. The observations are expressed in the world coordinate system W when they are stored in $\mathbf{Y}_{\mathcal{S}r}$ as the system proceeds one time step. Obviously it is straightforward to transform them into the vehicle's coordinate system, using the rotation matrix $R^{EW} = (R^{WE})^{\mathrm{T}}$.

As depicted earlier the lanes are modeled using the polynomial (3). Let us assume that the white lane markings are approximately parallel with the road border. In order to allow the number of lanes to change, without simultaneously changing the curvature, we extend

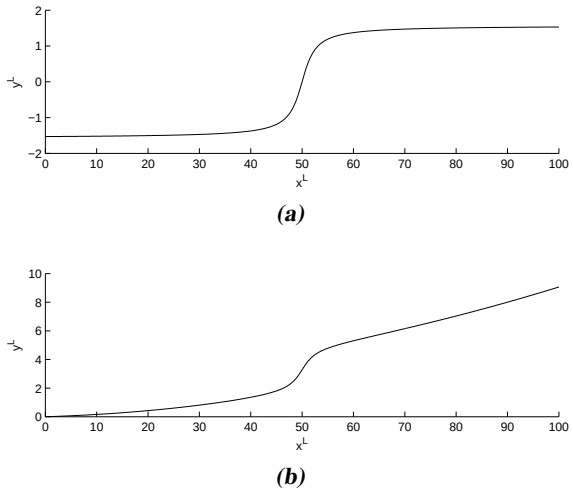

Figure 4: *A pure* $\arctan$ *is shown in Figure (a), whereas the complete expression* (9) *is shown in Figure (b) for a typical example.*

the second order model (3) with a fourth element. Hence, a linear predictor is provided by

$$\hat{y}_1^E(x^E, \boldsymbol{\theta}_{1l}) = l_0 + l_1 x^E + l_2 (x^E)^2 + l_3 (x^E)^3, \tag{8}$$

which is a third order polynomial, describing the road's left border, given in the ego vehicle coordinate frame.

By analyzing road construction standards, such as VGU (2004), we assume that the increment and decrement of the number of lanes can be modelled using the $\arctan$ function illustrated in Figure 4a. This allows for a continuous, but possible rapid, change in shape. Let us now, as a second approach, extend (3) and form the following nonlinear predictor

$$\hat{y}_2^E(x^E, \boldsymbol{\theta}_{2l}) = l_0 + l_1 x^E + l_2 (x^E)^2 + k \arctan \tau (x^E - b), \tag{9}$$

where the parameter b indicates where $\arctan$ crosses zero. The slope τ and magnitude k could be chosen according to typical road construction constants. An example of the complete nonlinear road border model (9) is shown in Figure 4b.

We will start describing the linear model (8) and come back to the nonlinear model (9) later in this section. Given the N_l observations in $\mathbf{Y}_{\mathcal{S}l}$, the parameters

$$\boldsymbol{\theta}_{1l} = \begin{bmatrix} l_0 & l_1 & l_2 & l_3 \end{bmatrix}^{\mathrm{T}} \tag{10}$$

can be approximated by rewriting the linear predictor (8) according to

$$\widehat{\mathbf{Y}}_{1l}^E = \Phi_l^E \, \boldsymbol{\theta}_{1l}, \tag{11}$$

where the regressors ($x_{S_i E_s} \in \mathbf{Y}_{\mathcal{S}l},\ i = 1, \ldots, N_l$)

$$\varphi_i^E = \begin{bmatrix} 1 & x_{S_i E_s}^E & (x_{S_i E_s}^E)^2 & (x_{S_i E_s}^E)^3 \end{bmatrix}^{\mathrm{T}}. \tag{12}$$

are stacked on top of each other in order to form

$$\Phi_l^E = \left[\varphi_1^E, \ldots, \varphi_{N_l}^E\right]^{\mathrm{T}}, \tag{13}$$

The parameters are found by minimizing the weighted least square error (7), here in matrix form

$$||\boldsymbol{Y}_l^E - \Phi_l^E\,\boldsymbol{\theta}_{1l}||_\Lambda^2 = (\boldsymbol{Y}_l^E - \Phi_l^E\,\boldsymbol{\theta}_{1l})^{\mathrm{T}}\Lambda(\boldsymbol{Y}_l^E - \Phi_l^E\,\boldsymbol{\theta}_{1l}), \tag{14}$$

where Λ is a weighting matrix

$$\Lambda = \mathrm{diag}(\begin{bmatrix}\lambda_1 & \cdots & \lambda_{N_l}\end{bmatrix}) \tag{15}$$

and the y-coordinates are given by

$$\boldsymbol{Y}_l^E = \left[y_{S_1E_s}^E, \ldots, y_{S_{N_l}E_s}^E\right]^{\mathrm{T}}. \tag{16}$$

The right hand side of the road is modeled analogously, using the following parameter vector,

$$\boldsymbol{\theta}_{1r} = \begin{bmatrix}r_0 & r_1 & r_2 & r_3\end{bmatrix}^{\mathrm{T}}. \tag{17}$$

The azimuth angle $\delta_{S_iE_s}$ is measured with lower accuracy than the range $d_{S_iE_s}$ in the radar system. This influences the uncertainty of the measurements, when transformed into Cartesian coordinates in accordance to the measured distance. Therefore, the elements of the weight matrix Λ in (14) are defined as

$$\lambda_i = \frac{1}{\log d_{S_iE_s}}, \quad i = 1, \ldots, N_l, \tag{18}$$

modeling the fact that stationary objects close to the vehicle are measured with higher accuracy than distant objects. Hence, the closer the object is, the hight the weight.

The problem of minimizing (14) can be rewritten as a quadratic program (Boyd and Vandenberghe, 2004) according to

$$\min_{\boldsymbol{\theta}_{1l}} \quad \boldsymbol{\theta}_{1l}^{\mathrm{T}}\,\Phi_l^{\mathrm{T}}\,\Lambda\,\Phi_l\,\boldsymbol{\theta}_{1l} - 2\left(\boldsymbol{Y}_l^E\right)^{\mathrm{T}}\,\Lambda\,\Phi_l\,\boldsymbol{\theta}_{1l}. \tag{19}$$

A straightforward solution of this problem will not work due to the simple fact that not all of the stationary objects detected by the radar stems from relevant objects for our purposes. For example, under some circumstances the radar also detects objects at the opposite side of the highway. These observations could for example stem from a guardrail or the concrete wall of a gateway from e.g., a bridge, see Figure 5b. If the road borders are estimated according to the quadratic program in (19) using these observations the result will inevitably be wrong. In order to illustrate that this is indeed the case the result is provided in Figure 5a. In the subsequent section we will explain how this situation can be avoided by deriving a set of feasibility conditions that the curve parameters $\boldsymbol{\theta}_{1l}$ and $\boldsymbol{\theta}_{1r}$ have to fulfill.

Let us briefly revisit the nonlinear model (9). Since this predictor is nonlinear, it cannot be factored in the same way as we did for the linear predictor in (11). Instead, we

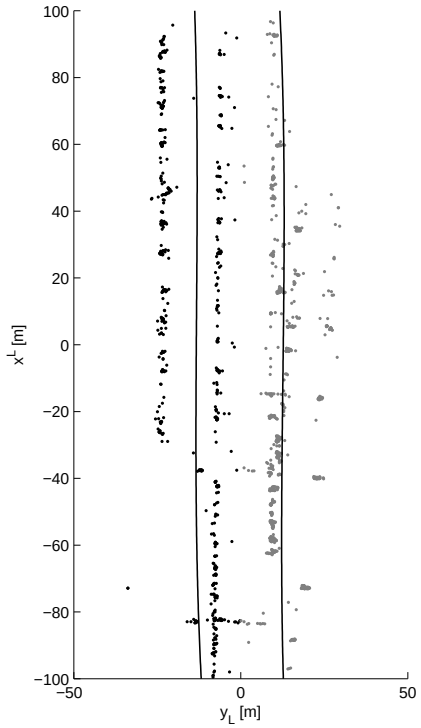

(a)

(b)

Figure 5: *The gateway shown on the opposite side of the highway in Figure (b) misleads the road boarder estimation. The stored observations are shown together with the estimated road boarders (lines) in Figure (a). The black points belongs to the left set* $\mathbf{Y}_{\mathcal{S}l}$ *and the gray points belongs to the right set* $\mathbf{Y}_{\mathcal{S}r}$*.*

have to keep the nonlinear form, resulting in the following optimization problem to be solved

$$\min_{\boldsymbol{\theta}} \quad \left\| \boldsymbol{Y}_l^E - \widehat{\boldsymbol{Y}}_{2l}^E(X_l^E, \boldsymbol{\theta}_{2l}) \right\|_\Lambda^2, \tag{20}$$

where $\boldsymbol{Y}_l^E$ was defined in (16) and similarly $\widehat{\boldsymbol{Y}}_{2l}^E$ are the nonlinear predictions

$$\hat{y}_{2li}^E(x_{S_iE_s}^E, \boldsymbol{\theta}_{2l}) = l_0 + l_1 x_{S_iE_s}^E + l_2 (x_{S_iE_s}^E)^2 + k \arctan \tau (x_{S_iE_s}^E - b) \tag{21}$$

stacked on top of each other. Hence, the parameters $\boldsymbol{\theta}_{2l}$ used in (20) are given by

$$\boldsymbol{\theta}_{2l} = \begin{bmatrix} l_0 & l_1 & l_2 & k & \tau & b \end{bmatrix}^{\mathrm{T}}. \tag{22}$$

The resulting problem (20) is a non-convex least-squares problem.

4.2 Constraining the Predictor

The predictor has to be constrained for the problem formulation to be interesting. More specifically, we will in this section derive constraints forming a convex set, guaranteeing that the resulting linear optimization problem remains quadratic. This problem can then be efficiently solved using a dual active set method[1], see e.g., Gill et al. (1991).

As we assume that the white lane markings (3) are approximately parallel with the road border (8), we could use the angle ψ_{RE} to constrain the second border parameter l_1 and we could use the curvature c_0 to constrain the third border parameter l_2 according to

$$(1-\Delta)\psi_{RE} - \epsilon_{\psi_{RE}} \leq l_1 \leq (1+\Delta)\psi_{RE} + \epsilon_{\psi_{RE}} \qquad \text{if } \psi_{RE} \geq 0, \tag{23a}$$

$$(1+\Delta)\psi_{RE} - \epsilon_{\psi_{RE}} \leq l_1 \leq (1-\Delta)\psi_{RE} + \epsilon_{\psi_{RE}} \qquad \text{if } \psi_{RE} < 0, \tag{23b}$$

$$\frac{(1-\Delta)c_0 - \epsilon_{c_0}}{2} \leq l_2 \leq \frac{(1+\Delta)c_0 + \epsilon_{c_0}}{2} \qquad \text{if } c_0 \geq 0, \tag{23c}$$

$$\frac{(1+\Delta)c_0 - \epsilon_{c_0}}{2} \leq l_2 \leq \frac{(1-\Delta)c_0 + \epsilon_{c_0}}{2} \qquad \text{if } c_0 < 0, \tag{23d}$$

where the allowed deviation Δ is chosen as 10%, i.e., $\Delta = 0.1$. A small value ϵ is added to avoid that both the upper and lower bounds are equal to 0 in case ψ_{RE} or c_0 is equal to 0. Several different approaches for estimating the road curvature c_0 are described by Lundquist and Schön (2008b).

The first border parameter l_0 is not constrained, because the number of lanes may change at e.g. a gateway. It should be possible for the border of the road to move in parallel to the ego vehicles motion without any conditions.

In order to create a feasibility condition for the fourth parameter l_3 of the linear model, the estimated position of the ego vehicle expressed in the reference frame R is saved at each time sample. A data entry is removed from the set if it lays more than $200\ \mathrm{m}$ behind the current position. Furthermore, the estimated curvature is used to extrapolate

[1] The QP code was provided by Dr. Adrian Wills at the University of Newcastle, Australia, see `http://sigpromu.org/quadprog`. This code implements the method described by Goldfarb and Idnani (1983), Powell (1985).

points $200\ \mathrm{m}$ ahead of the vehicle. These points together with information about the ego vehicle's earlier positions are used to derive a driven path as a third order polynomial

$$y^E = l + \psi_{RE} x^E + \frac{c_0}{2}(x^E)^2 + \frac{c_1}{6}(x^E)^3. \tag{24}$$

Especially the parameter c_1 is of interest and can be used to constrain l_3. Hence, the final inequality, which will further constrain (19) is given by

$$\frac{(1-\Delta)c_1 - \epsilon_{c_1}}{6} \leq l_3 \leq \frac{(1+\Delta)c_1 + \epsilon_{c_1}}{6} \qquad \text{if } c_1 \geq 0, \tag{25a}$$

$$\frac{(1+\Delta)c_1 - \epsilon_{c_1}}{6} \leq l_3 \leq \frac{(1-\Delta)c_1 + \epsilon_{c_1}}{6} \qquad \text{if } c_1 < 0. \tag{25b}$$

To summarize, the constrained optimization problem to be solved based on the linear predictor (8) is given by

$$\begin{aligned} \min_{\boldsymbol{\theta}_{1l}} \quad & \|\boldsymbol{Y}^E - \widehat{\boldsymbol{Y}}^E_{1l}(X^E, \boldsymbol{\theta}_{1l})\|^2_\Lambda \\ \text{s.t.} \quad & (23) \\ & (25) \end{aligned} \tag{26}$$

The parameter b, of the nonlinear model (9) is constrained by the measurement distance and the parameters k and τ are constrained by road construction standards. The resulting nonlinear least-squares problem is finally given by

$$\begin{aligned} \min_{\boldsymbol{\theta}_{2l}} \quad & \|\boldsymbol{Y}^E - \widehat{\boldsymbol{Y}}^E_{2l}(X^E, \boldsymbol{\theta}_{2l})\|^2_\Lambda \\ \text{s.t.} \quad & (23) \\ & b_{\max} \leq \ b \ \leq -b_{\max} \\ & k_{\max} \leq \ k \ \leq -k_{\max} \\ & \tau_{\max} \leq \ \tau \ \leq \tau_{\min}. \end{aligned} \tag{27}$$

4.3 Outlier Rejection

The difference between the observed point and the calculated road border lines is used to separate and remove outliers which lie more than 1.5 lane width (w) from the lines. Subsequently the quadratic program (19) is used a second time and the result is shown in Figure 6. For this case, the two predictor models yields approximately the same result.

An advantage of the nonlinear model is its ability to model changes in the number of lanes, as can be seen in Figure 7a, where the number of lanes changes from two to three. Recall that it is the use of the $\arctan$ function that allows us to model changes in the number of lanes. The new lane originates from an access road to the highway. The corresponding camera view is shown in Figure 7b.

4.4 Computational Time

We have compared the computation time for the two proposed predictors with constraints. The nonlinear least square problem (27) was solved using the function `fmincon` in MATLABS optimization toolbox. Furthermore, we have used two different methods for solving

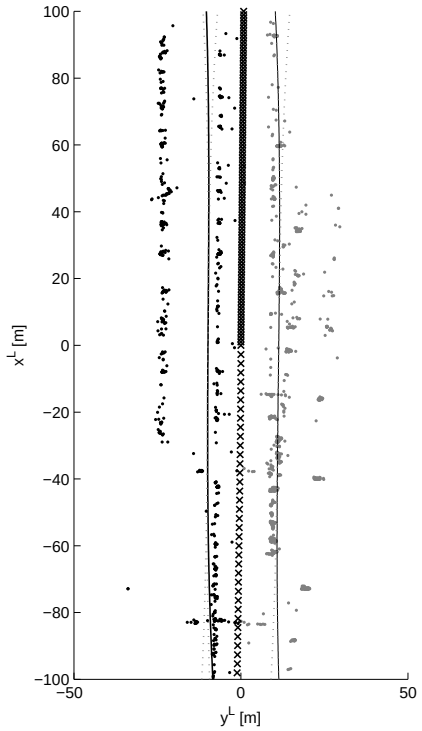

Figure 6: *Road border estimation for the same situation as in Figure 5a, but the additional constraints are now used. The feasible set for the parameters l_1, l_2 and l_3 is between the dashed lines. The crosses shows the driven path (for $x < 0$) and the estimated path (for $x > 0$).*

the quadratic problem (26). The first method is the active set method mentioned earlier, where parts are written in C-code, and the second method used is `quadprog` in MATLABS optimization toolbox. The computational time was averaged over a sequence of 1796 samples. The sample time is 0.1 s, implying that the measurements were collected during 179.6 s highway driving. The results are shown in Table 1.

The computation time of the nonlinear predictor is about 38 % higher than it is for the linear predictor proposed in this paper. The MATLAB function `quadprog` needs 149 % more computational time. This indicates that the computational time of the nonlinerar predictor can possibly be reduced by utilizing an optimized C-code implementation.

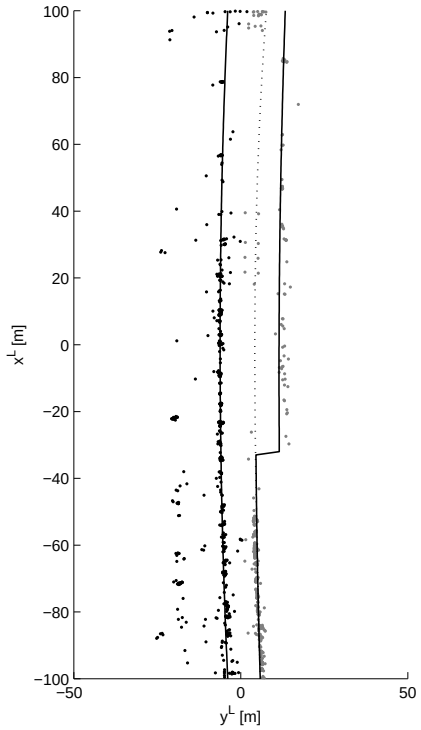

(a)

(b)

Figure 7: *A change in the number of lanes is modeled accurately using the* arctan *function in the nonlinear predictor, as shown by the solid line in Figure (a). The dashed line is the result of the linear predictor. The camera view of the traffic situation is shown is Figure (b).*

Table 1: *Average computational time for one sample.*

Method	Time [ms]
Linear Predictor (this paper)	84
Linear Predictor (`quadprog`)	209
Nonlinear Predictor	116

5 Calculating the Free Space

The free distance to the left and the right road borders is now easily calculated by considering the first parameters l_0 and r_0 respectively. The number of lanes on the left hand side is given by

$$\max\left(\left\lfloor\frac{l_0 - L}{w}\right\rfloor, 0\right) \tag{28a}$$

and the number of lanes on the right hand side is given by

$$\max\left(\left\lfloor\frac{-r_0 - R - 2}{w}\right\rfloor, 0\right). \tag{28b}$$

In the expressions above L and R are the distances from the sensor in the ego vehicle to the left and right lane markings of the currently driven lane. We assume that the emergency lane is $2\ \mathrm{m}$ on the right hand side of the road according to VGU (2004).

The number of observed stationary objects depends on the surrounding environment. A guardrail or a concrete wall results in more observations than for example a forest. Hence, the estimated border lines are accompanied by a quality measure which depends on the number of observations and their variance. The variance is calculated before and after the outliers have been removed.

It is still a problem to detect the distance to the road border if there is a noise barrier some meters to the right of the road. This wall generates many observations with small variance and cannot be distinguished from a guardrail. However, one solution might be to include camera information in a sensor fusion framework.

5.1 Border Line Validity

A very thrilling problem with the present curve fitting approach is that there are no gaps to properly leave or enter the road at a gateway. A collision avoidance system would brake the vehicle automatically if leaving the road at a gateway when simultaneously crossing the border line. This leads us to the conclusion that the border lines should only be defined if the number of observations around it lies above a certain limit.

In a first step we calculate the distance between the line and the observations in the set $\mathbf{Y}_{\mathcal{S}l}$

$$d_{l,i} = \left| y^E_{S_i E_s} - \left(\psi_{RE} x^E_{S_i E_s} + \frac{c_0}{2}(x^E_{S_i E_s})^2\right)\right| \quad \text{for} \quad i = 1, \ldots, N_l \tag{29}$$

and compare it with a constant or variable, e.g., the lane width w

$$n_i = \begin{cases} 1 & \text{if } d_{l,i} > w \\ 0 & \text{otherwise.} \end{cases} \tag{30}$$

In a second step the border line is segmented in valid and not valid parts. The start and end points of the valid parts are given by identifying the indices of two non equal and adjoined elements in the vector n. By applying the XOR function ($\oplus$) according to

$$c = n_{2:N_l} \oplus n_{1:N_l-1}, \tag{31}$$

the start and end points of the border line are identified as the indices with $c = 1$. These indices are stored in two additional sets for the left and right border lines, respectively. An example is shown in Figure 8a and the corresponding camera view in Figure 8b. The gateway to the right leads to a gap in the right border line, between $48 - 73$ m ahead of the ego vehicle. One of the leading vehicles lies between the ego vehicle and the guardrail, this is the reason whey there are so few stationary object on the left hand side from about 70 m ahead and why no line could be drawn.

6 Conclusions and Future Work

In this contribution we have derived a method for estimating the free space in front of a moving vehicle, making use of radar measurements originating from stationary objects along the road side. There is no need to introduce any new sensors, since the radar sensor is already present in modern premium cars. It is just a matter of making better use of the sensor information that is already present.

Two different road border models are introduced, one linear model containing four parameters and one nonlinear model containing six parameters. These models do not depend on the fact that a radar sensor is used, implying that it is straightforward to add more sensor information from additional sensors. In other words, the approach introduced here fits well within a future sensor fusion framework, where additional sensors, such as cameras and additional radars, are incorporated.

The present approach has been evaluated on real data from both highways and rural road in Sweden. The results are encouraging and surprisingly good at times. It is of course not always perfect, but it is much more informative than just using the raw measurements. The problems typically occur when there are to too few measurements or if the measurements stems from other objects than the road side objects.

Currently there is a lot of activity within the computer vision community to be able to handle non-planar road models, making use of parametric models similar to the ones used in this paper. A very interesting avenue for future work is to combine the idea presented in this paper with information from a camera about the hight differences on the road side within a sensor fusion framework. This would probably improve the estimates, especially in situations when there are too few radar measurements available.

7 Acknowledgement

The authors would like to thank Dr. Andreas Eidehall at Volvo Car Corporation for providing data and for initial discussions on the topic. The idea of using the $\arctan$-function in the predictor was brought to our attention by Professor Anders Hansson. Furthermore, we would like to thank the SEnsor Fusion for Safety (SEFS) project within the Intelligent

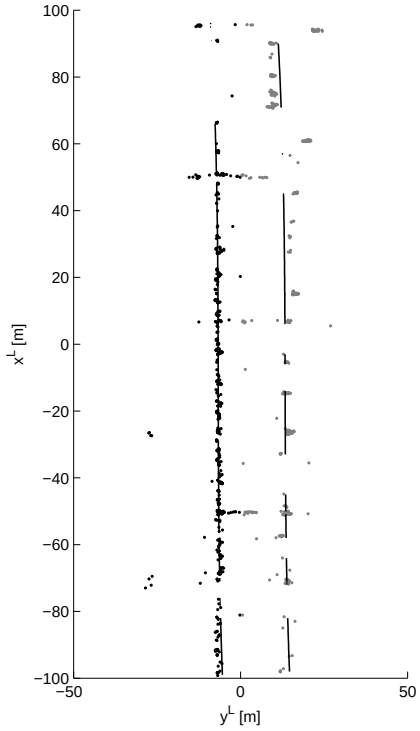

(a)

(b)

Figure 8: *The gateway to the right in Figure (b) leads to a gap in the right border line, between* $48 - 73$ m *ahead, as shown in Figure (a).*

Vehicle Safety Systems (IVSS) program and the strategic research center MOVIII, funded by the Swedish Foundation for Strategic Research (SSF) for financial support.

References

Björck, Å. (1996). *Numerical methods for least squares problems*. SIAM, Philadelphia, PA, USA.

Boyd, S. and Vandenberghe, L. (2004). *Convex Optimization*. Cambridge University Press.

Buehler, M., Iagnemma, K., and Singh, S., editors (2008a). Special Issue on the 2007 DARPA Urban Challenge, Part I, volume 25 (8). *Journal of Field Robotics*.

Buehler, M., Iagnemma, K., and Singh, S., editors (2008b). Special Issue on the 2007 DARPA Urban Challenge, Part II, volume 25 (9). *Journal of Field Robotics*.

Buehler, M., Iagnemma, K., and Singh, S., editors (2008c). Special Issue on the 2007 DARPA Urban Challenge, Part III, volume 25 (10). *Journal of Field Robotics*.

Dickmanns, E. D. (2007). *Dynamic Vision for Perception and Control of Motion*. Springer, London, UK.

Elfes, A. (1987). Sonar-based real-world mapping and navigation. *IEEE Journal of Robotics and Automation*, 3(3):249–265.

Fukae, T., Tamiya, N., and Mandai, H. (1996). Lateral distance measurement using optical spread spectrum radar. In *Proceedings of the IEEE Intelligent Vehicles Symposium*, pages 1–6, Tokyo, Japan.

Gern, A., Franke, U., and Levi, P. (2000). Advanced lane recognition - fusing vision and radar. In *Proceedings of the IEEE Intelligent Vehicles Symposium*, pages 45–51, Dearborn, MI, USA.

Gern, A., Franke, U., and Levi, P. (2001). Robust vehicle tracking fusing radar and vision. In *Proceedings of the international conference of multisensor fusion and integration for intelligent systems*, pages 323–328, Baden-Baden, Germany.

Gill, P. E., Murray, W., Saunders, M. A., and Wright, M. H. (1991). Inertia-controlling methods for general quadratic programming. *SIAM Review*, 33(1):1–36.

Goldfarb, D. and Idnani, A. (1983). A numerically stable dual method for solving strictly convex quadratic programs. *Mathematical Programming*, 27(1):1–33.

ISO, I. O. f. S. (1999). *Passenger cars – Test track for a severe lane-change manoeuvre – Part 1: Double lane-change*. ISO 3888-1:1999. Geneva, Switzerland.

Kaliyaperumal, K., Lakshmanan, S., and Kluge, K. (2001). An algorithm for detecting roads and obstacles in radar images. *IEEE Transactions on Vehicular Technology*, 50(1):170–182.

Kirchner, A. and Ameling, C. (2000). Integrated obstacle and road tracking using a laser scanner. In *Proceedings of the IEEE Intelligent Vehicles Symposium*, pages 675–681, Dearborn, MI, USA.

Kirchner, A. and Heinrich, T. (1998). Model based detection of road boundaries with a laser scanner. In *Proceedings of the IEEE Intelligent Vehicles Symposium*, pages 93–98, Stuttgart, Germany.

Lakshmanan, S., Kaliyaperumal, K., and Kluge, K. (1997). Lexluther: an algorithm for detecting roads and obstacles in radar images. In *Proceedings of the IEEE Conference on Intelligent Transportation System*, pages 415–420, Boston, MA, USA.

Lundquist, C. and Schön, T. B. (2008a). Road geometry estimation and vehicle tracking using a single track model. In *Proceedings of the IEEE Intelligent Vehicles Symposium*, pages 144–149, Eindhoven, The Netherlands.

Lundquist, C. and Schön, T. B. (2008b). Road geometry estimation and vehicle tracking using a single track model. Technical Report LiTH-ISY-R-2844, Department of Electrical Engineering, Linköping University, SE-581 83 Linköping, Sweden.

Lundquist, C., Schön, T. B., and Orguner, U. (2009). Estimation of the free space in front of a moving vehicle. Technical Report LiTH-ISY-R-2892, Department of Electrical Engineering, Linköping University, SE-581 83 Linköping, Sweden.

Ma, B., Lakshmanan, S., and Hero, A. (2000). Simultaneous detection of lane and pavement boundaries using model-based multisensor fusion. *IEEE Transactions on Intelligent Transportation Systems*, 1(3):135–147.

Mayhan, R. and Bishel, R. (1982). A two-frequency radar for vehicle automatic lateral control. *IEEE Transactions on Vehicular Technology*, 31(1):32–39.

McCall, J. C. and Trivedi, M. M. (2006). Video-based lane estimation and tracking for driver assistance: Servey, system, and evaluation. *IEEE Transactions on Intelligent Transportation Systems*, 7(1):20–37.

Nikolova, M. and Hero, A. (2000). Segmentation of a road from a vehicle-mounted radar and accuracy of the estimation. In *Proceedings of the IEEE Intelligent Vehicles Symposium*, pages 284–289, Dearborn, MI, USA.

Powell, M. (1985). On the Quadratic Programming Algorithm of Goldfrab and Idnani. *Mathematical Programming Study*, 25(1):46–61.

Sparbert, J., Dietmayer, K., and Streller, D. (2001). Lane detection and street type classification using laser range images. In *Proceedings of the IEEE Intelligent Transportation Systems Conference*, pages 454–459, Oakland, CA, USA.

Tamiya, N., Mandai, H., and Fukae, T. (1996). Optical spread spectrum radar for lateral detection in vehicles. In *IEEE 4th International Symposium on Spread Spectrum Techniques and Applications Proceedings*, pages 195–198, Mainz, Germany.

Thrun, S., Burgard, W., and Fox, D. (2005). *Probabilistic Robotics*. Intelligent Robotics and Autonomous Agents. The MIT Press, Cambridge, MA, USA.

VGU (2004). *Vägar och gators utformning – Landsbygd - Vägrum*. Vägverket, Swedish Road Administration, Borlänge, Sweden. 2004:80.

Wedel, A., Franke, U., Badino, H., and Cremers, D. (2008). B-spline modeling of road surfaces for freespace estimation. In *Proceedings of the IEEE Intelligent Vehicles Symposium*, pages 828–833, Eindhoven, The Netherlands.

Wijesoma, W. S., Kodagoda, K. R. S., and Balasuriya, A. P. (2004). Road-boundary detection and tracking using ladar sensing. *IEEE Transactions on Robotics and Automation*, 20(3):456–464.

Zomotor, Z. and Franke, U. (1997). Sensor fusion for improved vision based lane recognition and object tracking with range-finders. In *Proceedings of IEEE Conference on Intelligent Transportation System*, pages 595–600, Boston, MA, USA.

Paper D

Tracking Stationary Extended Objects for Road Mapping using Radar Measurements

Authors: Christian Lundquist, Umut Orguner and Thomas B. Schön.

Edited version of paper originally published in *Proceedings of the IEEE Intelligent Vehicle Symposium*, Xi'an, China, 2009.

Preliminary version published as Technical Report LiTH-ISY-R-2892, Department of Electrical Engineering, Linköping University, Linköping, Sweden.

Tracking Stationary Extended Objects for Road Mapping using Radar Measurements

Christian Lundquist, Umut Orguner and Thomas B. Schön

Department of Electrical Engineering,
Linköping University,
SE–581 83 Linköping, Sweden.
E-mail: (lundquist, umut, schon)@isy.liu.se.

Abstract

It is getting more common that premium cars are equipped with a forward looking radar and a forward looking camera. The data is often used to estimate the road geometry, tracking leading vehicles, etc. However, there is valuable information present in the radar concerning stationary objects, that is typically not used. The present work shows how stationary objects, such as guard rails, can be modeled and tracked as extended objects using radar measurements. The problem is cast within a standard sensor fusion framework utilizing the Kalman filter. The approach has been evaluated on real data from highways and rural roads in Sweden.

Keywords: extended objects, object detection, radar imaging, road vehicle radar, object tracking, road mapping, stationary objects

1 Introduction

For a collision avoidance system it is imperative to have a reliable *map* of the environment surrounding the ego vehicle. This map, consisting of both stationary and moving objects, has to be built in real time using measurements from the sensors present in the ego vehicle. This is currently a very active research topic within the automotive industry and many other areas as well. Great progress has been made, but much remains to be done. Current state-of-the-art when it comes to the problem of building maps for autonomous vehicles can be found in the recent special issues by Buehler et al. (2008a,b,c) on the 2007 DARPA Urban Challenge. In these contributions measurements from expensive and highly accurate sensors are used, while we in the present paper utilize measurements from off-the-shelf automotive radars.

Obviously, these stationary radar measurements are not enough to fully explain the road borders. However, as we will see, there is surprisingly much information present in these measurements.

In this contribution we consider the problem of estimating the position and shape of stationary objects in front of the vehicle, making use of echoes from a standard automotive radar. Hence, there is no need to introduce any new sensors, it is just a matter of making better use of the sensor information that is already present in a modern premium car. We represent the stationary objects as

- points, with sources such as delineators or lampposts or
- lines, where measurements stem from e.g. guard rails or concrete walls.

The lines are modeled as extended objects, since an object is denoted extended whenever the object extent is larger than the sensor resolution. Put in other words, if an object should be classified as extended does not only depend on its physical size, but also on the physical size relative to the sensor resolution. Extended object tracking is extensively described by e.g., Ristic et al. (2004), Gilholm and Salmond (2005) and it has received quite recent attention by Vermaak et al. (2005), Angelova and Mihaylova (2008) where Monte Carlo methods are applied and by Koch (2008) which is based on random matrices.

The problem of road border estimation has been investigated in the literature during the last decade. The approaches presented mainly differ in their models for the road borders and the different types of sensors used in the estimation. The third order approximation of the two sided (left and right) "clothoid model" has been used in connection with Kalman filters by Kirchner and Heinrich (1998) and Polychronopoulos et al. (2004) for laser scanner measurements and radar measurements, respectively. Lundquist and Schön (2009) proposed two road border models, one of which is very similar to the model proposed by Polychronopoulos et al. (2004), and used a constrained quadratic program to solve for the parameters. A linear model represented by its midpoint and orientation (one for each side of the road) is utilized by Wijesoma et al. (2004) with ladar sensing for tracking road-curbs. Later, Kodagoda et al. (2006) enhanced the results of Wijesoma et al. (2004) with the addition of image sensors. A similar extended Kalman filtering based solution is given by Fardi et al. (2003), where a circular road border modeling framework is used. Recently, the particle filters (also referred to as condensation in image and video processing) have been applied to the road border estimation problem by Wang et al. (2008) with an hyperbolic road model.

The present solution extends an already existing sensor fusion framework by Lundquist and Schön (2008), which among other things provides a good road geometry estimate. This framework improves the raw vision estimate of the road geometry by fusing it with radar measurements of the leading vehicles and information from various proprioceptive sensors. The idea is that the motion of the leading vehicles reveals information about the road geometry as described in e.g., Zomotor and Franke (1997), Gern et al. (2000, 2001). Hence, if the leading vehicles can be accurately tracked, their motion can be used to improve the road geometry estimates. Furthermore, we used a solid dynamic model of the ego vehicle allowing us to further refine the estimates by incorporating several additional sensor measurements from the CAN bus. The resulting, rather simple, yet useful *map* of the environment surrounding the ego vehicle consists in

- Road geometry, typically parameterized using road curvature and curvature rate.
- Position and velocity of the leading vehicles.
- Ego vehicle position, orientation and velocity.
- Position and shape of stationary objects.

The stationary objects are tracked by casting the problem within a standard sensor fusion framework. Since we use a linear model and assume Gaussian noise we use the standard Kalman filter (Kalman, 1960).

The approach has been evaluated on real data from highways and rural roads in Sweden. The test vehicle is a Volvo S80 equipped with a forward looking 77 GHz mechanically scanned frequency modulated continuous-wave (FMCW) radar and a forward looking vision sensor (camera).

2 Geometry and Notation

Lundquist and Schön (2008) provide a sensor fusion framework for sequentially estimating the parameters l_E, ψ_{RE}, c_0 in the following model of the road's white lane markings,

$$y^E = l_E + \psi_{RE} x^E + \frac{c_0}{2}(x^E)^2, \tag{1}$$

where x^E and y^E are expressed in the ego vehicle's coordinate frame E. The angle between the longitudinal axis of the vehicle and the road lane is ψ_{RE}, see Figure 1. It is assumed that this angle is small and hence the approximation $\sin\psi_{RE} \approx \psi_{RE}$ is used. The curvature parameter is denoted by c_0 and the offset between the ego vehicle and the white lane is denoted by l_E.

In this paper we will use the planar coordinate transformation matrix

$$R^{WE} = \begin{bmatrix} \cos\psi_{EW} & -\sin\psi_{EW} \\ \sin\psi_{EW} & \cos\psi_{EW} \end{bmatrix} \tag{2}$$

to transform a vector, represented in the ego vehicle's coordinate frame E, into a vector, represented in the world reference coordinate frame W, where ψ_{EW} is the angle of rotation from W to E. We will refer to this angle as the yaw angle of the vehicle, and in order to simplify the notation we will use $\psi \triangleq \psi_{EW}$. The point O_W is the origin of W and O_E is the origin of E situated in the vehicles center of gravity. The geometric displacement vector $\boldsymbol{d}^W_{EW}$ is the straight line from W to E represented with respect to frame W. The angles and distances are shown in Figure 1. Hence, a point P^E represented in the ego vehicle coordinate frame E is transformed to be represented in the world coordinate frame W using

$$P^W = R^{WE} P^E + \boldsymbol{d}^W_{EW}. \tag{3}$$

An observation m will be referred to as a stationary object $\mathcal{S}_m$ in the point S_m. The radar in the ego vehicle measures the azimuth angle $\delta_{S_m E_s}$ and the range $d = ||\boldsymbol{d}^E_{S_m E_s}||_2$. These are transformed into Cartesian coordinates $\boldsymbol{y}^E_{\mathcal{S}_m} = \begin{bmatrix} x^E_{S_m E_s} & y^E_{S_m E_s} \end{bmatrix}^{\mathrm{T}}$.

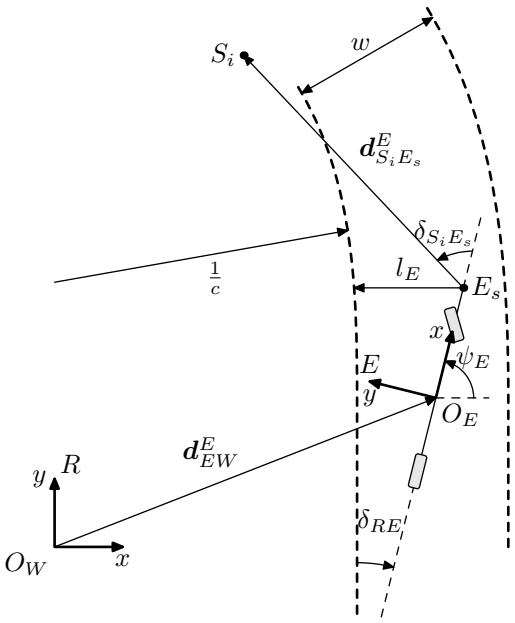

Figure 1: *The ego vehicle's coordinate frame E has its origin O_E situated in the vehicle's center of gravity. A stationary object $\mathcal{S}_i$ is observed at a distance $||\boldsymbol{d}^E_{S_m E_s}||_2$ and an angle $\delta_{S_m E_s}$ with respect to the radar. The angle between the vehicle's longitudinal axis and the road lane is ψ_{RE}, the distance to the left lane marking is l_E and the road curvature is c_0.*

3 Extended Object Model

In this section we introduce models for the tracked stationary object, i.e., points and lines. To take care of the lines a model with the object's shape, size, position and orientation is introduced.

3.1 Process Model of the Stationary Objects

Stationary objects are modeled as points $\mathcal{P}$ or lines $\mathcal{L}$. A point $\mathcal{P}_i$ is represented using a position in the planar world coordinate frame W, according to

$$\boldsymbol{x}_{\mathcal{P}_i} \triangleq \begin{bmatrix} x^W_{\mathcal{P}_i W} & y^W_{\mathcal{P}_i W} \end{bmatrix}^{\mathrm{T}}. \tag{4}$$

A line $\mathcal{L}_j$ is represented as a second order polynomial in its coordinate frame L_j

$$y^{L_j} = a_0 + a_1 x^{L_j} + a_2 \left(x^{L_j}\right)^2. \tag{5}$$

The coordinate frame L_j is initiated together with the line and is equal to the ego vehicles coordinate frame at the moment the line is created. Unlike the ego vehicle's frame it is fixed to the world frame, i.e., $r^W_{L_j W}$ and $\psi_{L_j W}$ are constant and it does not follow the vehicles movement.

The state of the line $\mathcal{L}_j$ is

$$\boldsymbol{x}_{\mathcal{L}_j} = \begin{bmatrix} a_{0,j} & a_{1,j} & a_{2,j} & s_j & e_j \end{bmatrix}^{\mathrm{T}}, \tag{6}$$

where s_j and e_j are the start and end points of the line given as scalar x^{L_j} values.

The process model of the stationary objects in the form

$$\boldsymbol{x}_{t+1} = F\boldsymbol{x}_t + \boldsymbol{w}_t, \quad \boldsymbol{w}_t \sim \mathcal{N}(0, Q), \tag{7}$$

is simple, since the objects are not moving. For the points, the system matrix, referred to as $F_{\mathcal{P}}$, is the identity matrix. The term $\boldsymbol{w}_t$ in (7) represents the process noise. We include some dynamics into the process model of the line. We assume that the lines are shrinking with a factor $\lambda < 1$ according to

$$s_{j,t+1} = s_{j,t} + \lambda(e_{j,t} - s_{j,t}), \tag{8a}$$

$$e^j_{j,t+1} = e_{j,t} - \lambda(e_{j,t} - s_{j,t}), \tag{8b}$$

leading to

$$F_{\mathcal{L}} = \begin{bmatrix} 1 & 0 & 0 & 0 & 0 \\ 0 & 1 & 0 & 0 & 0 \\ 0 & 0 & 1 & 0 & 0 \\ 0 & 0 & 0 & 1-\lambda & \lambda \\ 0 & 0 & 0 & \lambda & 1-\lambda \end{bmatrix}. \tag{9}$$

This shrinking behavior for the lines allows us to automatically adjust the start and end points of the lines according to the incoming measurements.

3.2 Measurement Model

The measurement equation describing the measurements relation to a point $\mathcal{P}_i$ is defined as

$$\boldsymbol{y}_{\mathcal{P}_i,t} = \boldsymbol{x}_{\mathcal{P}_i,t} + \boldsymbol{e}_{\mathcal{P},t}, \quad \boldsymbol{e}_{\mathcal{P},t} \sim \mathcal{N}(0, R_{\mathcal{P}}), \tag{10}$$

where the output $\boldsymbol{y}_{\mathcal{P}_i,t} = \boldsymbol{y}^W_{\mathcal{S}_m}$ is the observation m in the world coordinate frame associated to the i^{th} point. The term $\boldsymbol{e}_{\mathcal{P},t}$ in (10) represents the measurement noise associated with the radar. The measurement equation describing the measurements relation to a line $\mathcal{L}_j$ is

$$\boldsymbol{y}_{\mathcal{L}_j,t} = \begin{bmatrix} 0 & 0 & 0 & h_{14} & h_{15} \\ 1 & x^{L_j}_{S_m L_j} & \left(x^{L_j}_{S_m L_j}\right)^2 & 0 & 0 \end{bmatrix} \boldsymbol{x}_{\mathcal{L}_j,t} + \begin{bmatrix} 0 \\ 1 \end{bmatrix} \boldsymbol{e}_{\mathcal{L},t}, \tag{11}$$

where $\boldsymbol{y}_{\mathcal{L}_j,t} = \boldsymbol{y}^{L_j}_{\mathcal{S}_m}$ is the observation m in the L_j coordinate frame and associated to line $\mathcal{L}_j$. The term $\boldsymbol{e}_{\mathcal{L},t} \sim \mathcal{N}(0, R_{\mathcal{L}})$ represents the measurement noise. The first row of the measurement matrix, which determines the update of the start and the end points, depends on the position of the observation in relation to the predictions of the start and the end points according to

$$\begin{bmatrix} h_{14} & h_{15} \end{bmatrix} = \begin{cases} \begin{bmatrix} 1 & 0 \end{bmatrix} & \text{if } x^{L_j}_{S_m L_j} \leq s_{j,t|t-1} \\ \begin{bmatrix} 0 & 1 \end{bmatrix} & \text{if } x^{L_j}_{S_m L_j} \geq e_{j,t|t-1} \\ \begin{bmatrix} 0 & 0 \end{bmatrix} & \text{otherwise.} \end{cases} \tag{12}$$

This type of measurement where some measured quantities ($x^{L_j}_{S_m L_j}$ in our case) appear as model parameters is not conventional in dynamic estimation literature and can be considered as an extension of the so-called "errors in variables" framework. In our application, this enables us to use the Kalman filter because the resulting model is linear.

4 Data Association and Gating

At every sampling time, the system receives a batch of $N_{\mathcal{S}}$ observations $\boldsymbol{y}_{\mathcal{S}_m}$, $m = 1, \ldots, N_{\mathcal{S}}$ from the radar. These new measurements can be associated to existing tracked points $\mathcal{P}_i$, $i = 1, \ldots, N_{\mathcal{P}}$ or to tracked lines $\mathcal{L}_j$, $j = 1, \ldots, N_{\mathcal{L}}$, or a new track is initiated. The number of association events (hypotheses) is extremely large. The classical technique to reduce the number of these hypotheses is called gating, see e.g., Bar-Shalom and Fortmann (1988). We apply gating and make a nearest-neighbor type data association based on likelihood ratio tests. Other more complicated data association methods like multiple hypothesis tracking, according to e.g., Reid (1979), or joint probabilistic data association, as described by e.g., Bar-Shalom and Fortmann (1988), can also be used in our framework. However, these are quite complicated and computationally costly approaches and the nearest neighbor type algorithm we used has been found to give sufficiently good performance for our case. The gating and the data association are performed according to the following calculations. The likelihood $\ell_{\mathcal{S}_m,\mathcal{P}_i}$ that the observation $\boldsymbol{y}_{\mathcal{S}_m}$ corresponds to the i^{th} point $\mathcal{P}_i$ is given by

$$\ell_{\mathcal{S}_m \mathcal{P}_i} = \begin{cases} \mathcal{N}(\boldsymbol{y}^W_{\mathcal{S}_m}; \hat{\boldsymbol{y}}_{\mathcal{P}_i,t|t-1}, S_{\mathcal{P}_i}), & \text{if } \boldsymbol{y}^W_{\mathcal{S}_m} \in \mathcal{G}_{\mathcal{P}_i} \\ 0, & \text{otherwise} \end{cases} \tag{13}$$

where $\hat{\boldsymbol{y}}_{\mathcal{P}_i,t|t-1}$ is the predicted measurement of the point $\mathcal{P}_i$ according to the model (10) and $S_{\mathcal{P}_i,t|t-1}$ is its covariance (innovation covariance) in the Kalman filter. The gate $\mathcal{G}_{\mathcal{P}_i}$ is defined as the region

$$\mathcal{G}_{\mathcal{P}_i} \triangleq \left\{ \boldsymbol{y} \,\middle|\, (\boldsymbol{y} - \hat{\boldsymbol{y}}_{\mathcal{P}_i,t|t-1})^{\mathrm{T}} S^{-1}_{\mathcal{P}_i,t|t-1} (\boldsymbol{y} - \hat{\boldsymbol{y}}_{\mathcal{P}_i,t|t-1}) \leq \delta_{\mathcal{P}} \right\} \tag{14}$$

where $\delta_{\mathcal{P}}$ is the gating threshold.

The likelihood that the observation m corresponds to the j^{th} line state is derived by considering the orthogonal distance between the line and the observation. To simplify the calculations we assume that the curvature of the line is small and that the orthogonal distance can be approximated with the y-distance between the observation and the line expressed using the lines coordinate frame L_j, i.e.,

$$\epsilon_{\mathcal{S}_m \mathcal{L}_j} = y^{L_j}_{S_m L_j} - \hat{y}^{L_j}_{S_m L_j}, \tag{15}$$

where

$$\hat{y}^{L_j}_{S_m L_j} \triangleq \begin{bmatrix} 1 & x^{L_j}_{S_m L_j} & \left(x^{L_j}_{S_m L_j}\right)^2 & 0 & 0 \end{bmatrix} \hat{\boldsymbol{x}}_{\mathcal{L}_j,t|t-1}. \tag{16}$$

The likelihood $\ell_{\mathcal{S}_m\mathcal{L}_j}$ that the observation corresponds to the j^{th} line is then given by

$$\ell_{\mathcal{S}_m\mathcal{L}_j} = \begin{cases} \mathcal{N}\left(\epsilon_{\mathcal{S}_m\mathcal{L}_j}; 0, \mathrm{E}\left(\Delta_{y_j}^2\right)\right), & \text{if } \begin{bmatrix} x_{S_mL_j}^{L_j} \\ y_{S_mL_j}^{L_j} \end{bmatrix} \in \mathcal{G}_{\mathcal{L}_j} \\ 0, & \text{otherwise} \end{cases} \tag{17}$$

where $y_j = y_{S_mL_j}^{L_j}$ and the gate $\mathcal{G}_{\mathcal{L}_j}$ is defined as

$$\mathcal{G}_{\mathcal{L}_j} \triangleq \left\{ \begin{bmatrix} x \\ y \end{bmatrix} \Big| \left(y - \hat{y}_{S_mL_j}^{L_j}\right)^2 \mathrm{E}\left(\Delta_{y_j}^2\right)^{-1} \leq \delta_{\mathcal{L}}, s_j - \delta_s < x < e_j + \delta_e \right\}. \tag{18}$$

In (17) and (18), $\mathrm{E}(\Delta_{y_j}^2)$ represents the uncertainty of the line in the y direction at the x-value $x_{S_mL_j}^{L_j}$. This covariance has to be calculated in terms of the state estimate $\hat{\boldsymbol{x}}_{\mathcal{L}_j,t|t-1}$ and its covariance $P_{\mathcal{L}_j,t|t-1}$. This derivation can be made by first rewriting the line equation (6) with mean parameters and a deviation Δ

$$y + \Delta_y = (a_0 + \Delta_{a_0}) + (a_1 + \Delta_{a_1})x + (a_2 + \Delta_{a_2})x^2, \tag{19}$$

where the superscripts and subscripts are discarded for the sake of brevity. This gives

$$\Delta_y = \Delta_{a_0} + \Delta_{a_1}x + \Delta_{a_2}x^2. \tag{20}$$

Considering the squared expectation of this deviation, we obtain

$$\begin{aligned} \mathrm{E}(\Delta_y^2) &= \mathrm{E}\left(\Delta_{a_0} + \Delta_{a_1}x + \Delta_{a_2}x^2\right)^2 \\ &= \mathrm{E}\Big(\begin{bmatrix} 1 & x & x^2 \end{bmatrix} \begin{bmatrix} \Delta_{a_0} & \Delta_{a_1} & \Delta_{a_2} \end{bmatrix}^{\mathrm{T}} \\ &\quad \times \begin{bmatrix} \Delta_{a_0} & \Delta_{a_1} & \Delta_{a_2} \end{bmatrix} \begin{bmatrix} 1 & x & x^2 \end{bmatrix}^{\mathrm{T}} \Big) \\ &= \begin{bmatrix} 1 & x & x^2 \end{bmatrix} \mathrm{E}\Big(\begin{bmatrix} \Delta_{a_0} & \Delta_{a_1} & \Delta_{a_2} \end{bmatrix}^{\mathrm{T}} \\ &\quad \times \begin{bmatrix} \Delta_{a_0} & \Delta_{a_1} & \Delta_{a_2} \end{bmatrix} \Big) \begin{bmatrix} 1 & x & x^2 \end{bmatrix}^{\mathrm{T}}. \end{aligned} \tag{21}$$

Now, the expectation above is given by the upper-left 3×3 partition of the covariance matrix $P_{\mathcal{L}_j,t|t-1}$ which we denote by $P_{\mathcal{L}_j,t|t-1}^{3\times3}$. Hence,

$$\mathrm{E}\left(\Delta_{y_j}^2\right) = \begin{bmatrix} 1 & x_{S_mL_j}^{L_j} & (x_{S_mL_j}^{L_j})^2 \end{bmatrix} P_{\mathcal{L}_j,t|t-1}^{3\times3} \begin{bmatrix} 1 & x_{S_mL_j}^{L_j} & (x_{S_mL_j}^{L_j})^2 \end{bmatrix}^{\mathrm{T}}. \tag{22}$$

Having calculated the likelihood values, we form two matrices of likelihood values, one matrix $\Gamma_{\mathcal{P}} \in \mathbb{R}^{n_{\mathcal{S}}\times n_{\mathcal{P}}}$ with the combinations of observations and points, according to (13), and one matrix $\Gamma_{\mathcal{L}} \in \mathbb{R}^{n_{\mathcal{S}}\times n_{\mathcal{L}}}$ with the combinations of observations and lines, according to (17).

First we find the the maximum value of $\Gamma_{\mathcal{P}}$, and call the corresponding point state i_m and measurement m_m. Thereafter we find the maximum value of the m^{th} row, corresponding to measurement m_m of matrix $\Gamma_{\mathcal{L}}$ and call the corresponding line state j_m. The likelihood ratio denoted by $\Lambda(\boldsymbol{y}_{\mathcal{S}_m})$ is now given by

$$\Lambda(\boldsymbol{y}_{\mathcal{S}_m}) \triangleq \frac{\ell_{S_m\mathcal{P}_{i_m}}}{\ell_{S_m\mathcal{L}_{j_m}}}. \tag{23}$$

The corresponding likelihood ratio test is

$$\Lambda(\boldsymbol{y}_{\mathcal{S}_m}) \underset{H_1}{\overset{H_0}{\gtrless}} \eta \tag{24}$$

where H_0 and H_1 corresponds to hypotheses that the measurement $\boldsymbol{y}_{\mathcal{S}_m}$ is associated to the point $\mathcal{P}_{i_m}$ and to the line $\mathcal{L}_{j_m}$, respectively. The threshold is selected as $\eta < 1$, since (13) is two dimensional and (17) is one dimensional. More theory about likelihood test is given by e.g., van Trees (1968).

No two measurements may originate from the same point source and no two sources may give rise to the same measurements. However, one line source may give rise to multiple measurements. This means that if measurement $\boldsymbol{y}_{\mathcal{S}_m}$ is associated to point $\mathcal{P}_i$, then the values in the m^{th} row of the two matrices as well as the i^{th} column of the point likelihood matrix must be set to zero to exclude the measurement and the point from further association. However, if $\boldsymbol{y}_{\mathcal{S}_m}$ is associated to line $\mathcal{L}_j$, then only the values in the m^{th} rows of the two matrices are set to zero because the line $\mathcal{L}_j$ can still be associated to other measurements. The procedure is repeated until all measurements with non-zero likelihood have been associated to either a point or a line. A new point is initiated if the observations could not be associated to an existing state. This is true when a measurement is not in the gate of a non-associated point or a line.

5 Handling Tracks

A line is initiated from tracked points under the assumption that a number of points form a line parallel to the road. In this section we will discuss track handling matters such as initiating and removing tracks.

5.1 Initiating Lines

All points $\mathcal{P}_i$ are transformed into the ego vehicles coordinate frame since the road's geometry is given in this frame. The road geometry is described by the polynomial given in (1). We consider hypothetical lines passing through each point $\mathcal{P}_k$ parallel to the road. For each such line, the corresponding lateral distance $l_{\mathcal{P}_k}$ is given by

$$l_{\mathcal{P}_k} = \hat{y}^E_{\mathcal{P}_k E_s} - \psi_{RE}\hat{x}^E_{\mathcal{P}_k E_s} - \frac{c_0}{2}\left(\hat{x}^E_{\mathcal{P}_k E_s}\right)^2. \tag{25}$$

The likelihood $\ell_{\mathcal{P}_i\mathcal{P}_k}$ that a point $\mathcal{P}_i$ is on the line of point $\mathcal{P}_k$ is then given by

$$\ell_{\mathcal{P}_i\mathcal{P}_k} = \begin{cases} \mathcal{N}\left(\epsilon_{\mathcal{P}_i\mathcal{P}_k}; 0, P^E_{\mathcal{P}_k,(2,2)}\right), & \text{if } \begin{bmatrix} \hat{x}^{L_E}_{\mathcal{P}_i E_s} \\ \hat{y}^{L_E}_{\mathcal{P}_i E_s} \end{bmatrix} \in \mathcal{G}_{\mathcal{P}_k} \\ 0, & \text{otherwise,} \end{cases} \tag{26}$$

where the lateral distance between the point $\mathcal{P}_i$ and the proposed new line of point $\mathcal{P}_k$ is given by

$$\epsilon_{ik} = \hat{y}^E_{\mathcal{P}_i E_s} - \hat{y}^E_{\mathcal{P}_k E_s}, \tag{27}$$

where

$$\hat{y}^E_{\mathcal{P}_k E_s} = l_{\mathcal{P}_k} + \psi_{RE}\hat{x}^E_{\mathcal{P}_i E_s} + \frac{c_0}{2}\left(\hat{x}^E_{\mathcal{P}_i E_s}\right)^2, \tag{28}$$

and the state covariance in the ego vehicles coordinate frame is given by

$$P^E_{\mathcal{P}_k} = \left(R^{EW}\right)^{\mathrm{T}} P_{\mathcal{P}_k} R^{EW}. \tag{29}$$

The notation $P^E_{\mathcal{P}_k,(2,2)}$ refers to the lower-right element, i.e., the variance in the diagonal corresponding to y^E. The gate $\mathcal{G}_{\mathcal{P}_k}$ is defined as

$$\mathcal{G}_{\mathcal{P}_k} \triangleq \left\{ \begin{bmatrix} x \\ y \end{bmatrix} \middle| \frac{\left(y - \hat{y}^E_{\mathcal{P}_k E_s}\right)^2}{P^E_{\mathcal{P}_k,(2,2)}} \leq \delta_{\mathcal{L}}, -\delta_s < x - \hat{x}^E_{\mathcal{P}_k E_s} < \delta_e \right\}. \tag{30}$$

From all combinations of likelihoods we form a symmetric matrix $\Gamma_{\mathcal{I}}$. The columns of $\Gamma_{\mathcal{I}}$ are summed and the maximum value corresponding to column k_m is chosen. If this column contains more than a certain number κ of non-zero rows, corresponding to points

$$\mathcal{P}_l = \{\mathcal{P} \mid \Gamma_{\mathcal{I}}(:, k_m) \neq 0\} \tag{31}$$

within the gate of $\mathcal{P}_{k_m}$, a line is formed from the points $\mathcal{P}_l$. The new line's states a_0, a_1 and a_2 are estimated by solving a least square problem using the points $\mathcal{P}_l$. The states s and e are the minimum and maximum x-coordinate value of the points, respectively. All elements in column k_m and rows i_m are set to zero and the procedure is repeated until no column contains more than κ non-zero elements.

5.2 Remove Lines or Points

For each state we introduce a counter. The counter is increased if the state is updated with new measurements and decreased if it was not updated during one iteration. A state is removed if the counter is zero.

6 Experiments and Results

Let us start by showing the information given by an ordinary automotive ACC radar, for the traffic situation shown in Figure 2a. The ego vehicle, indicated by a circle, is situated at the $(0, 0)$-position in Figure 2b, and the black dots are the radar reflections, or stationary observations, at one time sample. The gray dots are former radar reflections, obtained at earlier time samples. Figure 2c shows the estimated points and lines for the same scenario. The mean values of the states are indicated by solid black lines or points. Furthermore, the state variance, by means of the 1σ confidence interval, is illustrated by gray lines or ellipses, respectively. Lundquist and Schön (2008) presented a new approach to estimate the road curvature (1), which we show here as gray dashed lines. We also show the tracked vehicle in front of the ego vehicle illustrated by a square.

In Figure 3a we see a traffic scenario with a freeway exit. The corresponding bird's eye view is shown in Figure 3b. The origin of the line's coordinate systems are illustrated with dots and a number which is repeated at each line. Line 1 indicates the guardrail to

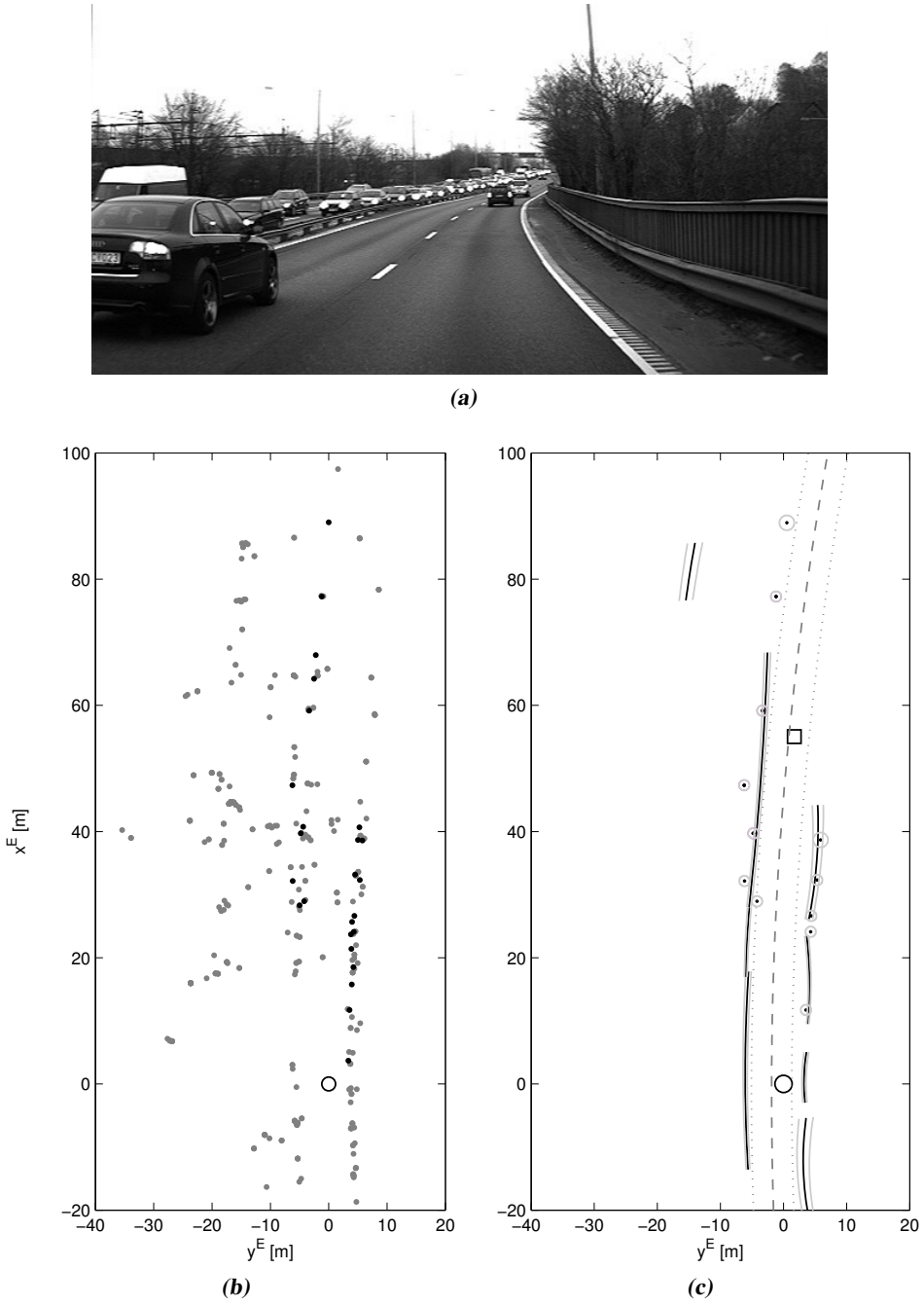

Figure 2: *A traffic situation is shown in Figure (a). Figure (b) shows the radar reflections, and Figure (c) the resulting tracked points and lines. The circle is the ego vehicle, the square is the tracked vehicle in front and the dashed gray lines illustrates the tracked road curvature.*

(a)

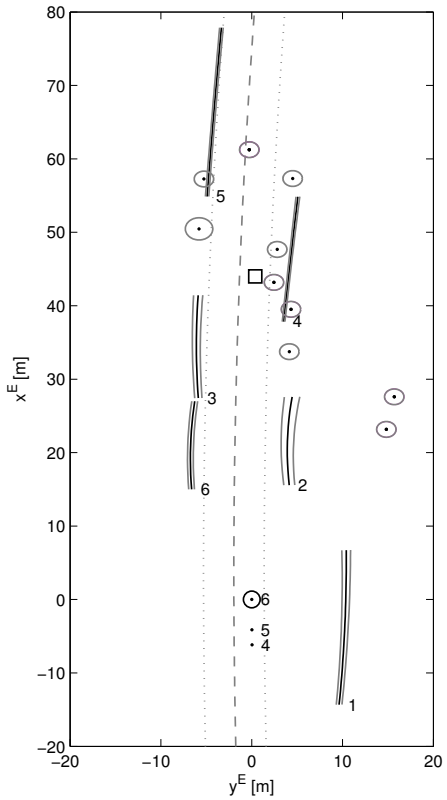

(b)

Figure 3: *Freeway exit with guardrails, the camera view is shown in Figure (a) and the bird's eye view with the estimated states in Figure (b).*

the right of the exit, line 2 is the guardrail starting at the exit sign. The gap between line 3 and line 5 is probably due to the dimple, where the radar signals are transmitted above the guard rail, hence not giving us any stationary observations in the desired region.

Our last example shows a situation from a rural road, see Figure 4a. The lines 5 and 6 are the guardrails of a bridge. Line 4 depicts a fence behind the bridge. From the camera view it is hard to recognize and also the radar has problems to track it, indeed the gray lines indicates a large uncertainty for this case.

7 Conclusion

In this contribution we have derived a method for tracking stationary objects as extended objects using radar measurements. Typically radar echoes stem from delineators or guardrails, which are tracked as points or lines, respectively, in a standard Kalman filter framework. A major part of the present approach is the data association and gating problem. The approach has been evaluated on real and relevant data from both freeways and rural roads in Sweden. The results are not perfect, but surprisingly good at times, and of course much more informative than just using raw measurements. Furthermore, the standard state representation of the objects should not be underestimated since it is compact and easy to send on a vehicle CAN-bus.

Acknowledgment

The authors would like to thank the SEnsor Fusion for Safety (SEFS) project within the Intelligent Vehicle Safety Systems (IVSS) program and the strategic research center MOVIII, funded by the Swedish Foundation for Strategic Research (SSF) for financial support.

References

Angelova, D. and Mihaylova, L. (2008). Extended object tracking using Monte Carlo methods. *IEEE Transactions on Signal Processing*, 56(2):825–832.

Bar-Shalom, Y. and Fortmann, T. E. (1988). *Tracking and Data Association*. Mathematics in science and engineering. Academic Press, Orlando, FL, USA.

Buehler, M., Iagnemma, K., and Singh, S., editors (2008a). Special Issue on the 2007 DARPA Urban Challenge, Part I, volume 25 (8). *Journal of Field Robotics*.

Buehler, M., Iagnemma, K., and Singh, S., editors (2008b). Special Issue on the 2007 DARPA Urban Challenge, Part II, volume 25 (9). *Journal of Field Robotics*.

Buehler, M., Iagnemma, K., and Singh, S., editors (2008c). Special Issue on the 2007 DARPA Urban Challenge, Part III, volume 25 (10). *Journal of Field Robotics*.

(a)

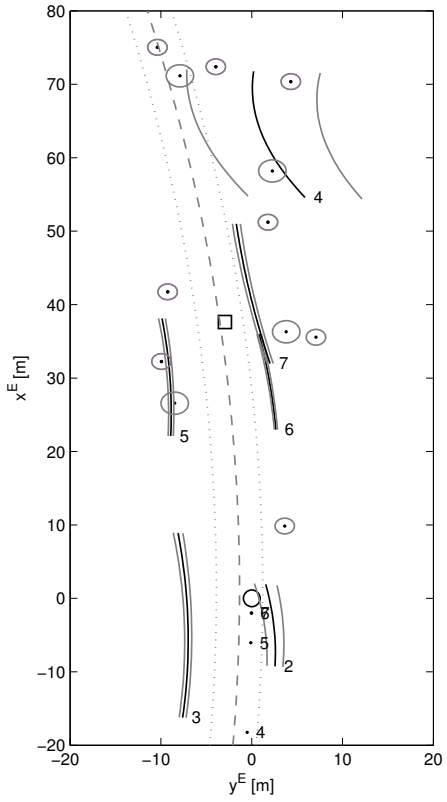

(b)

Figure 4: *A traffic scenario from a rural road, with guardrails on both sides of a bridge is shown. Note that the fence behind the bridge in Figure (a) is illustrated by line* 4 *in Figure (b), observe the large uncertainty.*

Fardi, B., Scheunert, U., Cramer, H., and Wanielik, G. (2003). Multi-modal detection and parameter-based tracking of road borders with a laser scanner. In *Proceedings of the IEEE Intelligent Vehicles Symposium*, pages 95–99, Columbus, USA.

Gern, A., Franke, U., and Levi, P. (2000). Advanced lane recognition - fusing vision and radar. In *Proceedings of the IEEE Intelligent Vehicles Symposium*, pages 45–51, Dearborn, MI, USA.

Gern, A., Franke, U., and Levi, P. (2001). Robust vehicle tracking fusing radar and vision. In *Proceedings of the international conference of multisensor fusion and integration for intelligent systems*, pages 323–328, Baden-Baden, Germany.

Gilholm, K. and Salmond, D. (2005). Spatial distribution model for tracking extended objects. In *IEE Proceedings of Radar, Sonar and Navigation*, volume 152, pages 364–371.

Kalman, R. E. (1960). A new approach to linear filtering and prediction problems. *Transactions of the ASME, Journal of Basic Engineering*, 82:35–45.

Kirchner, A. and Heinrich, T. (1998). Model based detection of road boundaries with a laser scanner. In *Proceedings of the IEEE Intelligent Vehicles Symposium*, pages 93–98, Stuttgart, Germany.

Koch, J. W. (2008). Bayesian approach to extended object and cluster tracking using random matrices. *IEEE Transactions on Aerospace and Electronic Systems*, 44(3):1042–1059.

Kodagoda, K. R. S., Wijesoma, W. S., and Balasuriya, A. P. (2006). CuTE: Curb Tracking and Estimation. *IEEE Transactions on Control Systems Technology*, 14(5):951–957.

Lundquist, C. and Schön, T. B. (2008). Road geometry estimation and vehicle tracking using a single track model. In *Proceedings of the IEEE Intelligent Vehicles Symposium*, pages 144–149, Eindhoven, The Netherlands.

Lundquist, C. and Schön, T. B. (2009). Estimation of the free space in front of a moving vehicle. In *Proceedings of the SAE World Congress*, SAE paper 2009-01-1288, Detroit, MI, USA.

Polychronopoulos, A., Amditis, A., Floudas, N., and Lind, H. (2004). Integrated object and road border tracking using 77 GHz automotive radars. In *IEE Proceedings of Radar, Sonar and Navigation*, volume 151, pages 375–381.

Reid, D. B. (1979). An algorithm for tracking multiple targets. *IEEE Transactions on Automatic Control*, 24(6):84–90.

Ristic, B., Arulampalam, S., and Gordon, N. (2004). *Beyond the Kalman Filter: Particle filters for tracking applications*. Artech House, London, UK.

van Trees, H. L. (1968). *Detection, Estimation, and Modulation Theory*. John Wiley & Sons, New York, USA.

Vermaak, J., Ikoma, N., and Godsill, S. J. (2005). Sequential Monte Carlo framework for extended object tracking. *IEE Proceedings of Radar, Sonar and Navigation*, 152(5):353–363.

Wang, Y., Bai, L., and Fairhurst, M. (2008). Robust road modeling and tracking using condensation. *IEEE Transactions on Intelligent Transportation Systems*, 9(4):570–579.

Wijesoma, W. S., Kodagoda, K. R. S., and Balasuriya, A. P. (2004). Road-boundary detection and tracking using ladar sensing. *IEEE Transactions on Robotics and Automation*, 20(3):456–464.

Zomotor, Z. and Franke, U. (1997). Sensor fusion for improved vision based lane recognition and object tracking with range-finders. In *Proceedings of IEEE Conference on Intelligent Transportation System*, pages 595–600, Boston, MA, USA.

Notation

Lower case letters are used to denote scalar variables, bold lower case letters are used for vector valued variables and upper case letters are used for matrix valued variables. A superscript letter is used to denote the coordinate frame, in which a variable or constant is represented. A calligraphic style subscript letter is used to denote the affiliation of a variable to a model or subsystem.

Symbols

$a(\cdot)$	continuous-time nonlinear process model
a_x	longitudinal acceleration
a_y	lateral acceleration
C_α	cornering stiffness
C_d	damper constant
C_s	spring constant
$c(\cdot)$	continuous-time nonlinear measurement model
c_0	road curvature
c_1	road curvature derivative
χ	pitch angle
Δz_f	axle height, front
Δz_r	axle height, rear
d	a displacement
$\boldsymbol{d}$	a displacement vector
d_{EW}	scalar (Euclidean) displacement from O_W to O_E
$d_{S_i E_s}$	range between ego vehicle's sensor and stationary object i
$d_{T_i E_s}$	range between ego vehicle's sensor and leading vehicle i

$\boldsymbol{d}_{EW}^{W}$	displacement vector from O_W to O_E, in the W-frame
δ_f	mean front wheel angle
δ_R	angle between the vehicle's velocity vector and the lane
δ_s	steering wheel angle
$\delta_{S_i E_s}$	azimuth angle between the ego vehicle's sensor and a stationary object i
$\delta_{T_i E_s}$	azimuth angle between the ego vehicle's sensor and a tracked (moving) target i
E	ego vehicle coordinate frame at CoG
E_f	ego vehicle coordinate frame at front wheel
E_r	ego vehicle coordinate frame at rear wheel
E_s	ego vehicle coordinate frame at sensor (radar, vison)
$\mathcal{E}$	ego model or subsystem
$\boldsymbol{e}$	measurement noise
F	discrete-time linear process matrix
F_z	vertical force
$f(\,\cdot\,)$	discrete-time nonlinear process model
$\mathcal{G}$	gate (data association)
H	discrete-time linear measurement matrix
$\boldsymbol{H}$	stacked measurement models on top of each other
$h(\,\cdot\,)$	discrete-time nonlinear measurement model
I_{zz}	moment of inertia about the vertical axis
K	Kalman gain
L	line coordinate frame
$\mathcal{L}$	modeled line
l_b	wheel base
l_E	offset between the ego vehicle and the left lane marking
l_f	distance between ego vehicle CoG and front axle
l_r	distance between ego vehicle CoG and rear axle
l_s	distance between ego vehicle CoG and sensors
l_{T_i}	lateral distance between leading vehicle and lane marking
$\ell(\,\cdot\,)$	likelihood function
m	vehicle mass
$\boldsymbol{m}$	map state vector or matrix
N	number of elements in a set
$\mathcal{N}(m, P)$	normal (Gaussian) distribution with mean value m and covariance matrix P
$\mathcal{N}(x\,;\,m, P)$	normal (Gaussian) probability density function with mean value m and covariance matrix P
n	number of elements in a vector
O_E	origin of E, at the vehicle's center of gravity

O_{L_i}	origin of a line frame L_i
O_{T_i}	origin of T_i at the tracked target
O_V	origin of V at the ego vehicles vision and radar sensors
O_W	origin of W
$\mathcal{O}$	measured object (by e.g., radar)
P	state covariance
$\mathcal{P}$	modeled point
$p(\boldsymbol{x})$	probability density function of $\boldsymbol{x}$
$p(\boldsymbol{x}, \boldsymbol{y})$	joint probability density function of $\boldsymbol{x}$ and $\boldsymbol{y}$
$p(\boldsymbol{x}\|\boldsymbol{y})$	conditional probability density function of $\boldsymbol{x}$ given $\boldsymbol{y}$
ψ_E	the ego vehicle's yaw angle
ψ_{T_i}	yaw angle of target i
ψ_{RE}	angle between the ego vehicle and the road tangent
Q	process noise covariance
R	rotation matrix
R	measurement noise covariance
R	road coordinate frame
$\mathcal{R}$	road model
$\mathbb{R}^n$	the set of real numbers in n dimensions
S	innovation covariance
S_i	position of stationary object i
$\mathcal{S}$	stationary object model
T	target coordinate frame
T	sample time
$\mathcal{T}$	target model
t	time
$\boldsymbol{\theta}$	parameter vector
$\boldsymbol{u}$	known deterministic input signal
V	coordinate frame in sensor pointing at leading vehicle
$V(\theta; \boldsymbol{x}, \boldsymbol{y})$	criterion function to be minimized
v_x	longitudinal velocity
v_y	lateral velocity
W	world coordinate frame
w	road width
$\boldsymbol{w}$	process noise
$\mathbf{X}$	set of state vectors
$\boldsymbol{x}$	state vector
$\boldsymbol{x}_{\mathcal{E}}$	state vector of ego vehicle
$\boldsymbol{x}_{\mathcal{L}_i}$	state vector of line i
$\boldsymbol{x}_{\mathcal{P}_i}$	state vector of point i
$\boldsymbol{x}_{\mathcal{R}}$	state vector of road

$\boldsymbol{x}_{\mathcal{T}_i}$	state vector of target i
x_{EW}^{W}	x-coordinate of a line from O_W to O_E, in W-frame
$\mathbf{Y}$	set of measurement vectors
$\boldsymbol{Y}$	stacked measurement vectors on top of each others
$\boldsymbol{y}$	measurement vector
y_{EW}^{W}	y-coordinate of a line from O_W to O_E, in W-frame

Operators

$\mathrm{diag}(a)$	a diagonal matrix with a as diagonal entry
$\dot{x}$	time derivative of x
$\triangleq$	equal by definition
$\sim$	denotes "is distributed according to"
$\in$	belongs to
$\forall$	for all
$\mathrm{Tr}\, A$	trace of matrix A
A^{T}	transpose of matrix A
A^{-1}	inverse of matrix A
$\mathrm{Cov}(x)$	covariance matrix of the random variable x
$\mathrm{E}(x)$	expectation of the random variable x
$\mathrm{Var}(x)$	variance of the random variable x
$\min$	minimize
$\max$	maximize
$\|x\|_A^2$	weighted vector norm, $\|x\|_A^2 = x^T A x$
$\lvert\cdot\rvert$	absolute value

Abbreviations and Acronyms

pdf	probability density function
s.t.	subject to
CAN	Controller Area Network
ECU	Electronic Control Unit
EKF	Extended Kalman Filter
FMCW	Frequency Modulated Continuous-wave Radar
IMU	Inertial Measurement Unit
KF	Kalman Filter
LRT	Likelihood Ratio Test
LS	Least-Squares
MAP	Maximum A Posteriori
ML	Maximum Likelihood
OGM	Occupancy Grid Mapping
QP	Quadratic Program
RLS	Recursive Least Squares

RMSE	Root Mean Square Error
SEFS	Sensor Fusion for Safety
SLAM	Simultaneous Localization and Mapping
UKF	Unscented Kalman Filter
WLS	Weighted Least Squares

Licentiate Theses
Division of Automatic Control
Linköping University

P. Andersson: Adaptive Forgetting through Multiple Models and Adaptive Control of Car Dynamics. Thesis No. 15, 1983.

B. Wahlberg: On Model Simplification in System Identification. Thesis No. 47, 1985.

A. Isaksson: Identification of Time Varying Systems and Applications of System Identification to Signal Processing. Thesis No. 75, 1986.

G. Malmberg: A Study of Adaptive Control Missiles. Thesis No. 76, 1986.

S. Gunnarsson: On the Mean Square Error of Transfer Function Estimates with Applications to Control. Thesis No. 90, 1986.

M. Viberg: On the Adaptive Array Problem. Thesis No. 117, 1987.

K. Ståhl: On the Frequency Domain Analysis of Nonlinear Systems. Thesis No. 137, 1988.

A. Skeppstedt: Construction of Composite Models from Large Data-Sets. Thesis No. 149, 1988.

P. A. J. Nagy: MaMiS: A Programming Environment for Numeric/Symbolic Data Processing. Thesis No. 153, 1988.

K. Forsman: Applications of Constructive Algebra to Control Problems. Thesis No. 231, 1990.

I. Klein: Planning for a Class of Sequential Control Problems. Thesis No. 234, 1990.

F. Gustafsson: Optimal Segmentation of Linear Regression Parameters. Thesis No. 246, 1990.

H. Hjalmarsson: On Estimation of Model Quality in System Identification. Thesis No. 251, 1990.

S. Andersson: Sensor Array Processing; Application to Mobile Communication Systems and Dimension Reduction. Thesis No. 255, 1990.

K. Wang Chen: Observability and Invertibility of Nonlinear Systems: A Differential Algebraic Approach. Thesis No. 282, 1991.

J. Sjöberg: Regularization Issues in Neural Network Models of Dynamical Systems. Thesis No. 366, 1993.

P. Pucar: Segmentation of Laser Range Radar Images Using Hidden Markov Field Models. Thesis No. 403, 1993.

H. Fortell: Volterra and Algebraic Approaches to the Zero Dynamics. Thesis No. 438, 1994.

T. McKelvey: On State-Space Models in System Identification. Thesis No. 447, 1994.

T. Andersson: Concepts and Algorithms for Non-Linear System Identifiability. Thesis No. 448, 1994.

P. Lindskog: Algorithms and Tools for System Identification Using Prior Knowledge. Thesis No. 456, 1994.

J. Plantin: Algebraic Methods for Verification and Control of Discrete Event Dynamic Systems. Thesis No. 501, 1995.

J. Gunnarsson: On Modeling of Discrete Event Dynamic Systems, Using Symbolic Algebraic Methods. Thesis No. 502, 1995.

A. Ericsson: Fast Power Control to Counteract Rayleigh Fading in Cellular Radio Systems. Thesis No. 527, 1995.

M. Jirstrand: Algebraic Methods for Modeling and Design in Control. Thesis No. 540, 1996.

K. Edström: Simulation of Mode Switching Systems Using Switched Bond Graphs. Thesis No. 586, 1996.

J. Palmqvist: On Integrity Monitoring of Integrated Navigation Systems. Thesis No. 600, 1997.

A. Stenman: Just-in-Time Models with Applications to Dynamical Systems. Thesis No. 601, 1997.

M. Andersson: Experimental Design and Updating of Finite Element Models. Thesis No. 611, 1997.

U. Forssell: Properties and Usage of Closed-Loop Identification Methods. Thesis No. 641, 1997.

M. Larsson: On Modeling and Diagnosis of Discrete Event Dynamic systems. Thesis No. 648, 1997.

N. Bergman: Bayesian Inference in Terrain Navigation. Thesis No. 649, 1997.

V. Einarsson: On Verification of Switched Systems Using Abstractions. Thesis No. 705, 1998.

J. Blom, F. Gunnarsson: Power Control in Cellular Radio Systems. Thesis No. 706, 1998.

P. Spångéus: Hybrid Control using LP and LMI methods – Some Applications. Thesis No. 724, 1998.

M. Norrlöf: On Analysis and Implementation of Iterative Learning Control. Thesis No. 727, 1998.

A. Hagenblad: Aspects of the Identification of Wiener Models. Thesis No. 793, 1999.

F. Tjärnström: Quality Estimation of Approximate Models. Thesis No. 810, 2000.

C. Carlsson: Vehicle Size and Orientation Estimation Using Geometric Fitting. Thesis No. 840, 2000.

J. Löfberg: Linear Model Predictive Control: Stability and Robustness. Thesis No. 866, 2001.

O. Härkegård: Flight Control Design Using Backstepping. Thesis No. 875, 2001.

J. Elbornsson: Equalization of Distortion in A/D Converters. Thesis No. 883, 2001.

J. Roll: Robust Verification and Identification of Piecewise Affine Systems. Thesis No. 899, 2001.

I. Lind: Regressor Selection in System Identification using ANOVA. Thesis No. 921, 2001.

R. Karlsson: Simulation Based Methods for Target Tracking. Thesis No. 930, 2002.

P.-J. Nordlund: Sequential Monte Carlo Filters and Integrated Navigation. Thesis No. 945, 2002.

M. Östring: Identification, Diagnosis, and Control of a Flexible Robot Arm. Thesis No. 948, 2002.

C. Olsson: Active Engine Vibration Isolation using Feedback Control. Thesis No. 968, 2002.

J. Jansson: Tracking and Decision Making for Automotive Collision Avoidance. Thesis No. 965, 2002.

N. Persson: Event Based Sampling with Application to Spectral Estimation. Thesis No. 981, 2002.

D. Lindgren: Subspace Selection Techniques for Classification Problems. Thesis No. 995, 2002.

E. Geijer Lundin: Uplink Load in CDMA Cellular Systems. Thesis No. 1045, 2003.

M. Enqvist: Some Results on Linear Models of Nonlinear Systems. Thesis No. 1046, 2003.

T. Schön: On Computational Methods for Nonlinear Estimation. Thesis No. 1047, 2003.

F. Gunnarsson: On Modeling and Control of Network Queue Dynamics. Thesis No. 1048, 2003.

S. Björklund: A Survey and Comparison of Time-Delay Estimation Methods in Linear Systems. Thesis No. 1061, 2003.

M. Gerdin: Parameter Estimation in Linear Descriptor Systems. Thesis No. 1085, 2004.

A. Eidehall: An Automotive Lane Guidance System. Thesis No. 1122, 2004.

E. Wernholt: On Multivariable and Nonlinear Identification of Industrial Robots. Thesis No. 1131, 2004.

J. Gillberg: Methods for Frequency Domain Estimation of Continuous-Time Models. Thesis No. 1133, 2004.

G. Hendeby: Fundamental Estimation and Detection Limits in Linear Non-Gaussian Systems. Thesis No. 1199, 2005.

D. Axehill: Applications of Integer Quadratic Programming in Control and Communication. Thesis No. 1218, 2005.

J. Sjöberg: Some Results On Optimal Control for Nonlinear Descriptor Systems. Thesis No. 1227, 2006.

D. Törnqvist: Statistical Fault Detection with Applications to IMU Disturbances. Thesis No. 1258, 2006.

H. Tidefelt: Structural algorithms and perturbations in differential-algebraic equations. Thesis No. 1318, 2007.

S. Moberg: On Modeling and Control of Flexible Manipulators. Thesis No. 1336, 2007.

J. Wallén: On Kinematic Modelling and Iterative Learning Control of Industrial Robots. Thesis No. 1343, 2008.

J. Harju Johansson: A Structure Utilizing Inexact Primal-Dual Interior-Point Method for Analysis of Linear Differential Inclusions. Thesis No. 1367, 2008.

J. D. Hol: Pose Estimation and Calibration Algorithms for Vision and Inertial Sensors. Thesis No. 1370, 2008.

H. Ohlsson: Regression on Manifolds with Implications for System Identification. Thesis No. 1382, 2008.

D. Ankelhed: On low order controller synthesis using rational constraints. Thesis No. 1398, 2009.

P. Skoglar: Planning Methods for Aerial Exploration and Ground Target Tracking. Thesis No. 1420, 2009.